WIND TUNNEL MODELLING

OF

BUOYANT PLUMES

KEVIN WILLIAM RUTLEDGE

WADHAM COLLEGE

OXFORD

A thesis submitted in partial fulfilment of the requirements of the degree of Doctor of Philosophy at the University of Oxford.

Michaelmas Term 1984

ACKNOWLEDGEMENTS

This study was carried out while the author was a member of the Oxford University Wind Engineering Research Group, and I would like to thank all the members of the group, past and present, for providing a lively and friendly atmosphere to work in.

I would like to thank Dr. Graham Thornton, my supervisor, for his critical view of the subject and his practical advice in designing the wind tunnel experiments.

Dr. Colin Wood, my college tutor, introduced me to fluid mechanics as an undergraduate and has always encouraged my interest in the subject.

Mr. Rex Belcher provided enthusiastic support for the computing requirements of this study, for which I am most grateful.

All the photographs in this thesis were carefully processed and printed by Mr. John Mooney.

Finally, I must thank my parents for all their help and encouragement throughout my studies. Without their support I would never have reached this stage.

WIND TUNNEL MODELLING OF BUOYANT PLUMES

KEVIN W. RUTLEDGE WADHAM COLLEGE

A thesis submitted in partial fulfilment of the requirements of the degree of Doctor of Philosophy at the University of Oxford.
Michaelmas Term 1984

ABSTRACT

The short range dispersion in the atmosphere of buoyant gases, such as hot air or natural gas, may be hazardous and dangerous. The available methods for studying this problem were reviewed. Wind tunnel studies were considered to be the most suitable method for studying near-field dispersion, and methods for accurately modelling the near-field behaviour of a buoyant plume of gas were examined. The experiments were performed in the Oxford University 4m x 2m low speed wind tunnel at a model scale of 1:200. The mean trajectory and rate of spread of a buoyant plume from a 60 m high (full-scale) stack were measured in the presence of a simulated natural wind.

The exact similarity requirements were derived from dimensional analysis and from the equations of motion. In practice, it is not possible to match all the necessary dimensionless groups and exact scaling of the exit gas density ratio and the exit Reynolds number is often relaxed. A series of experiments was performed to examine the effect of these two groups on mean plume behaviour, with the intention of providing guidance for correct simulation of plume dispersion at reduced-scale.

The exit density ratio was found to have little effect on the near-field plume behaviour, provided all the other dimensionless groups were matched. Plumes with low Reynolds number were found to rise significantly higher than plumes with higher 'turbulent' Reynolds numbers. This difference in trajectory could not be correlated with the plume exit momentum flux.

The effect of the cross-flow on near-field dispersion was examined by performing experiments in four different simulations of the earth's atmospheric boundary-layer. The behaviour of the plume was found to be sensitive to both the velocity profile and the turbulence intensity of the cross-flow. To study dispersion in the wind tunnel, the cross-flow should be an accurate simulation of the velocity profile and turbulence intensity components of the natural wind.

CONTENTS

LIST OF FIGURES AND TABLES

SYMBOLS

A	frontal area of a building [m^2]
a_2	constant in Batchelor's (1950/52) expression
a	constant in Chatwin's (1968) expression for cloud velocity
b	plume radius [m]
b	constant in eqn. 2.18
b	exponent in power-law representation of plume trajectory
C	a constant
C_D	drag coefficient
C_p	specific heat at constant pressure [kJ/kg K]
c	gas concentration [p.p.m.]
D^2	variance of the temperature profile [m^2]
d	stack exit diameter [m]
Ec	Eckert number (= U^2/C_pT)
Er	non-dimensional error in plume trajectory see eqn. 6.17
F_b	exit buoyancy flux (= $w_s g r^2 (\rho_a - \rho_s)/\rho_a$) [m^4/s^{-3}]
F_{ax}	body-force in the x-direction [N]
F_m	exit momentum flux (= $\rho_s w_s^2 r^2/\rho_a$) [m^4/s^{-2}]
F_{rd}	densimetric Froude number (= $gd(\rho_a - \rho_s)/\rho_a U^2$)
g	acceleration due to gravity [m/s^2]
H	stack height [m]
h	heat transfer coefficient [W/m^2K]
K	eddy diffusivity [m^2/s]
k	thermal conductivity [W/m^2K]
k_2	geometrical constant (Moore, 1966)
L	integral length scale [m]
L	Monin-Obukov length (eqn. 2.18 only) [m]
l	mixing length [m]

l_b buoyancy length-scale (= F_b / U^3) [m]

l_m momentum length-scale (= $\sqrt{F_m / U^2}$) [m]

l_v velocity length-scale (= $w_s r / U$) [m]

m mass flow-rate [kg/s]

Nud Nusselt number (= hd/k)

n =2/3(1+p), exponent in Murthy's (1970) plume rise formula

n frequency [s^{-1}]

$\hat{n}$ modal frequency [s^{-1}]

dn spectral width [s^{-1}]

Pr Prandtl number (= $C_p \mu / k$)

p pressure [N/m^2]

p exponent in Murthy's (1970) mean velocity profile

Q stack exit heat flux [MW]

Q source strength per unit area [m^{-2}]

Q radial heat flux through model stack [W/m]

q volumetric concentration of helium

$R(\tau)$ autocorrelation function, see eqn. 2.24

R_e Reynolds number (= $\rho Ud/\mu$)

R_{ex} stack exit Reynolds number (= $\rho_s W_s d / \mu_s$)

Ri bulk Richardson number (= $\Delta T L g / TU^2$)

Ro Rossby number (= $U/L\Omega$)

R_{mom} momentum ratio (= $\rho_s w_s^2 / \rho_a U_a^2$)

R_v velocity ratio (= w_s / U_a)

r stack exit radius [m]

S(X) scaling of a property in the model and prototype

S(n) power spectral density [m^2/s]

T temperature [K]

T integral time-scale [s]

t time [s]

τ reference value of time [s]

U velocity in the X-direction [m/s]

U_a wind velocity at stack height [m/s]

U_* friction velocity [m/s]

U' overall heat transfer coefficient [W/mK]

V velocity in the Y-direction [m/s]

V_e entrainment velocity [m/s]

Var variance of the longitudinal velocity component [m^2/s^2]

W velocity in the Z-direction [m/s]

w_s stack exit velocity of the plume [m/s]

X distance downstream of stack centre [m]

X^* downstream distance term in Moore's (1974) plume rise formula [m]

Y lateral distance from plume centre-line [m]

Z height above the ground (or stack exit) [m]

Z_o roughness length [m]

Z_* reference height in Djurfors & Netterville (1978) expression for the wind velocity profile [m]

α molecular diffusivity [m^2/s]

α_1 entrainment constant

β momentum correction factor

γ exponent in Djurfors & Netterville (1978) expression for the wind velocity profile

θ_* friction temperature ($=-\overline{w'T'}/U_*$) [K]

θ temperature above ambient [K]

μ dynamic viscosity [Ns/m^2]

ν kinematic viscosity [m^2/s]

ρ gas density [kg/m^3]

$\Delta\rho$ density difference $(\rho_a - \rho_s)$ [kg/m^3]

σ_x standard deviation of temperature profile [m]

σ_u standard deviation of velocity component [m/s]

$\sigma_u/\bar{u}$ turbulence intensity

χ gas concentration [p.p.m.]

Subscripts

a ambient conditions

amb " "

s properties at stack exit

x,y,z components in the X,Y,Z direction

u,v,w property of the velocities in the X,Y,Z directions

Superscripts

— time-averaged mean value

' fluctuating component

or non-dimensional term

1. INTRODUCTION

Our present industrial society produces large quantities of waste products in gaseous form, from many sources, including coal-burning, internal combustion engines and chemical plants. The release of these gases into the atmosphere, either accidentally or deliberately, can cause many problems and hazards. Normally, it is assumed or hoped that the gases will mix with the atmosphere and become diluted before they can cause damage to man or the environment. The atmosphere may appear to be a rather large volume of air capable of safely diluting any pollutant and in the past this seems to have been the approach adopted by many people. However, there are two major flaws in this simplistic approach; firstly, it takes time (and distance) for the pollutant to become diluted and secondly, even minute quantities of a gas may be harmful. If we are going to release potentially dangerous gases into the atmosphere we must know more about their subsequent dispersion.

The problems caused by gases released into the atmosphere occur both over short and medium range. In the short range, the gases may not have been sufficiently diluted and are still potentially dangerous due to their temperature, flammability or toxicity. While for the medium range, although the gases are well mixed with the air, they may still be harmful despite the small concentrations of toxic gas present.

In short range or 'near-field' pollution the gases are often released into an environment consisting of buildings, structures and machinery. In such a situation, the dispersion of gases will be greatly influenced by the flow field of this complex topography. There are several possible forms and sources of short range pollution and we will consider the more important examples.

Fuel gases released accidentally from storage containers or pipelines will mix with the air to form a flammable mixture, and since there are likely to be further quantities of flammable gases or chemicals nearby, the possible 'knock-on' effect could be disastrous. Similarly, the release of toxic gases in an industrial area would be dangerous. Recently, the risk of accidental releases of radioactive gases from nuclear power stations has become a cause for concern; this may not only be a short range but also a medium range problem.

The above are examples of accidental releases. However, some controlled, continuous releases may also be potentially harmful. The hot exhaust gases from gas turbines fall into this category. The gases are very hot with temperatures up to 500°C. The turbines may be operating in a chemical plant, on board a ship or on an offshore structure. It is upon this latter situation, due to the expanding North Sea oil and gas industry, that a great deal of attention has recently been focused.

Hot gases on offshore structures give rise to a number of potential hazards. For example, the possibility of hot gases blowing over the helideck may cause helicopters to suddenly lose lift in the last few vital metres of descent or for their engines to stall. The hot exhaust gases, which often include quantities of highly toxic hydrogen sulphide, can be drawn into the air intakes for the living quarters or even back into the turbines themselves. Finally, the effect of hot gases on machinery and structures may be detrimental to their performance and often creates, in addition, a hostile environment for men working on the rig. These are real problems which must be taken into account in the design and operation of production platforms.

In the case of medium range or 'far-field' pollution, we are concerned with the release of gases which, even when well mixed with the

air, are potentially hazardous. The hazard may be due to small concentrations (parts per million, p.p.m.) of toxic or radioactive gases, or due to the accumulation of certain pollutants above safe levels during continuous releases. In medium range pollution we are often interested in measuring concentration levels up to several kilometres from the source. In such circumstances, the turbulent mixing by the atmosphere controls the dispersion.

The classic medium range pollution problem is the dispersion of gases from power station chimney stacks. In this situation, we are not too concerned with the nature of the actual source but rather the dispersion of the gases over many kilometres. We will want to measure ground-level concentration (g.l.c.) of gases, such as sulphur dioxide, in order to satisfy health regulations.

Most of the above pollutants are lighter-than-air gases. Although there are potential dense gas pollutants, e.g. liquid natural gas, this study will consider only positively buoyant gases. The dispersion of dense gases is often considered as a separate subject since the method of dispersion and the sources are different.

Having considered some of the possible sources of pollution, we should now consider which measurable properties of the pollution we wish to determine and why we need to know their values. The information required will vary depending on the source of the pollution and the nature of the hazard. For example, in the case of a fractured gas pipeline, we would want to know the region of flammable gas so that we could define a dangerous area from which people would have to be evacuated. On an offshore structure we would want to know the peak temperature, due to exhaust gases, which men may be exposed to, to ensure that it is not dangerously high. There are regulations concerning the levels of sulphur dioxide to which people may be exposed,

and so before building a power station chimney stack it must be demonstrated to the relevant authority that these levels will not be exceeded in inhabited areas.

The distinction between short and medium range dispersion, which we have already referred to, becomes more marked when we consider the quantities we wish to determine and the methods available to study the problems. Short range dispersion is often associated with complex environments, such as chemical plants or offshore structures, and with relatively large values of concentrations which may fluctuate greatly, e.g. thermal pollution. Medium range pollution is normally associated with simpler topography and very small values of concentration.

The easiest quantity to determine or predict is the mean concentration at a point. We may need this information to describe the mean environment which people or machinery are exposed to; health regulations may require the mean concentration of a certain gas to be below a certain value. We may want to know the extent of a polluted region or where the peak mean value occurs and this requires making measurements at many points throughout the region to map out concentration contours.

However, concentration values in the atmosphere are fluctuating quantities and the peak value may be more critical than the mean value. For example, although the mean concentration of a flammable gas may be below the lower flammable limit the peak value may be above the limit. We may only need to measure fluctuating concentrations at certain points, such as a point of ignition, or we may need to make measurements over a large region to find the maximum concentration.

In fact, we may want to measure the concentration fluctuations over the complete range of frequencies. We could then construct a spectrum of the concentration fluctuations to identify any dominant or

isolated frequency. We could also construct a probability density function which will tell us the probability of any concentration occurring at a point. The probability density function would be useful in defining flammable regions and in joint probability calculations of risk. These extensive measurements are normally only needed for short range dispersion where there is a serious hazard.Mediumrange dispersion normally only requires mean measurements to be made.

The information we require about a dispersion problem and the nature of the topography will normally determine how we attempt to examine the problem. For example, to study the mean ground-level concentrations of sulphur dioxide from an isolated chimney stack in a uniform, flat enviroment a theoretical model of dispersion may be adequate. Whereas it may be necessary to carry out full-scale tests to measure fluctuating concentrations of pollutants in a complex chemical plant.

The obvious way to study a pollution problem which already exists is to carry out full-scale tests. We can set-up our monitoring equipment at the relevant points of interest and measure concentration levels (or temperature). However, wind direction and speed vary with time and in order to make any sense of the results, we must be able to monitor the meteorological conditions at the same time. Obviously, we have no control over the wind's behaviour and if we want to study the effect of the wind from a certain direction we may have to wait a long time for that condition to occur. Also, we will find that in atmospheric flows averaging times up to 1 hour are required to give statistically significant results. We may want results at many points and this requires either duplication of, possibly expensive, monitoring equipment or repeating the experiments several times. Thus full-scale experiments consume a great deal of time, equipment and effort. They

are, therefore, very expensive and so are seldom carried out.

In spite of the difficulty and expense of carrying out full-scale tests, they do yield actual results which, provided the experiments were carried out carefully, can be used with confidence in assessing an existing pollution problem. Full-scale tests, unlike alternative methods, do not require any assumptions or scaling relaxations to be made and so provide the true result for any pollution study, within the usual limits of experimental uncertainty.

There are two further methods of studying dispersion: reduced scale studies and theoretical methods. Both may be used to predict the effect upon dispersion of changes in the surrounding environment or to study off-design conditions. Both methods are quicker and less expensive to perform than full-scale tests. For these reasons, reduced scale studies and theoretical methods are used extensively to study dispersion. However, both methods require certain assumptions or scaling relaxations to be made. If we are going to use these alternative methods, we must be confident that, in spite of the assumptions made, they provide sufficiently accurate results. Full-scale tests provide the only means of assessing the accuracy of these methods. Unfortunately, few rigorous comparisons have been made between full-scale and laboratory results.

Theoretical methods are widely used because they avoid the need to carry out full-scale or model tests. Also, they do not require any special equipment other than a computer. Using theoretical methods, the values of parameters such as wind speed, gas temperature or velocity, may be varied at will. Thus a wide range of conditions may be studied. Also, we may study proposed designs before they are constructed. For example, we could determine the effect, on pollution levels, of changing the height of a chimney stack.

The basic approach of theoretical studies is to solve the equations governing the motion and dispersion of the effluent in the atmosphere, i.e. the equations of continuity, momentum and energy. These equations are non-linear and consequently difficult to solve analytically. To solve the equations simplifying assumptions have to be made which means that the results are only applicable to a few idealised situations. For example, it is often assumed that the wind speed is constant with height and that the terrain is flat and homogeneous in surface roughness. These assumptions severely limit the situations in which theoretical methods may be used.

All theoretical methods require some empirical input to solve the equations. For example, plume rise models require an empirical expression to describe the rate of entrainment of ambient air into the plume. The values of these empirical terms can only be determined from full-scale data and cannot be determined from first principles. Their values may vary from one situation to another and this greatly limits the confidence with which we can predict concentration levels. In fact, theoretical methods may be so dependent on the empirical input that they become empirical expressions rather than theoretical solutions.

A great deal of effort has been spent in developing theoretical techniques for predicting dispersion in two simple cases; ground-level release of pollutants over flat homogeneous terrain and dispersion of pollutants from an elevated source (e.g. a chimney stack) also in a flat, uniform environment. It would appear that in these circumstances reasonably accurate (±30%) predictions of concentration levels may be made.

However, as soon as we introduce any complex topography the theoretical methods become inadequate. This is because we cannot solve the equations of motion for turbulent flow around obstacles. Even in

the relatively simple case of dispersion around a cube we have to resort to empiricism. So clearly, in complex environments such as city centres, chemical plants or offshore structures we cannot completely describe the flow field or determine the pollution levels without making great simplifications. Thus, in many real situations theoretical methods cannot be used and alternative methods must be used.

It is in complex environments that we can best make use of reduced-scale methods. We can use a wind tunnel or water tank to model the full-scale situation and by using suitable models we can study dispersion in complex environments. (Henceforth, we will refer mainly to wind tunnel studies but many of the remarks will also be relevant to water tank studies.) An important advantage of model tests is that we can study situations which do not already exist. Thus we can examine proposed developments at the design stage, e.g. wind tunnel tests are often used to study pollution from power station chimney stacks before construction. The various parameters can easily be controlled, e.g. wind speed and direction, gas temperature and velocity. Thus unlike full-scale studies, we do not have to wait for the right meteorological conditions to occur and this saves a great deal of time. Also, because we are working at reduced scales, the time-scale of fluctuations in the flow field is reduced which means that the averaging times required are only a fraction of those at full-scale. Thus model scale tests can be carried out quickly and for this reason tend to be less expensive than full-scale tests.

If we are going to study dispersion at model scale we must be confident that the flow fields are similar at model and full-scale. The Reynolds number (which represents the ratio of inertial to viscous forces) is very different in the model and full-scale. The use of reduced length scales and velocity scales in the model study means that

the fluid used in the model study 'appears' to be more viscous than the full-scale fluid. Consequently, the flow fields in the model and prototype will never be exactly the same. Nevertheless, it is possible that the Reynolds number in the model may be large enough that the flow becomes fully turbulent (i.e. the viscous forces are negligible) and behaves similarly to the full-scale flow. It is this hypothesis of 'Reynolds Number Independence' which is at the heart of reduced-scale modelling. Different flow situations will require different critical Reynolds numbers to be exceeded before the flow field becomes independent of the Reynolds number, e.g. flow in a tube, flow around a cylinder. In wind tunnel studies we must ensure that all the critical Reynolds numbers in the model are exceeded and in many situations this may be difficult to achieve. Despite the widespread use of the hypothesis of 'Reynolds Number Independence' the mismatch in Reynolds number is the limiting factor in using reduced scale models to study dispersion.

In addition to the Reynolds number criteria, we must also ensure that the boundary conditions imposed on the flow are correct. Not only must the model be correctly scaled geometrically but the air flow over the model must have the same characteristics as the natural wind. Air flowing over the earth's surface produces an atmospheric boundary-layer (a.b.l.) in which the properties of the flow, such as the mean velocity and turbulence intensity, vary with height. How accurately do we need to model the natural wind? Do we need to model only the mean flow or also the fluctuating component? An additional meteorological factor which may need to be modelled is the stability of the atmosphere. The atmospheric stability represents the buoyancy forces acting on a parcel of air as it rises adiabatically through the atmosphere, and it is determined by the vertical temperature gradient in the atmosphere.

If the vertical temperature gradient in the atmosphere is such that air rising adiabatically is always at the same temperature and pressure as its surroundings, the atmospheric stability is said to be neutral. There are only a few wind tunnels in the world which can model any stability conditions other than neutral stability. Neutral stability normally prevails during high winds (> 10 ms^{-1}).

If we can model the flow field accurately then reduced scale studies offer a very useful means of studying atmospheric dispersion since we can study pollution problems in real, complex environments. To validate these methods we should compare their results with full-scale data. Unfortunately, suitable full-scale data is scarce and limited, and as a result few comparisons have been possible. Thus, in absolute terms the accuracy of model tests has not been fully examined. However, an alternative approach is to study the accuracy of model tests in relative terms by a process of testing the sensitivity of dispersion to variations in the experimental variables.

From the equations of motion and by dimensional analysis, we can determine the similarity requirements for exact modelling of a full-scale dispersion problem, i.e. which parameters must be matched. If we could achieve exact similarity of these parameters in the model and the prototype then the results in the model and prototype would be exactly similar since the governing equations would be exactly the same. However, in practice, we cannot achieve exact similarity and are forced to relax the scaling of certain parameters. It is the relaxation of these parameters which needs to be examined and justified. If we can show that the relaxed parameters have little effect on the results then we can be confident that we are modelling the full-scale situation. By this process we can validate model scale studies of atmospheric dispersion.

As we shall see later, in the Literature Review, there have been very few rigorous attempts to investigate the validity of reduced scale studies by considering the sensitivity of the results to the scaling parameters. Nevertheless, wind tunnel tests are now widely used to study pollution problems. It is the purpose of this study to investigate the validity of wind tunnel methods and the techniques used. To do this, I will consider the effect of relaxing the scaling of certain parameters in order to determine which parameters are important. By this means, I intend to determine how we can accurately model atmospheric dispersion in a wind tunnel.

2. LITERATURE REVIEW

In this literature review I will describe in more detail some of the previous studies of atmospheric dispersion. As mentioned earlier, these studies may be divided into three categories:

1. Full-scale studies,
2. Theoretical methods,
3. Reduced scale studies.

By reviewing the previous work, we will be able to see more clearly the applicability and limitations of each method.

This review will be conducted from the viewpoint of the wind tunnel modeller who wants to model atmospheric dispersion accurately in a wind tunnel. Therefore, when considering full-scale studies we will be looking for results which may be compared with wind tunnel results to validate wind tunnel methods. We will discuss the various theoretical methods so that we are aware of which results may be applied to wind tunnel studies and to understand the limitations of theoretical methods. Finally, in reviewing wind tunnel tests we will describe the range of studies which have been carried out and discuss the practical techniques employed. Then, in the next chapter, we will consider in detail the theoretical similarity requirements for wind tunnel modelling of dispersion and will review how these requirements have been applied by previous workers.

2.1 FULL-SCALE STUDIES

Full-scale studies are the most direct means of studying atmospheric dispersion. For a given situation they produce the most useful and reliable results, assuming the experiments are carried out carefully.

However, full-scale experiments are very difficult and time

consuming to carry out. The main problem is determining the meteorological conditions under which the results were obtained, it is important to know these conditions because they will greatly influence the results. Ideally, the wind speed and direction should be measured at several heights close to the source of pollution. Also, the vertical temperature gradient (and the resulting atmospheric stability) is an important factor, and would need to be measured to relate the results to different stability classes. The effluent exit conditions are normally easier to determine. However, it may not be possible to vary them greatly from the normal operating conditions.

Atmospheric dispersion is controlled by many parameters and since it is not possible to completely isolate each parameter, full-scale results inevitably show a degree of scatter in their values. In order to obtain meaningful results the experiments should be repeated several times and ensemble averages calculated. Long averaging times will be required to obtain mean values. There is a gap in the wind energy spectrum at about one hour, so this would be a suitable averaging time. Unfortunately, it may not be possible to make measurements for such a length of time and the exit conditions or the wind direction may change during this period.

For the above reasons, there are few full-scale studies of atmospheric pollution reported in the literature. Two main types of experiments have been reported, ground-level release of gas over relatively flat terrain and studies of pollution from power station chimney stacks. Studies of pollutant dispersion in complex environments have been limited to a few studies of pollution in urban areas. Presumably other studies have been carried out but the results are not widely available. Thus most of the data refers to medium range pollution.

The earliest pollution studies in the United Kingdom were carried

out on Salisbury Plain by the Chemical Defence Establishment, Porton in 1923. They consisted of releasing a harmless smoke at ground level and then measuring the smoke concentration downstream. The smoke concentration was measured by collecting samples on filter paper and then comparing them with laboratory prepared specimens. Further experiments were carried out at Cardington in 1931 and 1934, when atmospheric turbulence measurements were also made using a bi-directional vane. The above experiments were performed to determine the lateral spread of a smoke cloud. The measurements of cloud width showed considerable scatter and this was probably due to variations in atmospheric stability, however, they did suggest that cloud width was proportional to the lateral turbulence intensity.

During the 1950's several experiments were performed in the U.S.A. on diffusion from ground-level 'point' sources. The experiments were performed at Round Hill, Massachusetts (Cramer et al., 1958), where the terrain was undulating and included small buildings and trees, and also on the Nebraska plains during Project Prairie Grass (Barad, 1959). Sulphur dioxide was used as a tracer gas and the meteorological conditions were measured accurately. The results showed a strong linear relationship between cloud width and lateral turbulence intensity. The lateral profiles of concentration were found to be closely Gaussian. It was also found that in neutral conditions the standard deviation of the lateral distribution of concentration (σy) increased as the downstream distance (X) raised to the power of 0.8 .

$$\sigma_y \propto X^{0.8} \qquad (2.1)$$

which agreed with the previous Porton experiments.

There have been a few studies of dispersion around buildings, e.g. Munn & Cole (1967). The results of such studies are clearly very dependent on the geometry of the buildings.

McCormick (1971) reviewed much of the available full-scale data in his paper 'Air Pollution in the Locality of Buildings'. The main interest appears to be in the dispersion of combuston products from car exhausts in urban areas, and there have been several studies of the dispersion of exhaust gases in 'city canyons' In McCormick's paper, the blackening of buildings is illustrated by photographs which show that the deposition of soot on the faces of buildings may be influenced by the aerodynamics of the flow around individual buildings.

Start et al. (1977) measured the downwind dispersion of a ground-level release near the reactor building of the Rancho Seco nuclear power station in California. SF_6 was used as a tracer gas and its concentration was measured at several downstream sampling points for averaging periods of 1 hour. The plant's two cooling towers were found to have an important effect, as one would expect. Similar studies have been performed in the U.K. by the C.E.G.B..

Sommers et al. (1980) have reported field measurements for the dispersion of the flue gases of gas fired heating units from buildings. The low gas concentrations, compared with the background level, were difficult to measure and highlight one of the problems of performing full-scale studies. The results of the full-scale study have been compared with results from several wind tunnel studies and some large discrepancies are apparent. The results of such full-scale studies can

be usefully compared with wind tunnel experiments to determine the validity of model scale studies. Studies of pollution in urban areas have focused on measuring concentrations of sulphur dioxide at several stations throughout the area and then relating the results to wind speed, direction and atmospheric stability. Such studies have been carried out in the U.K. in Leicester ,1937-39 (D.S.I.R., 1945), Reading, 1964-65 (Marsh & Withers, 1969), and London (Smith & Jeffrey, 1971).

The available data on the dispersion of chimney plumes can be divided into two categories: visual observations of smoke plumes and ground level concentration (g.l.c.) measurements. Smoke plumes have been studied photographically to determine a mean trajectory. Long-exposure photographs have been used and the trajectory determined as the mid-point between the upper and lower edges. Alternatively, many instantaneous photographs have been taken, the instantaneous trajectory determined and then the mean trajectory of several photographs calculated. The main problem with such experiments is determining the meteorological conditions since the wind speed and direction need to be known at the stack exit, which may be several hundred feet above ground level. In several studies the wind speed and direction have been measured at much lower heights and then extrapolated to the stack height using previously measured atmospheric data.

The main motivation to determine plume rise has been to fit the results to empirical formulae. Several studies in Britain and the U.S.A. have suggested that plume rise is inversely proportional to the wind speed. Slawson and Csanady (1967) observed the plume from the Lake View Generating Station, Ontario and found that in neutral conditions the mean plume rise (Z) was described by:

$$Z \propto X^{2/3} \qquad (2.2)$$

where X is the downstream distance.

Briggs (1969) examined data from many sources and found that they agreed quite well with the '2/3 power-law'. Hogstrom (1964) studied the plumes from several Swedish power stations. Later Bringfelt (1969) analysed the results and found general agreement with the '2/3 power-law' but also found considerable variation in the exponent.

Studies similar to those described above have been carried out in the U.K. by the Central Electricity Generating Board. From visual observations, Scriven (1966) pointed out that chimney plumes frequently breakdown into discrete puffs and suggested a mechanism for this breakdown. The C.E.G.B. has also made measurements of ground level concentrations of pollutants downstream of the Tilbury and Northfleet power stations, Lucas et al. (1967), Hamilton (1967). Such experiments are very valuable in validating theoretical models, Moore (1975), or wind tunnel tests, Robins (1980). Robins (1980) has actually modelled the full-scale situation in a wind tunnel, at a scale of 1:500, and then investigated the effect of different modelling techniques on the results obtained. Such studies are very important to wind tunnel modellers, in that they suggest which modelling techniques yield results closest to the full-scale results. They also allow us to determine how accurately we can expect our model scale results to agree with the full-scale results. (Robins' (1980) studies will be referred to again later.)

In Canada, an extensive investigation has been carried out by Syncrude Canada Ltd. into the rise and dispersion of a plume from the 183m tall stack at Syncrude's Mildred Lake oil plant, Slawson et al. (1978). Throughout 1977 the plume was studied photographically and ground-level concentration measurements were made. Meteorolgical data were also recorded in the form of wind speed and direction, and temperature profiles. The resulting data have provided a valuable source of information on plume dispersion. Slawson et al. (1980) have

used the data to test several theoretical models of plume rise and spread, with the intention of developing a 'site-tuned plume dispersion model'.

Similar studies have been carried out in Germany, see Brotz et al. (1982), to study the dispersion from conventional and nuclear power stations. Tracer element techniques have been used to make measurements of concentration (using SF_6 tracers for example) and aircraft have been used to make measurements within the elevated plumes.

One of the few reported studies of short-range dispersion is by Hoult et al. (1977), who studied the exhaust flow downwind of a large gas turbine by photographic methods. They also modelled the situation in a wind tunnel. The results for mean plume rise varied from run to run in both the model and full-scale by up to a factor of three. This was probably due to too short an averaging time being used. Within the large scatter of the results there was some quantitative agreement.

The study of Hoult et al. illustrates one of the main problems of full-scale studies, namely, scatter in the results. This is caused by the constant variation in the conditions, such as wind speed and direction, and also because averaging times of too short a duration are used. Thus measured values of plume-rise and ground-level concentration can show variations of up to $\pm$100%. Thus only the main trends in atmospheric dispersion can be determined from full-scale experiments.

The experimental scatter in full-scale results makes it difficult to isolate results due to a specific set of conditions and to compare them with either wind tunnel or theoretical results. Thus, comparing full-scale results with wind tunnel results often proves to be an unsatisfactory and inconclusive method of validating wind tunnel tests. Then, in order to validate wind tunnel methods an alternative technique may have to be used. As suggested earlier, by examining the effect of

relaxing parameters we will be able to determine which parameters are important and which have negligible effect. Then, having rigorously justified the relaxation of certain parameters and the matching of others, we will be able to validate wind tunnel techniques.

The uncertainty in full-scale results should also be borne in mind when using theoretical methods. Theoretical methods should be used to give an estimste of the results and to describe the main features of the dispersion. In the light of the above, we should carefully consider whether elaborate numerical techniques are necessary or can be justified.

2.2 THEORETICAL METHODS FOR PREDICTING DISPERSION

Theoretical methods are an attractive, alternative means of studying atmospheric dispersion. However, if we are going to use these methods we should be aware of their physical basis and the conditions imposed upon them. In this way, we will see the reasons for their limitations and the need to use alternative techniques (i.e. wind tunnel tests) when theoretical methods cannot be used.

Also, in reviewing theoretical methods we will see that they require an empirical input, which can only come from full-scale data. Often, the results of theoretical methods are very dependent on the empirical input and then the method becomes empirical rather than theoretical.

Theoretical methods start with the equations of motion and then attempt to solve these equations. The governing equations for fluid flow and dispersion are complex and non-linear, and can only be solved in a few idealised situations. Hence, we find that most methods can only be used to describe dispersion either from ground-level or elevated sources (chimney stacks) over flat, uniform terrain. There are few

methods reported in the literature for studying dispersion in complex environments. Traditionally, the studies have been divided into two areas, firstly the rise of buoyant gases, and secondly, the diffusion of gases in the atmosphere. Analytical solutions to the equations were first sought, these required simplifying assumptions, but more recently numerical techniques have been used widely, but they still require certain assumptions to be made.

We will now review the development of theoretical methods for:

1) the rise of buoyant plumes,

2) atmospheric dispersion from ground-level sources,

3) atmospheric dispersion from elevated sources,

4) atmospheric dispersion near buildings.

We will concentrate on methods relevant to the dispersion of buoyant gases from chimney stacks.

2.2.1 THE RISE OF BUOYANT PLUMES

Most plume rise models yield solutions for the mean plume rise and some also give the rate of spread of the plume. Nearly all the plume models consider the plume's cross-section normal to its axis to be circular and the mean plume rise represents the mean trajectory of the centre of the plume's cross-section. However, it is well known that the actual cross-section is kidney-shaped and that the maximum velocity and temperature within the plume may not occur at the geometric centre. Nevertheless, these analytical models have been found to be in reasonable agreement with full-scale measurements of smoke plumes, when presumably the centre of the plume was taken to be the point mid-way between the visible edges of the plume.

The analytical models for describing plume rise can be divided into two classes, those based on a differential formulation and those

using an integral approach. The differential approach was developed in Germany between the 1920's and 50's to describe plumes and jets in a calm atmosphere. It is based on solving the appropriate boundary-layer equations and produces self-similar solutions for the profiles of velocity and temperature within the plume (N.B., it does not assume self-similar profiles). This method requires an empirical expression for the local eddy viscosity as an input. The integral approach, based on the early work of Priestley and Ball (1955) and Morton, Taylor and Turner (1956), is based on the conservation of mass, momentum and buoyancy over the plume's cross-section. This method requires either an assumption of self-similarity (Priestley and Ball) or an expression for the entrainment rate (Morton et al.). Thus both methods require an empirical relationship to provide a solution. The integral approach has proved more popular for modelling chimney plumes and we will concentrate on this method. For a review of similarity solutions a recent paper by Yih (1981) is recommended.

Before describing the various solutions it is worth considering the assumptions that are common to all but the very recent numerical techniques. Firstly, in nearly all solutions the cross-flow is assumed to be a uniform wind, i.e. no vertical wind shear. The only way in which the turbulence of the external flow enters the solution is through the empirical constants, i.e. the entrainment coefficients. Secondly, the Boussinesq Approximations is assumed to hold. This states that changes in density are ignored in the inertia terms but retained in the buoyancy terms.

Some of the earliest plume rise formulae were produced by Scorer (1958). By simple physical arguments, Scorer deduced that, when ejected normal to a cross-flow, a buoyant plume would rise as $X^{2/3}$, whereas a jet (no buoyancy) would rise as $X^{1/3}$, (X is the distance downstream).

Scorer looked closer at the physical aspects of plume behaviour and pointed out the phenomenon of bifurcation of plumes. He noticed that plumes frequently exhibited two counter-rotating vortices which often bifurcated the plume leaving ambient air in between. In fact, similarity solutions clearly show the plume to consist of two symmetrical vortices (see Yih (1981) p.475). Thus, it is well known that the plume's cross-section is not circular but elliptical, with the horizontal width being greater than the vertical height. Nevertheless, as we will see later, most plume rise models assume the plume's cross-section to be circular.(Similarity solutions also yield identical power-law solutions to those given by Scorer for plume and jet rise.)

Applying dimensional analysis to the problem, Briggs (1965) confirmed Scorer's conclusion for the buoyancy induced rise of a plume and took the solution a step further. He identified the buoyancy length, $l_b = F_b/U^3$, as the significant length scale for buoyant plumes and showed that the plume rise could be expressed as:

$$\left(\frac{Z}{l_b}\right) = C\left(\frac{X}{l_b}\right)^{2/3} \qquad (2.3)$$

where C is a constant, U is the cross-wind velocity,

$F_b = r^2 g w_s (\rho_a - \rho_s)/\rho_a$, buoyancy flux at the exit.

From limited observations of power station chimney plumes, Briggs confirmed the form of the above expression, with $C \sim 2.0$.

Moore (1966) and Scriven (1966) observed the chimney plumes from several English power stations and found that the plumes often broke down into discrete puffs soon after leaving the stack. Scriven suggested a mechanism for this breakdown and Moore showed that this phenomenon would have an important effect on the subsequent plume rise. By solving the equations for conservation of buoyancy and momentum and using empirical relationships to describe the volume of the plume (or

puff), Moore deduced that a continuous plume would rise as $Z \propto X^{2/3}$ whereas a plume that broke down into discrete puffs would follow $Z \propto X^{1/2}$. For the continuous plume:

$$\frac{Z}{l_b} = \frac{3}{2K_2}\left(\frac{X}{l_b}\right)^{2/3} \qquad (2.4)$$

K_2 = geometrical constant. (For a 'lumpy' plume which recombines $Z \propto X^{3/4}$) *

Through his analysis, Moore illustrated two important points; firstly, the buoyancy force starts to dominate the initial momentum when:

$$\frac{X}{U} > \frac{F_m}{F_b} \qquad (2.5)$$

$F_m = l_s w_s^2 r^2 / l_a$ = Exit momentum flux

And secondly, atmospheric stability has little effect on plume rise close to the stack (he suggested X>400m for any significant effect, in high winds).

Clearly, by the end of the 1960's the "2/3 power-law" was widely accepted and this was recognised by Briggs in 1969 when he reviewed thirty theoretical and empirical plume rise formulae. Summarizing all the results Briggs suggested the following formulae for plume rise:

$$Z = 2.3\,\frac{F_m^{1/3} X^{1/3}}{U^{2/3}}\left(1 + \frac{F_b X}{2F_m U}\right)^{1/3} \qquad (2.6)$$

Close to the stack

$$\frac{F_b X}{2F_m U} < 1 \Rightarrow \qquad Z = 2.3\left(\frac{F_m}{U^2}\right)^{1/3} X^{1/3} \qquad (2.7)$$

When buoyancy dominates the motion, i.e. $F_b X/2F_m U > 1$, then Briggs suggests the following formulae:

$$\left(\frac{Z}{l_b}\right) = 1.6\left(\frac{X}{l_b}\right)^{2/3} \qquad (2.8)$$

Further support for the "2/3 power law" came from the work of Slawson and Csanady (1967). Slawson and Csanady recognised that the plume's motion could be divided into several phases depending on which mechanism of entrainment was dominant. They defined three phases, an initial phase in which the plume's self generated turbulence dominated,

* Moore (1974) found that the expression $Z = 2.4\,Q^{1/4} X^{*3/4}/U$ was a good representation of the plume trajectories from several power stations for 400<X<2500. X^* = X for X<1000m and Q is the rate of heat emission (MW).

a second phase in which enviromental turbulence in the inertial sub-range dominates mixing and a final phase when the energy containing eddies of the enviromental turbulence dominate. The plume was assumed to be bent-over (almost horizontal) soon after leaving the stack, to travel with the wind velocity (assumed uniform with height) and to have "top-hat" profiles of velocity and temperature.

They used the entrainment hypothesis of Morton, Taylor and Turner (1956) to represent the entrainment of ambient air into the plume by an entrainment velocity, V_E. In the initial phase the entrainment velocity was assumed proportional to the plume's vertical velocity i.e. $V_E = \alpha_1 W$, where α_1 is an entrainment constant.

By solving the equations of conservation of mass, momentum and buoyancy, over the plume's cross-section they obtained the following solution for the plume rise at a distance from the stack where the initial plume velocity and radius are negligible:

$$\frac{Z}{l_b} = \left(\frac{3}{2\alpha_1^2}\right)\left(\frac{X}{l_b}\right)^{2/3} \qquad (2.9)$$

They also found that the plume radius (b) would be proportional to the plume rise, i.e. $b = b_o + \beta Z$, where β is a constant.

Using Batchelor's (1950,1952) expressions for atmospheric mixing in the intermediate and final phase, Slawson and Csanady obtained expressions for the gradual levelling-off of the plume's trajectory. They also obtained identical results using an eddy viscosity approach to the problem.

From observations of the smoke plume from a power station chimney stack, Slawson and Csanady found good agreement with the "2/3 power-law" for conditions of neutral atmospheric stability.

Murthy (1970) considered the effect of vertical wind shear in the Slawson and Csanady model. He used the following expression, to

represent the variation in wind velocity with height, $U(Z) = U_H (1 + Z/H)^P$ where H is the stack height. Solving the same equations as Slawson and Csanady but now with U as a variable, he found the following expression for plume rise:

$$\left(\frac{Z}{\ell_b}\right) \propto \left(\frac{X}{\ell_b}\right)^{2/3(1+P)} \qquad (2.10)$$

Hence, the vertical wind shear (p>0) will tend to lower the plume rise compared with a uniform wind (p=0). Note that since 0 > p > 1 in the atmosphere, then the exponent, let $n=2/3(1+p)$, in the above expression must lie between 1/3 and 2/3. From wind tunnel tests, Murthy found that for $X/\ell_b < 100$, n = 1/3 but for $X/\ell_b > 100$, n = 2/3. One wonders whether this difference is due to the wind shear or because the plume exhibits an initial jet region and then behaves as a bent-over plume, as suggested by Briggs (1969). Murthy concluded from the above information that ' although non-uniform wind conditions prevail in the atmosphere their effect on buoyant chimney plume rise is almost negligible and the 2/3 power-law is probably a good approximation.'.

Djurfors and Netterville (1978) have extended the work of Murthy to consider the effects of non-uniform winds under different conditions of atmospheric stability. By solving the equations of the Slawson and Csanady model but using $U = U_H(1+ Z/Z_*)^\gamma$ - where Z_* and γ are constants dependent on the atmospheric stability, they derived expressions for the plume rise. For neutral conditions the solution reduced to:

$$Z \propto X^{2/(3+\gamma)} \qquad (2.11)$$

which means that the vertical wind shear will reduce the plume rise (as found previously by Murthy). However, they were unable to present any experimental results to support this.

Hoult, Fay and Forney (1969) extended the work of Slawson and Csanady by representing the entrainment process by two entrainment

coefficients. The coefficients represent entrainment due to velocity differences between the air and the plume, parallel and normal to the plume's axis. Also, they did not assume the plume to be bent-over. They found that the solutions depend on the relative magnitude of a buoyancy length-scale and a momentum length-scale. The buoyancy length-scale is that previously defined by Briggs (1965) $l_b = F_b / U^3$, the 'momentum' length-scale is strictly a velocity length-scale defined as $l_m = r w_s / u$.(N.B. Briggs (1969) suggested a 'true' momentum length given by $l'_m = r \left(\frac{\rho_s w_s^2}{\rho_a u^2} \right)^{1/2}$)

The solutions were summarized by Hoult and Weil (1972) and are given in table 2.1. From the results, we can see that the mean trajectory of a pure jet rises initially as $X^{1/2}$ and then as $X^{1/3}$, while a forced plume rises as $X^{1/2}$ and then as $X^{2/3}$, see table 2.1 p.44a.

In a recent review, List (1982), who uses a similar method to Hoult et al. (1969), divided the solution into two cases, depending on the relative values of l_m and l_b . (l_m as defined by Hoult and Weil above.) The results are summarized in table 2.2, p. 44a.

Recent developments in plume rise theory have concentrated on solving the equations of Slawson and Csanady numerically. Typical of these methods is that used by Bouchardy (1980) who divides the atmosphere into several layers, so that the properties may vary with height. The equations are solved for each layer and the conditions at the top of one layer are used as the initial conditions for the next layer, in this way the solution steps upwards. Bouchardy showed that for a typical chimney plume, atmospheric stability has little effect on plume rise within the first 500m downstream. Slawson et al. (1980) have used numerical integration methods to solve the basic equations under various conditions e.g. different stability classes, using various forms for the entrainment velocity and not using the Boussinesq approximation.

They compared their results with full-scale data previously obtained, Slawson (1978), and found typical discrepancies of 20% or more between the theoretical and full-scale mean trajectory.

Petersen and Cermak (1979) have used numerical techniques to solve the equations of momentum and continuity. They assume the plume's cross-section to be circular (while acknowledging that it is actually kidney-shaped) and used a range of entrainment constants. They compared their results with wind tunnel results for the mean trajectory but actually varied the entrainment constant to give the minimum error between the theoretical and wind tunnel results. They found reasonable agreement for low turbulence intensity cross-flows. However, for high turbulence intensity flows the agreement was poor. Petersen and Cermak do not suggest a method for pre-selecting the value of the entrainment coefficients other than suggesting a range of values e.g. $\alpha_2 = 0.65$ to 1.34.

In conclusion,it is clear that power-law forms for the mean plume rise have been suggested by many authors and are now widely accepted. There is supporting evidence, both full-scale and model-scale, for the various indices for the different regions, e.g. Melbourne (1968), Briggs (1965), Pratte and Baines (1967). Also, various length-scales have been defined to non-dimensionalise the plume co-ordinates in each region. However, the entrainment constants need to be empirically defined and would appear to be a function of several variables, e.g. plume density, plume Reynolds number, cross-flow turbulence intensity.

In addition, there are several features of plume behaviour suggested by theoretical models. The plume may bifurcate into two separate flows due to the presence of two counter-rotating vortices. Atmospheric stability may be expected to have negligible effect in the

first phase of plume development. Thus, for the first phase we do not need to model atmospheric stability in wind tunnel studies. Finally, it is suggested that wind shear (i.e. wind velocity increasing with height) will reduce the plumes rise as compared with a uniform cross-flow (-this should be obvious from simple physical arguments). Therefore, we should model the wind shear in wind tunnel studies.

2.2.2 ATMOSPHERIC DIFFUSION FROM GROUND LEVEL SOURCES

Theories of atmospheric diffusion have developed separately from the methods for predicting plume rise. This was because a great deal of the early work involved the ground level release of non-buoyant gases released with zero initial velocity; in this case, the dispersion is controlled by the atmospheric turbulence. The theories developed to describe ground level releases were then applied to the atmospheric diffusion of elevated plumes. As with plume rise theories, analytical solutions to the governing equations were first sought and more recently numerical techniques have been used. All methods require certain simplifying assumptions and empirical data.

We will first review methods for ground level releases and then consider their extension to elevated sources. The theories apply to uniform flat terrain without any obstacles, such as buildings or trees and assume that the diffusion is dominated by atmospheric turbulence.

Three main theories have been developed to describe atmospheric diffusion for a ground level release of gas. They are Statistical Theory, Similarity Theory and Gradient Transfer Theory. An extensive discussion of these methods has been provided by Pasquill in his book 'Atmospheric Diffusion' (1974) and also by Robins and Fackrell (1979). We will briefly review these methods and summarize their results.

i) Gradient Transfer Theory

The general form of the diffusion equation may be written as:

$$\frac{\partial \chi}{\partial t} = -\left[\frac{\partial (u\chi)}{\partial x} + \frac{\partial (v\chi)}{\partial y} + \frac{\partial (w\chi)}{\partial z}\right] \qquad (2.12)$$

Writing the velocities and concentrations as a mean plus a fluctuating term and then averaging the equation, we obtain:

$$\frac{\partial \bar{\chi}}{\partial t} + \bar{u}\frac{\partial \bar{\chi}}{\partial x} + \bar{v}\frac{\partial \bar{\chi}}{\partial y} + \bar{w}\frac{\partial \bar{\chi}}{\partial z} = -\left[\frac{\partial (\overline{u'\chi'})}{\partial x} + \frac{\partial (\overline{v'\chi'})}{\partial y} + \frac{\partial (\overline{w'\chi'})}{\partial z}\right] \qquad (2.13)$$

Now by analogy with molecular diffusion, we assume that turbulent concentration fluxes are proportional to the mean concentration gradient (in that direction),i.e.

$$\overline{u'\chi'} = -K_x \frac{\partial \bar{\chi}}{\partial x} \qquad (2.14)$$

Thus the equation may be written as:

$$\frac{\partial \chi}{\partial t} + \bar{u}\frac{\partial \bar{\chi}}{\partial x} + \bar{v}\frac{\partial \bar{\chi}}{\partial y} + \bar{w}\frac{\partial \bar{\chi}}{\partial z} = \frac{\partial}{\partial x}\left(K_x \frac{\partial \bar{\chi}}{\partial x}\right) + \frac{\partial}{\partial y}\left(K_y \frac{\partial \bar{\chi}}{\partial y}\right) + \frac{\partial}{\partial z}\left(K_z \frac{\partial \bar{\chi}}{\partial z}\right) \qquad (2.15)$$

K is called the eddy diffusivity (from classical mixing-length theory $K_z = \overline{w'l}$,where l is the mixing-length).

The solution to the above equation depends on the eddy diffusivities (K), and a great deal of effort has been spent trying to determine the values of K in the atmosphere (N.B. K = K(x,y,z)). It is known that K_z is a complicated function of height and the atmospheric stability, as shown by Moore (1975, fig.1). The simplest solution is obtained by assuming K_z to be a constant. For a cross-wind line source emitting at a steady rate, at ground-level, into a uniform cross-flow, eqn. 2.15 is greatly simplified since $\frac{\partial}{\partial t} = \frac{\partial}{\partial y} = 0$, V = W = 0, and the longitudinal diffusion may be neglected.

Thus 2.15 reduces to:

$$\bar{u}\frac{\partial \bar{\chi}}{\partial x} = \frac{\partial}{\partial z}\left(K_z \frac{\partial \bar{\chi}}{\partial z}\right) \qquad (2.16)$$

which may be solved to give:

$$\chi = \frac{\sqrt{2}\,Q}{\sqrt{\pi}\,u\,\sigma_z} e^{-z^2/2\sigma_z^2} \qquad (2.17)$$

where $\sigma_z = \sqrt{\frac{2K_z x}{u}}$

The main assumption of Gradient Transfer Theory is that the size of the cloud is much larger than the scales of atmospheric turbulence dispersing the cloud. Thus, this theory could be used to describe the vertical diffusion from ground level sources or for large plumes caused by multiple sources. Note, this assumption will not be valid for the lateral spread and also it is known that K_y is also a function of X, the downstream distance.

A great deal of effort has been spent solving the diffusion equation numerically, using power-law forms for K and U. However, in a review of these methods Hanna (1982) concludes that "In many cases models use very crude approximations to U and K profiles, but very sophisticated finite difference techniques".

If we could specify the eddy diffusivities more accurately Gradient Transfer Theory would suggest an accurate method of modelling the vertical diffusion from ground level sources. However, simple analytical solutions provide useful approximations to the solution and there seems little point in developing more elaborate numerical methods to solve the basic equation.

A possible alternative method of solving the basic equation is to define the mean concentration fluxes $\overline{u\chi}$. We can attempt to describe the turbulent transport processes by mathematical models. Such methods are being developed, e.g. Fackrell and Robins (1979) and Goddard et al. (1980), and require mean velocity and concentration fields as an input.

ii) Similarity Theory

The basis of the Similarity Theory of Diffusion, first suggested by Monin (1959), is that within the constant stress-layer of the atmospheric boundary-layer the velocity is a function of only the friction velocity U_* and the heat flux at the surface, $\rho C_p u_* \theta_*$, where

θ_* is a friction temperature defined as $-\overline{w'T'}/u_*$, where $\overline{w'T'}$ represents the turbulent transport of heat, analogous to $\overline{w'u'}$ for the transfer of momentum.

By dimensional arguments, it then follows that for a passive gas released at ground level, the mean vertical displacement is given by:

$$\frac{d\bar{z}}{dt} = b u_* \Phi\left(\frac{z}{L}\right) \tag{2.18}$$

where b is a constant (normally taken to be equal to the Von Karman constant, 0.4), L = Monin-Obukov length, and in neutral stability $\Phi = 1$ Chatwin (1968) has shown that the cloud moves with the mean velocity at a height $a\bar{Z}$ (a = 0.56), thus the longitudinal displacement is given by:

$$\frac{d\bar{x}}{dt} = \bar{u}(a\bar{z}) \tag{2.19}$$

Combining the above equations and assuming a logarithmic velocity profile $\frac{u}{u_*} = \frac{1}{k} \ln \frac{z}{z_o}$, where Z_o is the roughness length, we obtain an expression relating Z and X in a neutral flow:

$$\bar{x} = \frac{\bar{z}}{kb}\left[\ln \frac{a\bar{z}}{z_o} - 1 + \frac{z_o}{\bar{z}}(1 - \ln a)\right] \tag{2.20}$$

For a continuous ground level line source, it is found that a good approximation to the exact solution of the above is:

$$\frac{\bar{z}}{z_o} \propto \left(\frac{x}{z_o}\right)^{0.9} \qquad \text{for } 10^5 < \frac{\bar{x}}{z_o} < 10^7 \tag{2.21}$$

Robins and Fackrell (1979) found good agreement between the predictions of Similarity Theory and wind tunnel tests for several simulated atmospheric flows.

It should be noted that Similarity Theory only applies to vertical diffusion and not to lateral diffusion. Also, because it applies to the constant stress region (which is typically 50m deep) it is unlikely to be useful in describing the diffusion of elevated plumes.

iii) Statistical Theory

The Statistical Theory of turbulent diffusion is based on the work of Taylor (1921) who related the random velocity fluctutions of a particle to the statistical properties of the flow field.

Consider a particle which has diffused a distance y, from a fixed axis after a time t due to a cross wind eddy velocity v'. The rate of change of y^2 with time is given by:

$$\frac{d(y^2)}{dt} = 2y\frac{dy}{dt} \qquad (2.22)$$

If we now consider the ensemble average of a large number of particles, denoting $\overline{y^2}$ by σ_y^2, we obtain:

$$\frac{d(\sigma_y^2)}{dt} = 2\overline{yv'} = 2\int_o^t \overline{v'(t).v'(t+\tau)}.d\tau \qquad (2.23)$$

If the turbulence field is homogeneous and stationary, we can define the auto-correlation coefficient as,

$$R_v(\tau) = \frac{\overline{v'(t)v'(t+\tau)}}{\sigma_v^2} \qquad (2.24)$$

where $\sigma_v^2 = \overline{v'^2}$, is the variance of the fluctuating velocity component. Substituting this in the above expression and integrating:

$$\sigma_y^2 = 2\sigma_v^2\int_o^T\int_o^t R_v(\tau).d\tau.dt \qquad (2.25)$$

The auto-correlation function must be a symmetrical function, such that R(0) = 1, and $\int_o^\infty R(\tau).d\tau$ = constant. These properties can be used to obtain the limiting form of the above expression.

For small t, $R \sim 1$ $\qquad \sigma_y^2 = \sigma_v^2 t^2$ $\qquad$ i.e. $\sigma_y \propto t$ $\qquad (2.26)$

For large t, $\int_o^\infty R(\tau).d\tau = T$, $\qquad \sigma_y^2 = 2\sigma_v^2 T t$ $\qquad$ i.e. $\sigma_y \propto t^{1/2}$ $\qquad (2.27)$

where T = Integral time-scale,

It is important to note that the requirement of homogeneous turbulence means that the Statistical Theory can only be applied to lateral diffusion from ground level sources, not to vertical diffusion.

However, it may be possible to use the theory as an approximate solution for elevated sources at a height where the turbulence properties are varying slowly with height.

Development of the above theory has concentrated on more accurate representation of the auto-correlation function and relating the Lagrangian properties to the more easily measured Eulerian properties (see Pasquill p.125-137).

It is worth noting, again, that increased complexity (e.g. in describing $R(\tau)$) is not necessarily a more fruitful path to follow. Robins and Fackrell (1979) compared the results of using three different forms of $R(\tau)$ (including a simple step spectrum) and found little difference in the results, any discrepancy being insignificant in comparison with 30% spread in the wind tunnel measurements of lateral spread.

2.2.3 ATMOSPHERIC DIFFUSION FROM ELEVATED SOURCES

There is one widely used theory to describe the diffusion from an elevated source, namely, the Gaussian plume model. It is an empirical formula, with little theoretical support, but it is found to fit available results quite well. Its basis is the Gradient Transfer Theory solution which assumes constant U and K, although, it is well known that U and K vary with height in the atmosphere. The model also assumes that the plume is diffusing from a constant height and therefore, should only be applied to a plume once it has levelled out. However, a simple model could probably be developed to incorporate varying height.

If we solve the diffusion equation for an elevated source at a height H, assuming constant U and K, we obtain the following solution:

$$\chi = \frac{2Q}{\pi u \sigma_y \sigma_z} \cdot e^{-y^2/2\sigma_y^2} \cdot e^{-(z-H)^2/2\sigma_z^2} \qquad (2.28)$$

where Q is the source strength per unit area, and

$$\sigma_y^2 = 2K_y X/\bar{u} \quad , \quad \sigma_z^2 = 2K_z X/\bar{u} \qquad (2.29)$$

The above solution does not allow for the ground (at Z=0) and to take this into account a reflected model is used: an imaginary source is placed at Z=-H. The complete solution is then:

$$\chi = \frac{Q}{2\pi u \sigma_y \sigma_z} \cdot e^{-y^2/2\sigma_y^2} \cdot \left[e^{-(z-H)^2/2\sigma_z^2} + e^{-(z+H)^2/2\sigma_z^2} \right] \qquad (2.30)$$

The ground-level concentrations are obtained by setting Z=0 in the above eqution.

The only unknowns in the above expression are the standard deviations of the cross-wind concentration profiles, σ_y and σ_z. Note that σ_y and σ_z are not necessarily the same, therefore, the plume's cross-section is not assumed to be circular. Defining σ has been the main area of development of the Gaussian Plume model and we will mention some of the main methods.

The simplest definitions of the σ's are simple powers of the downwind distance X. Statistical Theory suggests a means of defining the lateral rate of spread; close to the stack, for X< integral length scale (L), then

$$\sigma_y = \left(\frac{\sigma_v}{u}\right) X \qquad (2.31)$$

for X>>L

$$\sigma_y = \sqrt{\frac{\sigma_v}{u} \cdot 2XL} \qquad (2.32)$$

where, $\frac{\sigma_v}{u}$ = lateral turbulence intensity.

For the vertical diffusion, the result of Gradient Transfer Theory is often used:

$$\sigma_z = \sqrt{2\bar{K}_z X/u} \qquad (2.33)$$

Strictly, for the Gaussian solution K_z is a constant, but in the

atmosphere K_z varies with height. It has been suggested that an average value of K_z is used in regions where K_z is varying slowly with height.

More complicated forms for the σ's have been suggested i.e. $\sigma = AX^a$, a is not an integer and may also vary with X, Bultynck(1972). The σ's have also been given in graphical form. The Pasquill-Gifford curves, Gifford (1968), give σ_y and σ_z for ground-level releases over flat, farmland for distances up to 1 km. For elevated sources the Brookhaven (Smith and Singer, 1966), or T.V.A. curves (Carpenter et al., 1971), should be used. Various curves are given for different stability conditions and methods are suggested for determining the stability class from the actual wind speed and cloud cover. However, the authors warn of an uncertainty of up to $\pm 20\%$ in the values of σ_y and σ_z which are derived.

We should check whether the above results are consistent with those obtained for the rate of spread from the Slawson and Csanady model for plume rise. In the initial phase of the Slawson and Csanady model, we find that $b \propto z$, where b = plume radius. Now in the initial jet-like region $z \propto x^{1/2}$, therefore $b \propto x^{1/2}$ which is in agreement with the vertical rate of spread given by the Gradient Transfer Theory. In the final phase of the Slawson and Csanady model it has been shown, Henderson-Sellers(1980), that the rate of spread will be the same as for Fickian diffusion, i.e. the same as Gradient Transfer Theory. We would expect this, since Batchelor's expression $\frac{db^2}{dt} = 2a_2 \sigma_v L$ can be integrated to give an expression similar to the Gaussian solution for constant K, i.e.

$$b^2 \propto \left(2a_2 \frac{\sigma_v}{u} . L\right) X \qquad (2.34)$$

The question arises as to how accurately the Gaussian distribution describes the actual profiles. Several full-scale measurements have been made and most have been found to be a good fit to the Gaussian distribution, especially the lateral profiles. However, because of the

scatter of the results, it is not possible to determine accurately whether the profiles are truly Gaussian or of a slightly different form, i.e. is the exponent in eq.2.26 actually 2.0 or (say) 1.8 ? But as Pasquill (p.350) has pointed out, quite large variations in the exponent (i.e. 1 to 2) have little effect on the goodness of fit of the distribution. Therefore assuming Gaussian profiles is considered accurate enough for predicting atmospheric diffusion. (There is some evidence that the vertical distribution is slightly skewed and for this reason Moore (1975) used K_{zu} and K_{zL} to describe the Gaussian distribution above and below the centre-line respectively.)

2.2.4 ATMOSPHERIC DIFFUSION IN THE VICINITY OF BUILDINGS

The presence of any obstacle will cause the flow field to be disturbed and the resulting flow field is often very complex, even for a simple structure such as a cube. In such circumstances, it will be very difficult to describe the flow field and even more difficult, if not impossible, to describe the dispersion of gases. For this reason, the prediction methods for dispersion are almost totally empirical.
A few numerical solutions of the governing equations have been attempted but they require many simplifying assumptions to be made. An extensive review of 'Turbulent Diffusion Near Buildings' is given by Meroney (1982).

One approach to the problem starts with the Gaussian plume expression for ground-level concentrations, Builtjes(1980):

$$\chi(x,0,0) = \frac{Q}{\pi \bar{u} \sigma_y \sigma_z} e^{-H^2/2\sigma_z^2} \qquad (2.35)$$

For $H < \sigma_z$, the expression can be approximated by:

$$\chi(x,0,0) = \frac{Q}{\pi \bar{u} \sigma_y \sigma_z} \qquad (2.36)$$

A popular empirical expression for the ground-level concentration close to a building is:

$$\chi = \frac{Q}{kA\bar{u}} \tag{2.37}$$

where A is the frontal area of the building and k is a constant to be determined. $k \sim 1$ is a simple choice but as may be expected a wide range of values has been determined experimentally, see Builtjes(1980).

2.2.5 COMMENTS ON THEORETICAL METHODS

The theoretical methods reviewed above could be used to predict dispersion downwind of a small ground-level or elevated source, if the surrounding terrain was flat and uniform. Under these ideal conditions, we could, at best, expect an accuracy of $\pm 30\%$ in the predictions, which may be adequate in many cases. However, it is likely that the accuracy would be poorer and it is worth considering the comments of the American Meteorological Society Committee on Atmospheric Turbulence and Diffusion (1978) who suggested that a factor-of-two accuracy is all that can be expected in applying these theories of atmospheric diffusion to full-scale situations with limited meteorological data. In practice, the terrain is rarely flat and is often obstructed by structures. In addition, sources of pollution are not necessarily 'point-sources' and may cover a large irregular area. In these real situations we find that theoretical methods are not suitable and proposed methods tend to be very empirical.

In fact, all theoretical methods require empirical inputs. These empirical inputs come from full-scale or wind-tunnel results and are often found to be peculiar to a certain situation. In such cases, theoretical methods become empirical descriptions of experimental results and there is little justification for replacing the experimental results by these 'theoretical' methods. Then, it would seem that

experimental methods should be used instead of theoretical methods.

A further limitation of theoretical methods is that they tell us little about the fluctuating concentration levels; this is especially true for dispersion in the wake of building. As pointed out earlier, the fluctuating concentrations are often more critical than the mean concentrations. Thus, in this important area of atmospheric dispersion, theoretical methods prove to be of little use.

Hence, theoretical methods are not suitable for studying many real pollution problems and an alternative is required. Wind tunnel modelling offers a possible solution to this problem. Wind tunnel methods can be used to study dispersion in complex environments and to study the time-dependent concentration values. In the next section, we will review the range of dispersion problems which have been studied using wind tunnels. Of course, if we are going to use wind tunnel methods we must be confident that the experiments are being performed correctly to yield accurate results. In the next chapter, we will examine the theoretical basis for wind tunnel modelling and consider the techniques that have been used.

2.3 WIND TUNNEL MODELLING OF DISPERSION

The starting point for all wind tunnel studies is the generation of a wind flow which has the same relevant characteristics as the natural wind. This will require the tunnel to have a long fetch upstream of the working section to generate either naturally or artificially a thick boundary-layer, about 1m deep. The requirements for modelling the atmospheric boundary-layer and the techniques employed are discussed in a separate chapter. In addition to having a long fetch the tunnel should also have a large cross-section so that large models can be used without causing blockage effects. The tunnel does not need

to be capable of running at high speeds since we will not need to exceed full-scale speeds which are rarely above 20 ms^{-1}. Several wind tunnels used for wind engineering studies have been described by Hunt and Fernholz (1975).

Most wind tunnel studies of atmospheric dispersion have been carried out in isothermal flows simulating neutral atmospheric stability. However, true neutral stability is a condition rarely achieved in the atmosphere. Conditions in high winds approximate to neutral stability but it is often under more extreme conditions of atmospheric stability that the more interesting and important characteristics of dispersion are observed. Since concentration levels may differ by an order of magnitude under varying stability conditions, the development of tunnels capable of simulating different stability conditions must be an important area of future research. At present, the Meteorological Wind Tunnel at Colorado State University is one of the few tunnels capable of producing flows of varying stability, Cermak (1971).

Various model scales have been used but because we are often interested in ground-level concentrations (g.l.c.) up to several kilometres from the source, very small scales are often used e.g.1:1000. (These scales are much smaller than those normally used to study wind loading on buildings.) For example, a scale of 1:800 has been used by Isyumov et al. (1976) and Wilson (1979b) while Petersen and Cermak (1979) have used 1:960. Typically, internal stack diameters are 5m which means model diameters of about 5mm. As we will see later, it will be very difficult (if not impossible) to produce a turbulent flow, as found in the full-scale stack, in the model for such small diameters. An additional problem at such small scales is ensuring the correct flow patterns around obstacles. Halitsky (1969) suggests that a 'building

Reynolds number' should be greater than 11,000. However, for buildings with curved surfaces we must ensure that the points of separation and reattachment are the same as would be expected at full-scale.

Cermak (1971) has modelled dispersion over large areas using a scale of 1:12,000. At such a large scale Cermak argues that a laminar model flow can model the turbulent full-scale flow; the viscous shear stresses in the model flow represent the turbulent Reynolds stresses at full-scale. Similarly, Cermak argues that molecular diffusion in the model flow (where there is no turbulent diffusion) represents the turbulent diffusion in the full-scale. Cermak found qualitative agreement between measurements of g.l.c. in the model and full-scale for distances of 1km to 5km. The above reasoning is open to question since the turbulent characteristics are variable properties of the flow field while the laminar characteristics are properties of the fluid.

Having generated a flow to represent the atmospheric boundary layer and having constructed a model of the situation to be studied, we must then introduce a gas to simulate the pollutant and observe how it disperses. Helium-air mixtures have been used in many studies to model buoyant gases. Numerous studies of dispersion from power station chimney stacks have been made by many authors using helium-air mixtures. General descriptions of these experiments and the techniques involved have been presented by Robins (1975) and Isyumov et al. (1976). Normally, in such studies, the purpose is to determine the mean ground-level concentrations at points of interest. Sampling tubes on the wind tunnel floor remove specimens of air which are then passed through a thermal conductivity cell to determine the helium concentrations, Isyumov et al. (1976). Such systems are capable of measuring p.p.m. of helium in air but have slow response times. Improved response times have been reported by Cermak et al. (1981) using

a thermistor bridge katharometer which has a time constant of about 1.0 second.

In order to measure fluctuating helium concentrations an aspirating gas concentration probe may be used, Netterville (1979) and Wood and Halstead (1982). Several designs have been suggested by different authors but the only commercially available probe is manufactured by Thermo Systems Inc., (for a review of various aspirating probes and their operation see Rutledge and Thornton (1982)). The aspirating probe would be expected to have a good frequency response since the sensing element is a hot-wire which is known to have a frequency response of several kHz. However, further consideration of the T.S.I. probe suggests a fluid dynamic effect, due to the sucking-in of the gas sample, which will severly limit the response time and more significantly, limits the spatial resolution to an area about 10mm in diameter. Thus the author does not consider the T.S.I. aspirating probe to be a suitable instrument for studying dispersion at small scales.

An alternative to measuring helium concentrations in helium-air mixtures is to use a tracer gas whose concentration can easily be measured. Flame ionisation detectors (F.I.D.'s) are capable of measuring parts per million of hydrocarbons and a measuring system based on F.I.D.'s has been developed by Fackrell and Robins at C.E.G.B.'s Marchwood laboratory. Propane, as a tracer gas ($\sim$ 10%), is mixed with helium and air to produce a suitable effluent gas, and subsequently the propane concentration is measured at points of interest. To obtain mean measurements gas is sucked from the flow field to a storage container before being analysed by a F.I.D.. By using several storage containers, simultaneous mean measurements may be made at many points, Robins(1975).

To measure fluctuating concentrations, Fackrell (1980) has developed an instrument based on a small F.I.D. which can be mounted in

the tunnel close to the sampling location. The resulting instrument is capable of detecting 1 p.p.m. of propane with an estimated 3dB frequency bandwidth of 300 Hz. Clearly, this instrument is very useful for studying the statistical properties of concentration fluctuations or it could be combined with a hot-wire anemometer to measure the concentration fluxes, $c'v'$.

Of course, we can use hot air to simulate buoyant gases and measure temperatures as an analogue of concentration. We will require a heat exchanger to produce the hot air and we must ensure that no unwanted temperature gradients are produced in the tunnel. One of the main advantages of using hot air is that gas temperatures may easily be measured using thermocouples. Fine wire thermocouples are easy to make and inexpensive, therefore it is quite possible to assemble large arrays of thermocouples to map out a temperature field quickly. Typically, a thermocouple system can provide measurements accurate to $\pm 0.2^{\circ}C$, which is acceptable for near field thermal pollution or flammable gas studies (-hot air being used to model flammable gases). However, in the far-field this accuracy is insufficient to cope with gas concentrations of the order of parts per million. Thus, some pollution studies, for example, measuring g.l.c. of medium range dispersion, could not be performed using hot air because the low concentrations could not be measured by thermocouples and we would have to resort to the gas analysis techniques, mentioned above.

The response time of even fine wire thermocouples is limited by considerations of heat transfer from the air to the thermocouple bead, typical response times are about 1 sec. Electrical compensation methods can be used to improve the response time, Sheppard and Warshawsky (1952), if the response time of the thermocouple is known. However, the response time varies with air velocity and temperature therefore the

response time could not be improved for the range of conditions encountered during an experiment. The limitation on response time is a major drawback if we wish to measure fluctuating temperatures; remember that processes in the wind tunnel are occurring faster than at full-scale.

Hot air has been used mainly in studies of near-field pollution. Hoult et al.(1977) studied dispersion from a large land-based gas turbine at a scale of 1:150 using hot air. Davies et al. (1979) studied the dispersion of hot exhaust gases on an offshore platform at a scale of 1:100. They made extensive temperature measurements over the platform and were able to construct mean temperature contours over the structure for various wind directions.

An alternative to the above quantitative methods is to observe the dispersion of gases by flow visualisation. By introducing smoke or oil vapour into the effluent gas, the subsequent dispersion may be photographed by instantaneous, time-exposure or video photography. Flow visualisation will yield mainly qualitative information about the mean path and mean spread and is especially useful for quickly studying the main features of dispersion around bluff bodies, e.g. Koga and Way (1979). Hoult et al. (1969) and Melbourne (1968) have compared the results of flow visualisation experiments for the mean plume trajectory with theoretical predictions, i.e. "2/3 power-law", and found reasonable agreement.

Studies of dispersion around buildings or from exhausts mounted on buildings have been carried out at larger scales, e.g. 1:300. There have been several studies of dispersion around simple rectangular buildings, e.g. Koga and Way (1979), Robins and Fackrell (1980), Li and Meroney (1983). Much of the work is concerned with the possible release of radioactive gases from the reactor building of a nuclear

power station. There have been a few studies of pollution in urban areas, either from chimney stacks or from motor car exhausts. Cermak and his associates have carried out several studies of urban pollution, see Cermak (1975) for further details.

The above is a brief review of the wide range of dispersion problems which have been studied in wind tunnels. Although the results are often compared with theoretical predictions, there have been very few comparisons with full-scale results. This means that the results of wind tunnel studies largely go unchecked by full-scale data, which is the ultimate verification of the validity of wind tunnel methods. Cermak (1971) compared model and full-scale results and suggests that there was qualitative agreement. Robins (1980) modelled the dispersion from Tilbury and Northfleet power station stacks at a scale of 1:500 in a wind tunnel. He found reasonable agreement with full-scale data for lateral plume spread and g.l.c., although inevitably there was some scatter in the full-scale results. As mentioned previously, scatter in full-scale results makes comparisons difficult.

In the first chapter an alternative means of verifying wind tunnel methods was suggested. Starting with dimensional analysis (or the governing equations) we can determine which parameters should be matched in the model and full-scale, then, by carefully justifying the relaxation of parameters, we can reduce the number of parameters so that the remaining significant parameters can be matched in wind tunnel studies. It is the relaxation of certain scaling parameters which needs to be carefully scrutinized. Most authors have justified their techniques by dimensional analysis and assertions about the importance of certain scaling parameters, without presenting any supporting practical evidence. It is the purpose of this study carefully to examine the effect of the various parameters and to question the

statements of previous workers about their relative importance. There have been a few previous studies of the effect of relaxing certain parameters by Isyumov and Tanaka (1979) and Robins (1980) and these will be referred to in the next chapter.

Table 2.1 Trajectory Equations for Buoyant Jets, Hoult & Weil (1972).

$$\frac{Z}{l_m} << 1 , \qquad \frac{Z}{l_m} = \left(\frac{R_v}{\beta R_v + \alpha}\right)^{1/2} \left(\frac{X}{l_m}\right)^{1/2}$$

$$\frac{X}{l_m} >> 1 , \qquad \frac{Z}{l_m} = \left(\frac{3}{\alpha^2}\right)^{1/3} \left(\frac{X}{l_m}\right)^{1/3}$$

$$\frac{X}{l_b} >> 1 , \qquad \frac{Z}{l_b} = \left(\frac{3}{2\alpha^2}\right)^{1/2} \left(\frac{X}{l_b}\right)^{2/3}$$

Note: α and β are entrainment constants,

R_v is the velocity ratio, w_s/u_a .

$l_m = R_v d/2$

$l_b = F_b/U^3$

Table 2.2 Trajectory equations for turbulent buoyant jet: evaluation of $\bar{z}(x)$ for jet in a crossflow , List (1982).

Cases for $l_M > l_b$			
RANGE	$D \ll \bar{z} \ll l_M \ll \bar{z} \ll \left(\frac{l_M}{l_b}\right)^{1/3} l_M \ll \bar{z}$		
$\bar{z}(x)/l_M$	$C_1(x/l_M)^{1/2}$	$C_2(x/l_M)^{1/3}$	$C_4(l_b/l_M)(x/l_b)^{2/3}$
Cases for $l_b > l_M$			
RANGE	$D \ll \bar{z} \ll l_M \ll \bar{z} \ll l_b \ll \bar{z}$		
$\bar{z}(x)/l_b$	$C_1(l_M/l_b)(x/l_M)^{1/2}$	$C_3(x/l_b)^{3/4}$	$C_4(x/l_b)^{2/3}$

Constants used in asymptotic trajectory laws

Investigator	C_1	C_2	C_3	C_4
Briggs[a] (1975)	—	1.8–2.1	—	0.85–1.3
Chu & Goldberg (1974)	—	1.44	—	1.14
Hoult et al. (1969)	1.8–2.5	—	—	—
Wright (1977)	1.8–2.3	1.6–2.1	1.4–1.8	$(0.85–1.4)(l_M/l_b)^{\frac{1}{3}}$

[a]Mean of 14 studies.

3. SIMILARITY REQUIREMENTS FOR WIND TUNNEL MODELLING OF BUOYANT PLUMES

It is the aim of this chapter to consider the theoretical background for wind tunnel studies of dispersion. Using both dimensional analysis and the governing equations, we will produce a set of dimensionless groups which should be matched in both the model and the prototype for exact similarity. We will then consider the significance of each group and whether every group can be matched or if we can justify relaxing the matching of certain groups.

We will consider the dispersion of gases from an isolated chimney stack. Buildings or obstacles will not be included since they would distort the flow field and cause additional effects which may confuse our results. We must be confident of being able to model the simple situation before we introduce further complications. The flow around bluff bodies is a separate branch of Wind Engineering but one which would have to be combined with the present study to justify the use of wind tunnel tests for studying dispersion in the vicinity of buildings. This study is hopefully the first step in achieving that aim.

Modelling the motion and dispersion of a buoyant plume in the earth's atmosphere involves many variables including the properties of the gases involved. However, by dimensional analysis the number of independent variables may be reduced to a smaller number of dimensionless groups. If we examine the resulting dimensionless groups, we find that it is impossible to match all of them in both the model and the prototype. It may be argued that the effect of certain groups on plume behaviour is negligible and the exact scaling of these groups can be relaxed. We are then left with a smaller number of dimensionless groups. However, as we shall see later, it may not be possible even to match all these groups. Certain groups are considered to be more

important than others in controlling plume behaviour and these are matched in the model and prototype, at the expense of the other groups. The choice and form of the matched groups is open to debate and there have been few studies to verify the choice of groups. Thus in examining the similarity requirements we must be critical in our choice of groups to be matched and those to be neglected. By this process we will produce a set of parameters which should be matched in the model and full-scale to accurately model atmospheric dispersion in the wind tunnel.

In the following discussion we will assume that the cross-wind flow has been modelled accurately to represent the wind at a certain model scale. The requirements for modelling the atmospheric boundary layer will be discussed in greater detail in a later chapter. We will characterise the cross-wind by its mean velocity U(z), at a height z.

3.1 DIMENSIONAL ANALYSIS

Firstly, let us consider all the parameters which are relevant to the dispersion of a buoyant plume in the atmosphere. Considering the situation shown in fig. 3.1, the following list of variables should completely describe the plume trajectory;

$$z = f(x, d, H, u, g, \rho_a, T_a, C_{pa}, K_a, \nu_a, w_s, \rho_s, T_s, C_{ps}, K_s, \nu_s) \quad (3.1)$$

The above 16 independent variables include 4 dimensions (m,l,t,T), hence by Buckingham's π Theorem they will form 12 dimensionless groups to describe the plumes's trajectory. Thus, after rearrangement;

$$\frac{z}{d} = f\left\{\frac{x}{d}, \frac{H}{d}, \frac{gd}{u^2}, \frac{w_s}{u}, \frac{\rho_s}{\rho_a}, \frac{\rho_a u d}{\nu_a}, \frac{\rho_s w_s d}{\nu_s}, \frac{C_{pa}\nu_a}{K_a}, \frac{C_{ps}\nu_s}{K_s}, \frac{C_{pa}T_a}{u^2}, \frac{C_{ps}T_s}{w_s^2}, \frac{K_a}{K_s}\right\} \quad (3.2)$$

The terms C_pT/U^2 are the inverse of the Eckert number and can be ignored for incompressible flows.

The parameters may now be divided into three categories, geometric properties, flow-field properties and fluid properties.

We will assume that complete geometric similarity is used, i.e. all dimensions are scaled by the same factor. Some authors, e.g. Barrett (1973), have distorted the stack diameter in order to scale other parameters. However, since this will change the rate of entrainment in the near-field it is not recommended as a technique to be used in near-field modelling, Robins (1980), Isyumov and Tanaka (1979).

Although dimensional analysis is useful in producing the relevant dimensionless groups it does not give us any additional information about the physical origin or significance of the groups. To obtain a greater understanding of the similarity requirements and to give a rigorous proof of dynamic similarity it is necessary to consider the governing differential equations. For the fluid properties, we will consider the diffusion equation and for the flow properties we will consider the equations of motion - the Navier-Stokes equations.

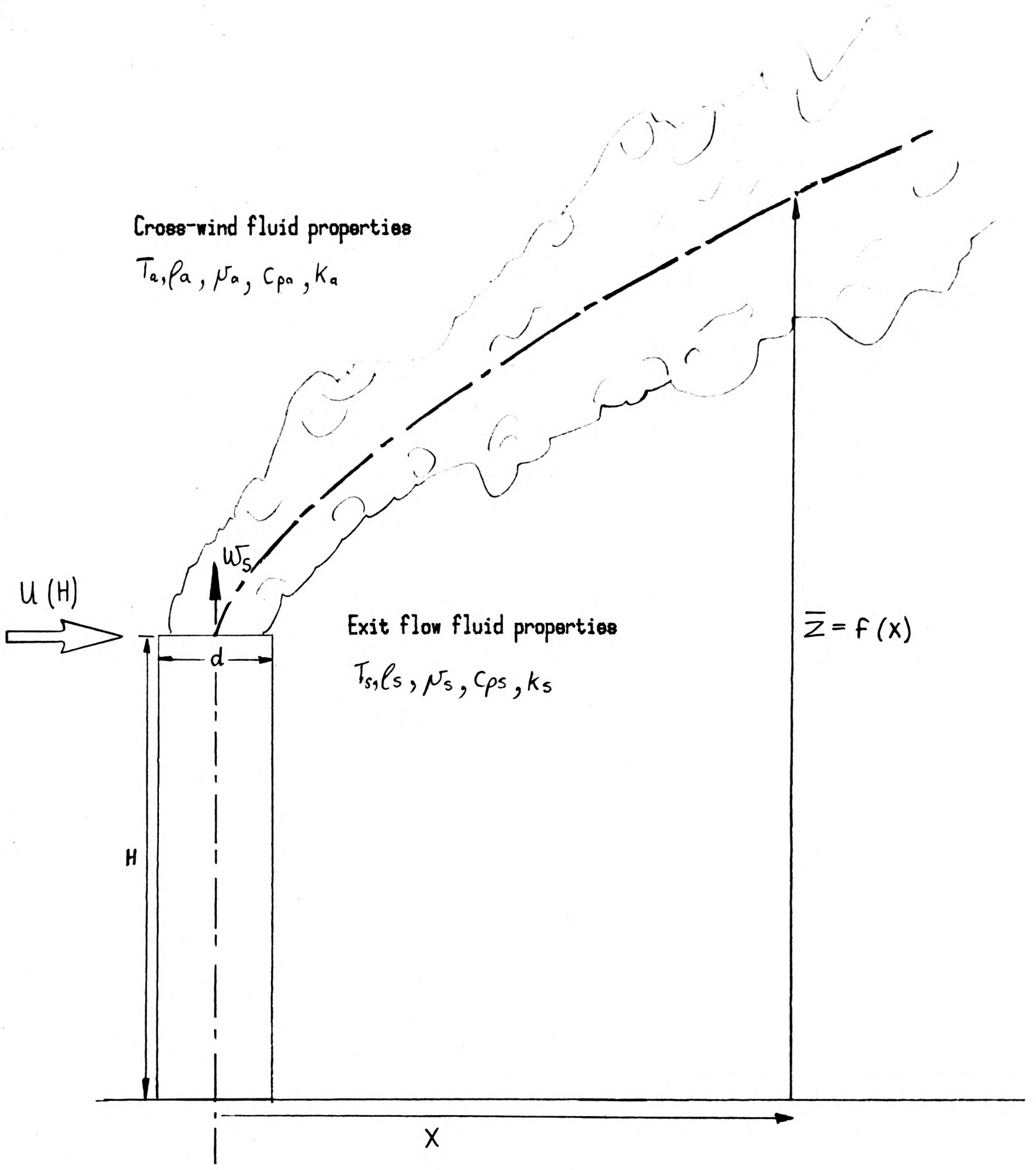

Fig. 3.1 Buoyant Plume in a Cross-Flow
(Definition of Parameters)

3.2 THE EFFECT OF MOLECULAR DIFFUSIVITY (FLUID PROPERTIES)

Once we have chosen a fluid to model the effluent gas, e.g. hot-air or helium-air, we have no control over the scaling of the fluid properties. However, let us consider the role played by the fluid properties by considering the diffusion equation which can be written in a general form as:

$$\frac{\partial T}{\partial t} + U\frac{\partial T}{\partial x} + V\frac{\partial T}{\partial y} + W\frac{\partial T}{\partial z} = (\alpha + K_T)\left(\frac{\partial^2 T}{\partial x^2} + \frac{\partial^2 T}{\partial y^2} + \frac{\partial^2 T}{\partial z^2}\right) \qquad (3.3)$$

We will consider the diffusion of heat, therefore $\alpha = k/\rho C_p$ is the molecular diffusivity of heat and K_T is the eddy diffusivity of heat which represents heat transfer due to turbulent mixing. (The equation for mass transfer would be very similar.) We have assumed that the turbulent heat flux can be represented as $-K_{Tx}\frac{\partial T}{\partial X} = \overline{U'T'}$. Strictly K_T may be different in each direction (α of course is not) but for simplicity we have assumed it to be constant and the same in each direction.

(We are assuming that the molecular and turbulent diffusions can be simply superimposed and that there is no interaction between the two. Mickelsen (1960) considered the possible interaction and by performing wind tunnel tests concluded that the molecular diffusion made only an independent contribution to the total dispersion. Therefore, we are justified in using the above expression.)

The next step is to non-dimensionalise the equation, writing $t'=t/\tau$, $T'=T/T_a$, $x'=x/d$, $U'=U/U_a$, where τ , T_a, d , U_a are reference values of time, temperature, length and velocity respectively, we obtain

$$\frac{d}{U_a\tau}\frac{\partial T'}{\partial t'} + U'\frac{\partial T'}{\partial x'} + V'\frac{\partial T'}{\partial y'} + W'\frac{\partial T'}{\partial z'} = \frac{(\alpha + K_T)}{U_a d}\left(\frac{\partial^2 T'}{\partial x'^2} + \frac{\partial^2 T'}{\partial y'^2} + \frac{\partial^2 T'}{\partial z'^2}\right) \qquad (3.4)$$

Now for exact similarity in the model and prototype the coefficients in the above equation must be the same in both cases. The first term, $d/U_a\tau$ is the Strouhal number which is common to all wind

tunnel tests and yields the condition for kinematic similarity and relates velocities and frequencies in the wind tunnel to full-scale.

The second term $(\alpha + K_T)/U_a d$ represents the effect of molecular and turbulent diffusion of heat. α is a property of the fluid whereas K_T and $U_a d$ are properties of the flow field. Hence, there is a complex interaction between fluid and flow properties governing the diffusion of heat. The two extremes for the above term occur when the flow is either laminar or turbulent. For laminar flow $K_T=0$ and molecular diffusion is the controlling process, for turbulent flows (e.g. the atmospheric wind) $K_T >> \alpha$ and turbulent diffusion dominates. Let us consider these two extremes in more detail.

3.2.1 Molecular Diffusion

$\alpha/U_a d$ is the inverse of the product of the Prandtl number and Reynolds number, and is known as the Péclet number (N.B. this product was also produced by the dimensional analysis).

If air is the working fluid for the model and prototype then the Prandtl number is matched, but the the Reynolds number will not be matched. Since velocities and lengths are reduced in the model, the model Reynolds number is typically 10^3 times smaller than in the full-scale. Thus the Péclet number is much smaller in the model, therefore, the inverse is much larger. This has the effect of greatly exaggerating the molecular diffusivity α, i.e. α in the model appears to be about 10^3 times larger than it should be for exact similarity.

If we were trying to model the molecular diffusion this mis-match would be significant. However, it is well known that in the atmosphere turbulent diffusion dominates molecular diffusion, i.e. $K_T >> \alpha$, therefore, we are trying to model the turbulent diffusion not the molecular diffusion. Thus, we can ignore the exaggeration of molecular diffusion in the model provided the turbulent diffusion is much greater.

This condition is often true and therefore the exaggeration of molecular diffusion has been ignored by wind tunnel modellers. However, it is possible that in some situations the molecular diffusion becomes significant. In reduced scale studies the molecular diffusion may be so exaggerated as to become comparable with the turbulent diffusion, we will return to this in 3.2.3.

3.2.2 Turbulent Diffusion

When $K_T >> \alpha$, the diffusion term reduces to $K_T/U_a d$. Thus to model the turbulent atmospheric diffusion, we must match this term in the model and the prototype. To illustrate how this is achieved we will use the Statistical Theory of Diffusion to express the lateral diffusion. (While this theory is limited in its application it serves to illustrate the basic technique involved.)

Statistical theory suggests the following expressions for K_{yT}, the lateral eddy-diffusivity, (see eqns. 2.26 & 27) :

$$K_{yT} = \overline{v'^2}\ t \qquad \text{for small } t, \tag{3.5}$$

$$K_{yT} = \overline{v'^2}\ T \qquad \text{for } t >> T \tag{3.6}$$

where T is the Lagrangian time-scale.

Re-writing the above expressions in terms of distance, i.e. $X = U_a t$,

for $X << L$ $\qquad K_{yT} = (\overline{v'^2}/U_a^2).(U_a X)$ (3.7)

and $X >> L$ $\qquad K_{yT} = (\overline{v'^2}/U_a^2).(U_a L)$ (3.8)

L = Lagrangian length scale.

Hence

$$K_{yT}/U_a d = (\overline{v'^2}/U_a^2).X/d \qquad X << L \tag{3.9a}$$

$$K_{yT}/U_a d = (\overline{v'^2}/U_a^2).L/d \qquad X >> L \tag{3.9b}$$

Now if all the lengths, including the integral length scale and all the velocities, including fluctuating components, are consistently scaled in the model and the prototype, the above term will be exactly matched in the model and prototype. Thus by matching the flow field we can model turbulent diffusion at reduced scales. The above analysis

suggests that to model three dimensional atmospheric diffusion we must model the components of turbulence intensity and the integral length scale in all three directions x,y,z. We will return to this requirement when we consider modelling the atmospheric boundary-layer in a later chapter.

3.2.3 Reduced Scale Studies.

The above arguments are valid when one form of diffusion dominates. However, it is possible that both terms may be important in small scale wind tunnel tests because of the exaggeration of the molecular diffusion. Let us consider both terms in $(\alpha + K_T)/U_a d$: for air $\alpha = 2\text{x}10^{-5}\ m^2 s^{-1}$ and typically $K_T = (\overline{v'^2}/U_a^2).U_a X$, now in wind tunnel tests $(\overline{v'^2}/U_a^2) \doteqdot 0.01$, $U \doteqdot 1\ ms^{-1}$ and taking a length-scale in the order of 1 cm, we find $K_T \doteqdot O[10^{-4}]$, (c.f. $K \doteqdot O[\ 1\ ]$ in the atmosphere). Thus, α and K_T are of similar magnitude and we must look more closely at the added effect of molecular diffusion on turbulent diffusion.

To illustrate the effect, let us consider the lateral diffusion from a line source, in a cross-wind of velocity U. The solution to the differential equation will give Gaussian lateral profiles for the temperature distribution;

$$T/T_o = \exp\ (-y^2/2D^2) \qquad (3.10)$$

where $D^2 = 2(\alpha + K_T)t$ is the variance of the lateral distribution. Using the expression above for K_T, we can write D^2 as:

$$D^2 = 2\alpha t + \overline{v'^2} t^2 \qquad (3.11)$$

In terms of the distance downstream:

$$D^2 = 2\alpha X/U + (\overline{v'^2}/U^2).X^2 \qquad (3.12)$$

Let us consider a typical wind tunnel test, where $(\overline{v'^2}/U^2) \doteqdot 0.01$, $U \doteqdot 1 ms^{-1}$

$$D^2 = (4\text{x}10^{-5} + X.10^{-2}).X \qquad (3.13)$$

So for downstream distances, X, of the order of millimeters the molecular term is significant.

To make this point clearer, let us calculate the exaggeration in the standard deviation of the cross-wind distribution due to the effect of the molecular term. We will consider model scales of 1:100, 1:400 and 1:1,000 and calculate D at various downstream distances and compare this value with the true value (scaled back to full-scale) we would calculate at full-scale. We take $\overline{v'^2}/U^2$ to be 0.01 and a full-scale velocity of $10ms^{-1}$, scaled by $\sqrt{\text{length-scale}}$. The results are presented in table 3.1 and shown in fig. 3.2.

There are two main points of interest. Firstly, the distortion is greatest nearest the source. The near-field (<100m) is the region of interest in thermal pollution and flammable gas studies. Thus in this important area, the molecular diffusion is being exaggerated and consequently the concentrations will be reduced below their true value. Secondly, the effect increases rapidly as the scale becomes smaller. For example, at 1:1,000 the exaggeration of the standard deviation is greater than 10% for the first 60m downstream and is still 4% at 200m.

In relating the above results to wind tunnel studies there are several points to consider. Although the above calculation refers to the lateral spread from a line source, the basic argument will be valid for the dispersion from any source modelled in the wind tunnel. For sources of finite size the near-field exaggeration will be smaller but still present.

The error in measuring D in the wind tunnel is often about 5%, so in many cases the exaggeration due to molecular diffusion will be much smaller than the experimental error. In small scale models we are often interested in dispersion far downstream of the source where the error will be small. However, in some situations turbulent mixing may not be very strong, e.g. low turbulence intensity flows over flat, smooth terrain, and the relative effect of molecular diffusion will be greater.

Clearly, there is no general rule but we must consider each individual situation in the light of the above discussion.

So far we have only considered modelling a full-scale hot-air plume by hot-air. However, helium-air mixtures are often used as an alternative fluid. In this case, we must consider the mass diffusion of helium instead of the diffusion of heat. The governing equation is similar, except that α now represents the molecular mass diffusivity of helium into air and K_T represents the turbulent mass diffusivity. The turbulent mixing process is considered to be the same for heat and mass, therefore, the K_T values will be the same for hot-air and helium-air plumes. Thus the turbulent mixing will be modelled as before. The value for mass diffusion of helium into air is $7.25 \times 10^{-5}\ m^2 s^{-1}$ (which is greater than for heat diffusion). Thus the exaggeration of molecular diffusion will be greater in the helium-air plumes than in the hot-air plumes. The comments made above will still apply but the distortion of the standard deviation of the lateral spread will be greater. Also, when molecular diffusion is significant, helium-air mixtures will spread more than hot air; see fig. 3.2 for a comparison of hot-air and helium-air.

It should be noted that the results presented in fig. 3.2 apply to 100% helium released from a point source. In practice, helium-air mixtures of about 50% helium (by volume) are used and are released from finite size sources. Thus in wind tunnel studies the errors will be smaller than those suggested in fig. 3.2. Nevertheless, the possibility of exaggerating the dispersion close to the source should be borne in mind when using very small scale models.

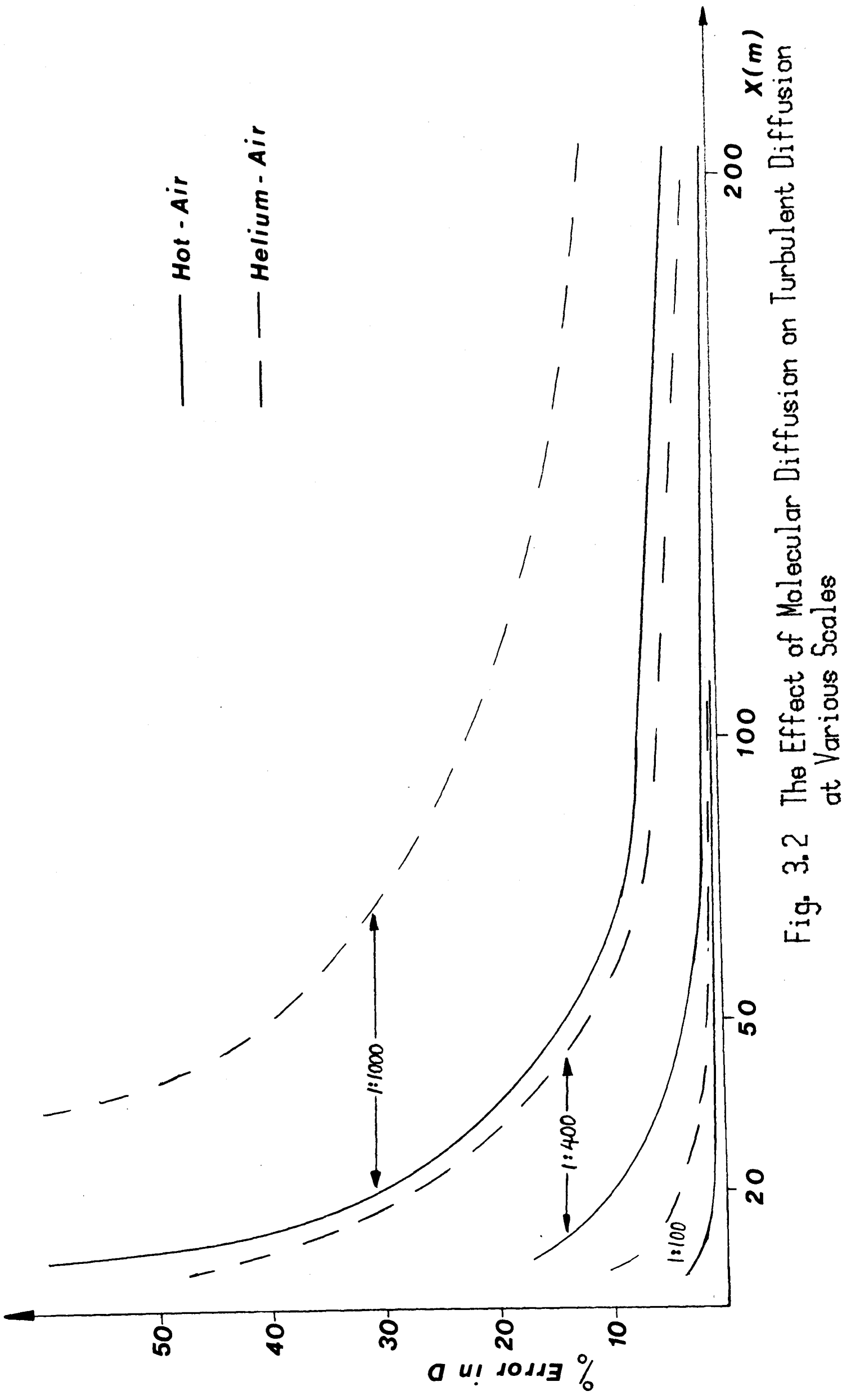

Fig. 3.2 The Effect of Molecular Diffusion on Turbulent Diffusion at Various Scales

	F-S Distance	Model Distance	Time (s)	$(\sigma_\theta X)^2$	$2\alpha t$	D.F-S	% Error $\Delta D/D$
Full-Scale $U = 10\ ms^{-1}$	10	10	1.0	1.0	4×10^{-5}	1.0	-
	50	50	5.0	25.0	2×10^{-4}	5.0	-
	100	100	10.0	100.0	4×10^{-4}	10.0	-
	200	200	20.0	400.0	8×10^{-4}	20.0	-
	400	400	40.0	1600.0	1.6×10^{-3}	40.0	-
1:100 $U = 1.0\ ms^{-1}$	10	.10	.10	10^{-4}	4×10^{-6}	1.02	2.0
	50	.50	.50	2.5×10^{-3}	2×10^{-5}	5.02	.4
	100	1.00	1.00	10^{-2}	4×10^{-5}	10.02	.2
	200	2.00	2.00	0.04	8×10^{-5}	20.02	.1
	400	4.00	4.00	0.16	4×10^{-4}	40.05	.1
1:400 $U = 0.5\ ms^{-1}$	10	.025	.05	6.2×10^{-6}	2×10^{-6}	1.15	14.9
	50	.125	.25	1.6×10^{-4}	1×10^{-5}	5.16	3.2
	100	.250	.50	6.2×10^{-4}	2×10^{-5}	10.16	1.6
	200	.500	1.00	2.5×10^{-3}	4×10^{-5}	20.16	0.8
	400	1.000	2.00	10^{-2}	8×10^{-5}	40.16	0.4
1:1000 $U = 0.32\ ms^{-1}$	10	.01	.032	10^{-6}	1.3×10^{-6}	1.52	51.8
	50	.05	.160	2.6×10^{-5}	6.4×10^{-6}	5.65	13.1
	100	.10	.320	1.2×10^{-4}	1.3×10^{-5}	10.73	7.3
	200	.20	.640	4.1×10^{-4}	2.6×10^{-5}	20.83	4.2
	400	.40	1.280	1.6×10^{-3}	5.1×10^{-5}	41.08	2.7

Note: All distances and D values in metres.

F-S = Full-Scale.

Table 3.1 Calculation of D Values at Various Scales

3.3 THE NAVIER-STOKES EQUATIONS (FLOW PROPERTIES)

To examine the significance of the flow properties we will consider the Navier-Stokes equations for the flow leaving the stack. Discussion of the cross-flow is included in a later chapter. We assume that if both flows (exit and cross flow) are modelled correctly, the interaction will be the same in the model and the prototype.

Firstly, consider the Navier-Stokes equation in the x-direction for an incompressible flow of constant viscosity:

$$\frac{\partial u}{\partial t} + u\frac{\partial u}{\partial x} + v\frac{\partial u}{\partial y} + w\frac{\partial u}{\partial z} = \frac{1}{\rho}\frac{\partial p}{\partial x} + \nu\left(\frac{\partial^2 u}{\partial x^2} + \frac{\partial^2 u}{\partial y^2} + \frac{\partial^2 u}{\partial z^2}\right) + \frac{F_{BX}}{\rho_s} \qquad (3.14)$$

where F_{BX} is a body force in the x-direction, which will be zero, and ν_s is the kinematic viscosity.

Let us non-dimensionalise the equation by a reference length, velocity and time-scale (d, w_s, τ) and denote the non-dimensional quantities by $'$:

$$\frac{w_s}{\tau}\frac{\partial u'}{\partial t'} + \frac{w_s^2}{d}\left\{u'\frac{\partial u'}{\partial x'} + v'\frac{\partial u'}{\partial y'} + w'\frac{\partial u'}{\partial z'}\right\} = -\frac{C_D \rho_a U_a^2}{2\rho}\frac{\partial p'}{\partial x'} + \frac{\nu w_s}{d^2}\left\{\frac{\partial^2 u'}{\partial x'^2} + \frac{\partial^2 u'}{\partial y'^2} + \frac{\partial^2 u'}{\partial z'^2}\right\} \qquad (3.15)$$

The pressure gradient acting in the x-direction is produced by the cross-flow flowing around the plume and may be compared to the drag-force on a cylinder in a cross-flow. Representing the pressure as the product of the cross-flow dynamic pressure and a drag coefficient, then we may non-dimensionalise the pressure as:

$$p = p'\ C_D \rho_a U_a^2/2 \qquad (3.16)$$

(Strictly, a pressure coefficient should be used in eqn. 3.16, but in order to relate the above equation to the motion of the complete plume a drag coefficient has been used.)

Rearranging yields :

$$\frac{d}{w_s \tau}\frac{\partial u'}{\partial t'} + u'\frac{\partial u'}{\partial x'} + v'\frac{\partial u'}{\partial y'} + w'\frac{\partial u'}{\partial z'} = -\frac{C_D}{2}\left\{\frac{\rho_a U_a^2}{\rho w_s^2}\right\}\frac{\partial p'}{\partial x'} + \frac{\nu}{w_s d}\left\{\frac{\partial^2 u'}{\partial x'^2} + \frac{\partial^2 u'}{\partial y'^2} + \frac{\partial^2 u'}{\partial z'^2}\right\} \qquad (3.17)$$

For the model and full scale flows to be similar, the coefficients in the equation (3.17) must be the same in model and prototype; i.e. $d/w_s\tau$, $w_s d/\nu_s$ and $C_D(\rho_a U_a^2/\rho_s w_s^2)$ must be matched.

The first term relates the scaling of velocity, length and time-scale in the model and prototype; having chosen a velocity and length scale, the time scale is then determined. The second term is the Reynolds number of the flow, and was also produced by dimensional analysis. The final term is a combination of two terms: the second half is the momentum ratio while the first half is a drag coefficient. We will consider these terms in greater detail later in this chapter, when we will consider each parameter individually.

Let us now consider the Navier-Stokes equation in the z-direction. The equation will be very similar to the x-direction except for two differences. Firstly, there will be a body force due to buoyancy in the z-direction, this force will be given by $(\rho_a-\rho)g$. Secondly, we assume there is no pressure gradient in the z-direction. Non-dimensionalising the equation and re-arranging as previously, we obtain:

$$\frac{d}{w_s\tau}\frac{\partial w'}{\partial t} + w'\frac{\partial w'}{\partial z'} + u'\frac{\partial w'}{\partial x'} + v'\frac{\partial w'}{\partial y'} = \frac{\nu}{w_s d}\left\{\frac{\partial^2 w'}{\partial z'^2} + \frac{\partial^2 w'}{\partial x'^2} + \frac{\partial^2 w'}{\partial y'^2}\right\} + \frac{(\rho_a-\rho)}{\rho}\frac{gd}{w_s^2} \qquad (3.18)$$

Two of the three coefficients in the above equation are the same as those in the x-component equation. The third term $(\rho_a-\rho_s).gd/\rho_s w_s^2$ is a densimetric Froude number. Note that the equations have produced a densimetric Froude number not a pure Froude number as the dimensional analysis produced.

Thus assuming complete geometric scaling and not including the time scaling ($w_s\tau/d$), the Navier-Stokes equations have yielded the following parameters to be matched for dynamic similarity;

$$\frac{w_s d}{\nu_s} \quad , \quad C_D\frac{\rho_a U_a^2}{\rho_s w_s^2} \quad , \quad \frac{(\rho_a-\rho_s)}{\rho_s}\cdot\frac{gd}{w_s^2} \qquad (3.19)$$

If we consider the N-S equation for the cross-flow, then the cross-flow Reynolds number, $U_a d/\nu_a$, would be added to the above.

Let us consider the flow parameters which the dimensional analysis and Navier-Stokes equations suggest should be matched for exact similarity. Dimensional analysis suggests the following set of dimensionless groups:

$$\frac{\rho_s}{\rho_a} \; , \; \frac{w_s}{U_a} \; , \; \frac{gd}{U_a^2} \; , \; \frac{w_s d}{\nu_s} \; , \; \frac{U_a d}{\nu_a} \qquad (3.20)$$

The Navier-Stokes equations produce the following four groups:

$$\frac{w_s d}{\nu_s} \; , \; \frac{U_a d}{\nu_a} \; , \; \frac{(\rho_a - \rho_s)}{\rho_s} . \frac{gd}{w_s^2} \; , \; C_D \cdot \left(\frac{\rho_a U_a^2}{\rho_s w_s^2} \right) \qquad (3.21)$$

If we assume that we can separate C_D from the momentum ratio $(\rho_a U_a^2 / \rho_s w_s^2)$ and that C_D is a function of the following variables ;

$$C_D = g\{ U_a \, , \, w_s \, , \, \rho_a \, , \, \rho_s \, , \, \mu_a \, , \, \mu_s \, , \, d \} \qquad (3.22)$$

Then by dimensional analysis ;

$$C_D = g'\{ \frac{U}{w_s} \, , \, \frac{U_a d}{\nu_a} \, , \, \frac{w_s d}{\nu_s} \, , \, \frac{\rho_a}{\rho_s} \} \qquad (3.23)$$

Thus the complete set of dimensionless groups produced by the N-S equations is:

$$\frac{\rho_a}{\rho_s} \; , \; \frac{U_a d}{\nu_a} \; , \; \frac{w_s d}{\nu_s} \; , \; \frac{(\rho_a - \rho_s)}{\rho_a} . \frac{gd}{U_a^2} \; , \; \frac{\rho_a U_a^2}{\rho_s w_s^2} \qquad (3.24)$$

(N.B. The velocity ratio is not included in 3.24 since it is not an independent group but can be produced from the momentum ratio and the density ratio. Also, the original densimetric Froude number has been combined with the momentum ratio to produce a Froude number based on the ambient air density ρ_a.)

The groups in 3.20 & 24 appear to be slightly different, however, closer examination will show that they are essentially the same; the densimetric Froude number may be produced from the pure Froude number

and the density ratio, and the momentum ratio is produced by combining the velocity ratio and density ratio. Thus both methods produce the same five groups and if we matched either of these sets of five parameters in the model and prototype, we would have exact dynamic similarity.

Problems arise when we do not match all the groups but relax the scaling of one or more of the groups. For example, if we did not match the density ratio (arguing that it has negligible effect) then should we match the velocity ratio or the momentum ratio ? The choice may have a significant effect on the results we obtain. When we start to relax the scaling of groups, dimensional analysis does not give us any guidelines as to which groups are important and which are not. (In fact, once the scaling of one group is relaxed, dimensional analysis may be used to produce virtually any combination of parameters.) To relate the dimensionless groups to the physical processes involved, we must examine the terms in the Navier-Stokes equations.

Let us now look closer at each of the terms in the N-S equations to see whether we can match all the terms, and if we cannot, can we justify neglecting certain terms.

3.4 DENSITY RATIO AND DENSIMETRIC FROUDE NUMBER SCALING

Variation of the density ratio (ρ_s / ρ_a) can be achieved using hot air or helium-air mixtures. Helium with its low density (0.163 Kg m^{-3} at N.T.P.) is favoured by many workers since it avoids using high temperatures in the wind tunnel. It can be shown quite easily (Thornton and Rutledge, 1981) that a hot air plume at a temperature, T, is modelled by a helium air plume with a volumetric concentration of helium, q, by:

$$T/T_{a_{HOT}} = 1/(1 - 0.861q)_{HE} \qquad (3.25)$$

Having scaled the density ratio, we must now scale the densimetric Froude number, $F_{rd} = gd.(\rho_a - \rho_s)/\rho_a U_a^2$.

At this point, let us define a scaling factor $S(X) = X_m/X_p$, where X is a property or combination of properties, and 'm' refers to the model and 'p' refers to the prototype; for exact scaling S(X) = 1.

Scaling the densimetric Froude number, assuming $S(\rho_a / \rho_s) = 1$, we find that: $S(U) = \sqrt{S(L)}$ (3.26)

i.e. the velocity, U, must be scaled as the square root of the length scale. This is where exact scaling presents a problem, since in most dispersion studies we need to use scales smaller than 1:100 which means that S(U) < 0.1, and thus for full-scale velocities of 10 ms^{-1} we need wind tunnel velocities of 1.0 ms^{-1} or less (10 ms^{-1} is a strong wind). Most wind tunnels are very difficult to control at such low speeds and the flow velocity becomes unstable. This is because low tunnel speeds will tend to make the time constant in any control system longer. The fans will also be operating at either low speed or low pitch where their performance is not as stable as at higher speeds. A further limitation to operating at low speeds is that the boundary-layer which is generated to simulate the wind may change its nature at low speeds. The atmospheric boundary-layer is a fully-rough boundary-layer. A general criterion for a fully-rough boundary-layer is that the roughness Reynolds number $U_* z_o/\nu > 2.5$, where U_* is the friction velocity and Z_o is the roughness length, given by the boundary-layer velocity profile:

$$U / U_* = \frac{1}{k} \ln (z/z_o) \qquad (3.27)$$

Therefore by operating at low speeds it may be possible to reduce $U_* z_o/\nu$ below its critical value. (k is von Karman's constant.)

For these reasons, many previous studies have opted to exaggerate the density difference in the densimetric Froude number in order to obtain higher wind tunnel speeds.

Thus $$S(U) = \sqrt{S(L).S(\Delta\rho)} \qquad (3.28)$$

where $\Delta\rho = \rho_a - \rho_s$, and we assume $S(\rho_a) = 1$.

In this way, we can obtain tunnel velocities approximately 50% greater and may avoid the problems mentioned above. (Helium with its low density is very useful in this respect.)

However, we have now relaxed density ratio scaling. We must now consider what effect this will have. Most authors have argued that mis-matching the density ratio will have a secondary effect and will have little effect on plume behaviour. Poreh and Kacherginsky (1981) in a discussion of modelling techniques stated that "Most modellers agree that the effect of density ratio on the simulation (of the plume) is not critical and would at most change the virtual origin of the plume by a few stack diameters". However, Cermak (1975) has pointed out that laboratory values of $\Delta\rho/\rho_a$ may be two or three times the prototype value while Hoult et al. (1977) warned that if $\Delta\rho/\rho_a > 0.4$ the mechanism of entrainment of air into the plume is modified.

Laboratory studies of the effect of $\Delta\rho/\rho_a$ add to the confusion. Hoult and Weil (1972) studied plumes with the same velocity ratio and densimetric Froude number but with $\Delta\rho/\rho_a$ varying from 0.1 to 0.4. They could find no dependence of the plume trajectory on $\Delta\rho/\rho_a$. Wilson (1979a) studied matched plumes with density ratios $\rho_s/\rho_a = 0.554$, 0.397, and 0.232 and found them to be very similar. Isyumov and Tanaka (1979) compared approximate modelling techniques which exaggerated $\Delta\rho/\rho_a$, with an exact simulation and found the plumes with exaggerated $\Delta\rho/\rho_a$ to rise higher but found the rate of spread (taken as the standard deviation of the concentration profiles) to be the same. Isyumov and Tanaka concluded that "the importance of scaling ρ_s/ρ_a may be greater than normally assumed in wind tunnel model studies of plume dispersion".

The effect of the density ratio on the entrainment process has been studied by Ricou and Spalding (1961). They studied jets in a calm atmosphere and found that the rate of entrainment (dm/dx) in a highly momentum-dominated jet obeys the relationship:

$$(1/\rho_a).dm/dx = C\,(\rho_s/\rho_a)^{1/2} w_s d \qquad (3.29)$$

where C is a constant. Since mismatching of the density ratio is used extensively to distort velocity ratio scaling and to raise wind tunnel speeds then account should be taken of the change in entrainment rate which may occur and its effect upon plume trajectory and rate of spread.

From the above discussion, we cannot come to any definite conclusion about the effect of the density ratio on plume behaviour. Therefore, this is an area in which a controlled set of experiments is required to study the importance of this parameter.

3.5 MOMENTUM RATIO OR VELOCITY RATIO SCALING

Having scaled the cross-wind velocity (U_a) in accordance with the densimetric Froude number, we must now scale the stack exit velocity (w_s) Dimensional analysis suggests that we should scale the velocity ratio, however, the Navier-Stokes equations suggest that we should scale the momentum ratio. If we were using complete scaling both ratios would yield the same scaling but if we relax density ratio scaling, the momentum ratio scaling will give a different scaling from velocity ratio scaling. Since momentum ratio scaling arises from the governing equations, it is generally considered to be more critical in controlling the initial trajectory of the plume than the velocity ratio. Many previous studies have preferred to use momentum ratio scaling, Robins (1975), Melbourne (1968), Isyumov et al. (1976), although velocity ratio scaling has been used successfully e.g. Hoult et al. (1977). In one of the few investigations of modelling techniques, Robins (1980) found

that techniques which matched the momentum ratio gave the best results. Snyder (1981) in his review of modelling methods recommends momentum ratio scaling for near-field modelling of plume behaviour.

In the Navier-Stokes equation the momentum ratio is combined with a drag coefficient C_D which should also be matched in the model and full-scale. It is known that the flow around the initial region of a jet issuing into a cross-flow is similar to the flow around a rigid cylinder, Moussa et al. (1977). Thus we would expect the drag coefficient to depend on the Reynolds number of the cross-flow. However, the interaction is clearly more comlpex in this case and we may expect C_D also to depend on the Reynolds number of the jet, the density ratio and the velocity ratio, see eq. 3.23. Thus the parameters which should be matched to model C_D are included in the parameters we are considering to model the general behaviour of the plume. However, as we shall see later, the Reynolds number of the model cross-flow is very much smaller than the full-scale value and this may result in the model C_D being different from the full-scale value (as it would be for a solid cylinder). There are no data relating C_D for a jet to its dependent parameters, so we don't know specifically how to match C_D . In such circumstances we can only try to match the other parameters in the hope that C_D will then also be matched.

3.6 STACK EXIT REYNOLDS NUMBER

The non-dimensional group of parameters ($\ell_s w_s d/\nu_s$) is the Reynolds number of the stack exit flow and is the most controversial scaling parameter in wind tunnel modelling of buoyant plumes. Reynolds numbers in the wind tunnel are several orders of magnitude smaller than full-scale values since;

$$S(R_{ex}) = S(w_s).S(d)/S(\nu_s) \qquad (3.30)$$

and $S(w_s) \doteq \sqrt{S(d)}$; typically $S(d) = 0.01$, so $S(R_{ex}) = 0.001$.

In many circumstances, we find that flow characteristics, such as the velocity profile or turbulence intensity, are constant over a wide range of Reynolds numbers, e.g. flow in rough pipes for Re > 4,000. It is normally considered that once a flow has become turbulent (i.e. above a critical Reynolds number) its properties are independent of the Reynolds number. It is this latter assertion which is widely abused in wind tunnel experiments. Many workers argue that because they are producing a 'turbulent' exit flow (using various devices such as wire trips, gauzes etc.), this flow must be similar to the full-scale flow, which is almost certainly a fully-developed turbulent flow. Few people actually make measurements of the flow to see what characteristics it possesses. Schlichting (1979) presents data on the velocity profile in pipe flow over a wide range of Reynolds numbers, 3.2×10^6 to 4×10^3, and shows that the profile changes only slightly over this wide range. The critical Reynolds number for pipe flow is 2.3×10^3 and in view of the above results we can argue that above a Reynolds number of 2.3×10^3 the stack exit velocity profile has a constant shape. However, few wind tunnel studies reach even this Reynolds number. Below this value the velocity must tend towards a parabolic laminar profile. Thus in model studies the velocity profile is laminar (or possibly transitional) while at full-scale it is fully turbulent. There appear to be two levels of

approaching this problem, some authors would argue that the mismatch is not important. For example Melbourne, (1968) states that "The effect of low Reynolds number on the initial phase of the path of the plume has been noted by many investigators to be negligible". While others acknowledge the problem and try to produce a turbulent velocity profile. They use such devices as wire trips, gauzes, internal roughening of the stack (Cermak, 1975) and porous plugs (Robins, 1975) to produce a flatter velocity profile. However, as pointed out by Isyumov and Tanaka (1979) such techniques won't work for very small diameter stacks where the Reynolds number is well below the critical value for pipe flow. Another technique frequently used, Barrett (1973), involves using a larger diameter stack with a short contraction to the correct diameter at the exit, this tends to produce a flatter exit velocity profile.

However, the exit velocity profile is not the only characteristic of the flow and the turbulence intensity could be an important parameter. In the initial phase of plume dispersion the entrainment is dominated by the self-generated turbulence. So surely the nature of the turbulence at the stack exit is going to be an important parameter. But the turbulence produced by gauzes, wire trips or a contraction will be different. There is increasing evidence that the exit turbulence structure is an important parameter in near-field modelling of buoyant plumes, D.J.Wilson (1979b) - we will return to this point later.

The few studies of Reynolds number effect that have been carried out do not clarify the situation but suggest that the results are very dependent on the experimental conditions. Hoult and Weil (1972) studied plumes with matched densimetric Froude number and velocity ratio but with varying Reynolds number. They studied plumes over the range of Reynolds numbers 28 to 2,800 and found that for Reynolds numbers above 300 the mean trajectory and rate of spread were independent of the

Reynolds number. This figure has been used by many authors because of the strong experimental evidence which Hoult and Weil presented. (Hoult and Weil's experiments were conducted in a tow tank and the plume was studied photographically by injecting ink into the stack flow. The flow was not tripped by any of the devices mentioned above.) Isyumov and Tanaka (1979) studied the effect of 'improving' the exit flow by using a contraction near the stack exit and found it to have little effect. However, it must be noted that they were studying plume dispersion in the wake of a building and we would expect the wake to dominate the dispersion. Kuhlman and Cheng-Chu (1981) compared plumes with matched velocity ratio and densimetric Froude number, and with supercritical but different Reynolds numbers, Re = 2,500 and 26,700. From extensive thermocouple measurements they found significant differences in the plume isotherms especially in the near field. Such results are very disconcerting because they occur at Reynolds numbers where we would normally expect Reynolds number independence to be valid. Can we then expect Reynolds number independence to be valid at much lower values ?

The most extensive study of the Reynolds number effect has been carried out by Wilson (1979b) who clearly recognises the problem. Initially, Wilson suggested that it was the difference in exit velocity profiles which would cause otherwise matched laminar and turbulent plumes to behave differently. Wilson sugested that the problem was in the momentum ratio ($\ell_s w_s^2 / \ell_a U_a^2$). This parameter is normally calculated using the mean velocity. However, strictly we should integrate the momentum leaving the stack to obtain the true momentum ratio. Thus for a circular stack :

$$R_{mom} = \int_0^{d/2} \frac{2\pi r \ell_s w_s^2(r)}{\pi d^2 \ell_a U_a^2/4} \cdot dr \qquad (3.31)$$

If we calculate the above integral for laminar and turbulent flows we will find that they have significantly different values of 1.33 and 1.02 respectively. Wilson suggested that this discrepancy could be accounted for by writing the momentum ratio as $\propto \rho_s w_s^2 / \rho_a U_a^2$. (Note that Wilson suggested that $\propto$ is the kinetic energy factor, when it would appear that it should be the momentum correction factor β , see Massey, 3rd ed. p.106). Wilson performed a set of experiments. Firstly, he compared the plume rise of a laminar plume with a low Reynolds number (300) with the same plume but now made turbulent by inserting a plug in the stack, with all other conditions held constant. Wilson found that the laminar plume rose higher than the turbulent plume, as might have been expected since it had a higher value of $\propto$. Wilson then matched the 'corrected' momentum ratio $\propto \rho_s w_s^2 / \rho_a U_a^2$ in the laminar and turbulent plumes - again, all the other parameters were matched. Wilson found no agreement between the two plumes and concluded that "these results do show that plume trajectories cannot be accounted for through a single correction factor $\propto$". (From Wilson's results it would appear that the same comment would apply if β had been used instead of $\propto$.)"The implication of this result is that plume rise is far more sensitive to the initial conditions than we first thought."

It is interesting to note that Wilson suggested that the full-scale flow will have a relatively low centre-line longitudinal turbulence intensity, 0.03. However, inserting plugs, gauzes etc. will increase the turbulence intensity well above this value (Wilson's plug produced a turbulence intensity of 0.20). Therefore, it would appear that inserting such devices to make the flow more 'turbulent' is the wrong approach, although it may improve the velocity profile slightly.

The above discussion shows that there is no accepted agreement on Reynolds number scaling. The experimental evidence is scarce and

conflicting. Many previous authors have made general statements about the role of the Reynolds number without any supporting practical results. The Reynolds number is a very important parameter since intuitively one would expect the nature of the exit flow to be very important in determining the subsequent near-field behaviour of the plume.

The Reynolds number appears as a scaling parameter because it represents the ratio of the inertial forces to the viscous forces in the stack flow and, as such, is a means of describing the exit flow. However, when we insert devices into the stack the Reynolds number has little significance and we need to refer to the flow characteristics, such as the exit velocity profile and turbulence intensity to describe the flow. The modeller needs to know which flow characteristics must be matched for accurate modelling, rather than the value of the Reynolds number that must be exceeded. We know that the full-scale flow is a fully turbulent flow so we should be trying to achieve the characteristics of that flow. There are many flow characteristics, so do we need to model them all or only a few ? Without full-scale plumes to compare with the model plumes, the alternative approach is to isolate certain characteristics and determine whether they have an effect on the plume's behaviour. Thus by varying different features of the exit flow, we should be able to determine whether it is the exit velocity profile or the turbulence intensity or some other feature of the flow which needs to be modelled to simulate a turbulent plume in the wind tunnel.

3.7 THE EXTERNAL STACK FLOW REYNOLDS NUMBER

The parameter $\rho_a U_a d / \mu_a$ is the Reynolds number of the flow around the stack and as with the internal Reynolds number it will be approximately 10^3 times smaller in the model than in the full-scale. It is a well known fact that the flow patterns around a circular cylinder vary with the Reynolds number, Goldstein (1938). The flow in the wake will produce a region of low pressure (suction) which may be capable of sucking the plume downwards into the wake itself (this phenomenon is normally called plume downwash).

We cannot model the full-scale flow pattern exactly at model scale; there are two possible solutions to this problem. Firstly, the effluent velocity may be large enough to eject the plume well above and beyond the influence of the wake region, and in such circumstances it is not considered necessary to model the stack wake accurately, Robins (1975), Snyder (1981). If downwash is important, it may be possible to achieve the same pressure distribution in the model as in the full-scale by roughening the outside of the stack. If the pressure distribution in the model and prototype are matched we would expect the suction effect of the wake also to be modelled. Let us now consider the two situations mentioned above.

To avoid plume downwash several 'rules of thumb' have been suggested. Wilson (1979b) suggested that the momentum ratio should be greater than 2.0 or the velocity ratio (w_s / U_a) should be greater than 1.5. Hoult and Weil (1972) found that (w_s / U_a) should be greater than 2.0 for non-buoyant jets and greater than 1.0 for buoyant plumes. From simple considerations of the pressure reduction in the wake of a cylinder, Rikhter et al. (1980) suggested that the plume's dynamic pressure should be greater than the static pressure reduction in the wake of the stack. Using this criterion they suggested $\rho_s w_s^2 / \rho_a U_a^2 > 2.4$

to avoid downwash. Summarizing the above, it would appear that downwash will be avoided if $w_s / U_a > 2.0$ or $R_{mom} > 2.4$. Having avoided downwash there is no need to model the flow around the stack accurately.

If plume downwash is likely to play an important role, we must make an attempt to model the flow around around the stack. Let us first consider some of the important flow features.

The development of the flow for increasing Reynolds numbers is shown in figs. 3.3 a to d, p.73. At low Reynolds numbers ($10^2 < Re < 10^5$) the flow separates on the rear surface of the cylinder and eddies are shed alternatively from each side forming a vortex street. The drag coefficient is approximately constant. At the critical Reynolds number, (about 3×10^5 but this value is sensitive to the surface roughness and the turbulence intensity), the boundary-layer over the cylinder changes from a laminar to turbulent flow. The turbulent boundary-layer can withstand a greater adverse pressure gradient, so the separation points move towards the rear of the cylinder. As a result, the wake becomes much narrower and the drag coefficient decreases significantly (to 0.3), the vortex shedding is more random. As the Reynolds number increases further the wake widens, the vortex shedding becomes more regular, and the drag coefficient increases to a constant value of about 0.7.

The above describes the flow around an infinite cylinder, however, for a finite cylinder in a shear flow the pressure distribution will vary with height and there will be a low pressure at the free end, this results in longitudinal flows along the cylinder as shown in fig. 3.5. The important feature from the point of view of plume behaviour is the upflow on the upper rear of the cylinder which rolls up into a pair of intense vortex sheets which may entrain and bifurcate the plume.

The main features of the pressure distribution around a cylinder are shown in fig. 3.4. The pressure distribution depends only on four

quantities; the minimum pressure coefficient C_{pm} and the angle at which it occurs θ_m, the base pressure coefficient C_{pb} and the angle at which it commences θ_b. The aim of the wind tunnel modeller is to produce a similar pressure distribution in the model as at full-scale. E.S.D.U. (1980/1) provide extensive data for the flow around cylinders which makes it possible to calculate the pressure distribution for any value of the Reynolds number, surface roughness and free stream turbulence.

Most wind tunnel stacks have Reynolds numbers well below 10^5 but the full-scale stack may have $Re > 10^7$. However, it is possible to achieve similar pressure distributions by roughening the stack's outer surface. The method has been illustrated by Lawson (1982) for some typical wind tunnel experiments. The examples computed by Lawson show how good the agreement between model and full-scale pressure distributions may be. Wind tunnel modellers should use the E.S.D.U. data and Lawson's method to match the pressure distributions around their model and prototype if downwash is expected to occur.

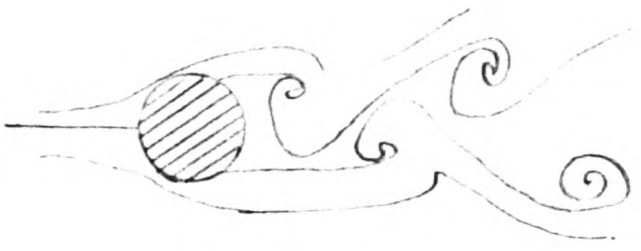

a) $40 < R_e < 150$

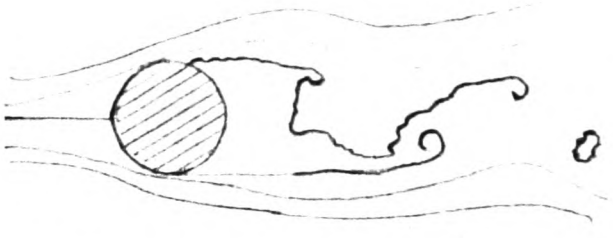

b) $150 < R_e < 3 \times 10^5$

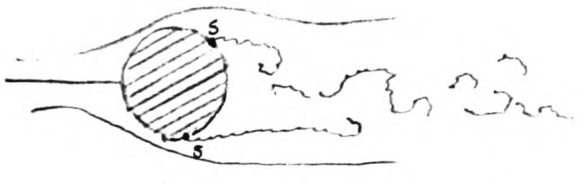

c) $3 \times 10^5 < R_e < 10^6$

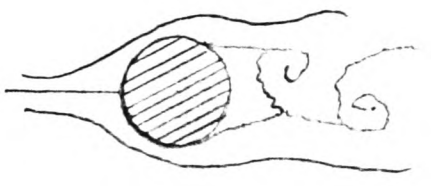

d) $R_e > 3 \times 10^6$

Fig. 3.3 Two Dimensional Flow Around a Cylinder

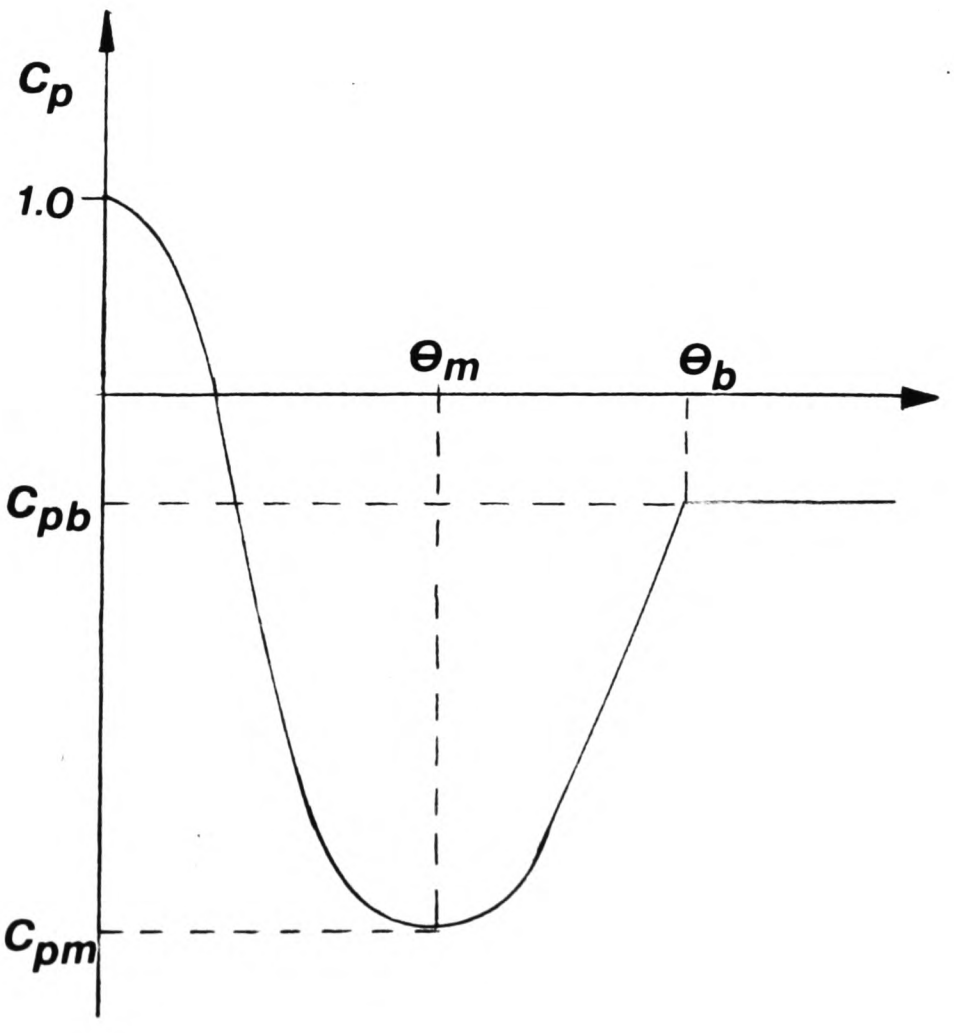

Fig. 3.4 Generalized Pressure Distribution Around a Cylinder

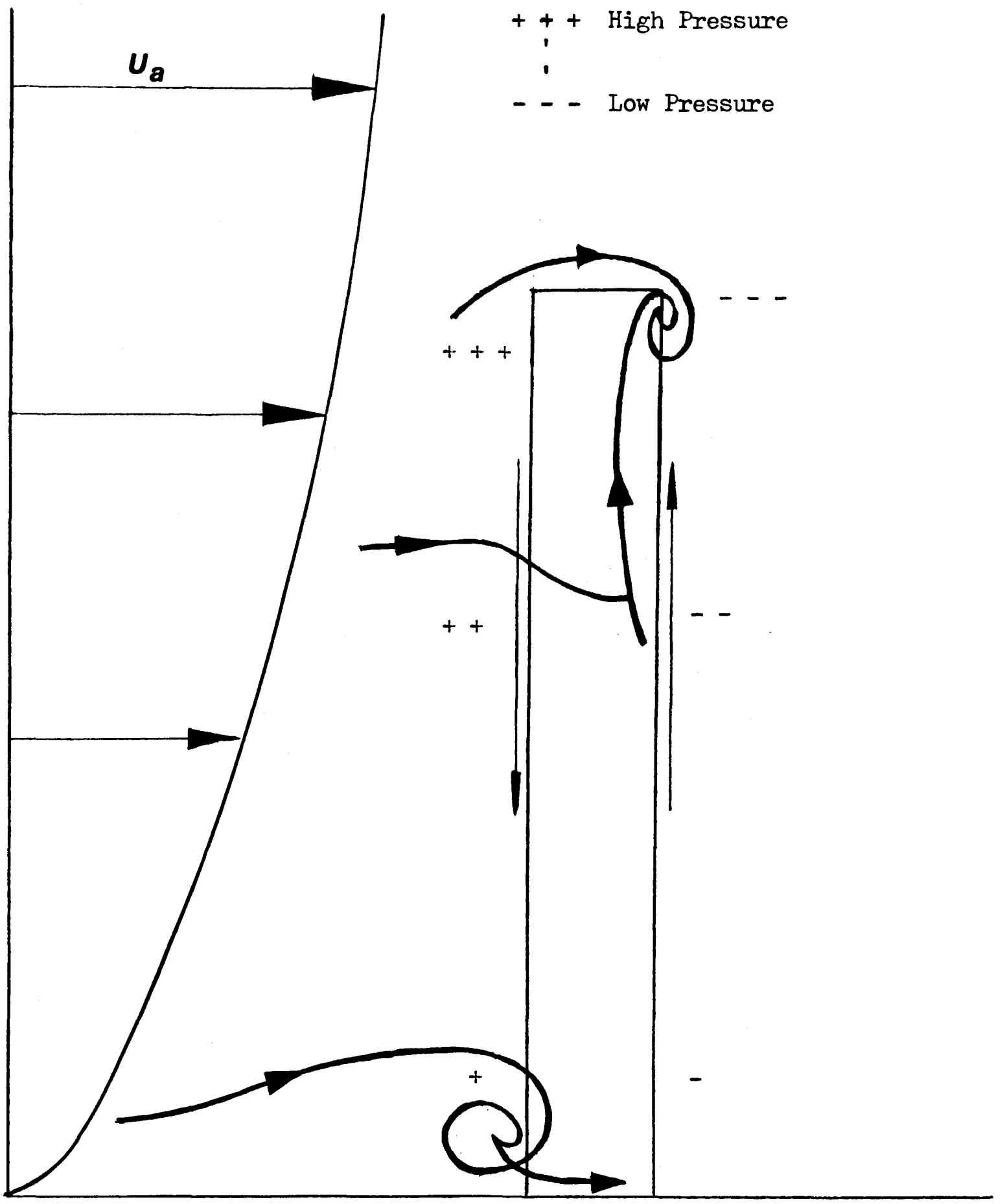

Fig. 3.5 Flow Around a Finite Length Cylinder in a Shear Flow

3.8 REVIEW OF MODELLING TECHNIQUES

We have seen above that it is impossible to achieve exact similarity between all the dimensionless groups in the model and the prototype. Most previous studies have reduced the problem to one of matching only a few groups. The Reynolds numbers cannot be matched but we will assume that attempts should be made to match the internal and external stack flows in the model and prototype. Also, assuming constant geometric scaling, we find that the similarity requirements reduce to only three dimensionless groups:

$$\frac{\ell_s}{\ell_a} \;,\; \frac{\ell_s w_s^2}{\ell_a u_a^2} \;,\; \frac{gd}{u_a^2}\frac{(\ell_a - \ell_s)}{\ell_a} \qquad (3.32)$$

The scaling of these three terms is often called complete or 'exact' scaling. However, as mentioned above, density ratio scaling is often relaxed in favour of scaling the densimetric Froude number. Thus, we are left with only two parameters to scale, one representing the velocity ratio or momentum ratio and one representing the buoyancy term. Now because we have relaxed density ratio scaling it is possible to combine the three terms to form various pairs of dimensionless groups. We will consider some of the pairs of parameters which have been used previously. (Density ratio scaling is relaxed unless otherwise stated.)

The most popular pair of groups is the densimetric Froude number and the momentum ratio:

$$\frac{\ell_s w_s^2}{\ell_a u_a^2} \;,\; \frac{gd}{u_a^2}\cdot\frac{(\ell_a - \ell_s)}{\ell_a} \qquad (3.33)$$

These are the parameters which Snyder (1981) in his "Guidelines for Fluid Modelling of Atmospheric Diffusion" recommends as his second choice for 'near-field' modelling, his first choice being 'exact' scaling as in 3.32. Velocity ratio and densimetric Froude number have also been used frequently, e.g. Cermak (1979).

To accompany his 'near-field' modelling Snyder suggested the following parameters should be matched for 'far-field' modelling:

$$\frac{\ell_s w_s^2}{\ell_a u_a^2} \quad , \quad \frac{gd}{w_s^2} \cdot \frac{(\ell_a - \ell_s)}{\ell_a} \tag{3.34}$$

where U_a in F_{rd} has been changed to w_s by multiplying F_{rd} by $(w_s^2 / U_a^2)^{-1}$.

Barrett (1973) used momentum-ratio modelling but introduced the parameter 'dimensionless discharge', to model the stack diameter to ensure correctly scaled exit flow rates. Exact geometric scaling was relaxed, i.e. $S(d/H) \neq 1$, with the following parameters matched:

$$\frac{gd}{u_a^2} \frac{(\ell_a - \ell_s)}{\ell_s} \quad , \quad \frac{\ell_s w_s^2}{\ell_a u_a^2} \quad , \quad \frac{w_s^2 d^2}{U_a^2 H^2} \tag{3.35}$$

Note also that the densimetric Froude number has had ℓ_a replaced by ℓ_s. Also, strictly, the momentum ratio scaling should be given by:

$$\frac{\ell_s w_s^2 d^2}{\ell_a u_a^2 H^2} \tag{3.36}$$

By this method the exit diameter is smaller than it would be for exact geometric scaling. Robins (1980) suggests that this distortion is unrealistic since it means incorrect initial plume trajectory. Also, Isyumov and Tanaka (1979) are unclear as to the advantages of such a distortion.

A modelling technique which is similar to the momentum ratio scaling method has been used by Skinner and Ludwig (1978) whereby densimetric Froude number is replaced by a new buoyancy parameter:

$$\frac{gd}{u_a^3} \cdot \frac{w_s}{(\ell_a - \ell_s)} \qquad \text{i.e. } F_{rd} \times \frac{w_s}{u_a} \tag{3.37}$$

This buoyancy parameter is the ratio of the onset wind momentum to buoyancy momentum, and is effectively the gradient of the linear part of the plume trajectory.

Finally, we should mention the modelling technique suggested by Poreh (1981). By analysis of simple non-buoyant jets and momentumless buoyant plumes, he deduced that the following two parameters were necessary for modelling plume rise:

a) Dimensionless Buoyancy Flux $$\frac{g d^2 w_s}{u_a^3 H} \cdot \frac{(\rho_a - \rho_s)}{\rho_a} \qquad (3.38)$$

b) Dimensionless Momentum Flux $$\frac{\rho_s w_s^2 d^2}{\rho_a u_a^2 H^2} \qquad (3.39)$$

Note that (b) is the general momentum ratio previously mentioned for $S(d/H) \neq 1$.

Little work has been done to compare the different modelling techniques suggested earlier. Only two extensive studies are reported in the literature. Isyumov and Tanaka (1979) have used a wind tunnel to model a plume exactly and then to compare the results with modelling the plume by several of the approximate methods. Robins (1980) also used a wind tunnel to model a plume by various methods but then compared his results with full-scale data.

Isyumov and Tanaka considered two situations; one with aerodynamic downwash (i.e. a nearby building) and an isolated stack. In the downwash situation only g.l.c measurements were made but it was found that velocity ratio scaling compared better with exact scaling than momentum ratio scaling. Also, as the density difference was exaggerated the similarity deteriorated. For an isolated stack, concentration measurements were made at several heights and at several positions downwind. Both velocity ratio and momentum ratio scaling overestimated the total plume rise quite significantly compared with the exact simulation (i.e. by 10% or more). But in most cases the maximum concentrations obtained in the approximate and exact simulations were in good agreement. Velocity ratio scaling underestimated the initial plume

rise. The tests were carried out using helium-air mixtures at a scale of 1:400. Isyumov and Tanaka concluded that only complete scaling should be used to ensure accurate modelling.

Robins tested several of the approximate methods, measuring not only g.l.c. but also plume rise. Firstly, he investigated an isolated stack in the wind tunnel using several approximate methods and exact scaling. He found that the following two modelling techniques were the only ones to give acceptable results when compared with exact scaling;

$$\frac{gdw_s}{u_a^3} \cdot \frac{(\ell_a - \ell_s)}{\ell_a} \quad , \quad \frac{\ell_s w_s^2}{\ell_a u_a^2} \tag{3.40}$$

(which is the method suggested by Skinner and Ludwig)

$$\frac{gd}{u_a^2} \cdot \frac{(\ell_a - \ell_s)}{\ell_s} \quad , \quad \frac{\ell_s w_s^2}{\ell_a u_a^2} \tag{3.41}$$

(which is essentially momentum ratio scaling but with the Froude number based on ℓ_s instead of ℓ_a).

Robins also modelled an actual power station site and compared his experimental results with full-scale data from the site. He found the two methods given above plus exact scaling to give the best agreement with the full-scale results. It is interesting to note that Robins found the method of Barrett, which scales the same parameters as in the second method above but also distorts the stack diameter, gives poor results. Robins suggests that in situations where downwash may be important, then only exact scaling should be used.

3.9 AREAS TO BE INVESTIGATED

We have reviewed the theoretical basis for wind tunnel modelling and produced a set of non-dimensional groups which should be matched for complete scaling. These groups may be divided into three categories: geometric properties, fluid properties and flow properties. We have assumed consistent geometric scaling throughout. Having chosen a working fluid, we have no control over its properties and we have warned of the possible exaggeration of molecular diffusivity in reduced scale studies. We then considered the remaining five flow properties.

It is not possible to match all the flow properies and the scaling of one group, the density ratio, is frequently relaxed for practical reasons, i.e. to achieve higher wind tunnel speeds. There have been few studies of the consequences of relaxing complete scaling, even though wind tunnel studies are widely used to study pollution problems. Most workers have performed their studies using a certain technique without comparing their results with either full-scale or other wind tunnel results. There are two areas where opinion regarding the scaling of the dimensionless groups is divided and there is no clear experimental evidence. Those two areas are density ratio scaling and modelling the stack exit flow.

To investigate the role played by these parameters we need to be able to isolate their effect. We can do this in the wind tunnel by holding all the dimensionless groups, except the one we are interested in, constant while varying the group being studied. Thus by varying the density ratio while holding all the other groups constant, we will be able to determine whether varying the density ratio has an effect on plume behaviour. The exit flow will be more difficult to study since it has several characteristics, e.g. velocity profile, turbulence intensity, turbulence spectrum. Nevertheless, if we can vary one

characteristic while attempting to hold the others constant, we will be able to study its effect. By this process of 'relative' wind tunnel tests, I hope to be able to improve our understanding of the modelling requirements for wind tunnel modelling of buoyant plumes.

For the purpose of this study, we will consider the plume from an isolated stack on flat terrain. It is expected that any effect due to the density ratio or the exit flow will be most pronounced in the near-field before atmospheric turbulence starts to dominate the dispersion. Therefore, we will study the behaviour of the plume in the near-field.

We have not yet considered, in detail, the modelling of the cross-flow (we will consider the modelling requirements in Chap. 5). Theoretical considerations would suggest that several characteristics of the cross-flow, such as velocity profile, turbulence intensities and spectra should be modelled. Therefore, most workers attempt to simulate these propeties at reduced-scale in the wind tunnel. However, they normally use only one simulation of the atmospheric boundary-layer which they consider appropriate for the situation being investigated. There have been few comparisons of the results obtained in different simulations. Thus, we have little experimental information as to how accurately we need to model the cross-flow. Hence, the role of the boundary-layer simulation is a third area which I hope to study. To do this, the behaviour of the same plumes will be studied in several different simulations of the atmospheric boundary-layer.

The remainder of this study is devoted to studying, experimentally, the following three areas:

i) the effect of the exit density ratio,

ii) the effect of the exit flow,

iii) the effect of the boundary-layer simulation.

4 EXPERIMENTAL EQUIPMENT

4.1 INTRODUCTION

This study was carried out in the Oxford University 4m x 2m Low Speed Wind Tunnel. The working section of the tunnel is 14.0m long and includes a 3.5m diameter turntable whose centre is 12.0m from the entry to the working section. The tunnel is described in greater detail by Greenway and Wood (1979) and is shown schematically in fig. 4.1. The working section upstream of the turntable is normally used to artificially generate a thick turbulent boundary-layer to simulate the earth's atmospheric boundary-layer. The simulation is generated by passive turbulence devices such as a grid, Counihan's fins, wooden blocks, bricks etc.. Details of the hardware used in this study are given in the next chapter.

The aim of this study is to examine the near field dispersion of a buoyant plume from an isolated chimney stack. The choice of model scale was influenced by several factors. Firstly, since we want to examine the near-field, the scale should be reasonably large i.e. below 1:300. Also, the wind tunnel speed must be greater than 0.5 ms^{-1}, since the tunnel cannot be satisfactorily controlled below that speed; bearing in mind that velocity scaling is as the square root of the length scale and for typical full-scale winds of 10 ms^{-1} or more this implies a scale greater than 1:400. (The Oxford tunnel is only capable of simulating neutral atmospheric conditions. Neutral conditions are normally achieved in high winds (>10 ms^{-1}), hence the range of full-scale speeds to be modelled.) In addition, we wish to study the dispersion in several different simulations (at the same scale) and since two 1:200 simulations already existed, this was chosen as the scale to be used (resulting in a velocity scaling of approximately 1:14).

It was decided to model a 60m high full-scale stack with an internal diameter of 5m. This was considered to be a typical industrial chimney stack and since we are not specifically trying to model a full-scale situation the choice is not critical to the experiments.

A working fluid (i.e. effluent) then had to be chosen. The choice was between hot air and helium-air (hydrocarbon tracer techniques have not been used in Oxford). Since we hoped to construct an array of sensing elements to study the plume, and in the light of previous experience, Thornton and Rutledge (1981), hot air was chosen, with thermocouples as the sensing instruments. The relatively slow response time of thermocouples meant that only mean temperature measurements could be made. Thus only the mean plume behaviour was studied quantitatively. In addition to quantitative measurements, flow visualisation was initially used to observe the main features of the dispersion and also to check that there was no downwash into the wake of the stack. Both instantaneous and time-exposure photographs were taken to give side and plan views of the plume.

We will now describe in greater detail the equipment used in this study.

4.2 HOT AIR SUPPLY

The air was supplied to the model stack from a regulated supply of air via rotameters and a heat exchanger. Half inch I.D. copper tubing was used between the various components. The arrangement is shown schematically in fig. 4.2. The stack was positioned on the centreline of the tunnel at the upstream edge of the turntable. The pipework and components were leak tested before use. Also shown in fig. 4.2 is the smoke generator and the 1/2" plastic piping which piped the smoke to the base of the stack where it was introduced into the air flow.

4.2.1 ROTAMETERS

The flow metering system is shown in fig. 4.3. Compressed air from the building supply was passed through a regulator and then through a bank of 'Rotameter' flow meters before flowing to the stack. In these meters, a given flow rate supports a conical float in a vertical, tapered tube by virtue of the pressure drop in the annular gap between the float and the tube wall. (The rotameters are from the Fisher 2100 series, manufactured by Fisher Controls Ltd., Croydon.) The flow rate was measured at ambient temperature. The rotameters were selected to cover the range 0 to 100 litres per minute, their respective ranges were 0.16 - 2.00, 1.67 - 15.0 and 15.0 - 100.0 $lmin^{-1}$. Only one rotameter was used at a time, the flow through the meters being controlled by diaphragm valves, each valve being matched to the range of the respective meter.

The rotameters were factory calibrated to $\pm 1\%$ of the full-scale reading but were further checked against a positive displacement meter and found to be accurate to within 2% of the indicated value. The flow rates during experiments remained steady to about 2% of the full-scale value.

4.2.2 HEAT EXCHANGER

The flow from the rotameters was piped into the tunnel, under the floor, to the heat exchanger which was next to the model stack, as shown in fig. 4.2 . The air was heated by passing it over a standard 1 KW fire element contained in a stainless steel tube, with an annular gap of 3.0 mm. The element was rewound with 18 S.W.G. nichrome wire to give a 3.2 Kw rating at mains voltage, with an allowance of about 200 w for heat conduction losses. The inner tube was encased by a 60.0 mm O.D. stainless steel tube and the gap between the two tubes was filled with glass wool to reduce the radial heat transfer. A drawing of the general assembly of the heat exchanger is shown in fig. 4.4.

Power was supplied at mains voltage by the temperature control unit, which is described in a later section and the performance of the combined system, heat exchanger and temperature controller, will be discussed then.

The heat exchanger was connected to the model chimney stack by a 40 mm length of 4.0 mm O.D. stainless steel tube (WT 0.25-0.50 mm).

4.2.3 MODEL CHIMNEY STACK

The model chimney stack is shown in fig. 4.5 . The model consists of a lower block, placed below the wind tunnel floor, which receives hot air from the heat exchanger via a 4.0 mm O.D. tube; an inner stainless steel tube of 24.5 mm I.D, surrounded by an outer tube of 50.0 mm O.D., the gap between the two tubes being filled with glass wool. The smoke generator is connected to the lower block by a 10.0 mm O.D. stainless steel tube and plastic tubing.

The design of the lower block was constrained by the 4.0 mm supply tube and the 24.5 mm inner tube. The block was mounted on legs to reduce conduction to the floor and was surrounded by glass wool to

reduce heat transfer to the tunnel floor. The third tube entering the lower block was the 10.0 mm O.D. smoke delivery tube; the smoke tube enters the block horizontally and then turns through a right-angle to run concentrically a short distance up the centre of the stack (- the smoke tube is shown dotted in the diagram). This arrangement was found necessary so that the main stack flow would draw the smoke out of the delivery tube, and to avoid condensation of oil droplets in the base of the stack (the smoke is a mixture of oil droplets and carbon dioxide).

The model stack is required to produce an exit flow which is very similar to the full-scale exit flow. The full-scale flow is a fully-turbulent flow with the familiar 1/7th power-law profile. In smooth pipes, with a smooth entrance, this would require an 'entry length' of 50 times the diameter; for a sharp entrance the 'entry length' may be reduced but probably not below 25 diameters. Thus the flow in our model stack will not be fully-developed (L/D = 14), therefore, we must attempt to produce an exit flow which has characteristics similar to a turbulent flow.

The exit flow was investigated by traversing a hot-wire anemometer across the exit plane to measure the exit velocity. Initially, the exit velocity profile was found to be badly skewed. This was thought to be caused by the entry flow from the 4 mm tube 'jetting' up the opposite wall of the stack. In order to reduce the asymmetry, since the full-scale exit flow is axisymmetric, an attempt was made to reduce the 'jetting' effect. Various gauzes and honeycombs were placed in the base of the stack in an attempt to break-up the incoming jet and produce a uniform, symmetric flow entering the inner tube. Finally, an annulus of tightly wrapped wire gauze was placed in the base of the block, the resulting exit velocity profile was found to be almost symmetric and very similar to a turbulent flow, see fig. 6.2.

The inner tube is surrounded by glass-wool and an outer concentric tube. The objective was to reduce the heat transfer to the outer tube and thus keep the temperature of the outer tube at a reasonable level. Heat transfer calculations were performed to determine the temperature of the outer tube for a range of external diameters. 50.0 mm was chosen because the resulting external temperatures were considered to be acceptable and this diameter was not too large as to be unrealistic. (All the plumes studied had momentum ratios which were large enough to suggest that entrainment into the wake of the stack would not occur and this was verified by flow visualisation.)

The rate of heat transfer from the stack was calculated for typical conditions, i.e. an exit temperature of 200 ^{o}C at a mean velocity of 2 ms^{-1}, with a cross-flow of 1 ms^{-1}. The stack dimensions are for the inner tube, 24.5 mm I.D., 25.0 mm O.D.; outer tube 44.0 mm I.D., 50.0 mm O.D.; height 300.0 mm.

The rate of heat transfer was calculated by considering in turn, convective heat transfer from the hot-air to the inner tube, then conduction through the stainless steel tubes and the glass wool, and finally convection to the cross-flow. The flows inside and outside the stack were assumed to be turbulent (expressions for the Nusselt numbers are from 'Heat Transfer' Bayley, Owen and Turner).

The overall heat transfer coefficient, U', is given by:

$$\frac{1}{U'} = \frac{1}{\pi d_{1i} h_{1i}} + \frac{1}{2\pi}\left\{\frac{\ln d_{1o}/d_{1i}}{k_{ss}} + \frac{\ln d_{2i}/d_{1o}}{k_{gw}} + \frac{\ln d_{2o}/d_{2i}}{k_{ss}}\right\} + \frac{1}{\pi d_{2o} h_{2o}} \qquad (4.1)$$

where h is the heat transfer coefficient,

k_{ss}, k_{gw} are the thermal conductivity of stainless steel and glass-wool, 20 $Wm^{-1}K^{-1}$ and 0.05 $Wm^{-1}K^{-1}$,

1 refers to the inner tube, 2 refers to the outer tube,

i refers to the inner diameter, o refers to the outer diameter.

For the inner tube, $Nud = h_{li}d_{li}/ k_{air} = 0.023\ R_{ed}^{0.8}\ Pr^{0.4}$, (4.2)

calculated at a mean film temperature of 450 K gives $h_{li} = 10.65\ Wm^{-2}K^{-1}$.

For the outer tube, $Nud = h_{2o}d_{2o}/ k_{air} = 1.1 \times .174\ R_{ed}^{0.618}\ Pr^{0.4}$,

evaluated at a mean film temperature of 300 K gives $h_{2o} = 13.18\ Wm^{-2}K^{-1}$.

Hence, $1/U' = 1.22 + 1.80 + .483 = 3.50$ (4.3)

Therefore, $\dot{Q} = U' \Delta T$, $\Delta T = 200 - 20 = 180$, $\Rightarrow \dot{Q} = 51.3\ Wm^{-1}$.

Thus the heat loss over the stack is 15.4 W, the internal temperature difference is 62.6°C and the outer temperature difference is 24.8°C .

The above heat transfer calculations suggested that for a centre-line temperature of 200°C the external wall temperature would be 25°C above ambient and that the heat loss over the stack would be 15.4 Watts i.e. about 12 % of the plume's exit heat content. Actual measurements showed that for a centre-line temperature of 190°C most of the outer wall was 19°C above ambient, however, the base of the stack was about 40°C above ambient. This higher temperature was thought to be caused by conduction from the lower block and two asbestos gaskets were inserted between the lower block and the stack in an attempt to reduce the flow of heat. Also, this area of higher temperature was remote from the plume and should not have a significant effect on plume behaviour.

A simple order of magnitude calculation for the effect of the heat transfer from the stack to the cross-flow, is to assune that all the heat goes into a wake of cross-section 300 mm x 50 mm. For a cross-wind speed of 1 ms^{-1}, the increase in the air temperature in the wake would be about 1°C. This rise in air temperature is very small compared with the initial temperature of the plume and is expected to have negligible effect on the plume behaviour.

4.2.4 TEMPERATURE CONTROLLER

The stack exit air temperature was controlled by a proportional temperature controller. The air temperature at the stack exit was sensed by a K-type thermocouple with the bead positioned at the centre of the stack in the exit plane (the presence of the thin lead wires was not expected to seriously intefere with the exit flow). The thermocouple was then connected to the Temperature Control Unit (TC4-643 3 KW version, Rosenforth Ltd., Glos.). The required temperature was set on the control unit and the control unit supplied power to the heat exchanger having compared the 'set' and actual temperatures. The temperature control system is shown schematically in fig. 4.7.

The control unit was housed in an instrument case placed outside the tunnel, see fig. 4.9. A L.E.D. thermocouple display unit was included which showed the actual exit temperature and also the ambient temperature measured by a thermocouple supported on a stand to the side of the stack.

In practice the temperature control system was found to operate very satisfactorily. Below 200 ^{o}C the temperature could be controlled to a few tenths of a degree, above 200 ^{o}C the temperature would be within 0.5 ^{o}C of the required value.

4.3 TEMPERATURE MEASUREMENTS

Temperature measurements were made using a linear array of eight thermocouples. The signal from the thermocouples was amplified 500 times and transmitted to a PDP 11/24 computer for sampling. Using this system mean temperature profiles in the plume could be determined. A general view of this arranngement is shown in fig. 4.10.

4.3.1 THERMOCOUPLES

K-type chromel-alumel thermocouples were used. The junctions were argon-arc welded from 0.003" (44 SWG) chromel-alumel wire. The wires were 1 m long and ran from the junction into the amplifier box to avoid generating any intermediate voltages. Between 0 ^{o}C and 400 ^{o}C the output voltage from the thermocouples can be assumed to be linear with temperature and is given as 40.30 μV/ ^{o}C. The thermocouples were mounted on 1.5 mm stainless steel tubes projecting horizontally from the main mast of the array.

The frequency response of the themocouples was not expected to be very good. Heat transfer calculations, treating the junction as a sphere, gave a time constant of about 0.5 s. Simple experiments in which the junction was heated in a stream of air and then the heat source removed, resulted in a time constant of about 1.0 s. Thus the time constant of the thermocouples was estimated to be about 1.0 s. Hence, we were only able to make mean temperature measurements and this system could not be used to make measurements of the fluctuating temperatures.

4.3.2 THERMOCOUPLE ARRAY

The thermocouple array is shown in fig. 4.8 . The array consists of a main tube onto which eight 10 mm long, 1.5 mm dia. stainless steel tubes are mounted perpendicularly. Each tube supports a thermocouple. The main tube is mounted on a stepper motor so that it may be moved up and down from outside the tunnel over a range of 30 cm. The stepper motor itself is attached to a support stand, as shown. The array can be adjusted so that vertical or horizontal traverses may be made. The base-plate of the support stand has 'V'-grooves cut into the underside which match up with a guide track placed centrally along the wind tunnel

floor. The guide track contained pegs with conical ends projecting about 1 mm above the track surface at 50 mm intervals. These pegs were located in holes in the base-plate and allowed the array to be moved positively downstream (x-axis) in 50 mm steps, see fig. 4.10 .

The thermocouple support tubes were spaced at 10 mm intervals and it was checked that the thermocouple junctions themselves were positioned at 10 mm intervals ± 0.5 mm. Using the arrangement above, the thermocouples could be positioned to ± 1.0 mm in each direction.

4.3.3 THERMOCOUPLE AMPLIFIERS

The thermocouple wires ran to an amplifier system housed in a steel instrument case (432 mm x 200 mm x 88 mm) placed well downstream of the stack and off the tunnel centreline (see fig. 4.10). The amplifier system consisted of eight Thermocouple Conditioning Units, a power supply and the various switches, input and output sockets required.

The thermocouple wires were connected to the amplifier system using chromel-alumel thermocouple connectors (RS type 467-829) and chromel-alumel wire ran from the connectors to the actual conditioning units. In this way, the cold junction was actually at the conditioning unit where the temperature was sensed by a platinum resistance thermometer in the conditioning unit. Thus no spurious intermediate E.M.F.'s should be generated in the thermocouple circuit.

A Thermocouple Conditioning Unit (Series TA 100, CIL Electronics Ltd., Worthing) was used to add the cold junction compensation (thus giving an absolute temperature rather than a temperature above ambient) and to amplify the thermocouple signal. The conditioning units were powered by a ± 15 V fixed voltage power supply (RS Type 591-124), see fig. 4.6 . The cold junction temperature was measured by a platinum

resistance thermometer which then adds a voltage proportional to the cold junction temperature to the thermocouple signal. The cold junction compensation must be set up initially for the particular type of thermocouple being used, for the K-type thermocouples used the c.j.c. was set up accurately to 4.030 ± 0.002 V. To set up the amplification the thermocouples must be disconnected and a D.C. voltage calibrator connected. With a zero volt input the zero setting on the amplifiers was adjusted, then by appling a voltage and monitoring the output the amplification was set up. The output from the thermocouples is 40.3μV/°c and an amplification of 500 was used, thus 0 - 5.0 V corresponds to the range 0 to 200°C, i.e. 25 mV/°C. The signal was then sent to the Analogue-to-Digital converter of the PDP 11/24 computer by multi-core screened cable. The 0 V line was common to all eight amplifiers.

In practice the amplifiers were found to be very reliable and very steady over several hours. The zero output could be set to 0.0 V $\pm$2 mV and the amplification factor could be set to 500 ± 1. At the end of each day the amplifiers were checked and the zeroes found to be 0.0 V $\pm$ 4 mV and the amplification was still 500 ± 1. Thus in terms of temperature, for an input temperature of 40°C the final signals were accurate ± 0.2°C rising to about ± 0.4 °C at 100°C.

4.3.4 DATA SAMPLING

The signal from the amplifier system was fed into the Analogue-to Digital converters of the PDP 11/24 before being sampled by the computer. The A-D's were used in bipolar configuration i.e. -5V to +5V. The resolution was 12 bit i.e. 2.44 mV per bit, or 0.1 C per bit. The sampling program controlled the rate of sampling and the sampling duration, and having collected the data, calculated the mean temperature for each thermocouple. The results were given in hard copy as a table

of thermocouple co-ordinates and temperatures. In this study, the sampling rate was 4 Hz, i.e. at least twice the estimated frequency response of the thermocouple, and the sampling duration was 100 s. The sampling duration was selected to be several times the period of the lowest significant frequency in the energy spectrum of the cross-wind (about 10 s) and also to give reasonably repeatable results. The value of 100s was found by experiment to give repeatable results and corresponds to a full scale averaging time of about 20 mins.

An initial test of the system was to place the thermocouples in an isothermal enclosure and to measure the temperature. This test was repeated several times and the readings were found to agree with each other and with a previously calibrated thermocouple to $\pm 0.5\,^{\circ}C$.

4.4 FLOW VISUALISATION

Smoke from the smoke generator was piped into the base of the model stack using 1/2" I.D. plastic tubing. The smoke then mixed with the heated air flow and made the resulting plume clearly visible. The plume was photgraphed using a 35 mm SLR camera to give side and plan views of the plume; both instantaeous and time exposure photographs were taken. To improve the contrast of the photographs, one wall and the floor of the tunnel were painted matt black. A simple white grid was marked on the floor and the side of the stack to allow the photos to be scaled. The smoke plume was illuminated by two 1 KW photographic lamps placed at an obtuse angle to the camera. The general arrangement is shown in fig. 4.11.

4.4.1 SMOKE GENERATOR

The smoke generator used was a '3020 Smoke Generator' manufactured by C.F. Taylor Ltd. The smoke is a mixture of a pure cosmetic grade oil

and carbon dioxide, the oil droplets in the 'smoke' are minute, about .5 microns in diameter; the smoke is neutrally buoyant with little tendency to either rise or fall. A pressure regulator is used to control the rate of emission of smoke and it can be reduced to just a trace of smoke. A balance had to be reached between using enough smoke to make the plume visible and not using too much as to intefere with the flow of hot air. A setting of the pressure regulator was found experimentally which produced enough smoke to make the plume visible and was not considered to be influencing the behaviour of the plume. For example, at an exit temperature of 200°C, the temperature would drop by 2 or 3°C when the smoke was switched on; thus the volumetric flow rate of CO_2 was about 2% of the flow rate of hot air, this was considered to be acceptable bearing in mind the qualtitative nature of flow visualisation. The smoke generator was always switched off when quantitative measurements were being made.

4.4.2 CAMERA AND LIGHTING

The camera could be mounted in two positions, at the side of the tunnel and on the tunnel ceiling. At the side of the tunnel, the camera was mounted on a tripod so that the centre of the lens was 30 cm above the tunnel floor and aligned with the stack exit, as shown in fig.4.11. The camera could be mounted on the roof, directly above the stack and looking vertically down, (the respective fields-of-view are shown in fig. 4.11).

The camera used was a manual Canon AT1 SLR with a f1.4 50mm lens. Ilford black and white film, FP4 (125 ASA), was used and processed normally. Flash pictures were taken using a flash (Hanimex TZ 855) mounted on the camera. Long exposure photographs were taken for 30 s, illumination being provided by two 1 KW photographic lamps.

4.5 EXPERIMENTAL PROCEDURE

To examine the behaviour of a plume the following procedure was followed. With the tunnel running, the speed at the stack would be set to a certain value using the wind tunnel control system. Calibration curves had been previously determined for the relationship between the 'set speed' on the control panel and the mean velocity at the stack exit, measured using a hot-wire anemometer (the curves were found to be linear). In this way the mean speed at the stack could be set up to 0.05 ms^{-1} of the required value. The required flow rate was then set up on the rotameters. Since the rotameters are at ambient temperature, account had to be taken of the air being heated to a certain exit temperature. The temperature control unit was then switched on and the set exit temperature gradually increased from ambient to the required value; this was necessary to avoid burning-out the heat exchanger by a sudden application of maximum power. Having reached the required exit temperature, the flow rate would be checked to ensure that the exit velocity and temperature were correct. During an experiment the temperature was constant to $\pm 1\,^{\circ}C$ and the flow rate constant to $\pm 0.02\ m^3h^{-1}$ for flows of 3.00 m^3h^{-1}.

With exit and cross-wind conditions set up, the thermocouple array would be positioned as required. The thermocouple amplifier system would have been set up previously. The ambient temperature could be measured either by a thermocouple on a stand to the side of the stack or by placing the array well away from the plume. With the array in position sampling would be initiated.

The experiment was controlled from outside the tunnel as shown in fig. 4.9. The exit temperature and ambient temperature were displayed on the temperature control unit, the position of the array was controlled and displayed on the stepper-motor control unit and the

sampling program was operated and monitored on a visual display unit. After each sampling duration the results were displayed on the V.D.U., to check for any possible irregularities before writing the results to disc. The longitudinal positioning of the array in the tunnel had to be changed manually and this could be achieved without affecting any of the experimental conditions. A typical run, measuring profiles at 6 downstream positions, took 30 minutes.

Photographs of the plume would be taken after completing the temperature measurements. One or two time-exposure and four flash photographs were taken from the side and above the plume.

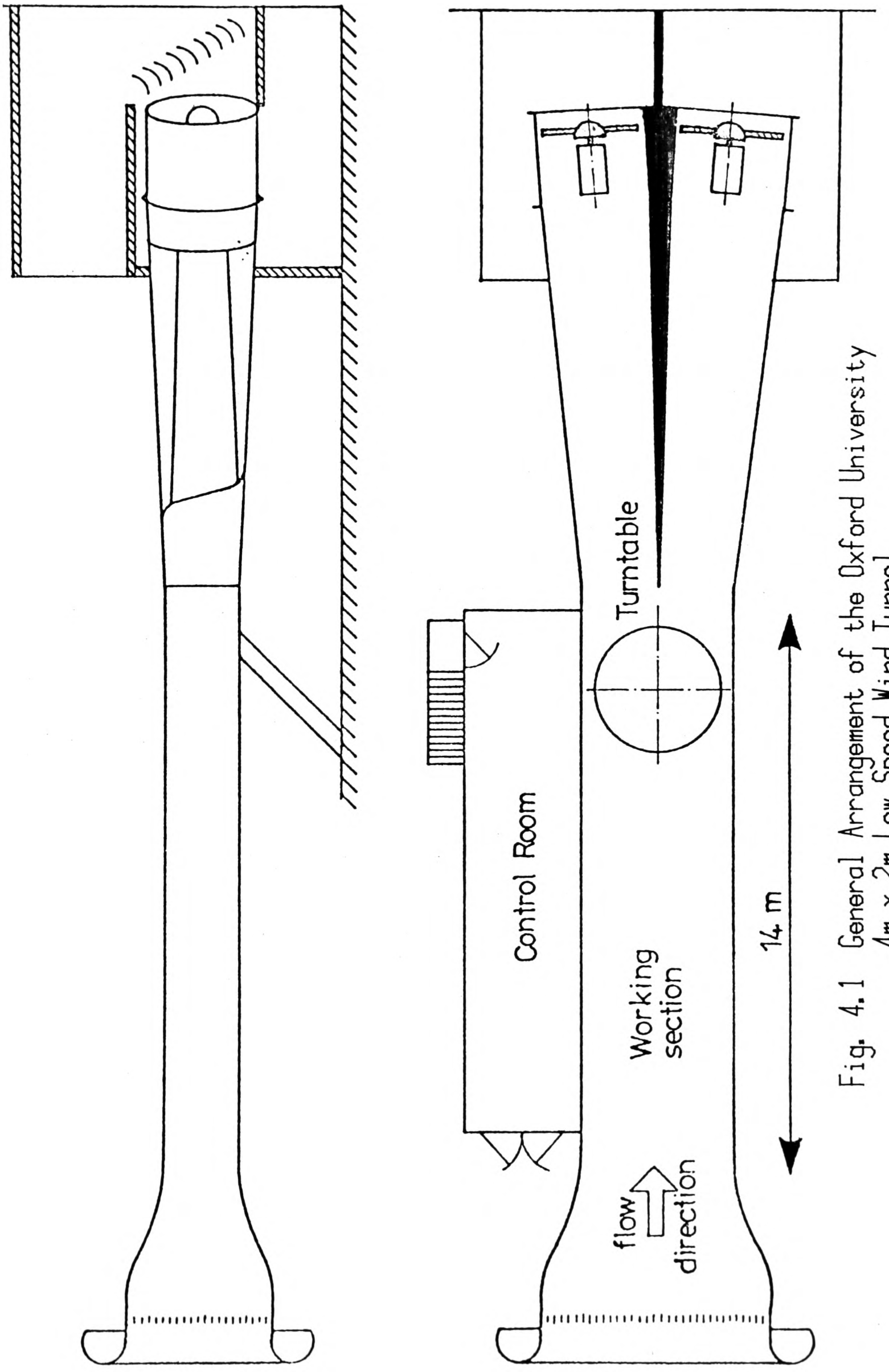

Fig. 4.1 General Arrangement of the Oxford University 4m x 2m Low Speed Wind Tunnel

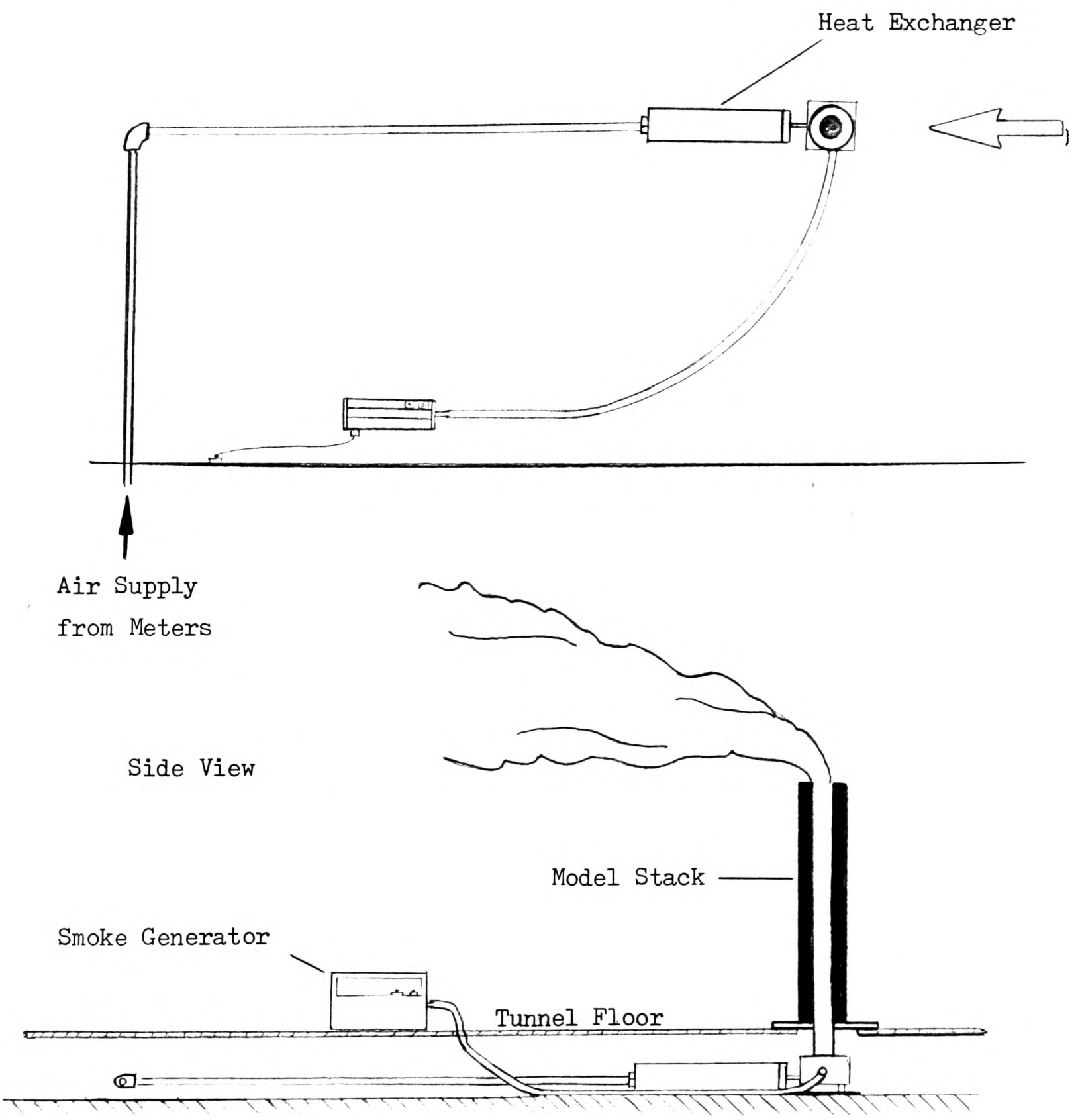

Fig. 4.2 Schematic Diagram of Air Supply Pipework, Heat Exchanger and Model Stack in the Tunnel

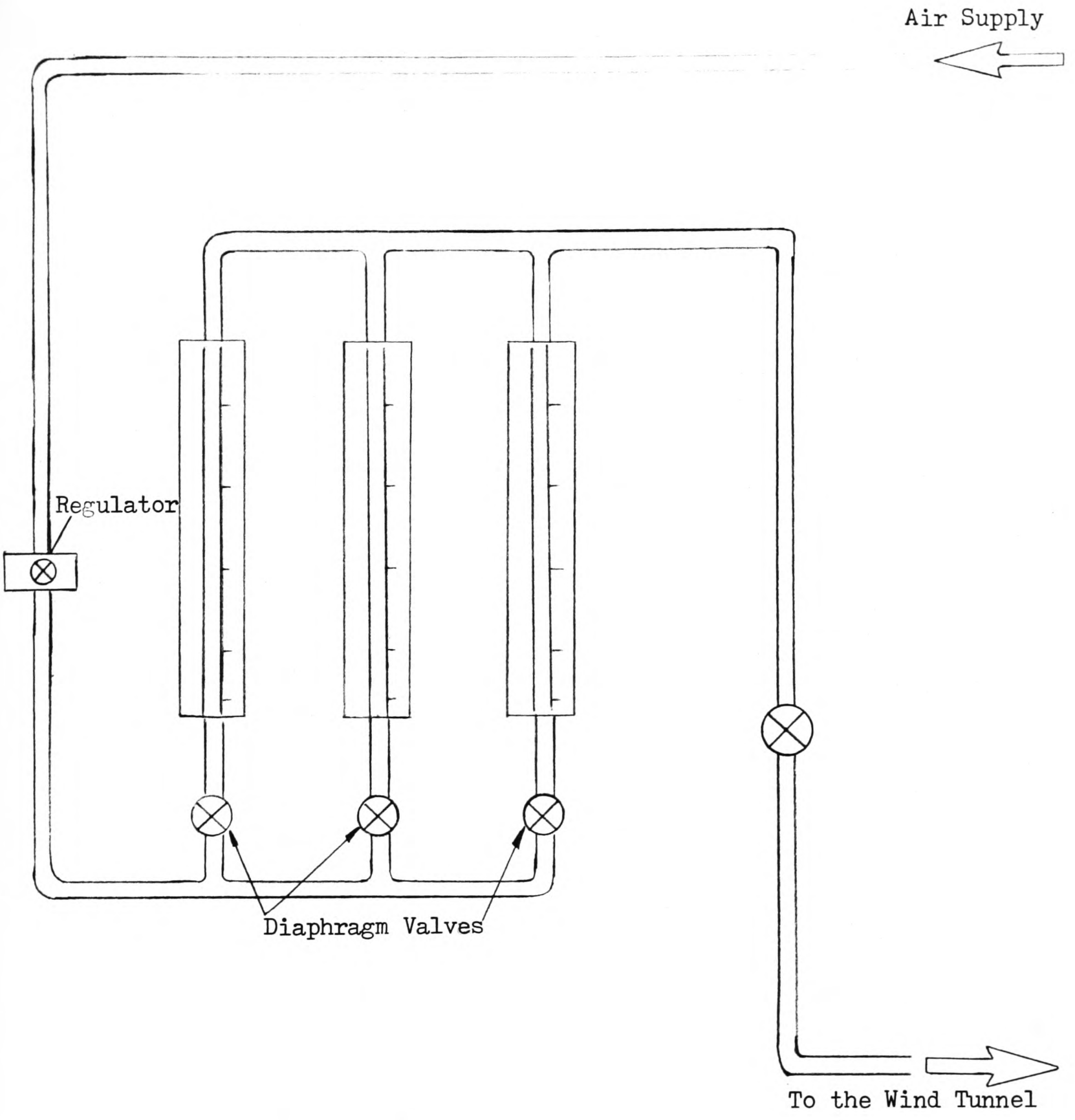

Fig. 4.3 Arrangement of Rotameter Flow Meters

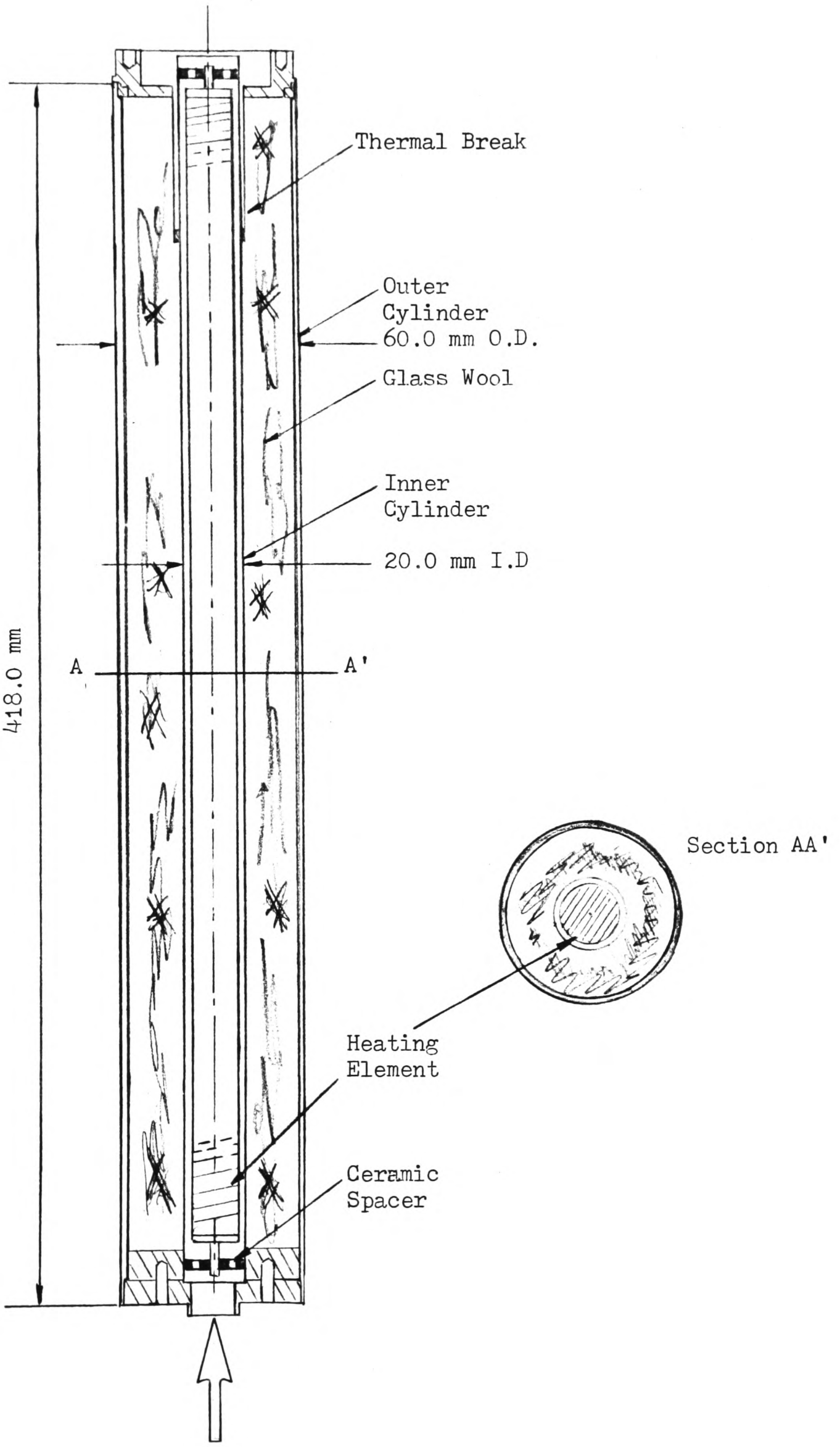

Fig. 4.4 Heat Exchanger

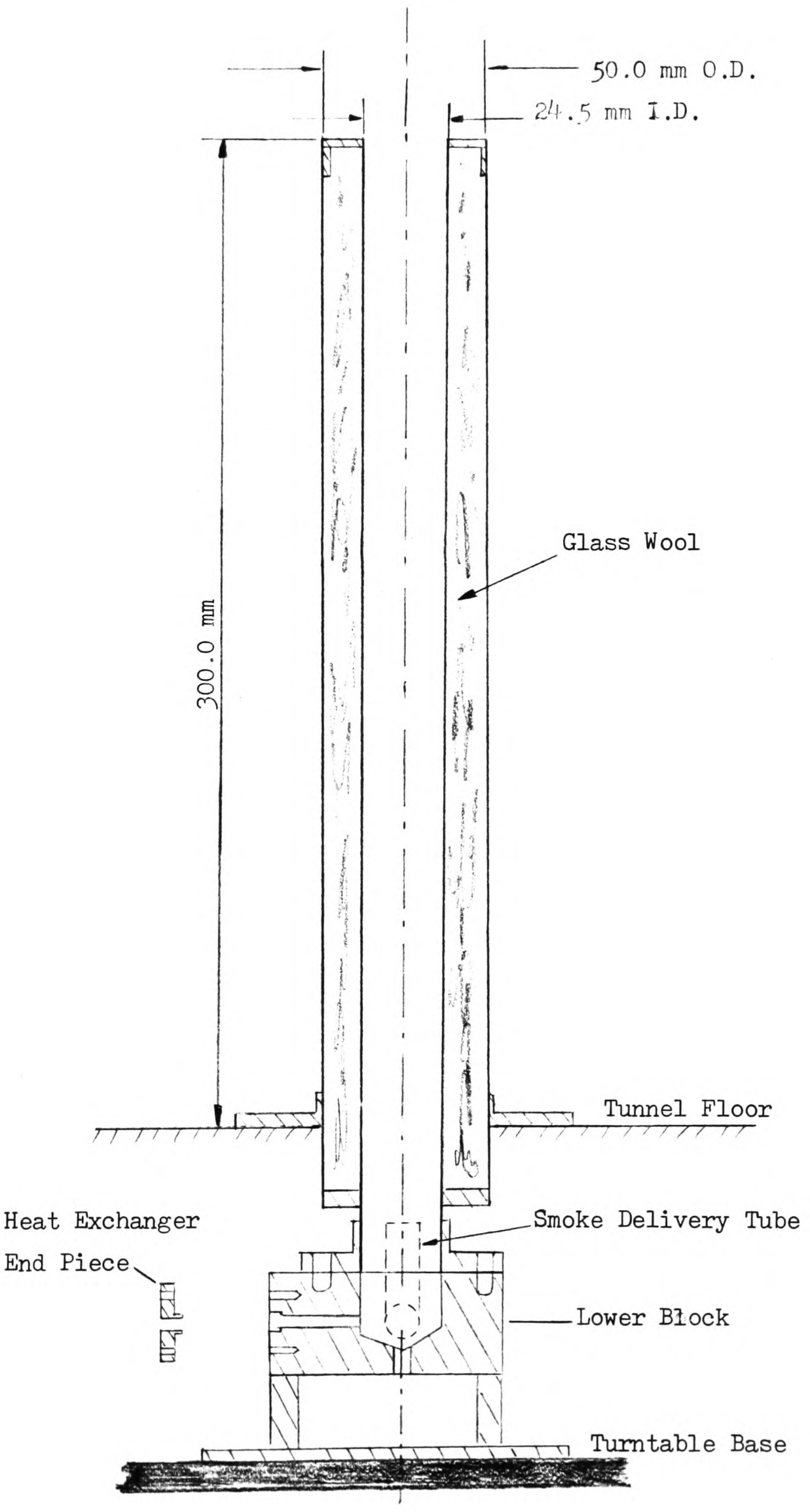

Fig. 4.5 Model Chimney Stack

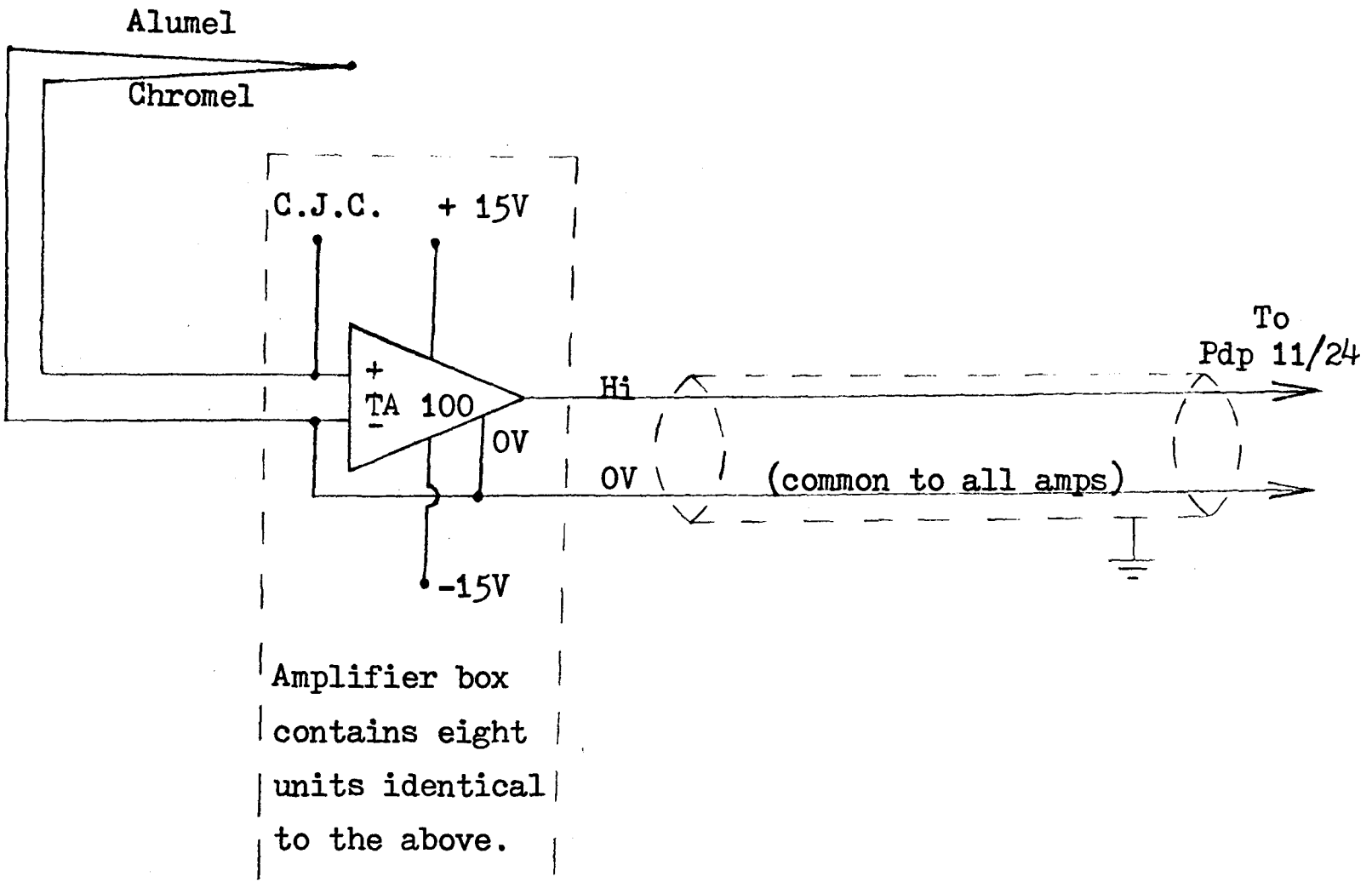

Fig. 4.6 Thermocouple Conditioning Unit

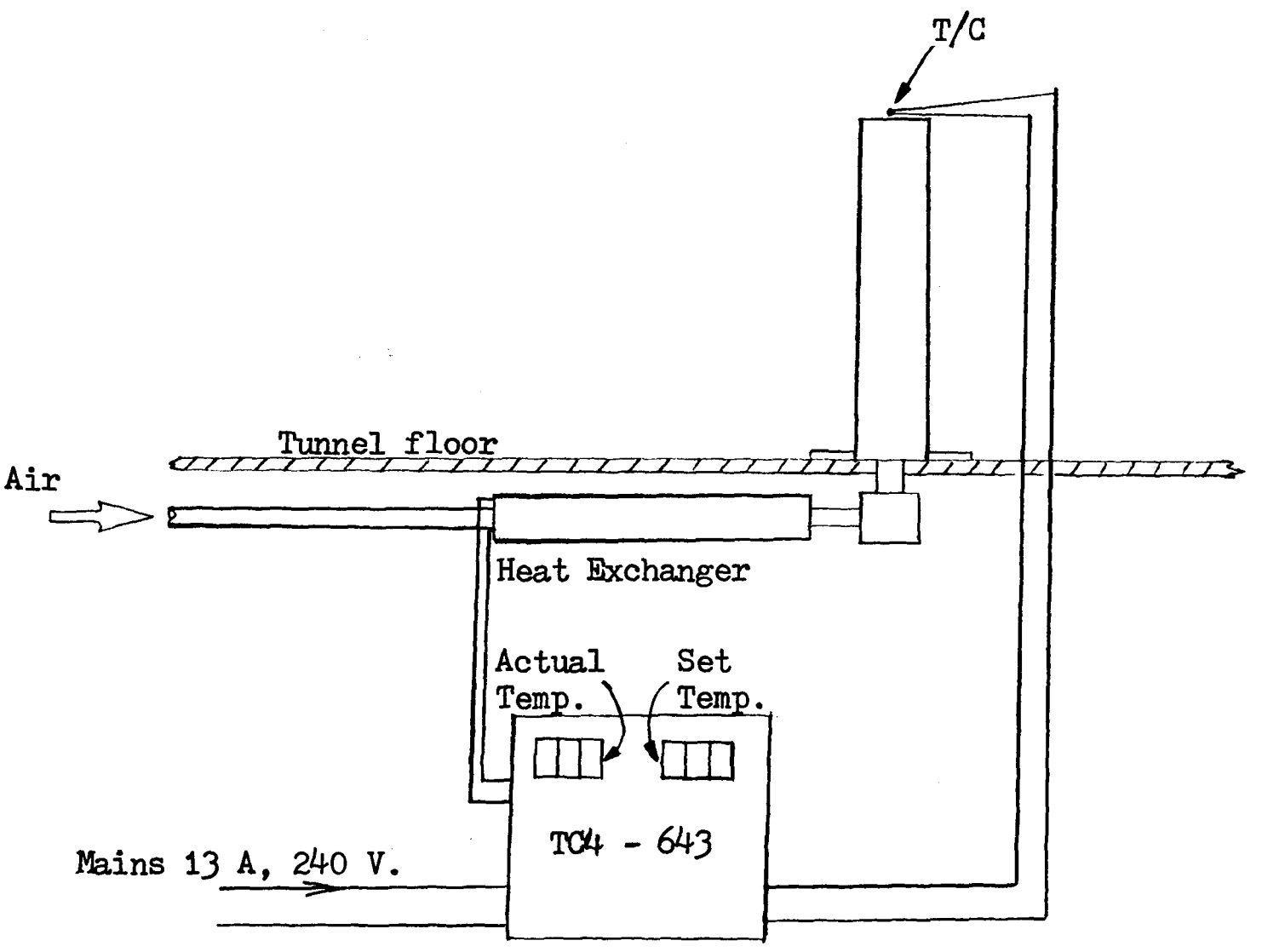

Fig. 4.7 Temperature Control System

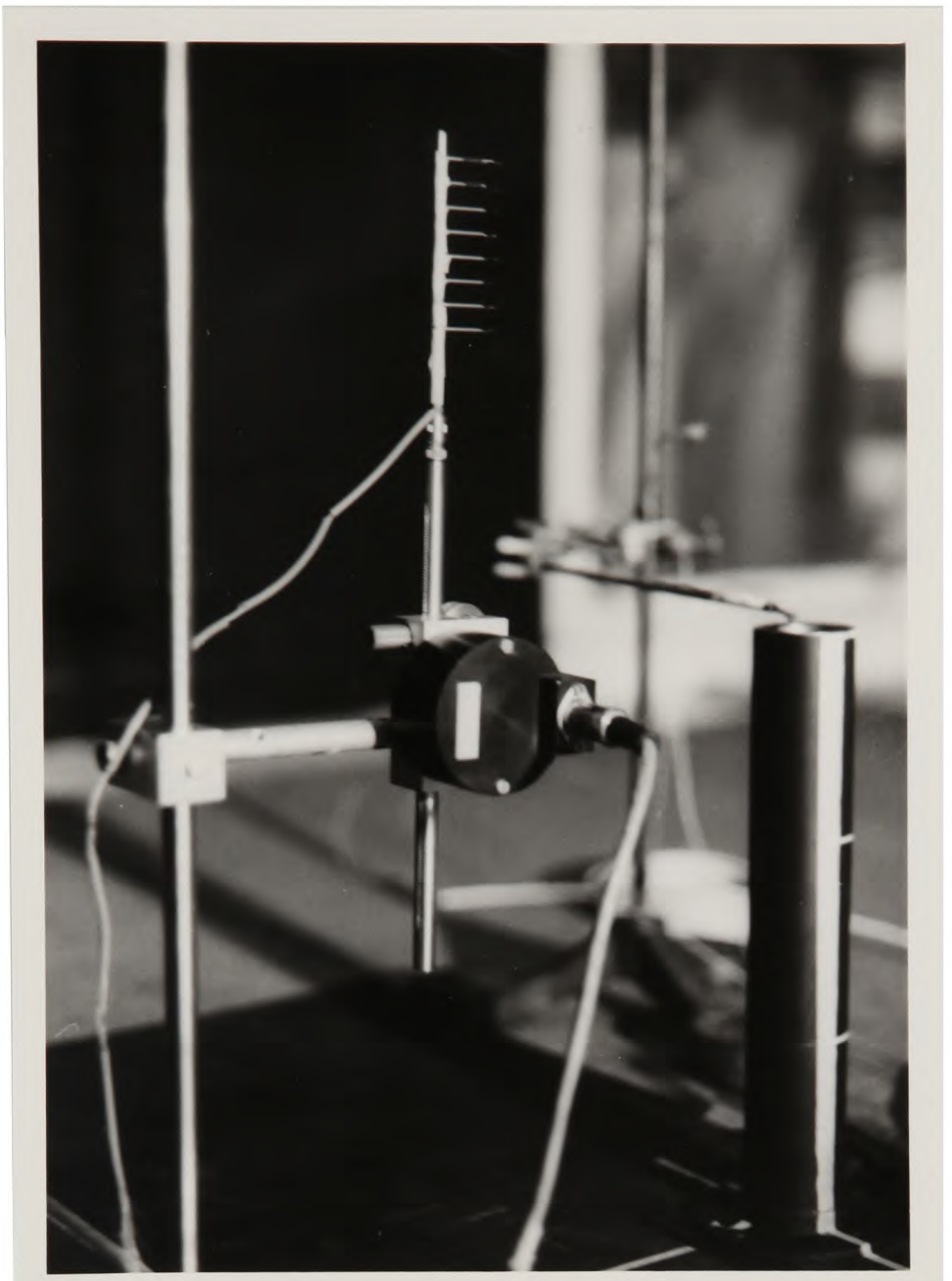

Fig. 4.8 Thermocouple Array

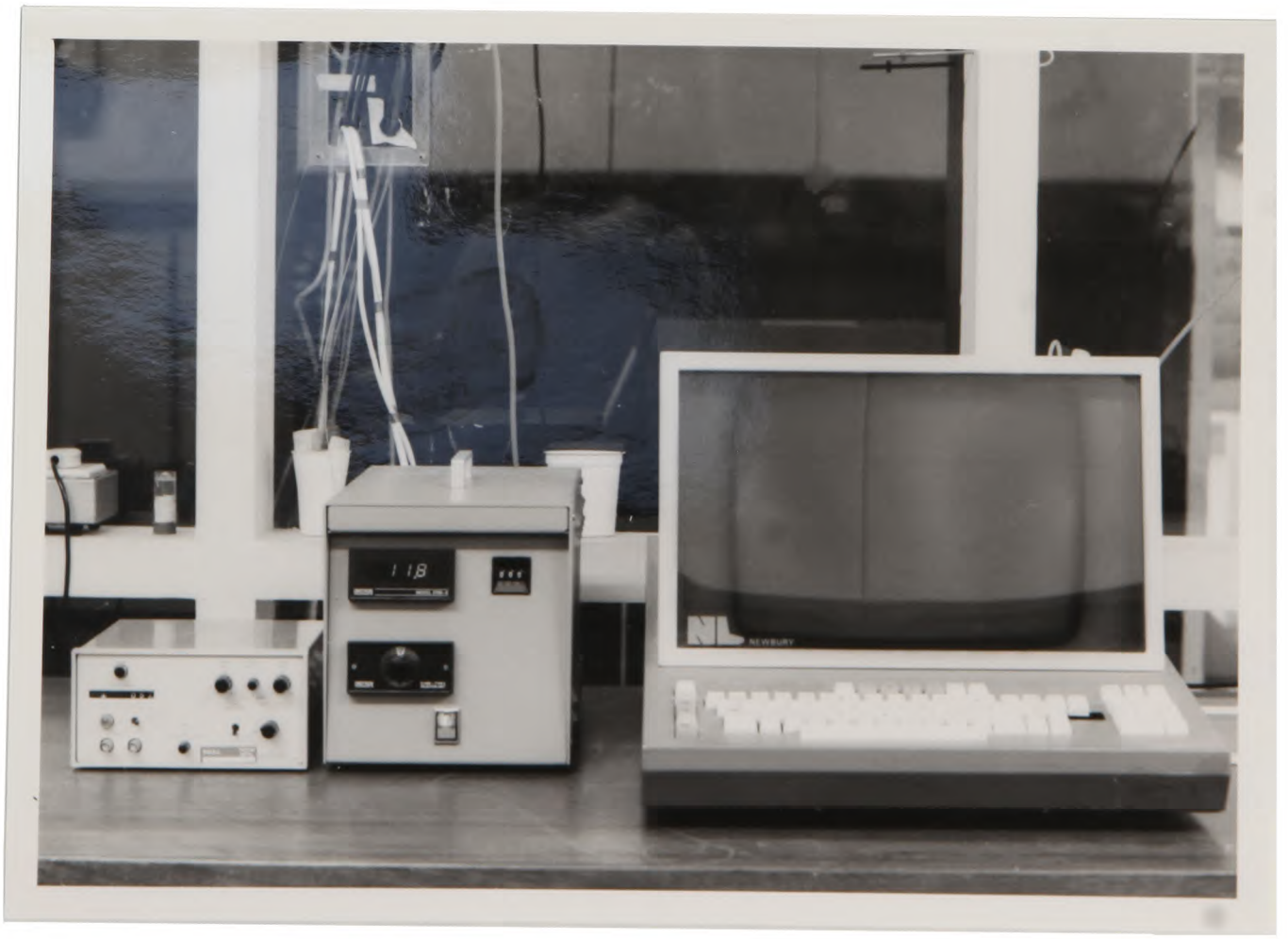

Fig. 4.9 Control of the Experiment From Outside the Tunnel

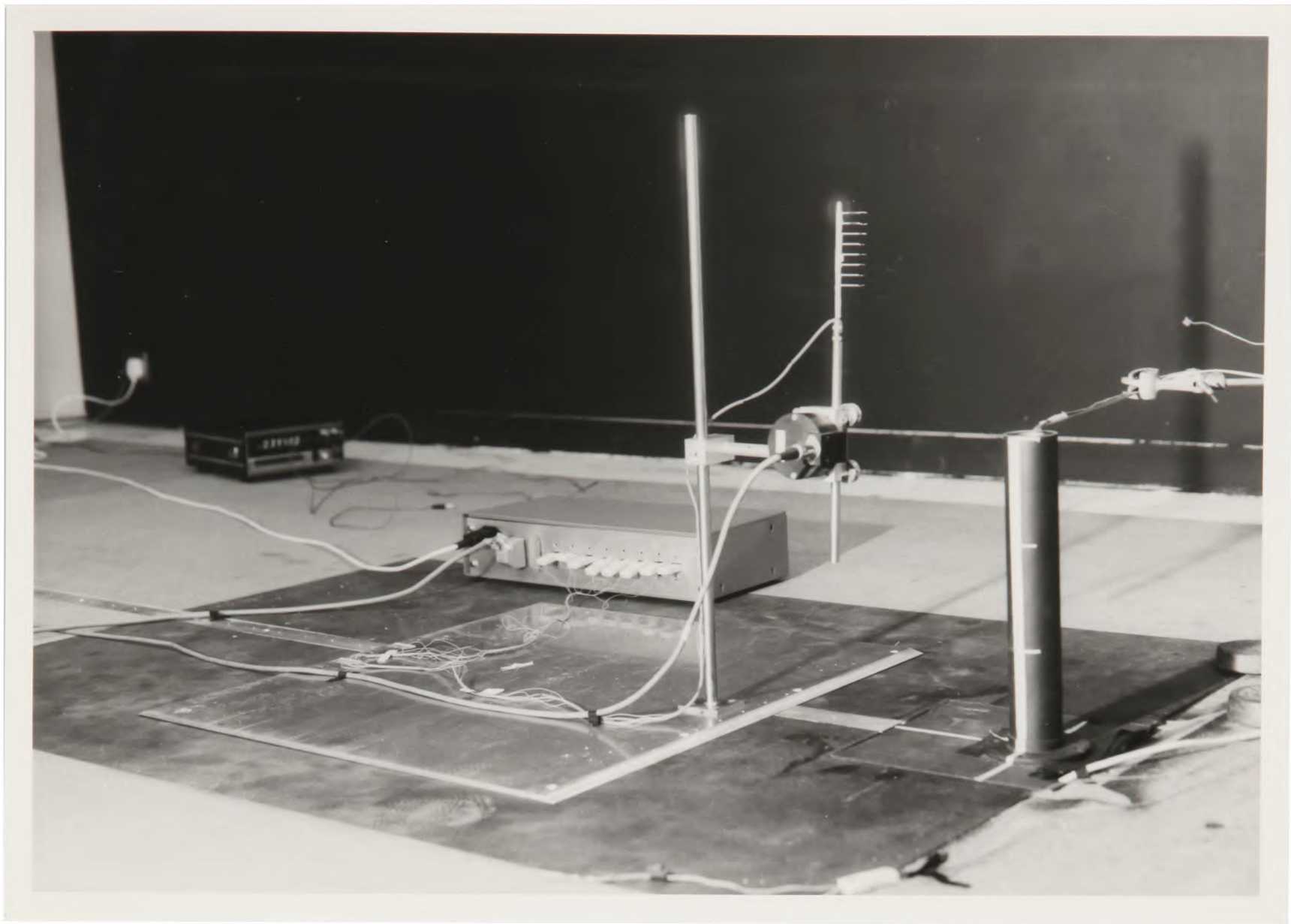

Fig. 4.10 General Views of the Experimental Set-Up

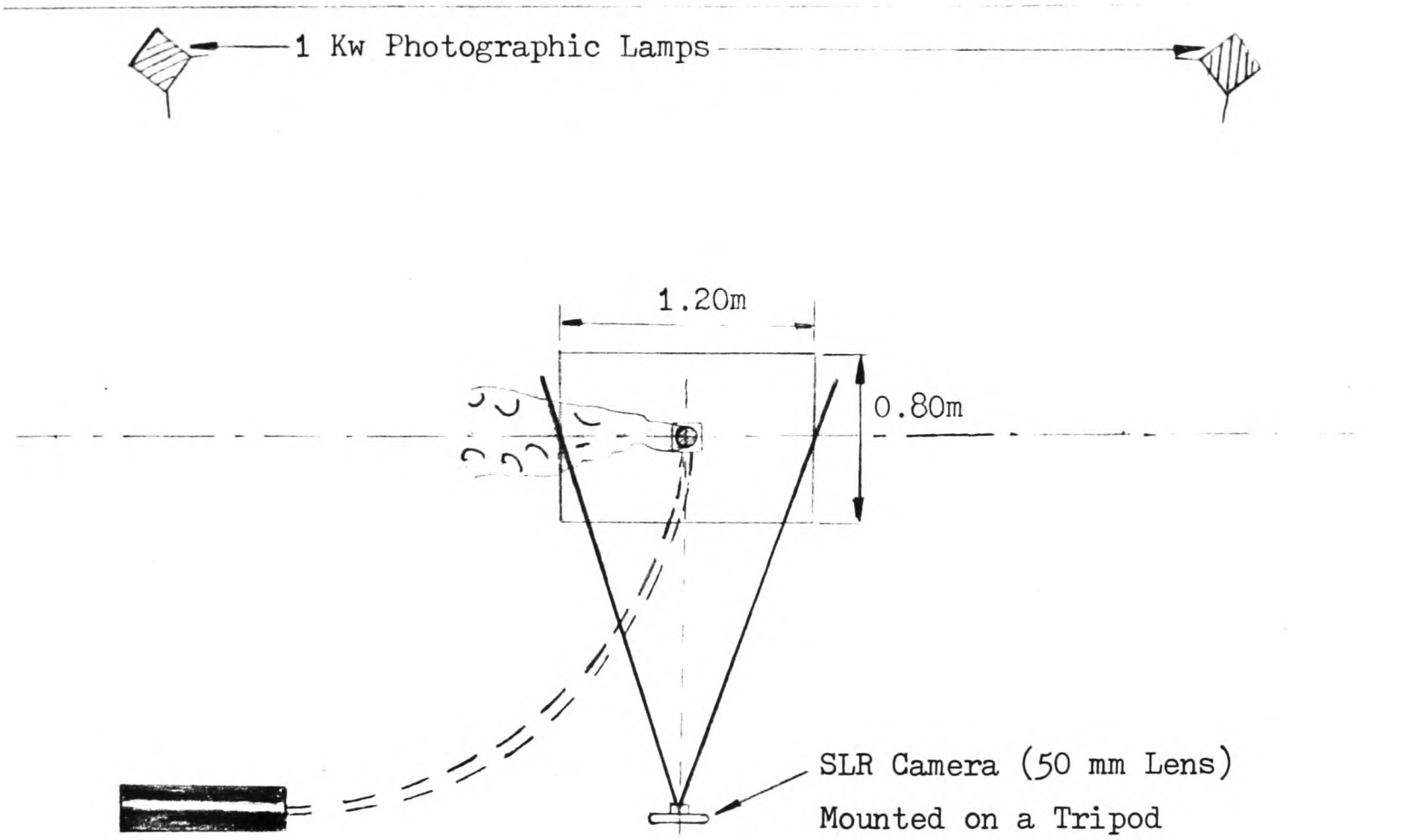

Fig. 4.11 Photographic Set-Up For Flow Visualisation (Showing Field-of-View)

5 ATMOSPHERIC BOUNDARY-LAYER SIMULATION

5.1 AIMS OF THE SIMULATION DEVELOPMENT

The cross-flow which the buoyant plume is exposed to must simulate the natural wind at the same geometric scale as the plume is modelled. Observation of full-scale smoke plumes shows that plume behaviour is very dependent on atmospheric conditions. Therefore, in the wind tunnel we must model the characteristics of the natural wind, such as wind speed, 'gustiness' and frequency of gusts. There are many statistical properties of the wind which can be defined, e.g. mean velocity profile, turbulence intensity in each direction, Reynolds stresses, and it will prove to be very difficult (if not impossible) to model them all precisely. We must decide which characteristics are going to be important in controlling the plume's behaviour and which characteristics we may neglect. Having decided on the full-scale characteristics to model, we then need full-scale data on which to model our reduced-scale simulation. The most complete set of data is given by E.S.D.U. (1972/74) who have examined most of the available data and summarized the results to give a set of standard curves for the various characteristics of the flow. It is found that for uniform, flat terrain the flow is completely specified by the wind velocity at a certain height and the roughness length Z_o . The roughness length is related to the nature of the surface roughness and E.S.D.U. gives values of Z_o for different terrain types, e.g. snow covered flat ground, farmland with many hedges. Thus, the wind tunnel modeller can determine a Z_o for the area he is trying to model, and the E.S.D.U. data will give values for the flow characteristics. The wind tunnel modeller then tries to match his simulation with the relevant E.S.D.U. data.

This process of matching the wind tunnel simulation to the E.S.D.U. data (or an alternative source) is used in all wind tunnel studies. However, there have been few studies of the effect of the simulation on plume behaviour, since most studies have only been performed in one simulation. In this study, I hope to simulate the cross-flow accurately for several different Z_o's, the aim being to investigate how sensitive the plume's dispersion is to the nature of the cross-flow and how accurately we need to model the cross-flow.

5.2 MODELLING REQUIREMENTS

Similarity requirements for wind tunnel modelling of atmospheric boundary-layers may be derived from the governing equations. If we non-dimensionalise these equations we find several non-dimensional groups which must be matched for the equations to be exactly similar in the model and prototype. However, for the resulting flows to be similar the boundary conditions must also be similar. We will consider these two sets of requirements.

Non-dimensionalising the governing equations produces the following groups to be matched (see Cermak (1971) for a detailed derivation):

$$\text{Reynolds number} \quad Re = UL/\nu$$

$$\text{Bulk Richardson number} \quad Ri = \Delta T L g / TU^2$$

$$\text{Rossby number} \quad Ro = U/L\Omega$$

$$\text{Prandtl number} \quad Pr = C_p \mu / k$$

$$\text{Eckert number} \quad Ec = U^2 / C_p \Delta T \qquad (5.1)$$

Complete matching of the dimensionless groups is not possible but relaxation of some of the groups can be justified. For neutral atmospheric conditions and strong winds $Ri \doteqdot 0$ and this can be modelled in the wind tunnel where, without temperature stratification, $Ri = 0$,

(i.e. isothermal conditions). The Rossby number, which takes account of the rotation of the earth in changing the wind direction with height (Ekman spiral), is not matched. But for short range effects (<5km) it has been shown to have no effect on dispersion, Pasquill (1969). By using air as the working fluid the Prandtl number is automatically matched and for incompressible flow the Eckert number is insignificant. The Reynolds number cannot be matched and may be several orders of magnitude smaller in the model than at full-scale. The requirement to match the Reynolds number is then replaced by a requirement to make the flow fully-turbulent. The flow characteristics of a fully turbulent flow are considered to be independent of Reynolds number. A roughness Reynolds number is defined which must be exceeded if a flow is to be aerodynamically rough (turbulent), which atmospheric flows are. It is defined as $U_* Z_o/\nu$, where U_* is the friction velocity and Z_o is the roughness length. These parameters can in turn be defined from the log-law form of the velocity profile:

$$U/U_* = 1/k.\ln(Z/Z_o) \qquad (5.2)$$

For an aerodynamically rough flow we require $U_* Z_o/\nu > 2.5$. If this condition is met, we can be certain that the boundary-layer is turbulent. However, the production of a fully-rough flow does not guarantee that the flow around bluff bodies will be exactly the same in the model and prototype. Further conditions, including a 'building Reynolds number', will have to be met to ensure the correct flow patterns around buildings.

Having fulfilled the requirements for matching the non-dimensional groups, we must also match the boundary conditions for the flows to be exactly similar. Obviously, one boundary condition is the geometric similarity which we have assumed throughout. Another condition is the vertical temperature profile. But as mentioned above we are using an

isothermal flow in the wind tunnel to simulate neutral atmospheric conditions. The third and most important boundary condition is the velocity field of the cross-flow. We must attempt to model the flow characteristics which are important in the dispersion of a buoyant plume. The earlier discussion of 'Theoretical Methods for Predicting Dispersion' would suggest that the following properties should be modelled:

i) the mean velocity profile,

ii) profiles of turbulence intensity (3 components)

iii) integral length scales L ,

where the turbulence intensity is σ_u/U and σ_u^2 is the variance of the velocity component. $L = UT$, (T is the integral time-scale) and L is a measure of the average size of the eddies in that direction. Condition (iii) can be extended to a requirement that the turbulent energy spectra are matched. This is an attempt to match the frequencies of the eddies which are dispersing the plume; the size and frequency of the dominant eddies in the mixing process will change as the plume grows, hence the requirement to model all the frequencies. Further properties, e.g. Reynolds stresses, could be matched but the above are of primary importance for modelling dispersion.

The full-scale values of the wind characteristics can be derived from E.S.D.U. (1972/74) and in the following sections the model results will be compared with the E.S.D.U. values. However, there is uncertainty in the full-scale values which E.S.D.U. present (especially in the spectra, see fig 10, 1974) and this should be borne in mind when considering the results of the wind tunnel simulations.

The scaling of the full-scale and model wind velocity has already been considered in section 3.4, i.e. $S(U) = \sqrt{S(d).S(\Delta\ell)}$. Having scaled the mean velocity by that ratio all other (turbulent) velocities should be scaled by the same ratio.

5.3 MODELLING TECHNIQUE

The wind flowing over the earth's surface produces a deep boundary-layer (about 600m in neutral conditions). A flat plate boundary-layer has very similar characteristics to the a.b.l.. Not only is the velocity profile similar but the ratios of the three components of turbulence intensity are also very similar for the flat plate boundary-layer and the a.b.l., (i.e. for the a.b.l. $\sigma u : \sigma v : \sigma w$ are 1.0:0.75:0.50, for the flat plate the ratios are 1.0:0.75:0.54). Thus if a flat plate boundary-layer of sufficient depth could be produced it would be a good simulation of the a.b.l.. To model the complete boundary-layer at a scale of 1:200 would require a wind tunnel at least 3m high and to grow such a boundary-layer naturally would require a fetch of at least several tens of meters. The alternative is to grow a turbulent boundary-layer artificially which models only part of the full boundary-layer depth. Several techniques have been developed using passive turbulence generating devices to produce 'part-depth' simulations. Such items as grids, wooden blocks, sand and more complicated arrangements have been used to disturb the flow in order to produce a boundary-layer with the required characteristics, see Counihan (1969), Cook (1973), Standen (1972). These devices must produce not only the correct velocity profile but also the three components of turbulence intensity ($\sigma u, \sigma v, \sigma w$) in the correct proportions.

Several methods have been developed at Oxford for producing part-depth simulations; most methods use a combination of a grid at the entry to the working section, and surface-mounted roughness elements. Four simulations were used in this study (all 1:200), and were developed from previous experience. The design of the four simulations and the terrain they represent is described below and the results are presented in the next section. The aim of the simulation development

was to produce flows with different characteristics in order to compare plume behaviour in each simulation.

The four flows are (descriptions from E.S.D.U.):

A) Empty tunnel, no shear, very low turbulence. This first flow is not an a.b.l. simulation. It is essentially a uniform, smooth cross-flow which will be used to show the need to simulate the a.b.l.

B) Z_o = 0.002 m, 'Natural snow surface (farmland)'. This represents the flow over a very smooth surface, but has appreciable shear and turbulence intensity compared with A.

C) Z_o = 0.01 m, 'level grass plains, few trees, wintertime' Although Z_o is larger than in B, the flow characteristics are very similar. Results in B and C could be compared to see how sensitive wind tunnel modelling of dispersion is to Z_o .

D) Z_o = 1.0 m, 'centre of large towns, (forests)'. A much more turbulent flow than the others and with slightly greater shear.

Some of the E.S.D.U. characteristics for the flows are shown in fig. 5.1 for comparison (mean velocity, longitudinal turbulence intensity profiles and turbulent energy spectra).

The hardware used to produce these simulations is shown in figs. 5.2 - 5.4 and described below.

A) Empty tunnel. The tunnel was cleared of all simulation devices and there was no grid. The floor and ceiling of the tunnel are painted wood and the walls are perspex. A thin boundary-layer would develop on all surfaces; the depth of the boundary-layer was measured to be about 15 cm at the turntable. The flow in the central section was expected to be uniform.

B) Z_o = 0.002 m. The simulation is shown in fig. 5.2. A grid was placed at the entrance to the working section consisting

of 11 vertical members and 4 horizontal members, evenly spaced. The bars were 9.5 cm wide and 3.5 cm thick. Some 20 cm downstream of the grid a fence, 12.5 cm high, was placed across the tunnel to trip the flow (the positioning of the fence was found to be very critical). Then three rows of building blocks (115 x 75 x 230 mm high) were placed on the painted wooden floor as shown, the first row being two bricks high. Then there was a 2.44 m fetch of small wooden blocks (45 x 45 x 25 mm high). The blocks were arranged in a pseudorandom manner to give an area coverage of approximately 7%. This was followed by a 2.44 m fetch of hardboard panels covered with sandpaper. The turntable, as in all simulations, was covered in hardboard with the rougher surface exposed.

C) Z_0 = 0.01 m. The simulation is shown in fig. 5.3, where the grid used is shown in detail. The floor downstream of the grid is covered in 2.44 m fetches of large inverted plastic cups, small inverted plastic cups, wooden blocks (x2) and sand. The large plastic cups are 400 cc volume truncated cones with a larger diameter of 85 mm, smaller diameter 73 mm, and height 95 mm. They were placed in a pseudorandom manner to give an area coverage of 7.6%. The smaller plastic cups are 92 mm high and have a larger diameter of 65 mm and smaller diameter of 46 mm; their area coverage is 8.7%. The wooden blocks and sand are as in B. An additional feature of this simulation are two hedges placed 2.75 m and 4.60 m upstream of the turntable centre. The hedges are 40 mm high, 30 mm wide and made from 'Hairlock' rubberised hair matting which is slightly porous.

D) Z_0 = 1.0 m. The grid consisted of three vertical bars, 21.0 cm wide, positioned as shown in fig. 5.4, and ten stacks of three bricks equispaced across the tunnel. Following the grid there was a 7.32 m fetch of large plastic cups and then smaller plastic cups to the edge of the turntable.

5.4 INSTRUMENTATION, SAMPLING AND DATA ANALYSIS

The flow characteristics were measured using single wire and cross-wire constant temperature hot wire anemometers, DISA K-type. A single wire probe was used to measure the longitudinal component, (i.e. mean velocity, turbulence intensity and power spectral density). The signal from the hot wire was processed by a DISA anemometer unit to give an output signal directly proportional to the velocity, (DISA type 55k01 main unit plus type 55k10 C.T.A. Standard Bridge). The wires were calibrated by placing them normal to the flow from a calibration nozzle; the velocity of the air leaving the nozzle had previously been determined and could be varied over a wide range of speeds. The cross wire probe was used to make measurements of the lateral and vertical components. Each wire was calibrated separately, as for a single wire, and the resulting velocity signals for each wire (inclined at plus and minus 45° to the mean flow) were combined by analogue methods to give an output proportional to the velocity in the plane of the wires normal to the mean flow. The resulting lateral or vertical velocity signal was then used as the input to the power spectral density program (which also calculates the variance of the signal).

The signal from a probe was conditioned by a dual Kemo switchable filter and passed through a D.C. preamplifier and an A-D converter (range 0 to 5 V) before being received by the PDP 11/24 computer. The computer program for the mean velocity and turbulence intensity measurements sampled the input signal at 100 Hz for 60 - 70 s (~15 mins full-scale) until a probability distribution of the signal was built-up. The probability distribution was displayed on an oscilloscope so that the operator could check for out-of-range signals or any irregularity. Tha data were then processed to give the mean velocity U and the turbulence intensity $\sigma u/U$, where U and σ_u^2 (variance) are respectively

the first and second moments of the probability distribution.

The power spectral density of each component could be obtained by using a Fast Fourier Transform program on the relevant velocity signal. The program gathered 28 separate blocks of data each containing 2048 instantaneous velocity readings; the velocity signal was sampled at twice the frequency of the highest coefficient to be determined. Having chosen the highest frequency to be measured, the lowest frequency was fixed by the sampling program. The frequency range for each spectrum was chosen to include most of the turbulent energy and to give an equal cut-off at each extreme frequency. Analogue filter settings were used to eliminate the mean and to avoid high frequency aliasing problems. A standard digital Fast Fourier Transform was used on each data block to give sets of real and imaginary coefficients. The coefficients of each block were then averaged to give a final smoothed spectrum which was plotted as a power spectral density curve. The spectra were plotted in a normalised form, $nS(n)/Var$ against the $\log_{10}$ of frequency, since this is a standard form given by E.S.D.U.. The variances of the lateral and vertical components determined above were used to determine the lateral and vertical turbulence intensities, $\sigma v/U$ and $\sigma w/U$.

5.5 SIMULATION RESULTS

The results of the simulation development will be presented and discussed in the following manner. Firstly, the mean velocity and turbulence intensity profile of the normal component will be considered and then the lateral and vertical components of turbulence intensity (derived from the spectral measurements) and finally, the turbulent power spectral densities of the three components measured at the stack exit, (all measured at the stack position, 70 cm upstream of the turntable centre, without the stack in place). These results are compared with values derived from the E.S.D.U. data. The lateral and longitudinal uniformity of the flows were also examined to ensure that the characteristics were not changing too rapidly in the near-field of the plume. (All heights refer to full-scale.)

5.5.1 SIMULATION A

The flow in the empty tunnel was not expected (or required) to represent an atmospheric flow, but rather, a standard low turbulence flow. Fig. 5.5a shows that above the boundary-layer the velocity and longitudinal turbulence intensity are essentially constant. The stack is 60 m high (full-scale), therefore the plume will be exposed to a uniform flow (no shear) of very low turbulence intensity, $\sigma u/U$ = 1%, which is much smaller than the value in atmospheric flows, which is usually > 10%.

The lateral and vertical turbulence intensities were only determined at the stack exit, since they were expected to be constant above the boundary-layer. The lateral turbulence intensity, $\sigma v/U$, was found to be 3% and the vertical turbulence intensity, $\sigma w/U$, was 3.7%. In most turbulent flows $\sigma_u > \sigma_v \gg \sigma_w$, e.g. flat plate boundary-layers, grid turbulence, and we would expect this to be the case in the empty tunnel. The discrepancy is due to the uncertainty in the measurement.

The discrepancy is thought to arise because the variance (σv^2) of these components is very small and any error in its value is exaggerated when calculating $\sigma v/U$. However, we may be certain that the turbulence intensities in this flow are significantly smaller than in atmospheric flows.

The three components of the turbulent energy spectrum measured at the stack height are shown in figs. 5.5b and 5.6. The above comments about the uncertainty in measuring the small variances in this flow also apply to the spectra since the spectra are non-dimensionalised by the variance. The important points to note are that the spectra are quite broad, the peak region covers almost a decade, and that the peaks occur at higher frequencies than in the later simulations. The E.S.D.U. curve for Z_o = 0.002 m is shown in fig. 5.5b for comparison and shows that there is a decade difference in the position of the peaks. (The w-spectra is badly chopped due to the filter setting but the main features may still be observed.)

A check of the lateral and longitudinal uniformity at the stack height revealed the flow to be constant within experimental error, with no observable trends for 50 cm either side of the centre-line and for 50 cm downstream of the stack.

5.5.2 SIMULATION B, Z_o = 0.002m

This simulation represents the flow over very smooth terrain - 'snow covered farmland' is the E.S.D.U. description. It could also probably be used to represent the flow over water.

The mean velocity profile agrees well with the E.S.D.U. curve for Z_o = 0.002 m (see fig. 5.7a). Also, the profile of the longitudinal component of turbulence intensity agrees well with the E.S.D.U. curve. The lateral and vertical component were determined from the power

spectral density measurements at 60 m and 100 m and are plotted in fig. 5.7b. The values for the lateral component agree reasonbly well with the E.S.D.U. curve, however, the values for the vertical component are too large. In fact, they are approximately 30% larger than required. Having developed a simulation it is very difficult to make changes in order to change one component since this will inevitably affect the whole flow. Therefore, no improvement could be made in the vertical component and this should be remembered when examining the plume's behaviour in this simulation.

Fig. 5.8 shows the spectra of the three velocity components. The longitudinal component agrees reasonably well with the E.S.D.U. curve. There is not quite enough energy at low frequencies and slightly too much at high frequencies. This is a problem which is often encountered in wind tunnel simulations. Since the vertical ordinate for these graphs is $n.S(n)/Var$ the discrepancy is not too important at high frequencies since there is little energy at those frequencies; the mismatch is more significant at low frequencies. The lateral component ($\sigma v/U$) also exhibits this mismatch and we may find that as a result plumes do not spread as much as we might expect. Although the magnitude of the vertical component of turbulence was found to be too large, the distribution of frequencies was in good agreement with the atmospheric data, fig. 5.8.

To check the uniformity of the flow, lateral traverses were made to 30 cm either side of the centre-line and a longitudinal traverse 50cm downstream of the stack, all at the stack height. The mean velocity was found to lie within 2% of the average value and the longitudinal turbulence intensity was within 5% of the average value. There were no observable trends, and the uniformity of the region of interest was considered to be good.

This simulation is considered to be a reasonably good model of an atmospheric wind, especially of the longitudinal component of velocity. However, the limitations in simulating the lateral and vertical component should be recalled. Since we are not specifically trying to model a full-scale situation but rather to compare plume behaviour in different simulations this mismatch is not considered to be too important in this study.

5.5.3 SIMULATION C, Z_o = 0.01 m

Although the Z_o value for this simulation is larger than for simulation B, the flow characteristics are very similar. From a practical point of view the E.S.D.U. values for mean velocity and the spectra are the same, see fig. 5.1. The main difference is that the turbulence intensities in C are about 10% greater than in B. Thus we may expect a plume in simulation C to spread more rapidly than in simulation B. Simple theoretical methods (Djurfors and Netterville, 1978) would predict that the mean plume rise would be the same in both simulations, however, one might expect the different rates of spread to have an effect on the plume rise.

It is interesting to note that simulations B and C are produced by very different hardware.

The profiles of the longitudinal mean velocity and turbulence intensity, see fig. 5.9a, show close agreement with the E.S.D.U. curve, although the turbulence intensity is slightly too great. The lateral and vertical turbulence intensities are shown in fig. 5.9b. The vertical component is well matched to the atmospheric values, the lateral component is in agreement at 60 m but at 100 m its value is too high (by 10%). From the limited data available it would appear that the lateral and vertical turbulence intensities are approximately constant

in the region 60 m to 100 m; this invariance with height has been found in several other wind tunnel simulations.

The turbulent energy spectra of the three components are shown in fig. 5.10. They show good agreement with the E.S.D.U. curve with, as we often find, slightly too much energy at high frequencies. The lateral and vertical components are well matched at low frequencies. This is important for dispersion modelling since it is these low frequencies which cause the plume to meander.

To examine lateral uniformity, measurements of the U-component were made at the stack exit height (60 m full-scale), for up to 50 cm either side of the stack. The velocity measurements were all within 1.5% of the mean value. The turbulence intensities were all within 5% of the mean value. The flow was examined up to 40 cm downstream of the stack. The mean velocity showed a slight decrease in value of 3% over this range; this may have been due to drift in the electronics of the anemometer. The turbulence intensities showed no significant trend and all values were within 5% of the mean value.

The above simulation is considered to be a good simulation of the atmospheric wind for Z_o = 0.01 m - 'level grass plains', and to be well suited to studying dispersion.

5.5.4 SIMULATION D, Z_o = 1.0 m

This simulation represents the wind in an urban environment and has a much higher Z_o than the other flows. The mean velocity profile and the longitudinal turbulence intensity profile, fig. 5.11a, show good agreement with the atmospheric data. Note that the velocity profile shows much greater shear than in the previous simulations and the turbulence intensity is also higher. The lateral and vertical turbulence intensities, fig. 5.11b, also show good agreement with the atmospheric

data, although the lateral component is slightly too small. The results suggest that the turbulence intensities are almost constant in the region 60 - 100 m, while full-scale data imply that they should be decreasing slowly.

The turbulent energy spectrum of each of the three components, shown in fig. 5.12, are a good match to the E.S.D.U. data, but with slightly too much energy at the higher frequencies. The spectra are well matched at the low frequencies.

A mean velocity and turbulence intensity profile was measured at 0.5m downstream of the stack and was found to be very similar to that measured at the stack. It would appear that the characteristics of the flow had not changed significantly over this fetch.

Simulation D is a good representation of the wind in a heavily built-up urban, industrial area. Since not only the longitudinal component but also the lateral and vertical components are well matched to the atmospheric data, this simulation is suitable for modelling atmospheric dispersion in an urban environment.

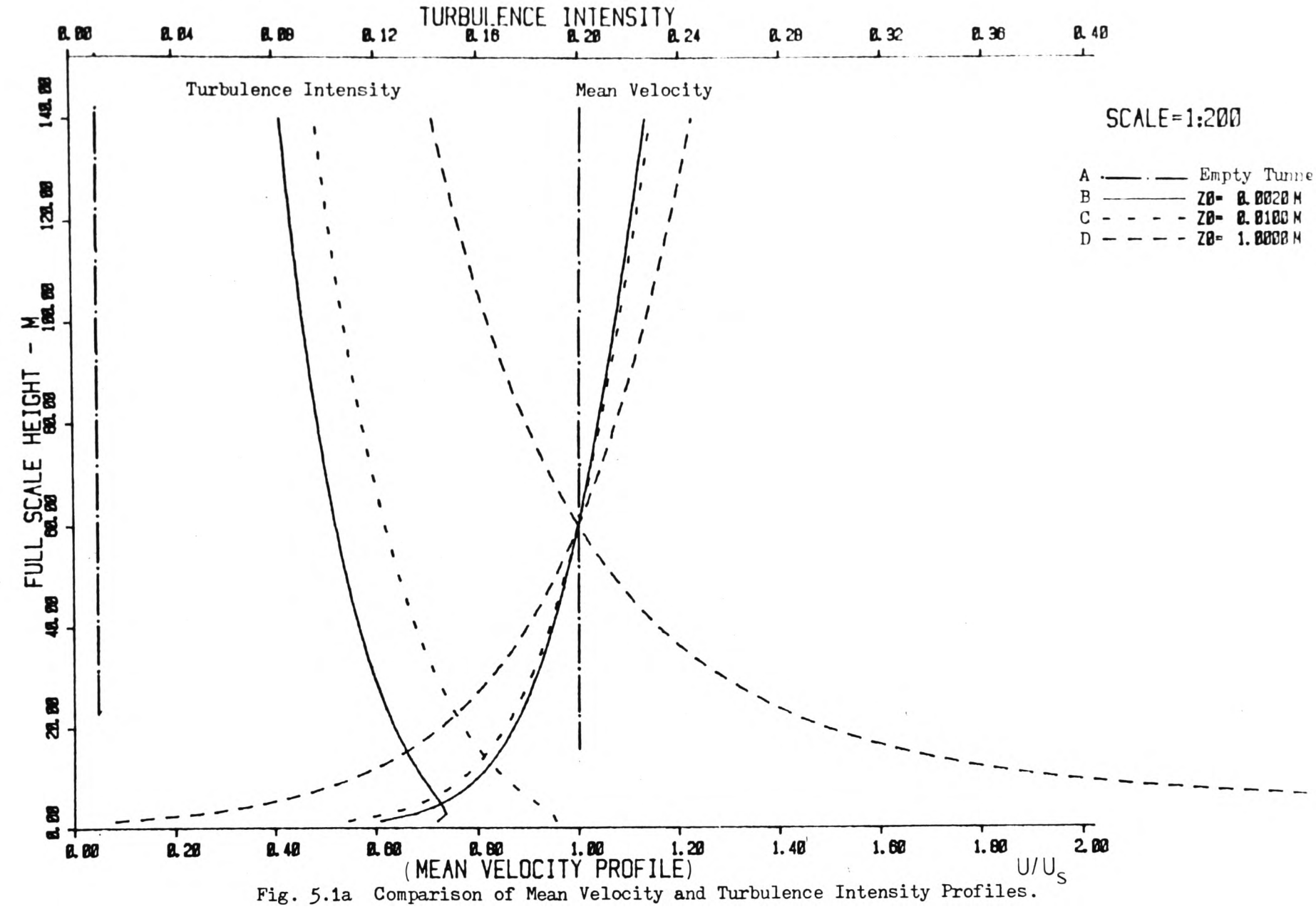

Fig. 5.1a Comparison of Mean Velocity and Turbulence Intensity Profiles.

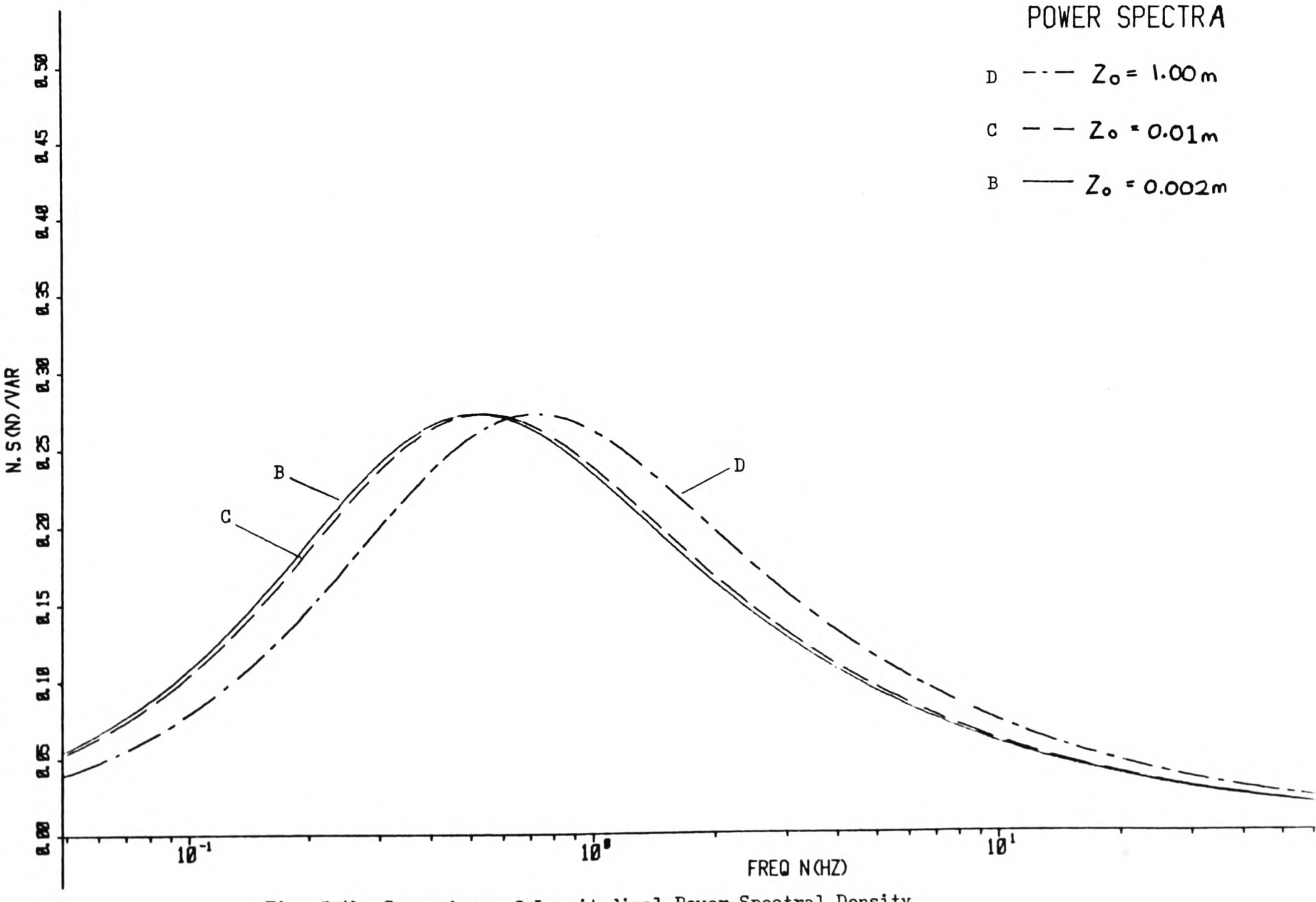

Fig. 5.1b Comparison of Longitudinal Power Spectral Density

Simulation B

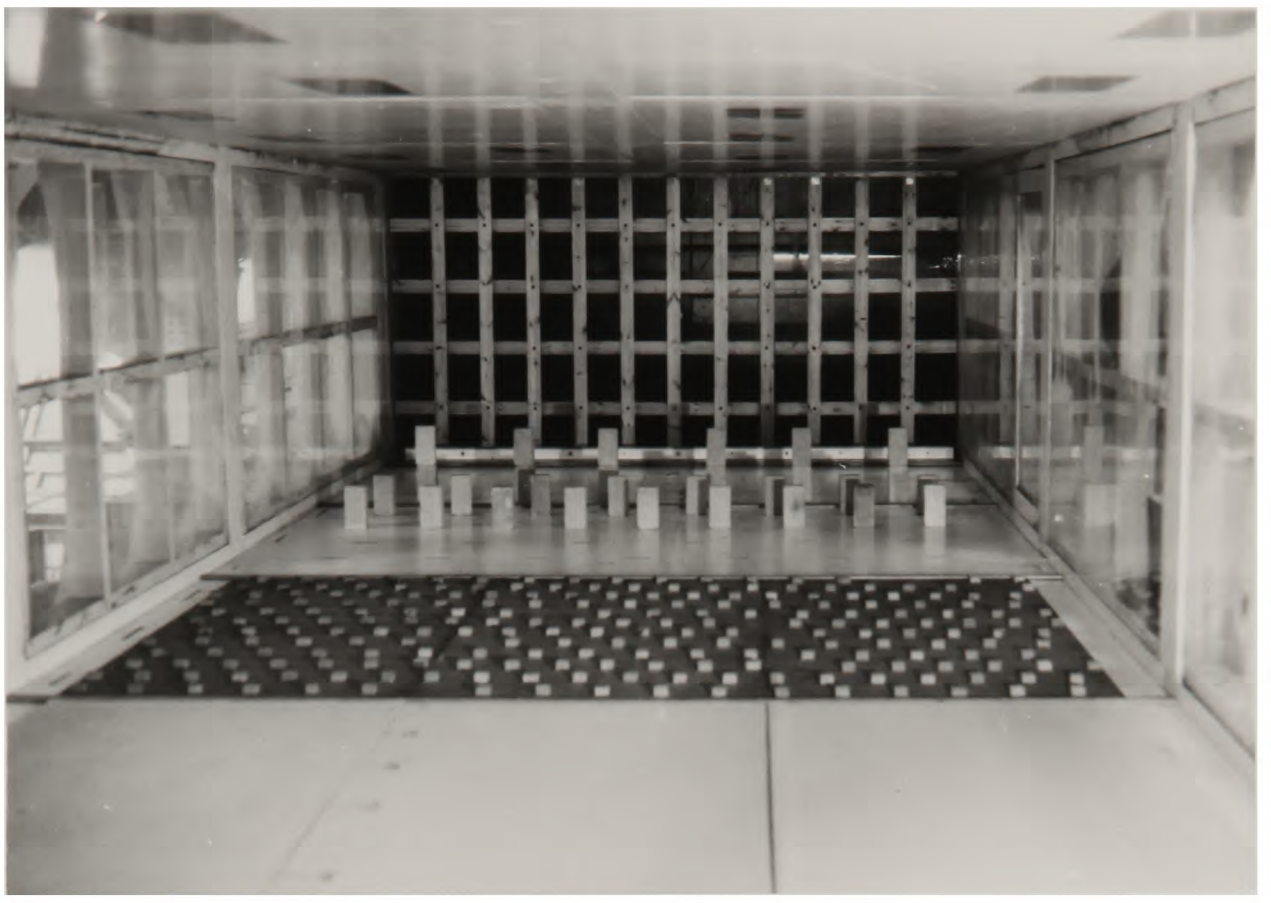

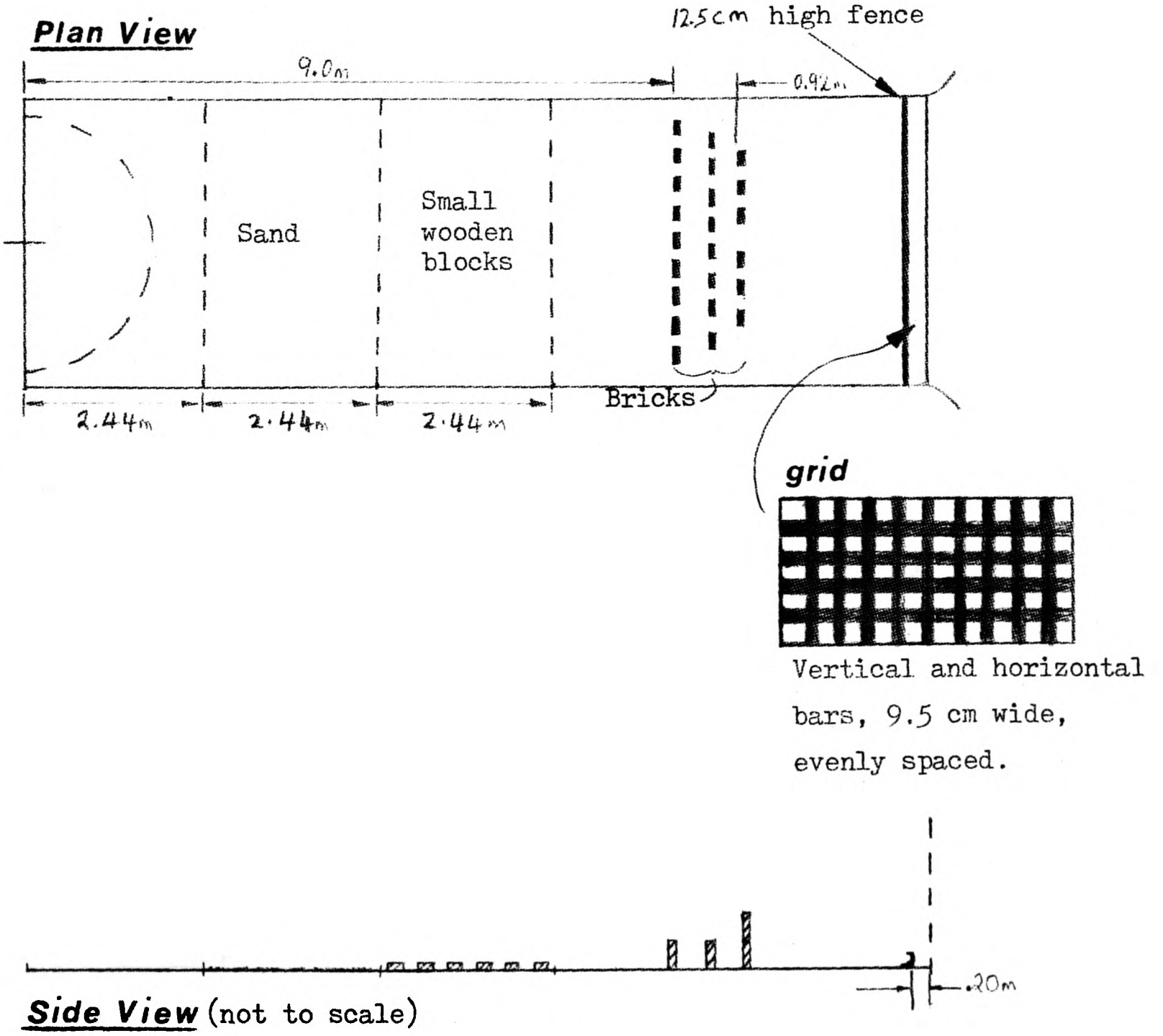

Fig. 5.2 SIMULATION B - Z_o = 0.002 m.

SIMULATION C

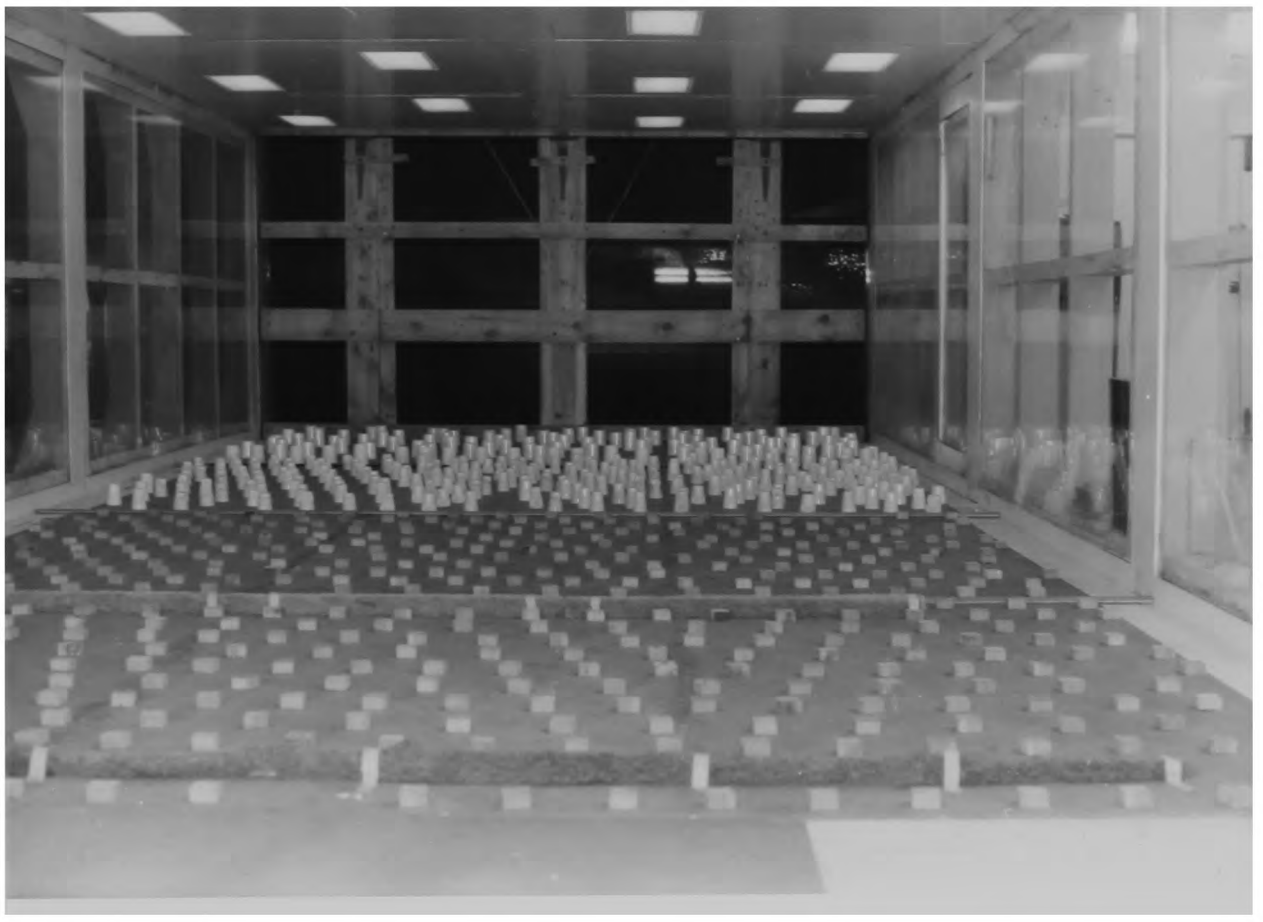

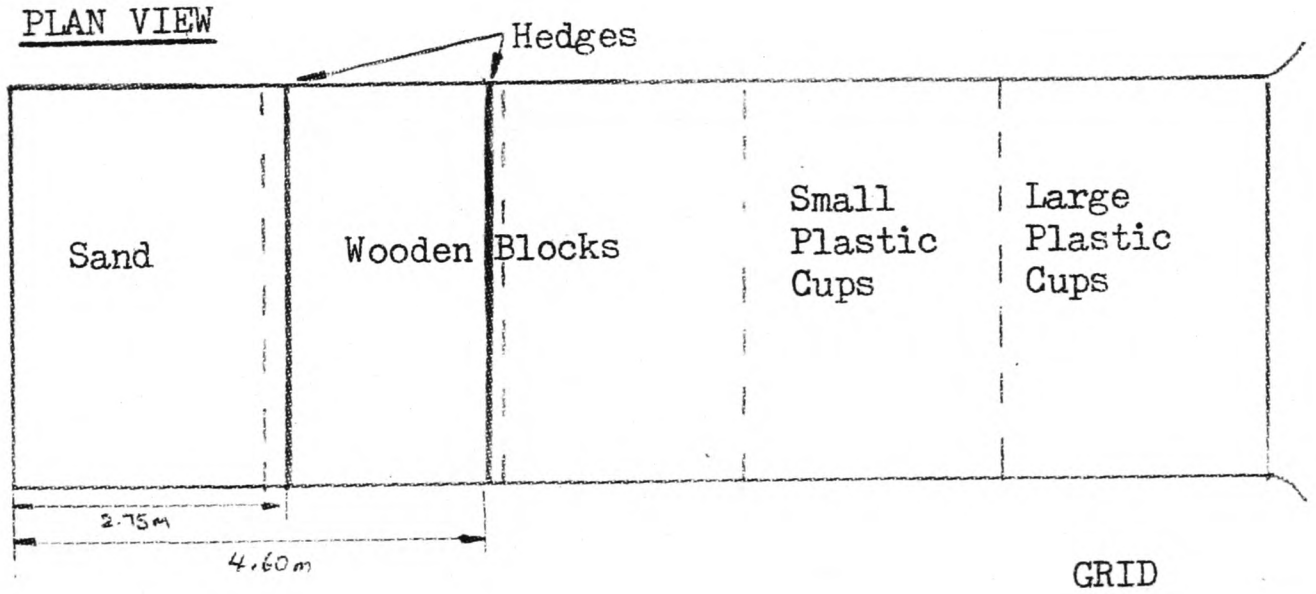

GRID

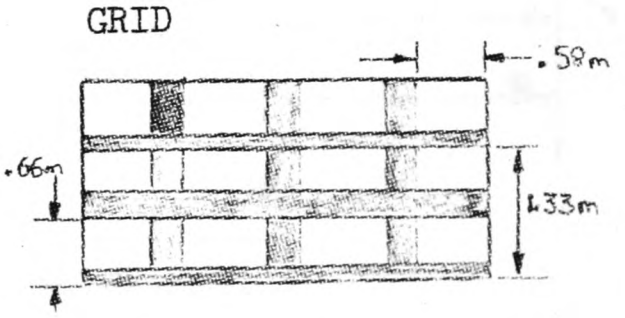

Vertical bars .31m wide.
Horizontal bars .105m wide
- middle bar double width.

SIDE VIEW (not to scale)

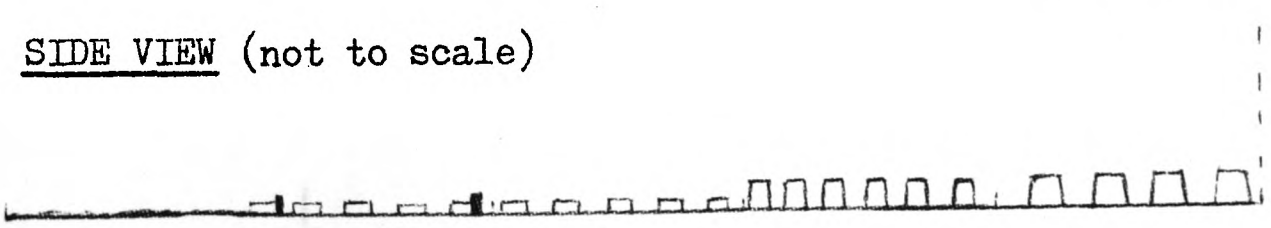

Fig. 5.3 SIMULATION C - Z_0 = 0.01 m

SIMULATION D

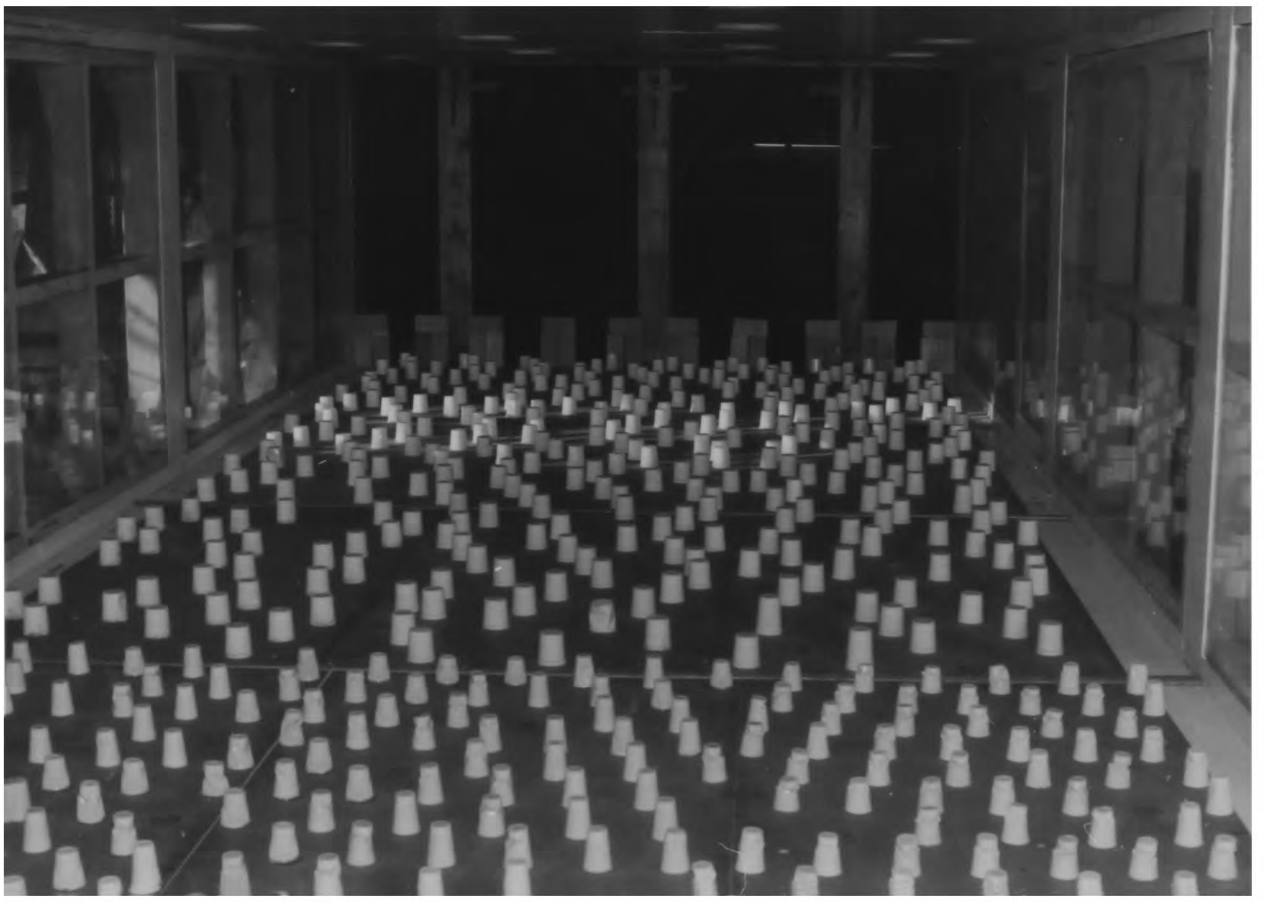

SURFACE ROUGHNESS ELEMENTS

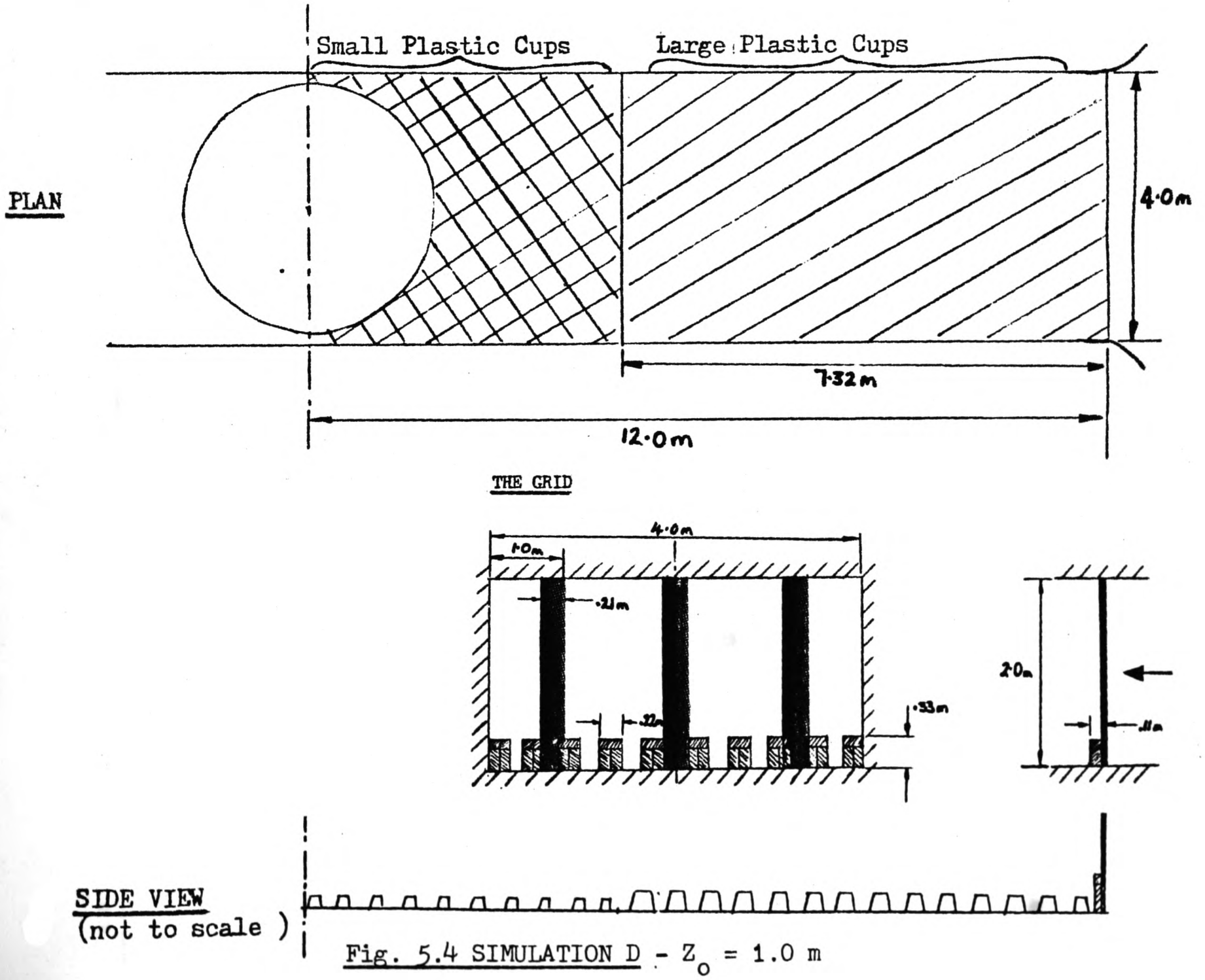

Fig. 5.4 SIMULATION D - Z_o = 1.0 m

SIMULATION A

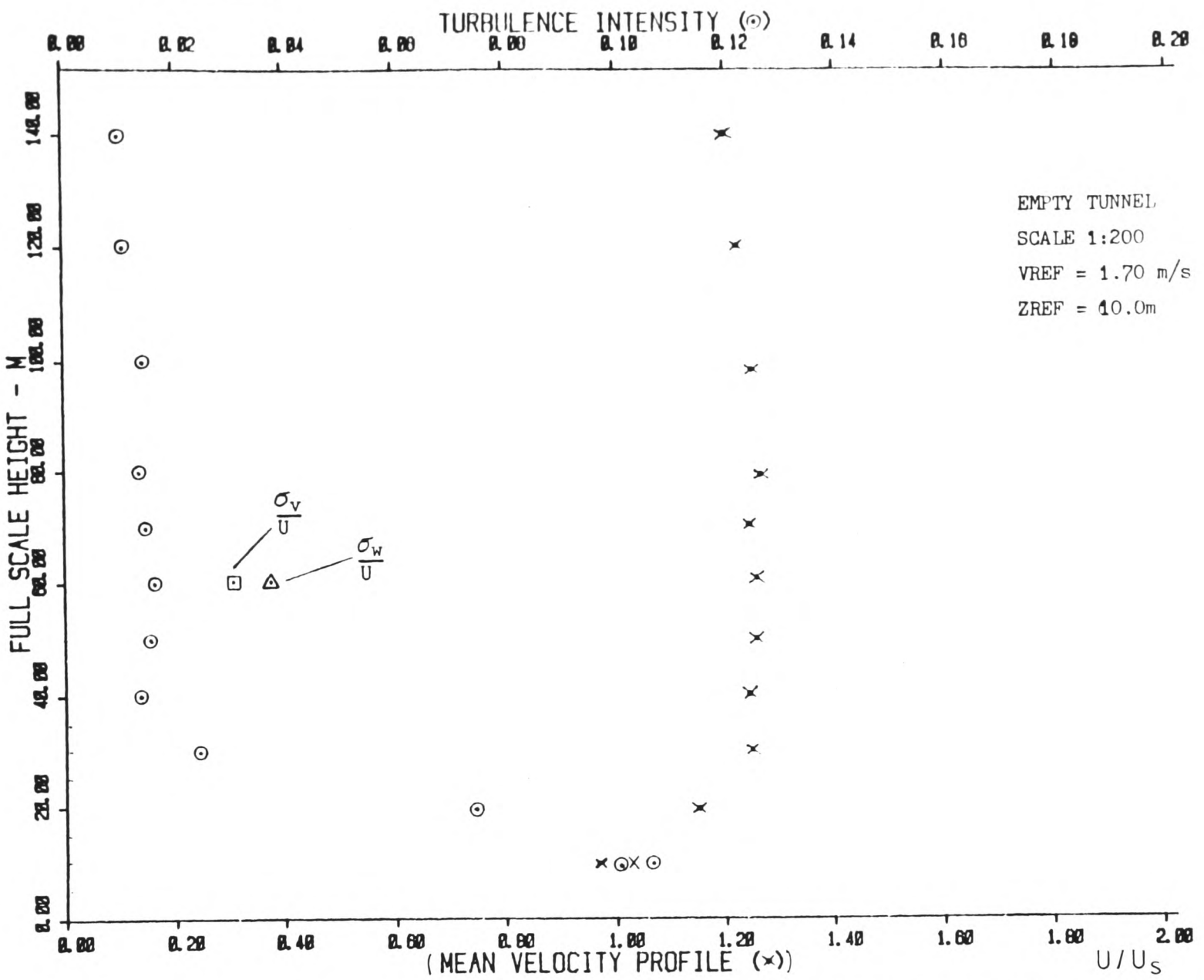

Fig 5.5a Mean Velocity and Turbulence Intensity Profile (Simulation A)

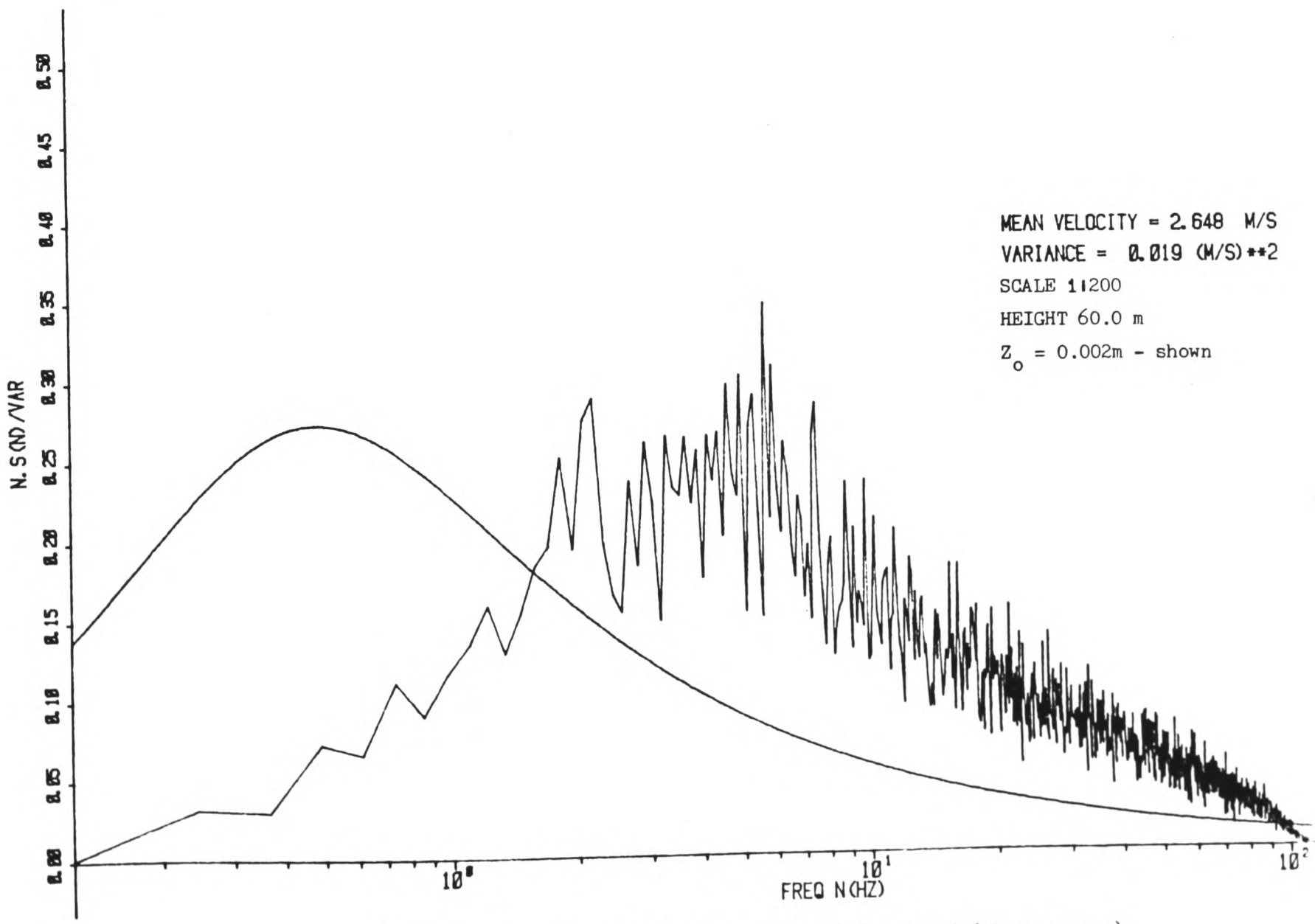

Fig. 5.5b Power Spectral Density of Normal Component (Simulation A)

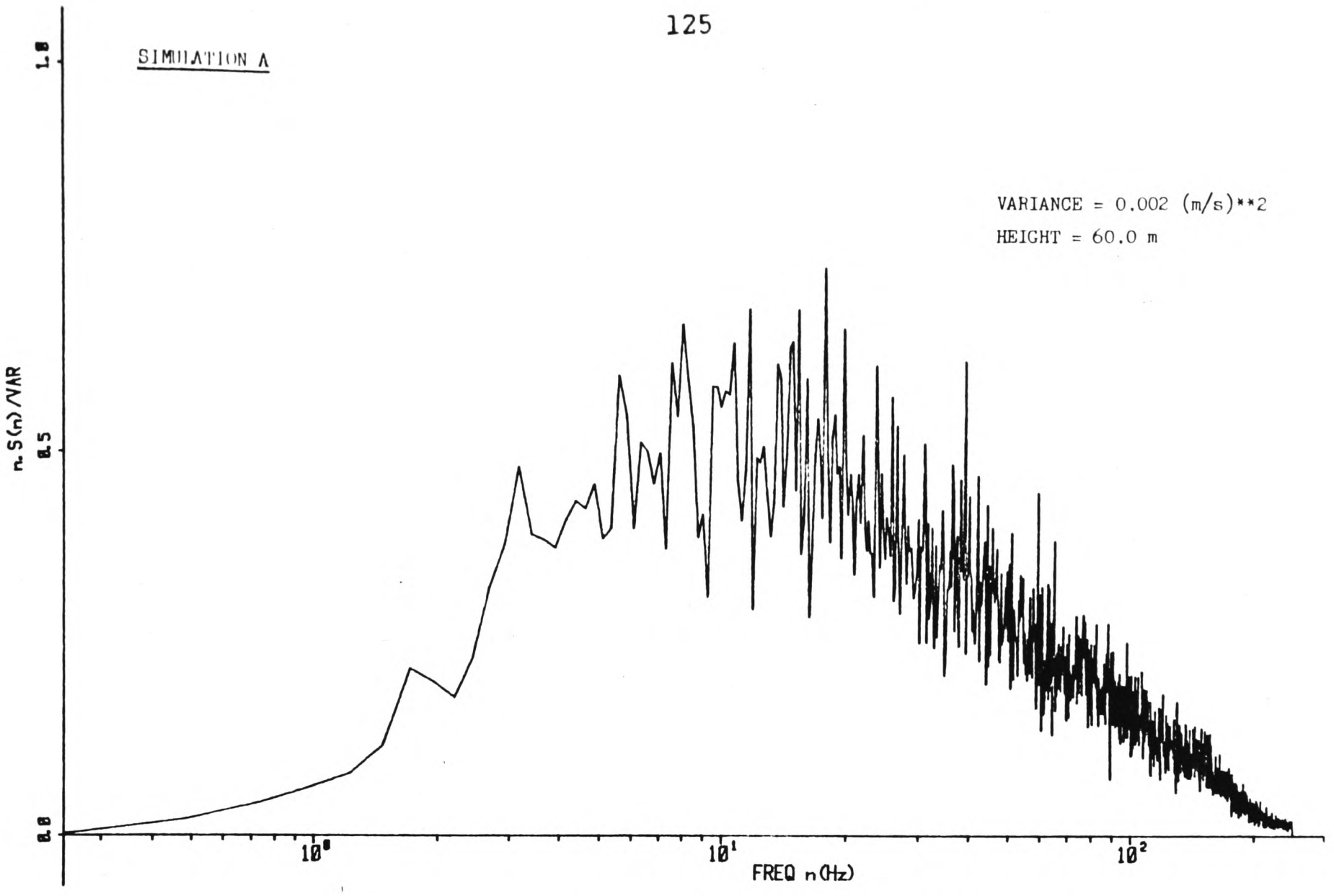

Fig 5.6a Power Spectral Density of Lateral Component at 60.0m f.s. (Simulation A)

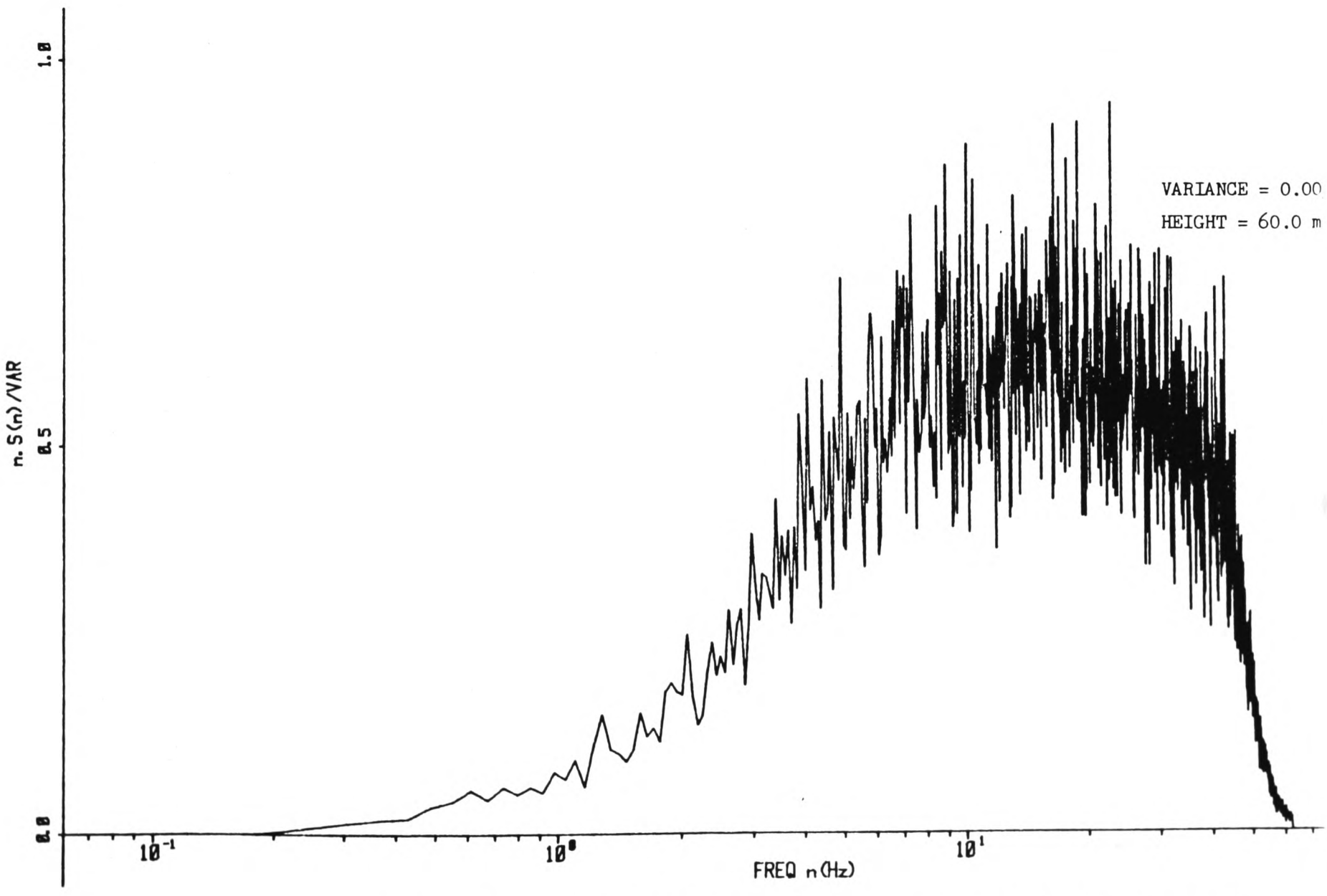

Fig 5.6b Power Spectral Density of Vertical Component at 60.0 m (Simulation A)

SIMULATION B

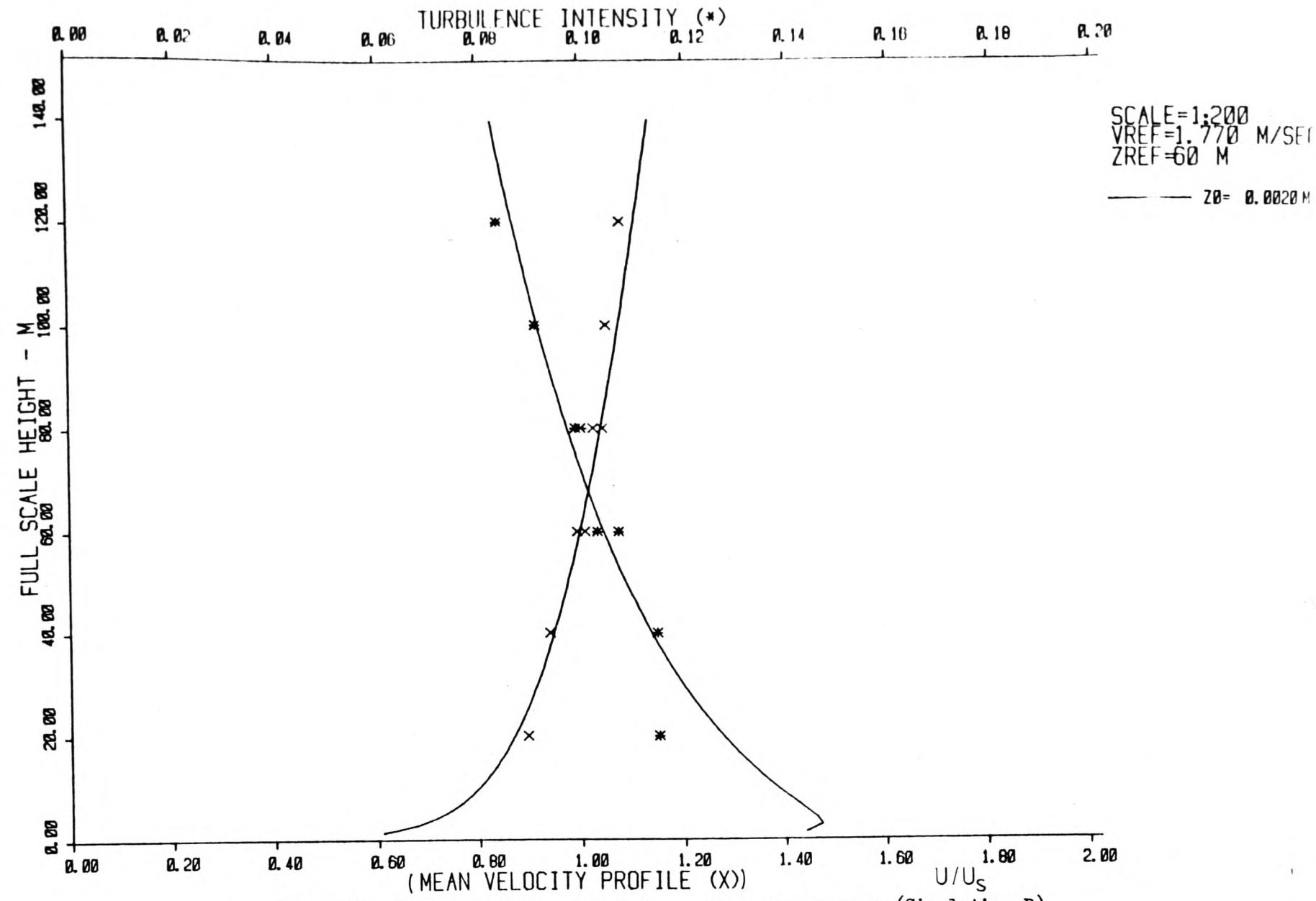

Fig. 5.7a Mean Velocity and Turbulence Intensity Profile (Simulation B)

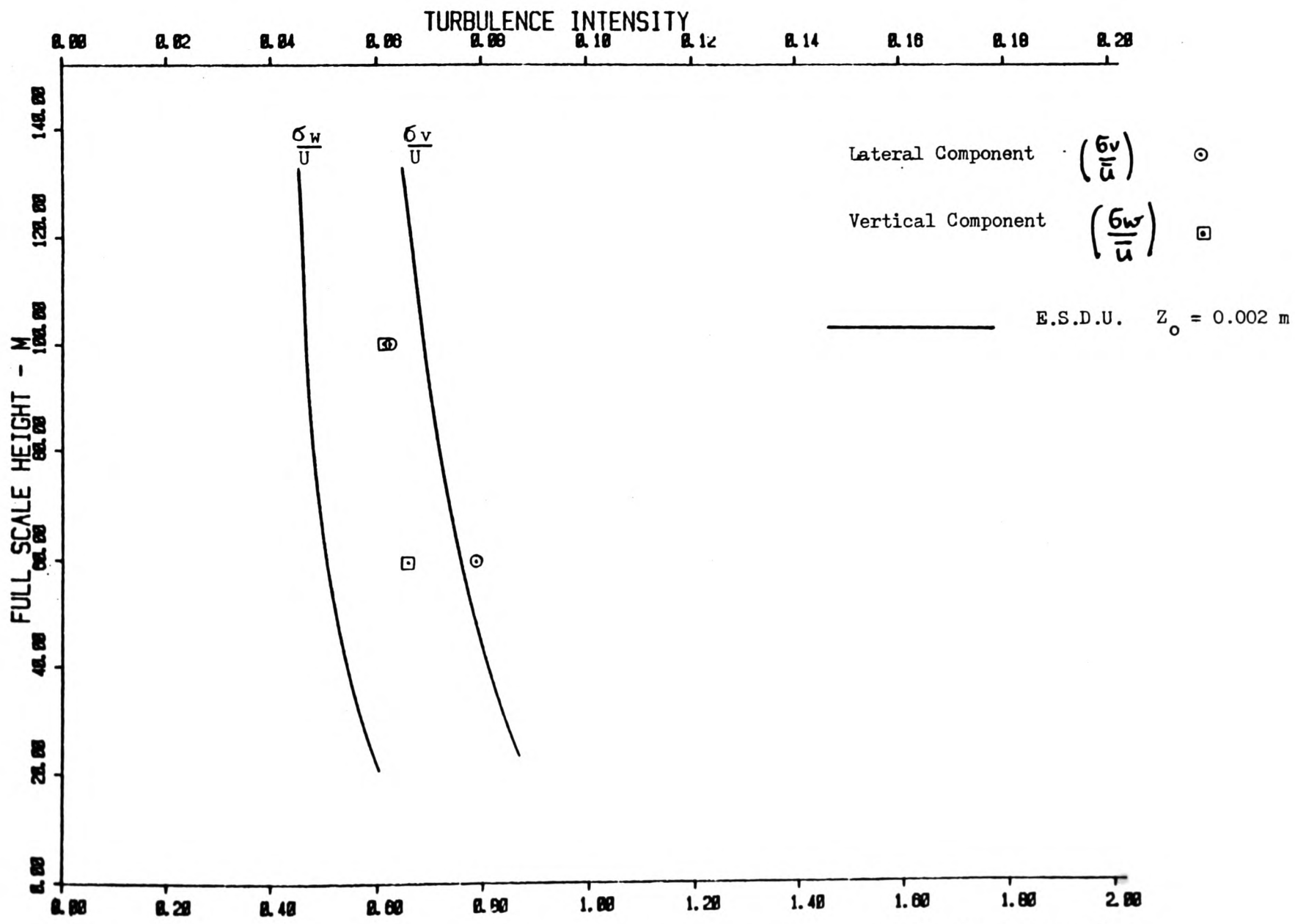

Fig. 5.7b Lateral and Vertical Turbulence Intensity Profiles (Simulation B)

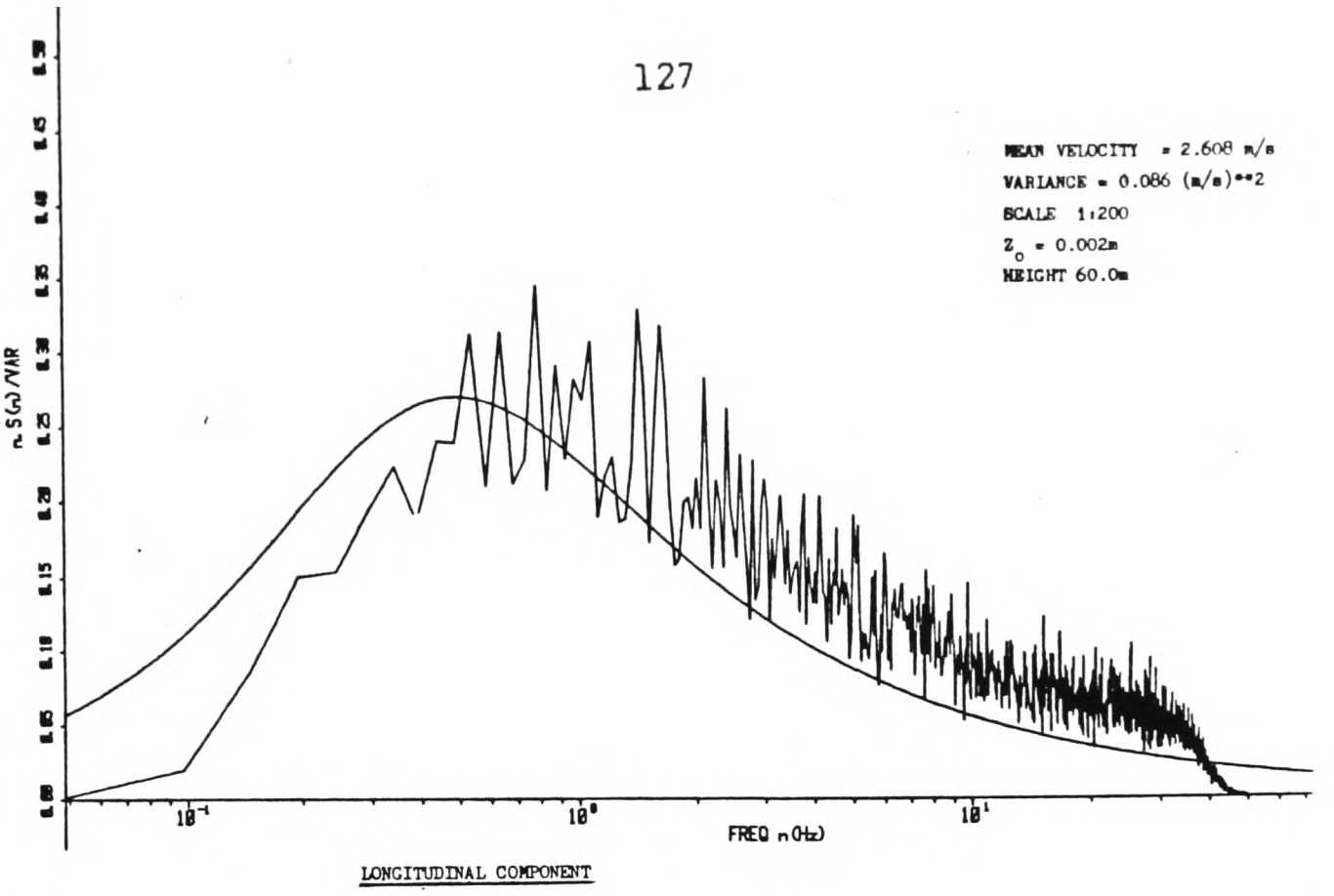

LONGITUDINAL COMPONENT

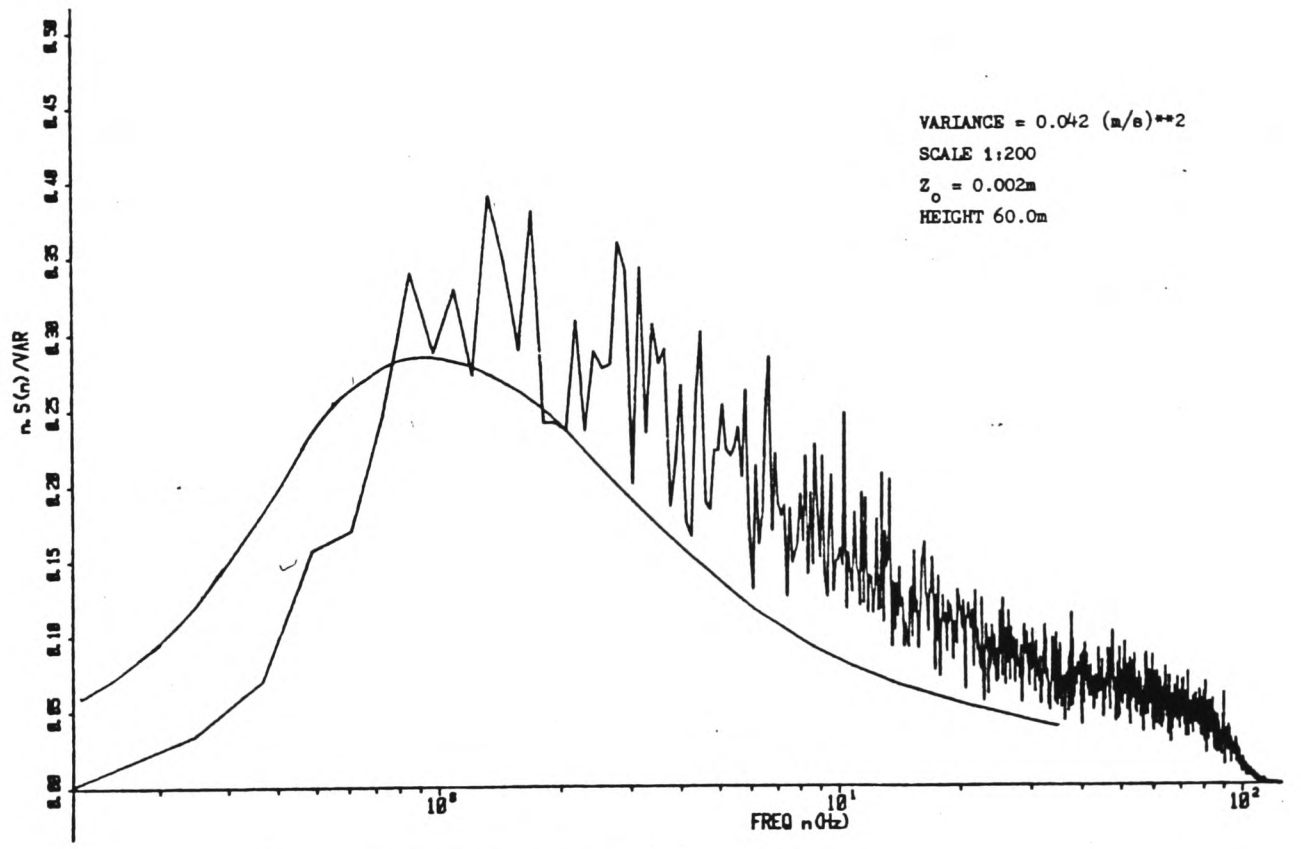

LATERAL COMPONENT

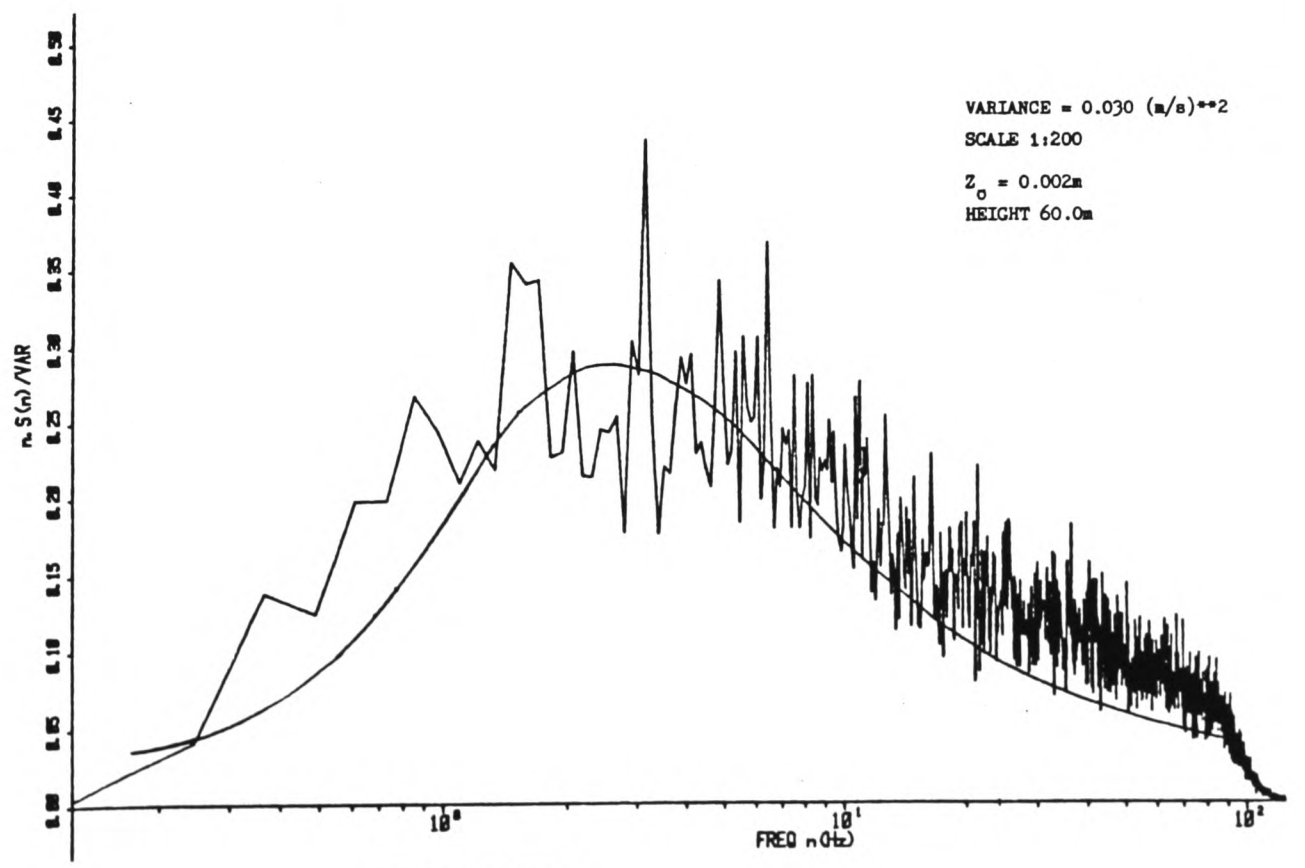

VERTICAL COMPONENT

Fig. 5.8 POWER SPECTRAL DENSITY SIMULATION B

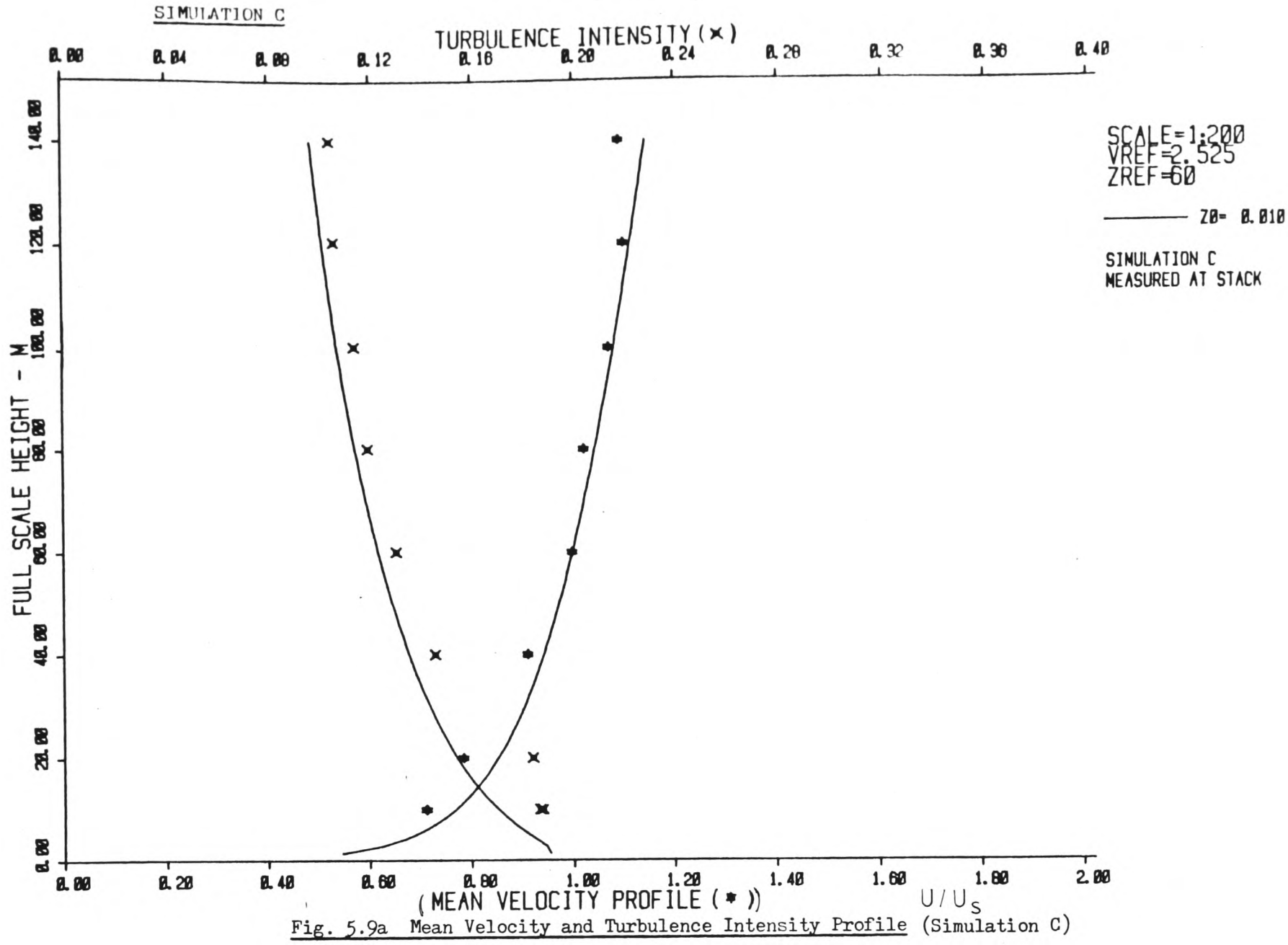

Fig. 5.9a Mean Velocity and Turbulence Intensity Profile (Simulation C)

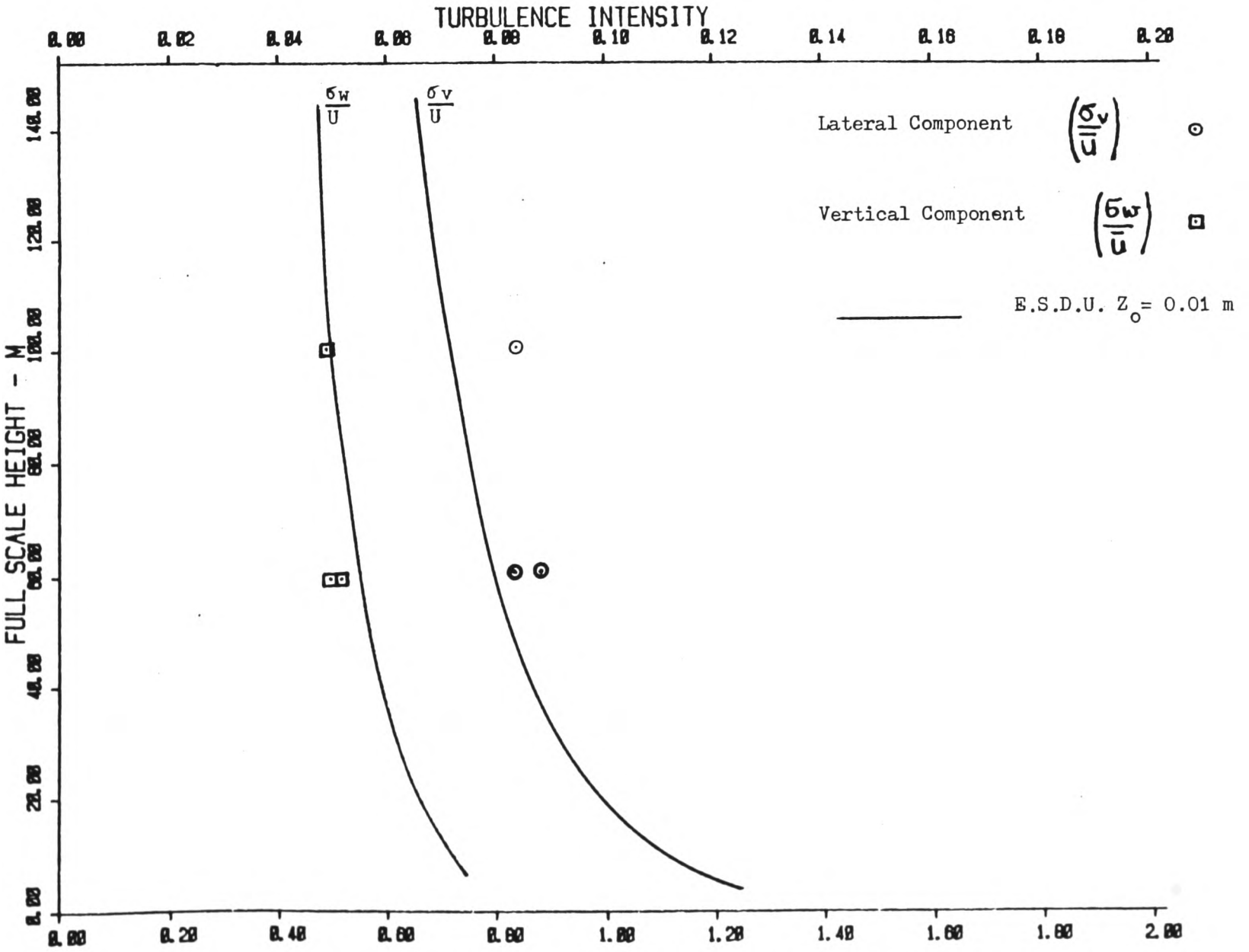

Fig. 5.9b Lateral and Vertical Turbulence Intensity Profiles (Simulation C)

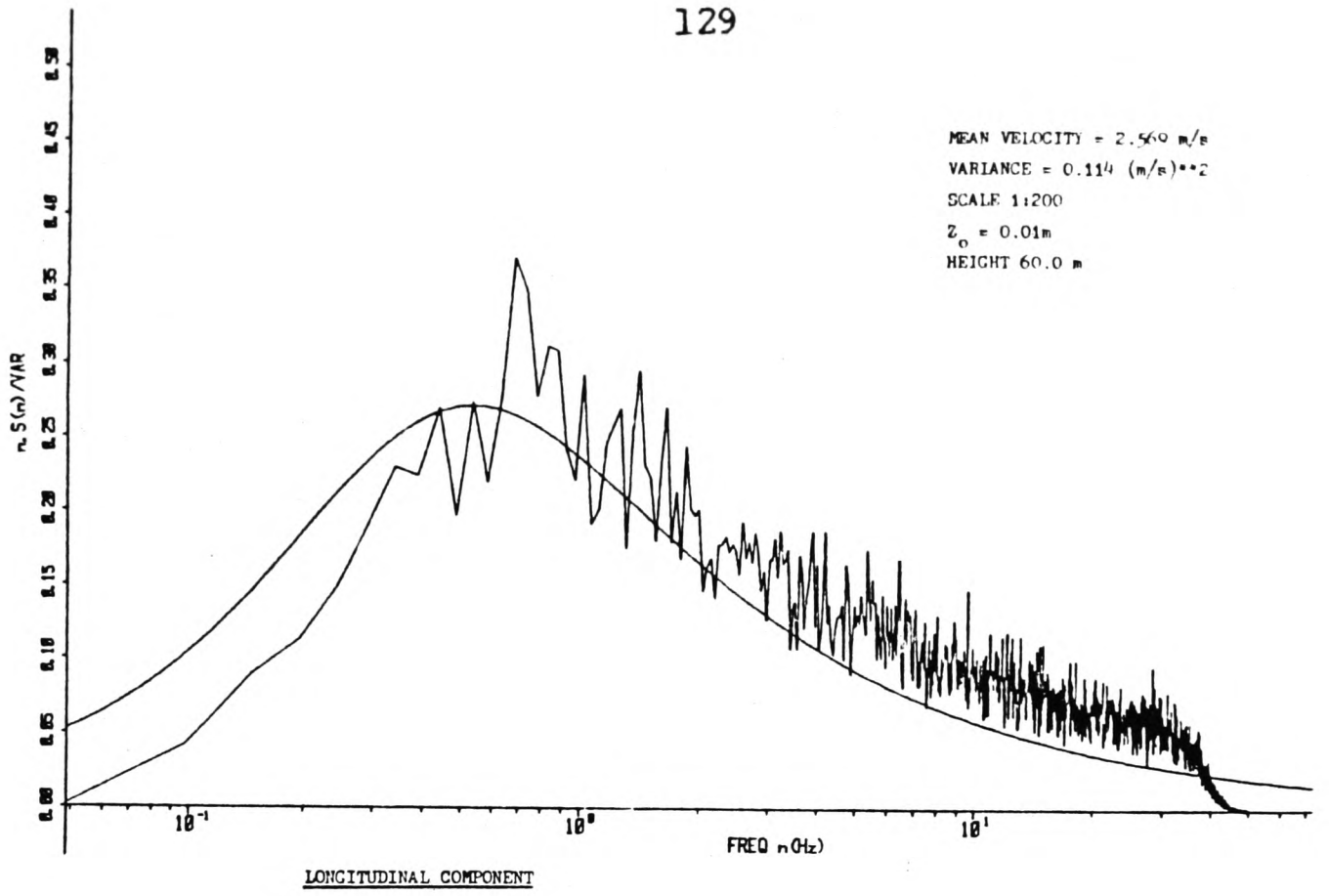

LONGITUDINAL COMPONENT

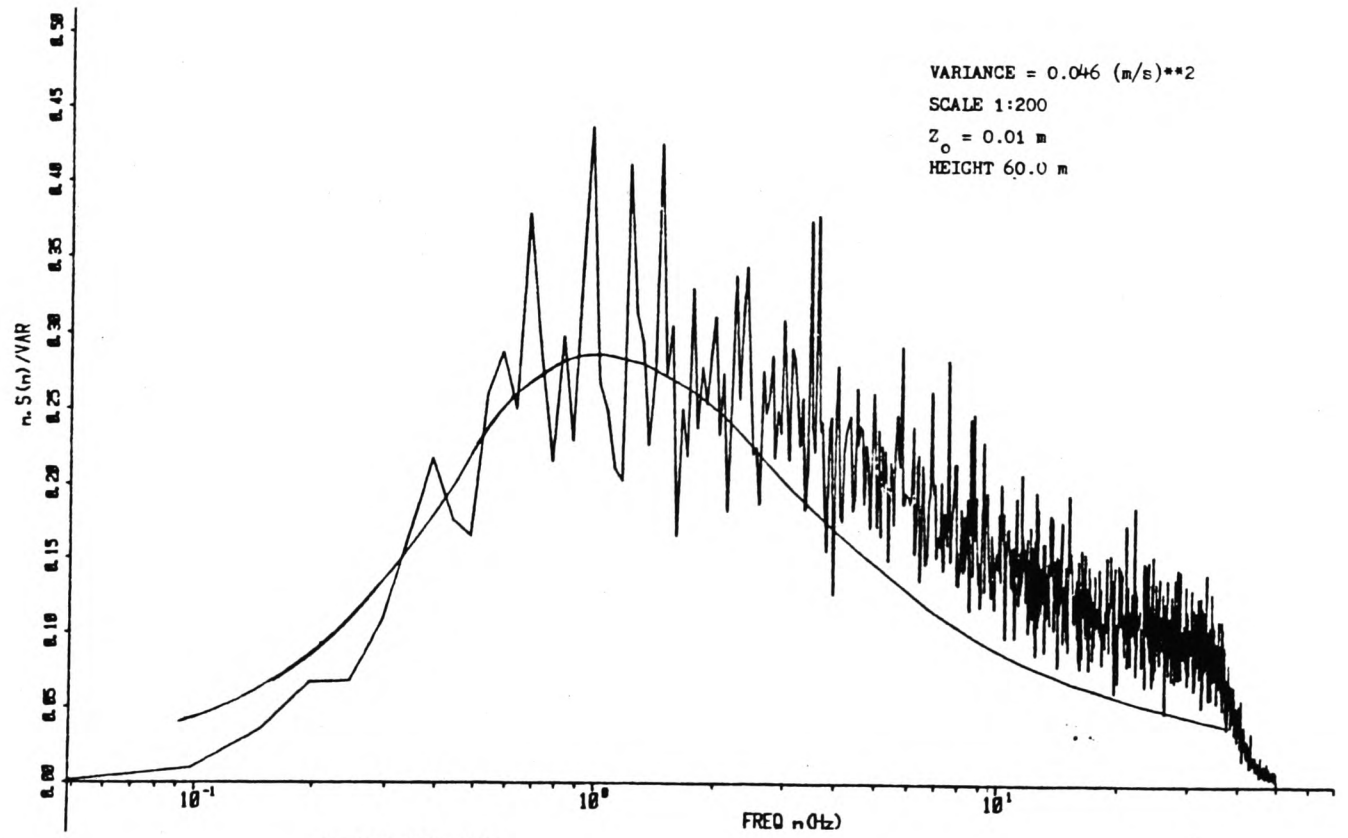

LATERAL COMPONENT

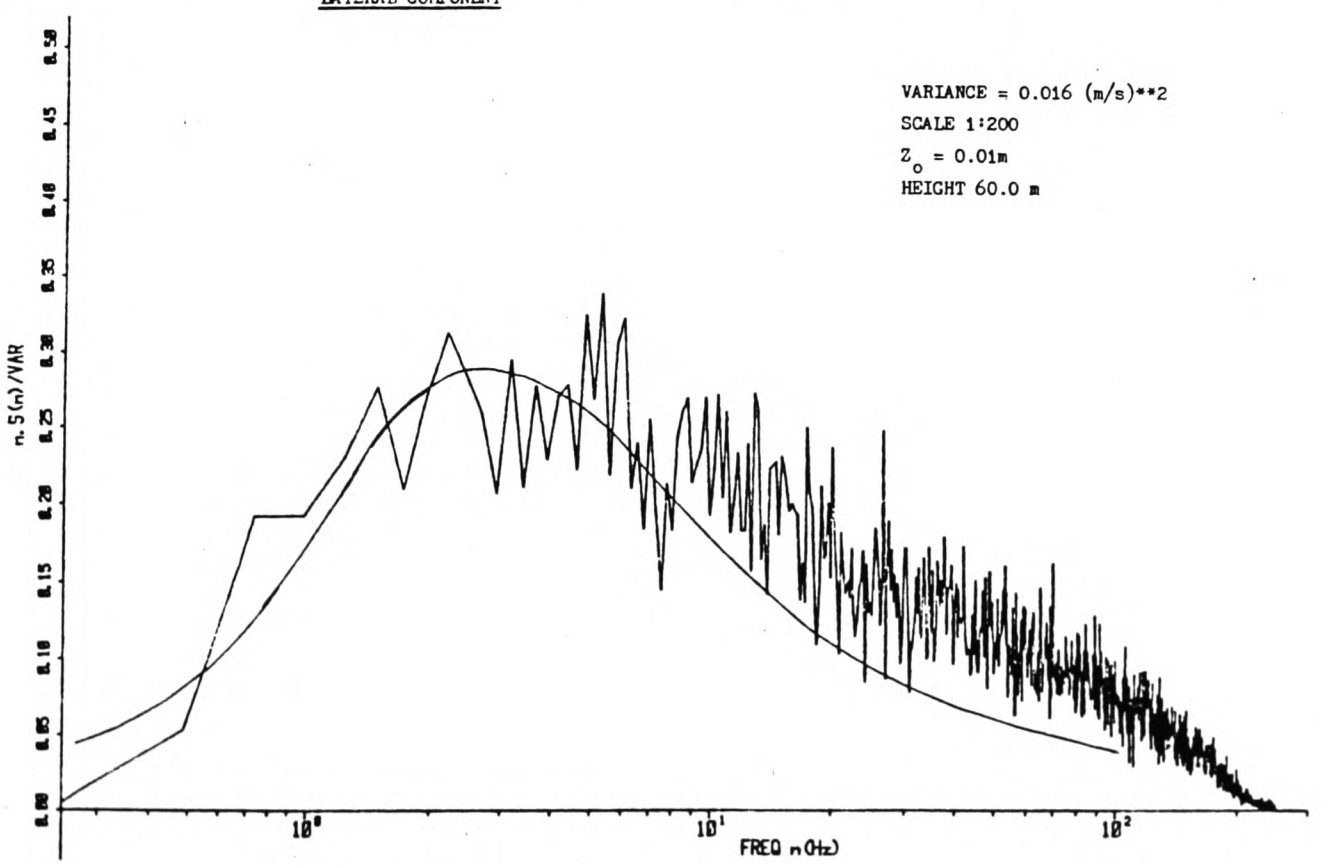

VERTICAL COMPONENT

Fig. 5.10 POWER SPECTRAL DENSITY SIMULATION C

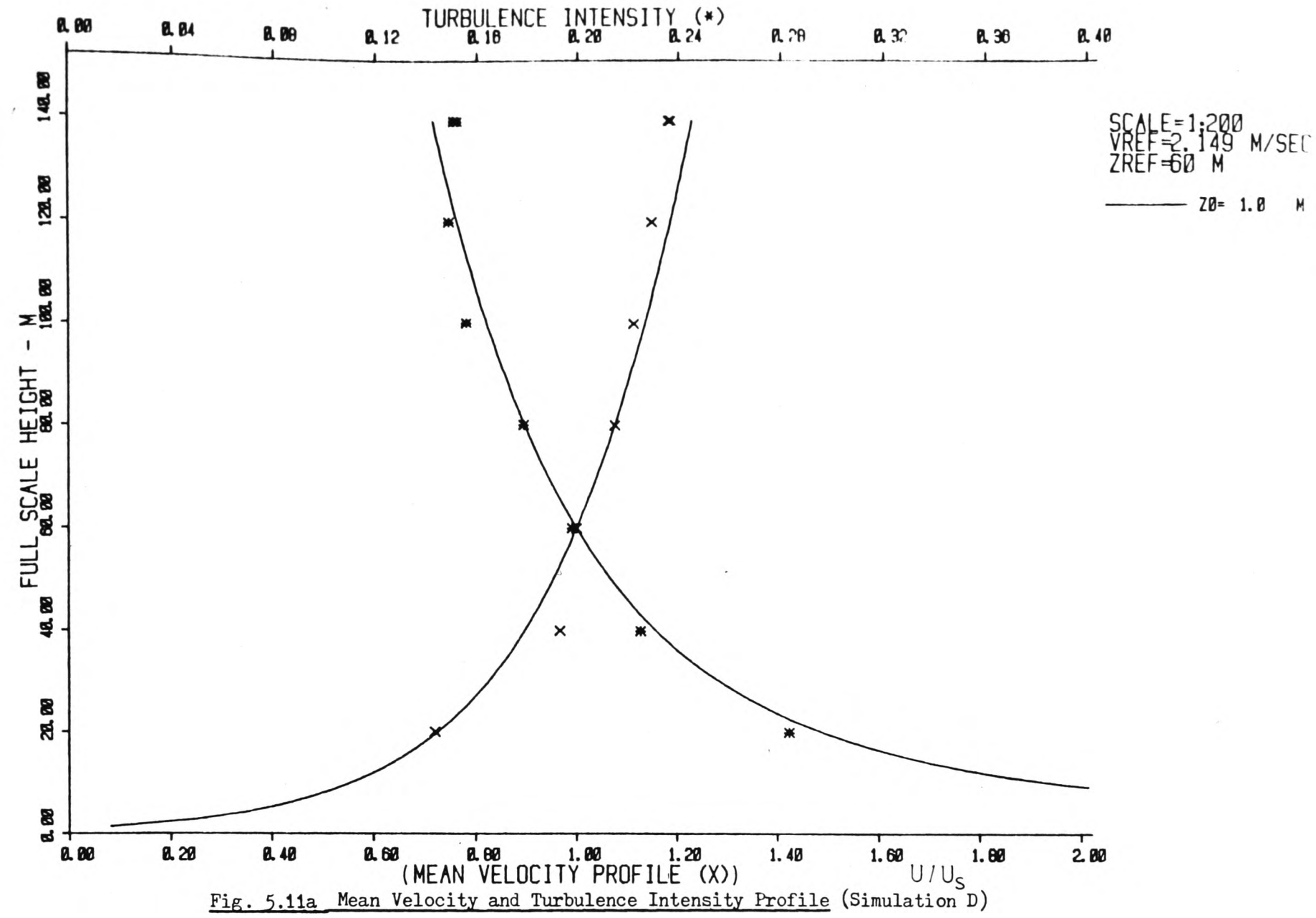

Fig. 5.11a Mean Velocity and Turbulence Intensity Profile (Simulation D)

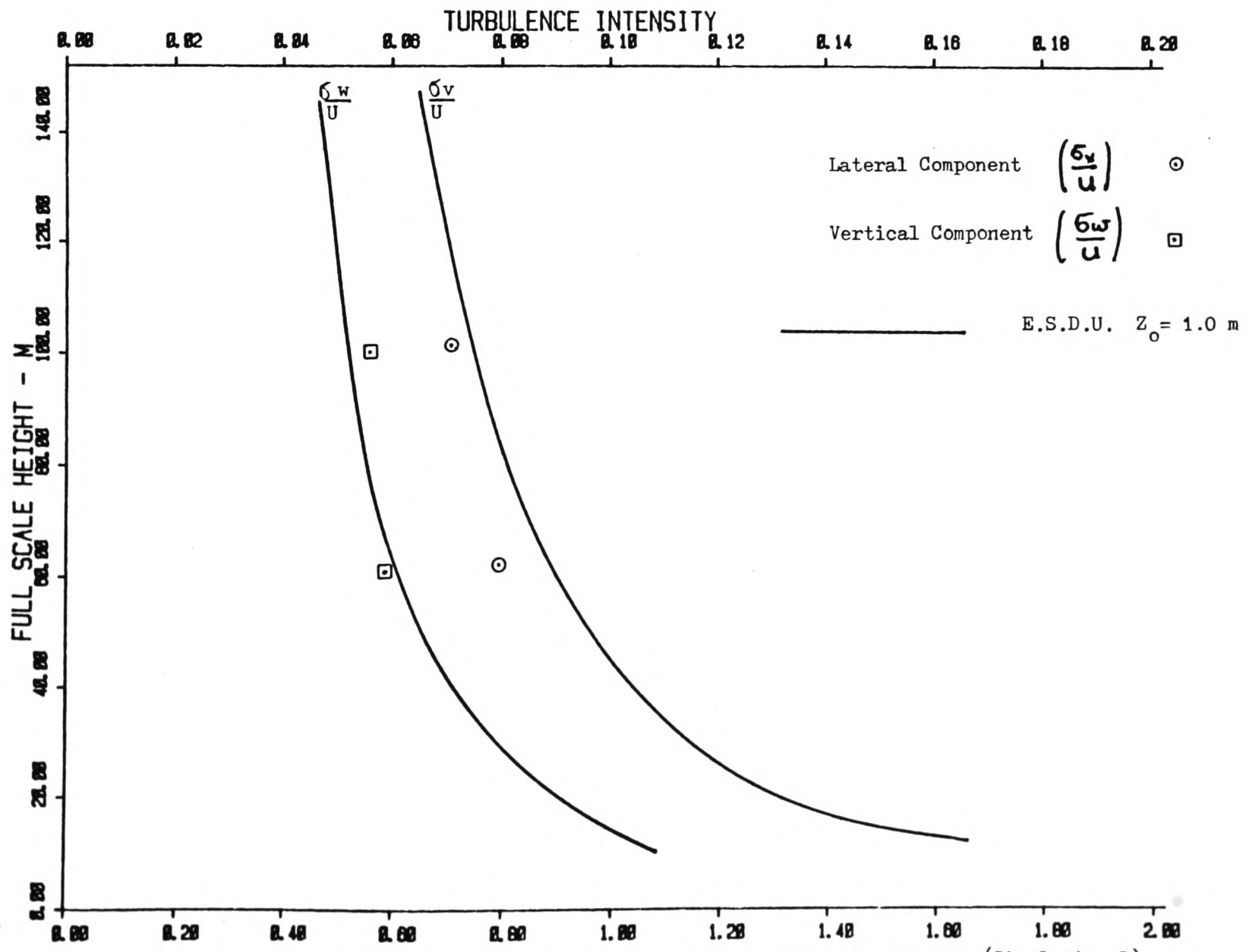

Fig. 5.11b Lateral and Vertical Turbulence Intensity Profile (Simulation D)

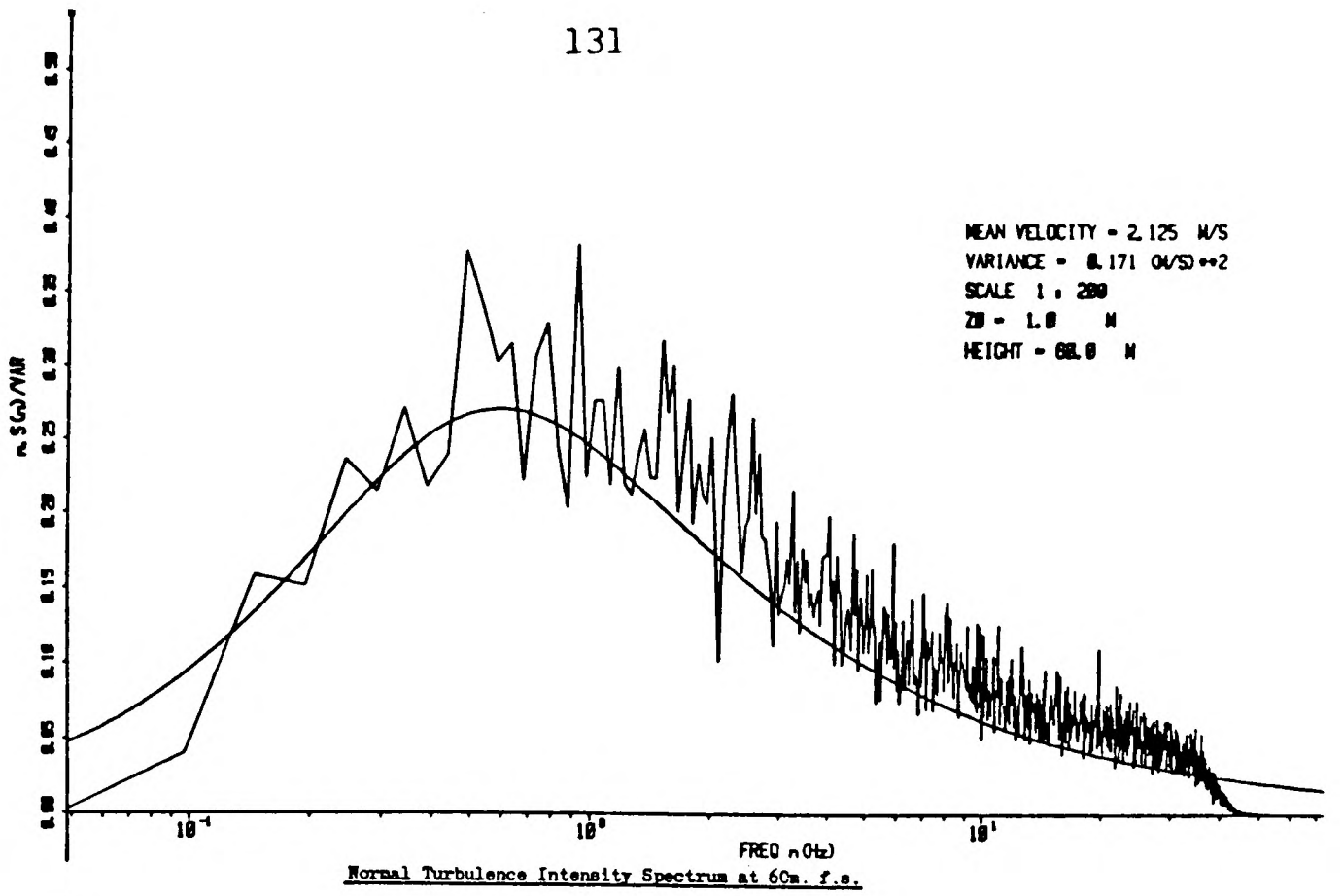

Normal Turbulence Intensity Spectrum at 60m. f.s.

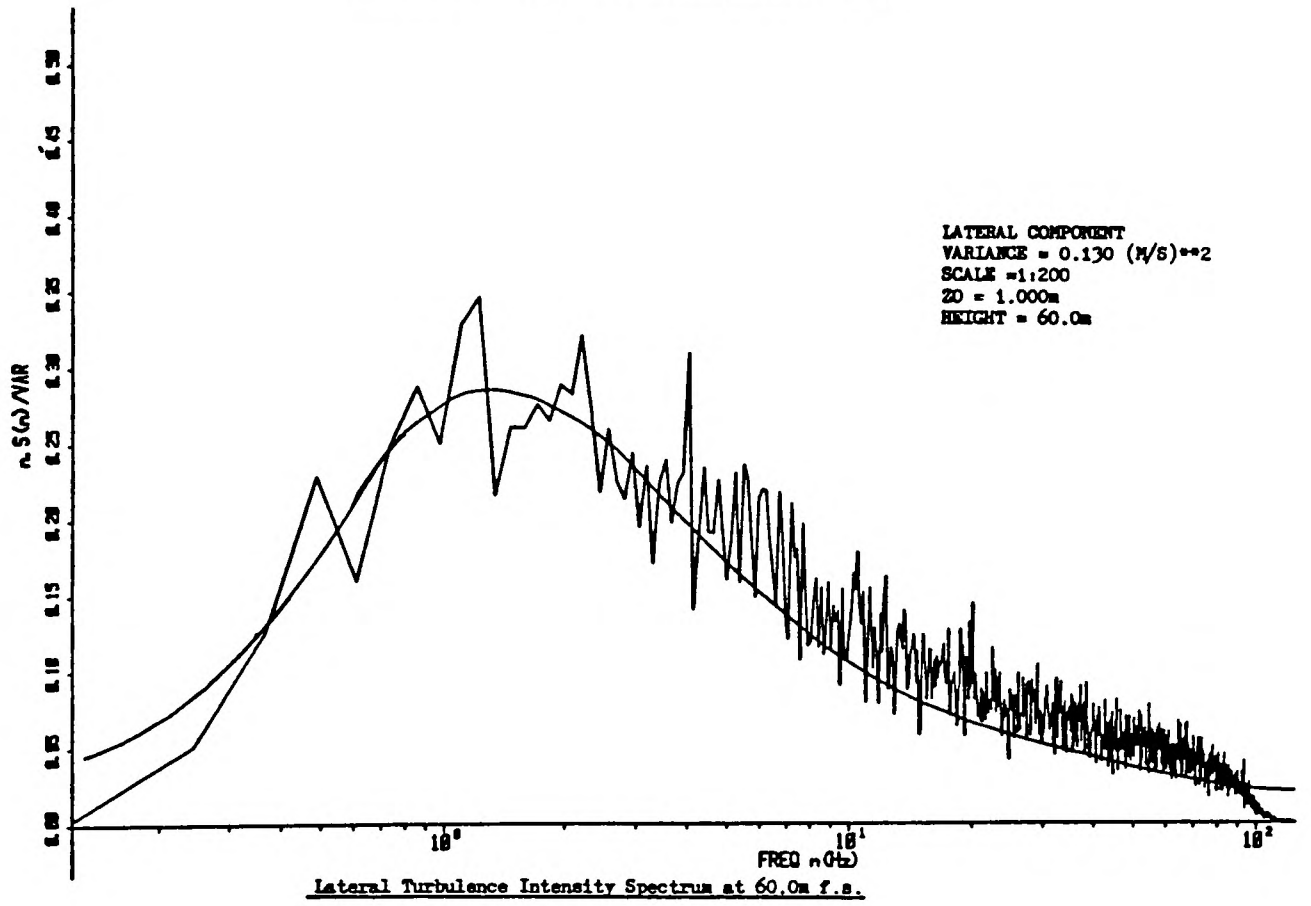

Lateral Turbulence Intensity Spectrum at 60.0m f.s.

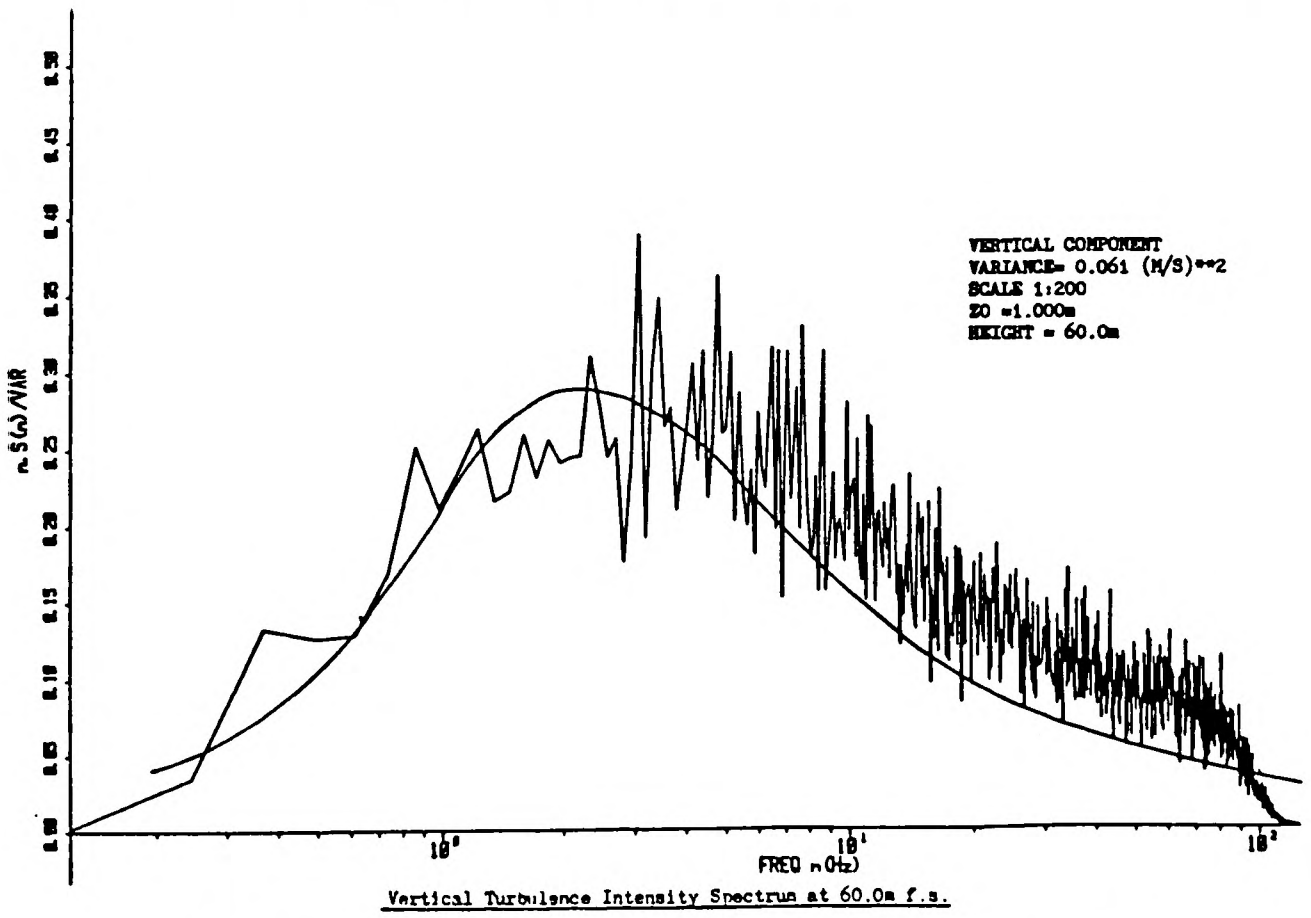

Vertical Turbulence Intensity Spectrum at 60.0m f.s.

Fig. 5.12 POWER SPECTRAL DENSITY SIMULATION D

6 CONDITIONS TO BE INVESTIGATED AND METHOD OF ANALYSIS

6.1 CONDITIONS TO BE INVESTIGATED

At the end of chapter 3 we outlined the three main areas to be studied and the method to be employed. We will now discuss in detail the experiments to be performed. As we discuss these experiments, the method of 'relative' wind tunnel tests should become evident.

In the initial phase of the experiments the plumes were examined by flow visualisation and some preliminary deductions were made. Then, in the second phase, certain plumes were studied more thoroughly using the thermocouple array to make quantitative measurements. Time constraints meant that not all the plumes were studied in the second phase. The results section will concentrate on the second phase because of the quantitative nature of those results. However, reference will be made to the results of the flow visualisation. The flow visualisation was the only means we had of studying the instantaneous behaviour of the plumes since the temperature measurements only yielded results for the mean trajectory and rate of spread.

The starting point for the experiments was the exact or complete similarity requirements for buoyant plume modelling (eqn. 3.24):

$$\frac{z}{d} = f\left\{\frac{x}{d}, \frac{\rho_s}{\rho_a}, \frac{\rho_s w_s^2}{\rho_a u^2}, \frac{gd(\rho_a-\rho_s)}{u^2 \rho_a}, \frac{w_s d}{\nu_s}\right\} \qquad (6.1)$$

It was proposed to study the effect of non-matching of the density ratio, mis-matching of the Reynolds number and the effect of the cross-flow simulation on plume behaviour. As mentioned earlier, the exit Reynolds number is a means of describing the exit flow and we will consider the exit flow characteristics rather than just the Reynolds number.

6.1.1 EXPERIMENTS TO STUDY THE EFFECT OF THE EXIT DENSITY RATIO

In order to determine how important it is to match the density ratio when modelling buoyant plumes, it was decided to study plumes that have all the dimensionless groups in eqn. 6.1, except the density ratio, matched. Thus the role of density ratio should be isolated.

Pairs of plumes were modelled in the wind tunnel such that the two plumes were exactly matched except for the stack gas density. Thus, the following equations express the conditions to be satisfied:

Momentum Ratio Matching:
$$\left(\frac{\rho_s w_s^2}{\rho_a u^2}\right)_a = \left(\frac{\rho_s w_s^2}{\rho_a u^2}\right)_b \qquad (6.2)$$

Densimetric Froude Number Matching:
$$\left(\frac{gd(\rho_a - \rho_s)}{u^2 \rho_a}\right)_a = \left(\frac{gd(\rho_a - \rho_s)}{u^2 \rho_a}\right)_b \qquad (6.3)$$

Exit Reynolds Number Matching:
$$\left(\frac{w_s d}{\nu_s}\right)_a = \left(\frac{w_s d}{\nu_s}\right)_b \qquad (6.4)$$

where the subscripts a and b refer to the two plumes in each pair (confusion with the use of subscript a for ambient conditions should not occur). d, the stack exit diameter, is a constant in these tests. Note that ν_s is a function of gas temperature; over the range of temperatures used this was modelled by a linear dependance on temperature;

$$\nu_s = \nu_{amb} + \nu'(T_s - T_{amb}) \qquad (6.5)$$

The above equations, 2, 3, 4, were solved simultaneously, to obtain relationships between plumes a and b;

$$\theta_a \theta_b = 1/\nu_*^2 \qquad (6.6)$$

where θ = temperature of stack gas above ambient,

$$\frac{w_{sa}}{w_{sb}} = \sqrt{\frac{\theta_a}{\theta_b}} \qquad (6.7)$$

$$\frac{u_a}{u_b} = \sqrt{\frac{(\theta \rho_a)_a}{(\theta \rho_a)_b}} \qquad (6.8)$$

where $\nu_* = \frac{\nu'}{\nu_{amb}}$ is a constant and $1/\nu_* \doteq 117\,^{\circ}C$.

A set of four pairs of plumes was chosen to be investigated. The stack exit temperatures (T) were chosen to cover a wide range of typical exit temperatures, and the temperature mismatch ($T_a - T_b$) was gradually decreased in the four pairs. Also in two pairs $T_a < 215^{\circ}C$, while $T_b > 215^{\circ}C$. These were chosen to examine Hoult and Weil's warning about the entrainment mechanism changing when $\ell_a - \ell_s / \ell_a > 0.4$, (i.e. $T_s = 215^{\circ}C$, for $T_{amb} = 20^{\circ}C$). The model values were chosen to be realistic for a 1:200 scale model of an industrial chimney stack (velocity scaling = 1:14) and the following criteria were considered in choosing the velocities used;

i) $U > 0.5\ ms^{-1}$, to avoid the problems of low speed operation of the wind tunnel,

ii) $w_s / U > 2.0$ and $R_{mom} > 2.5$, to avoid stack downwash of the plume,

iii) $w_s d / \nu_s > 2000$, to ensure a turbulent exit flow.

The four pairs of plumes are detailed in Table 6.1a.

6.1.2 EXPERIMENTS TO STUDY THE EFFECT OF THE EXIT FLOW

In this section we want to examine not only the effect of the Reynolds number but also the role of other exit flow characteristics, e.g. mean velocity profile, turbulence intensity. The Reynolds number is only one parameter describing the exit flow and the actual flow characteristics themselves are probably more significant.

The experiments can be divided into two sets; a set in which the plume's exit Reynolds number was increased from 1,000 to 3,000, and a set in which the exit flow characteristics were deliberately distorted in order to study their effect. Measurements of the following exit flow characteristics were made for all the plumes studied and are discussed in the next section; mean velocity profile, turbulence intensity profile and power spectral density. It was hoped that plume behaviour could

then be related to these characteristics rather than the general Reynolds number term.

In order to investigate the effect of the Reynolds number on plume behaviour it was decided to study a set of plumes which were matched except for the Reynolds number and to vary the Reynolds number over as wide a range as possible.

Originally, it was intended to match plume momentum ratio and densimetric Froude number while varying the Reynolds number. This required the following equations to hold:

Momentum Ratio Matching:
$$\left(\frac{\ell_s w_s^2}{\ell_a u^2}\right)_a = \left(\frac{\ell_s w_s^2}{\ell_a u^2}\right)_b \qquad (6.9)$$

Densimetric Froude Number Matching:
$$\left(\frac{gd}{u^2}\left(\frac{\ell_a - \ell_s}{\ell_a}\right)\right)_a = \left(\frac{gd}{u^2}\left(\frac{\ell_a - \ell_s}{\ell_a}\right)\right)_b \qquad (6.10)$$

In addition the following conditions were imposed on the plumes:

i) $U > 0.5$ ms^{-1}, to avoid low speed operation of the tunnel,

ii) $w_s/U > 2.0$ and $R_{mom} > 2.5$ to avoid downwash,

iii) $d = 24.5$ mm, only one model stack used.

Solving the above equations and applying the above conditions, we found that the range of Reynolds numbers would be limited. The results are summarized in fig. 6.1. Each curve shows the variation with temperature of the Reynolds number of a matched plume, when the original plume has the temperature marked on the curve and unity exit velocity. For example, at 200°C the original plume has a Reynolds number of 715 while a matched plume at 300°C (say) would have $R_{ex} = 645$. Clearly the range can be increased by using a higher initial velocity but for realistic conditions the upper limit would be about 4 ms^{-1}. To overcome these problems it was decided to relax densimetric Froude number scaling since it was believed that Reynolds number effects would mainly be important in the near-field which is controlled by the momentum ratio

rather than the densimetric Froude number. Therefore, momentum ratio and exit gas density were matched:

Momentum Ratio matching $$\left(\frac{\rho_s w_s^2}{\rho_a u^2}\right)_a = \left(\frac{\rho_s w_s^2}{\rho_a u^2}\right)_b \qquad (6.11)$$

Exit Density Ratio matching $$(\Delta\rho/\rho_a)_a = (\Delta\rho/\rho_a)_b \qquad (6.12)$$

This means that having matched the exit gas density, the exit velocities (w_s) can be chosen arbitrarily and then the onset wind velocities are scaled as the exit velocities (note that since the exit gas density is constant this is equivalent to velocity ratio matching). In this manner, a wider range of Reynolds numbers was achieved. A set of four plumes, with realistic conditions, was studied with conditions given in Table 6.1b, p. 172.

As we can see, the Reynolds number was varied by a factor of two, and although this is not a wide range, the flow visualisation showed that there was an effect on plume behaviour. Clearly, we would have liked to have examined a wider range of Reynolds numbers but without changing the stack diameter or using unrealistic exit velocities this would not be possible. Due to time constraints, the number of plumes which could be studied was limited and it was decided to study plumes with Reynolds numbers close to the critical Reynolds number since the greatest effect on plume behaviour would be expected in this range. Also, this range is typical of those normally used in wind tunnel studies. Different exit diameters could not be used since this would distort geometric scaling. Exaggerated exit velocities would not help since it is the low Reynolds number flows which are difficult to achieve. We cannot achieve low Reynolds numbers (for the given exit diameter) because we cannot use low enough exit velocities without downwash of the plume into the stack wake. And we cannot reduce the cross-flow below about 0.5 ms^{-1} because the tunnel flow then becomes

non-stationary. (The author realises that the exit diameter used may be considered quite large and that using a smaller diameter would have produced smaller Reynolds numbers. However, the above comments relate to the range of Reynolds numbers possible and using a smaller diameter would have produced small Reynolds numbers. In fact, it may not have been possible to produce a flow above the critical Reynolds number (2000) without significantly exaggerating the velocities. Then the conditions would not be modelling a realistic prototype. Nevertheless, this would have been a means of achieving a wider range of Reynolds numbers in this study. An additional reason for using the 24.5 mm diameter was that we could accurately measure exit profiles with the equipment available. With a smaller diameter it would have been very difficult to have distinguished between different exit profiles since, as we shall see later, the profiles are very similar for the Reynolds numbers investigated.)

Plumes 6,7,8 were studied by temperature measurements in the second phase of the study. It was not possible to study plume 5 because a stationary flow could not be achieved in the tunnel at 0.54 ms^{-1}.

In addition to plumes 6,7,8, two other plumes with different exit flow characteristics were studied. Firstly, plume 7b in which a 7.5 cm length of honeycomb was placed in the upper part of the stack. The honeycomb was made from metal foil and aligned with the stack so that it divided the main flow into several stream tubes of about 4 mm x 10 mm. The openings in the honeycomb were irregular in shape, the exit plane with the honeycomb in position is sketched in fig 6.7. The honeycomb was used to produce a distorted exit velocity profile so that we could study the role of the profile in plume behaviour.

The final plume studied, 6b, had the upper 10 cm of the inside of the stack roughened by placing a tube of sandpaper in the stack. The

average grain diameter was 0.020", giving a roughness factor R/k = 24.1. Placing the sandpaper in the stack also reduced the effective diameter of the stack by about 1 mm. Roughening the inside of the stack is a technique often used by modellers to produce a 'turbulent' exit flow. Therefore, this plume was studied to examine what effect roughening the stack has on the exit flow characteristics and on plume behaviour, and whether it produces a more 'turbulent' flow. Schlichting(1979) presents data for turbulent flows in pipes which shows that roughness reduces the velocity near the wall and causes the velocity profile to deviate from that for a fully turbulent flow in a smooth pipe, i.e. expressing the profile in power law form results in n = 1/4 to 1/5.

6.1.3 MEASUREMENTS OF THE EXIT FLOW CHARACTERISTICS

The exit flow characteristics at different Reynolds numbers were measured using a single wire, hot wire anemometer. The characteristics measured were the mean velocity profile, longitudinal turbulence intensity profile and the power spectral density. The experiments were made in the wind tunnel with no cross-flow. The hot wire was placed as close as possible to the exit plane and traversed across the exit plane using a stepper motor. The fragile nature of the hot wires meant that in practice the wire had to be about 1 mm above the exit plane. It was considered that the flow would not change significantly in this short distance, although, the flow at the edge will be changing due to the removal of the shear stress at the wall.

The exit velocity profile was measured at Reynolds numbers of 1000, 2500 and 7200; the results are shown in fig. 6.2. The most obvious feature is that the values of the centre-line velocity decrease with increasing Reynolds number. We would expect this since it is well known that for a laminar flow $\hat{U}/\bar{U}$ is 2.00 and that for fully turbulent

flow it is 1.22 (-as for the flow at R_{ex} = 7200), where $\hat{U}$ is the peak velocity. Clearly the flow at R_{ex} = 1000 is not laminar and the flow at R_{ex} = 2500 is not fully turbulent.

If we actually integrate the velocity profile to determine the momentum leaving the stack and non-dimensionalise the result by the momentum based on the mean velocity, we obtain the momentum correction factor:

$$\beta = \int_0^{d/2} \frac{2\pi r\, u(r)^2 .dr}{\pi d^2 \bar{u}^2/4} \qquad (6.13)$$

For a laminar flow, β = 1.33; for a turbulent flow, β = 1.02. Thus momentum ratios based on the mean velocity will underestimate the true momentum in a laminar flow by 33%.

It is this discrepancy which Wilson (1979b) tried to correct by writing the momentum ratio as $\beta \rho_s w_s^2 / \rho_a U^2$. (However, as mentioned earlier, Wilson was unable to explain the differences that he found in the plume trajectories of laminar and turbulent plumes by this correction factor. We will return to this point in greater detail in the next chapter.)

A value for β was calculated for R_{ex} = 1000, 2500 and 7200 by numerical integration of the results and found to be 1.22, 1.20 and 1.06 respectively. Thus the actual difference in β values for R_{ex} = 1000 and 2500 is very small in our experiments.

The above discussion refers to an isothermal exit flow. In practice, there will be an exit temperature profile for hot plumes. The exit temperature was measured using thermocouples for an exit centre-line temperature of 81 °C and R_{ex} = 2,300, and is shown in fig. 6.3. The exit profile is 'flat-topped' and similar to the turbulent velocity profile. We would expect this since Reynolds' Analogy suggests that heat and momentum are diffused similarly in a turbulent flow of a fluid with a Prandtl number close to unity.

The effect of the temperature profile will be to make β values based on the peak temperature even greater.

Thus
$$\beta' = \int_0^{d/2} \frac{2\pi r\, \ell(r)\, u(r)^2 \cdot dr}{\pi d^2\, \ell(r{=}0)\, \bar{u}^2/4} \qquad (6.14)$$

For a turbulent flow $\beta' = 1.18$, for a laminar flow $\beta' = 1.57$. Numerical integration of the above temperature profile for $R_{ex} = 2500$ gave $\beta' = 1.19$. This value is suprsingly close to the value for a turbulent flow. The temperature profile was not measured at a lower Reynolds number but since the velocity profiles are not very different at $R_{ex} = 1000$ and 2500 we may expect the the temperature profiles to be similar (Reynolds' Analogy). Thus the values of β' at $R_{ex} = 1000$ and 2500 would probably be quite similar and probably not differ by more than 10%.

To examine the velocity profiles further, the previous results were plotted on log-log axes and are shown in fig. 6.4. These plots illustrate the difference between the profiles more clearly. First, consider the high Reynolds number flow ($R_{ex} = 7200$). The profile is quite steep and almost linear, and is close to the '1/7th power-law' we would expect for a turbulent flow. The profiles at the lower Reynolds numbers are linear in the central region but exhibit a region of high shear in the outer 4 mm. The lower Reynolds number flow ($R_{ex} = 1000$) has a lower relative velocity in the outer region.

Also shown in fig. 6.4 is the profile that results from roughening the inside of the stack, at $R_{ex} = 2500$. The effect of roughening the inside of the stack has been to reduce significantly the velocity in the outer region (close to the wall). In fact, roughening the inside of the stack has made the flow (at $R_{ex} = 2500$) more like the lower Reynolds number flow ($R_{ex} = 1000$). Thus it has not produced a turbulent exit velocity profile but has had the opposite effect, producing a more laminar-like profile. There is no reason to suppose that the same

effect would not occur in the lower Reynolds number flows.

The longitudinal turbulence intensity was also measured and the resulting profiles are shown in figs. 6.5 for R_{ex} = 1000, 2500 and 7200. The profiles have a minimum on the centre-line of 4% (very close to the fully-turbulent value of 3%, Hinze (1959) fig. 7-59), and then rise to a much higher value of about 20% at the outer edge. The profile at R_{ex} = 1000 is not as flat as at higher Reynolds numbers and, perhaps more significantly, the turbulence intensity does not reach as high a value at the outer edge. For R_{ex} = 2500 and 7200, $\sigma u/U$ is above 20% at the edge, whereas for R_{ex} = 1000 it was below 20% (Hinze suggests that $\sigma u/U$ reaches a value of about 30% for a fully-turbulent flow at the wall).

Roughening the inside of the stack, at a Reynolds number of 2500, had no discrenible effect on the turbulence intensity profile.

Plume 7b, in which a 7.5 cm length of honeycomb was placed in the upper stack, was used to investigate the effect of having a distorted exit velocity profile. The resulting exit flow was measured for a nominal Reynolds number based on stack diameter of 2500. The results are presented in fig 6.7. Clearly, the mean velocity profile does not show a smooth form and consists of several peaks as we might expect since the honeycomb causes several smaller jets to be formed. It was not possible to calculate the exit momentum flux (or β) since this would require a very extensive set of velocity measurements. But clearly the exit velocity profile is unlike any other flow used in this study and should show how important it is to model the exit velocity profile for plume modelling. The turbulence intensity profile was also measured and is unlike those previously discussed, it shows low values of turbulence intensity (<4%) over a large section of the profile.

Finally, the power spectral density was determined from the velocity signal, at the centre of the stack and 1 mm from the edge. The

results for R_{ex} = 1000 and 2500 are shown in figs. 6.6a & b. The results at R_{ex} = 7200 and with the stack roughened were very similar to those at R_{ex} = 2500, and are not shown.

In order to derive some quantitative measurements from the spectra, in an attempt to differentiate between spectra which visually are very similar, the following characteristics were derived. Firstly, a measure of the width of the spectra was given by the ratio of the width of the spectrum (dn), to the modal frequency ($\hat{n}$), and also, in order to relate the spectra to length scale, the relative position of frequencies corresponding to the pipe diameter were determined. (The modal frequency was determined by considering a smooth curve through the spectrum rather than taking the absolute peak value.)

The results are given in Table 6.2. They suggest that at the centre of the stack the relative width of the spectrum decreases as the Reynolds number increases and that roughening the stack does actually increase this trend (and makes the flow more like a turbulent flow). At the edge of the stack the trend is reversed and the low Reynolds number flow is relatively narrower, this can be observed in fig. 6.6b.

The frequencies corresponding to the pipe diameter were calculated and marked on the graphs, see figs. 6.6a & b. There is clearly much more 'relative' turbulent energy (n.S(n)/var) at frequencies corresponding to the pipe diameter in the higher Reynolds number flow. Bearing in mind that

$$\int_{n_1}^{n_2} \frac{n\,S(n)}{Var}\,.\,d(\ln n) \qquad (6.15)$$

represents the fraction of the total turbulent energy between frequencies n_1 to n_2(-the integral from 0 to ∞ is, of course, unity). Then, we can see that there is relatively more energy in frequencies corresponding to the pipe diameter, and smaller lengths, in the higher Reynolds number flow. This is especially true at the centre of

the stack but also true at the edge.

At the highest Reynolds number investigated (R_{ex} = 7200) the frequency corresponding to the pipe diameter was almost coincident with the modal frequency. Thus there is a significant increase in the amount of turbulent energy in eddies of the pipe diameter, and smaller, as the Reynolds number increases. The amount of energy between the frequencies corresponding to the pipe diameter and the pipe radius were determined for R_{ex} = 1000, 2500 and 7200, at the stack centre, and were found to be 0.9%, 5.7% and 10.5% respectively of the total energy in the spectrum.

A large fraction of the energy in the spectra, especially at R_{ex} = 1000, corresponds to length scales greater than the pipe diameter. However, most of the energy is at length scales smaller than 35 cm, the length of the inner tube, which suggests that this energy is caused by fluctuations in velocity along the tube. These fluctuations are probably caused by the several changes in pipe diameter in the supply pipeline (including the heat exchanger).

Finally, we should consider the significance of the above flow characteristics for plume behaviour. The momentum correction factor β, will have an effect on plume trajectory since the 'near-field' behaviour is momentum dominated. However, for the plumes used in our experiments the β values were not expected to vary by more than 10%, therefore this may not be an important factor in this study. Also, plume 7b should reveal the significance of the exit velocity profile.

The effect of the flow characteristics on the rate of entrainment may be more important since spreading in the 'near-field' is considered to be dominated by self-generated turbulence. In the Slawson and Csanady plume model, the rate of entrainment in the initial phase is proportional to the vertical centre-line velocity. In the flows at R_{ex} = 1000 and 2500 the non-dimensional centre-line velocities only

differed by 5%, therefore, we would expect the rates of entrainment to be quite similar.

Considering the physical nature of entrainment further, it has been suggested by several authors, e.g. List (1982), Townsend (1980), that the initial entrainment in jets is caused by large-scale motions at the edge of the jet. Flow visualisation, List (1982), has clearly shown large vortices which trap ambient air and transport it into the jet where it mixes further with the turbulent fluid. The diameter of these vortices is initially about the size of the pipe radius. We have seen above that there is significantly more energy at such length scales in flows at R_{ex} = 2500 than at R_{ex} = 1000. Therefore, we might expect the rate of entrainment in the higher Reynolds number plumes to be greater.

The above discussion would seem to suggest that we might expect the rate of entrainment to vary with the Reynolds number and consequently to have an effect on the plume trajectory.

6.1.4 EXPERIMENTS TO STUDY THE EFFECT OF THE ATMOSPHERIC BOUNDARY-LAYER SIMULATION

In the first phase of this study the above experiments were performed in all four simulations described in the previous chapter. The plumes were studied by flow visualisation and some striking differences in plume behaviour in the different simulations were evident (these will be presented in the next chapter). In the second phase, it was only possible to study a few plumes in each simulation. Nevertheless, any differences in plume behaviour should be revealed even by this small sample.

The characteristics of the four simulations used are quite different and it was hoped that these experiments would reveal the significance of different characteristics for plume modelling. For

example, the effect of wind shear on mean plume rise could be studied since simulation A has no shear whereas simulation D exhibits a large degree of shear, and simulations B and C show moderate shear. Similarly the importance of the cross-flow turbulence intensity in the spreading of the plume could be investigated since the simulations all have different turbulence intensities.

A further aim of these experiments was to determine how accurately we need to model the atmospheric boundary-layer in the wind tunnel. By determining how sensitive our results are to certain flow characteristics, we should be able to discover to what extent we need to model the full-scale characteristics, e.g. does the turbulence intensity need to be modelled to $\pm 5\%$ or to $\pm 25\%$? The author knows of no previous experimental study that has defined how accurately modelled our a.b.l. simulation should be, in order to achieve accurate results for plume dispersion.

NOTE: From now on plumes will be referred to by a letter and number e.g. A5, C1a; the first letter refers to the simulation and the number is the plume number.

6.2 METHOD OF ANALYSIS OF TEMPERATURE PROFILES

Mean temperature profiles, lateral and vertical, of the plumes being studied were measured at the following distances downstream of the stack centre, X = 2.5, 5.0, 10.0, 15.0, 20.0, 40.0 cm. The vertical profiles (on the tunnel centre-line) were measured first, measurements being made every 10 mm, except close to the stack where measurements were made every 5 mm. The lateral temperature profile was then measured, at each downstream position, at the height of the maximum temperature in the vertical profile.

The set of profiles, six for each plume, was plotted on one graph so that the mean plume trajectory and rate of spread could easily be determined. The temperature profile for each downstream position was plotted on an axis which begins at $0^{\circ}C$, at the relevant downstream position. A typical set of profiles is shown in figs. 6.8a & b, the profiles show no sudden change in temperature and appear to be symmetrical about the peak. A smooth curve was drawn through the results, by hand, to give a complete profile. Close to the stack the profile is slightly skewed as the temperature of the cross-flow is above ambient due to heat transfer from the stack.

6.2.1 MEAN PLUME TRAJECTORY

To determine the mean plume trajectory we must define the mean centre of the plume at each position. The centre of the plume can be defined in various ways: for example, the centre of momentum, the position of the peak temperature or velocity, or the point mid-way between the two 'edges'. Since the temperature profiles appear to be symmetrical about the peak (we will examine this assertion later) the clearest definition of the plume centre is where the peak temperature occurs.

The position of the peak temperature could easily be located to ±5 mm and probably more accurately near the stack, i.e. ± 2.5 mm. However, at X = 40 cm the profiles where much flatter and the peak position could only be located ± 10.0 mm. Having determined the mean plume centre at each position, the results were recorded and plotted on another graph to show clearly the mean trajectory and to avoid confusion with the temperature profiles, e.g. fig. 6.10.

6.2.2 THE RATE OF SPREAD

In order to define the width of a profile, we must specify where the edge of the profile occurs. The edge may be defined in several ways, for example, the point where the temperature returns to ambient, the point where the temperature is 10% of the peak value, or one standard deviation from the peak (assuming the profile to be Gaussian). The first definition is not practical to use since it is difficult to locate precisely where the temperature returns to ambient. The other definitions would essentially be the same (i.e. they would be related by a constant) if the profiles were taken to be Gaussian. As mentioned earlier, lateral concentration profiles in the atmosphere are found to be closely Gaussian, and most theoretical models assume that the profiles are Gaussian. To examine how well our results fitted a Gaussian distribution several profiles, under varying conditions, were chosen and a Gaussian distribution fitted to the data.

Six profiles, under different conditions, were chosen at random (3 vertical, 3 lateral) and a Gaussian distribution fitted as follows. The position of the peak (but not its value) was taken from the profiles already drawn (- in order to be consistent with the previously defined plume centre, rather than calculating a new plume centre), then a best-fit Gaussian curve was fitted to the data using a least squares

program (points where the temperature had returned to ambient were not included since the Gaussian distribution cannot be expected to fit in this region of constant temperature).

The results are shown in figs. 6.9. The vertical profiles show reasonable agreement with the Gaussian curve (though not perfect agreement) and the profiles do appear to be slightly skewed. Fitting separate curves above and below the centre-line, as suggested by Moore (1975), would probably improve the fit. The lateral profiles show good agreement with the Gaussian curves and show no sign of being skewed. These results while not proving conclusively that the profiles are Gaussian, do justify the use of the Gaussian profile to define the width of the plume by the standard deviation (σ) of the profile (and support the choice of the temperature peak for the plume centre.)

Now σ_z or σ_y can be quickly determined from the previously hand drawn profiles. This was done by finding the width of the profile when the temperature had fallen to $1/e$ of the peak value (all temperatures above ambient), this width is $2\sqrt{2}\,\sigma$.

To compare the above methods of determining σ with other possible methods, the values derived from the hand-drawn curves and those from the best-fit curves and the actual standard deviation of the data were calculated for the above six profiles. The following values of σ were determined: i) σ_{prof} from the hand drawn profiles,

ii) $\sigma_{b\text{-}f}$ from the best-fit curves,

iii) σ_{calc} the actual standard deviation of the data.

The three values derived for each profile are given in Table 6.3.

For each profile the values of σ agree within 1.5 mm, except for plume B1b which was measured at the furthest downstream position and the discrepancy is ± 3.0 mm. Thus our method of determining σ from the hand drawn profiles is in good agreement with the other methods and was used

throughout this study. From the above examples, it is suggested that the uncertainty in the σ values is ± 2.0 mm, for X < 20 cm, and $\pm$ 4.0 mm for X = 40 cm. However, in some cases (especially at X = 40 cm) the form of the profile may suggest larger uncertainty in the σ values.

In general, an uncertainty of $\pm 10\%$ in the values of σ should be assumed. This experimental uncertainty is still significantly better than we would expect from full-scale results. (This uncertainty in measuring σ values, wind tunnel and full-scale, should be remembered when using theoretical methods.)

6.2.3 NON-DIMENSIONALISING THE MEAN PLUME TRAJECTORY

Having determined the mean plume trajectories, we now want to compare plumes measured under different conditions, i.e. different momentum ratios and Froude numbers. For example, we want to compare plumes with different density ratios, e.g. 1a & b, and we want to compare our results with theoretical predictions. To do this we must non-dimensionalise our results by the appropriate length-scale. Simply non-dimensionalising our results by the pipe diameter will not suffice since we want to be able to compare plumes with different cross-flow velocities, exit velocities etc. Three main length-scales have been suggested in the literature, and we will now consider which ones are appropriate to our results.

The three length scales discussed in the literature are:

i) Buoyancy length (l_b), Briggs (1969), where $l_b = F_b / u^3$

ii) Momentum length (l_m), Briggs (1969), where $l_m = \left(\frac{\rho_s w_s^2}{\rho_a u^2}\right)^{1/2} \frac{d}{2}$

iii) Velocity length (l_v), referred to as a 'momentum-scale' by Hoult & Weil (1972) and List (1982), where $l_v = \frac{w_s}{u} \cdot \frac{d}{2}$

Hoult and Weil, and List suggest that for $l_v > l_b$, l_v will be the

appropriate length-scale for the initial region; for all our plumes we find that $l_v > l_b$ (i.e. buoyant jets). To test this theoretical suggestion, we need to determine whether we can collapse our results onto a curve (or set of curves) by non-dimensionalising our results by one of the above length-scales.

We assume that by using the appropriate length-scale (l_m say) we can collapse our results onto a curve of the form:

$$(Z/l_m) = a.(X/l_m)^b \qquad (6.16)$$

This assumes that a and b are constants, however, they may be dependent on exit density, Reynolds number or the simulation used. And of course, this is just what we are trying to study in these experiments. So to a great extent, examining whether we can collapse our results on to a single curve, is investigating whether a and b (and hence plume behaviour) are dependent on the exit density or Reynolds number. For this reason, we did not use plumes from different simulations or with very different Reynolds numbers. However, we did use plumes 1 - 4, which have very different exit density ratios, so we are simultaneously determining the length scale and the effect of density ratio.

The following procedure was applied, firstly to individual plumes and then to groups of plumes. The co-ordinates of the mean plume trajectory were non-dimensionalised by one of the length-scales, a best-fit curve of the form $Z' = aX'^b$ was then fitted using a least-squares program to all the points and a and b were determined. To determine how well the data agreed with the fitted curve a non-dimensional error (Er) was calculated, where:

$$Er = \sqrt{\frac{1}{m}\sum_{n=1}^{m} \frac{Z'_n - a X'^b_n}{a X'^b_n}} \qquad (6.17)$$

and (X', Z') are the non-dimensional data points, a and b are

determined from the best-fit curve; for a single plume m = 6.

Note: Er for a single plume is a constant and does not depend on the length-scale. However, the Er values determined for a single plume show the degree of experimental scatter in the raw data, i.e. how well they fit the curve, and also suggest a value of Er to be attained by a set of plumes if they are to collapse onto one curve within the experimental scatter. For comparison, an error of ± 5 mm on a typical curve gave Er = 0.07.

The error values for individual plumes and for groups of plumes are given in tables 6.4 and 6.5, p.174.

The error values for individual plumes are no greater than 0.07, except for plumes B2a (Er = .091) and B3a (Er = .117), see table 6.4. The uncharacteristically large error for plume B3a plus the fact that its trajectory levels-off rapidly (see fig. 7.1c, p.179) made one cautious of using the data from B3a, and it was not considered in the subsequent choice of length-scales (- an experimental error is suspected). Since the error values are below the value due to the experimental uncertainty, this suggests that within the experimental uncertainty the trajectories each fit a curve of the form $Z' = aX'^{b}$. The average error for all the plumes was 0.054 (excluding B3a).

The same procedure was used for groups of plumes. However, the co-ordinates of each plume were non-dimensionalised by the relevant length-scale for each plume and all the points fitted to a single curve. The choice of length-scales now affects the error since the length-scales were different for each plume. The results for various groups of plumes using the three length-scales and unity length-scale, and the actual values of the length-scales are given in Table 6.5.

Examining the results, we see that l_m and l_v give significantly smaller values for Er than l_b. The errors using l_m and l_v are very

similar and not significantly greater than the 'experimental' error. The relatively small values of Er for unity length-scale are a result of many of the plumes having similar length-scales (because of the nature of these experiments). The effect of non-dimensionalising the results is shown in fig. 6.10 & 6.11; in fig. 6.10 the raw data for plumes B1 to B4 is presented, while in fig. 6.11 the same data non-dimensionalised by the velocity length-scale for each plume is shown. We can see that non-dimensionalising the data tends to collapse the points onto one curve. This is especially true in the lower diagram of fig. 6.11. Note that the raw data do not show a great spread of values because all the plumes have similar velocity (and momentum) ratios. The effect would be more marked for plumes with a wider range of momentum ratios, see Pratte and Baines (1967). The scatter is greatest at the furthest downstream position and this is probably due to the uncertainty in locating the peak there. Error bars corresponding to $\pm$10 mm have been drawn on those points.

From the results in table 6.5 and because of the form of the theoretical predictions of Hoult and Weil (1972) and List (1982), the velocity length-scale, $l_v = w_s d/2U$, was chosen to non-dimensionalise the plume trajectory data. (Whether the above analysis shows that the trajectory is independent of the exit density ratio or not will be discussed in the next chapter.)

6.2.4 NON-DIMENSIONALISING THE PLUME WIDTH

Our results for the plume width and height (lateral and vertical, respectively) also need to be non-dimensionalised, if we are going to compare plumes measured under different conditions. Having non-dimensionalised the plume trajectory by the velocity length-scale it is consistent to use the same length-scale for the spread of the plume,

since we would expect the plume trajectory and rate of spread to be related.

Strong support for using the velocity-length scale to non-dimensionalise the plume spread (and trajectory) comes from the work of Pratte and Baines (1967). They studied turbulent jets in a cross-flow and found that for a wide range of velocity ratios (5 - 35), their results for the rate of plume spread against downstream distance would collapse onto a single curve when non-dimensionalised by the velocity length-scale. Therefore, the velocity length-scale was used to non-dimensionalise our results for plume width and height.

6.3 ERROR ANALYSIS

Before examining the results of the experiments, we should consider the accuracy of the experiments. We should estimate how accurately we can specify the experimental conditions and how accurately we can measure the results. The experimental conditions are specified by the dimensionless groups and the boundary-layer simulation; the results are given by the mean plume trajectory and rates of spread.

6.3.1 UNCERTAINTY IN THE DIMENSIONLESS GROUPS

The primary sources of error in specifying the dimensionless groups were considered to be:

i) Mean cross-flow speed, ± 0.05 ms^{-1}, which gives a maximum error of $\pm 6\%$, for a 0.8 ms^{-1} cross-wind.

ii) Exit flow rates, ± 0.02 m^{3}h^{-1}, which yields a maximum error of $\pm 1\%$ for a flow rate of 2.08 m^{3}h^{-1} (-the lowest used).

iii) Exit and ambient temperature, $\pm 1^{\circ}$C, which gives a maximum error in $\Delta\ell/\ell$ of $\pm 4\%$ for a 50°C temperature difference (T_{amb} = 20°C).

Errors in the fluid properties and the stack diameter were considered to be negligible. The following are the maximum uncertainties in specifying the dimensionless groups:

Density Difference, $\Delta\ell/\ell$, $\pm 4\%$

Momentum Ratio, $\ell_s w_s^2/\ell_a U^2$, $\pm 14.6\%$

Densimetric Froude No., $gd.\Delta\ell/\ell_a U^2$, $\pm 16.0\%$

Exit Reynolds No., $\ell_s w_s d/\mu_s$, $\pm 1\%$

In practice, the actual uncertainties will be less than the maximum, but we can expect an uncertainty of $\pm 10\%$ for R_{mom} and F_{rd} and about $\pm 2\%$ for $\Delta\ell/\ell$ and R_{ex}. (The main source of uncertainty is due to the cross-wind speed which appears squared in R_{mom} and F_{rd}.)

6.3.2 ACCURACY OF THE ATMOSPHERIC BOUNDARY-LAYER SIMULATION

The results for the boundary-layer simulation were presented in the previous chapter. The flow properties recorded were measured quite accurately, e.g. i) Mean velocity measurements were accurate to $\pm 2.5\%$

ii) Longitudinal Turbulence intensity measurements were accurate to $\pm 5\%$.

iii) lateral and vertical turbulence intensities were determined from the power spectral density measurements and should be as accurate as the longitudinal component.

However, how well each simulation models an atmospheric boundary-layer flow is rather subjective. We have seen in Chapter 5 that the agreement with the E.S.D.U. data is quite good for the properties measured. In addition, the uncertainty in the actual E.S.D.U. curves themselves should be recalled, e.g. $\pm 15\%$ uncertainty in the $\sigma u/U$ values and greater in the power spectral density. In this study, we are not trying to model a particular full-scale situation, so it is more important that we know the flow properties accurately (i,ii,iii above) rather than Z_o.

6.3.3 UNCERTAINTY IN THE RESULTS

The thermocouple array could be positioned accurately to ± 1.0 mm in each direction, the spacing between thermocouples was 10.0 ± 0.5 mm. The actual uncertainty in the results is a combination of the spatial uncertainty, accuracy of the temperature measurements and accuracy of the analysis technique. In the previous sections, we estimated the uncertainties to be:

i) Mean Plume Trajectory The plume centre could be located to ± 5 mm which means a fractional uncertainty of less than $\pm 10\%$.

ii) Vertical and Lateral Spread In Sect. 6.2.2 an uncertainty of ±10% in the standard deviation of the temperature profiles was suggested.

From the above analysis, we can see that there is a ±10% uncertainty in most values determined in these experiments and we should bear this in mind in our subsequent discussion of the results.

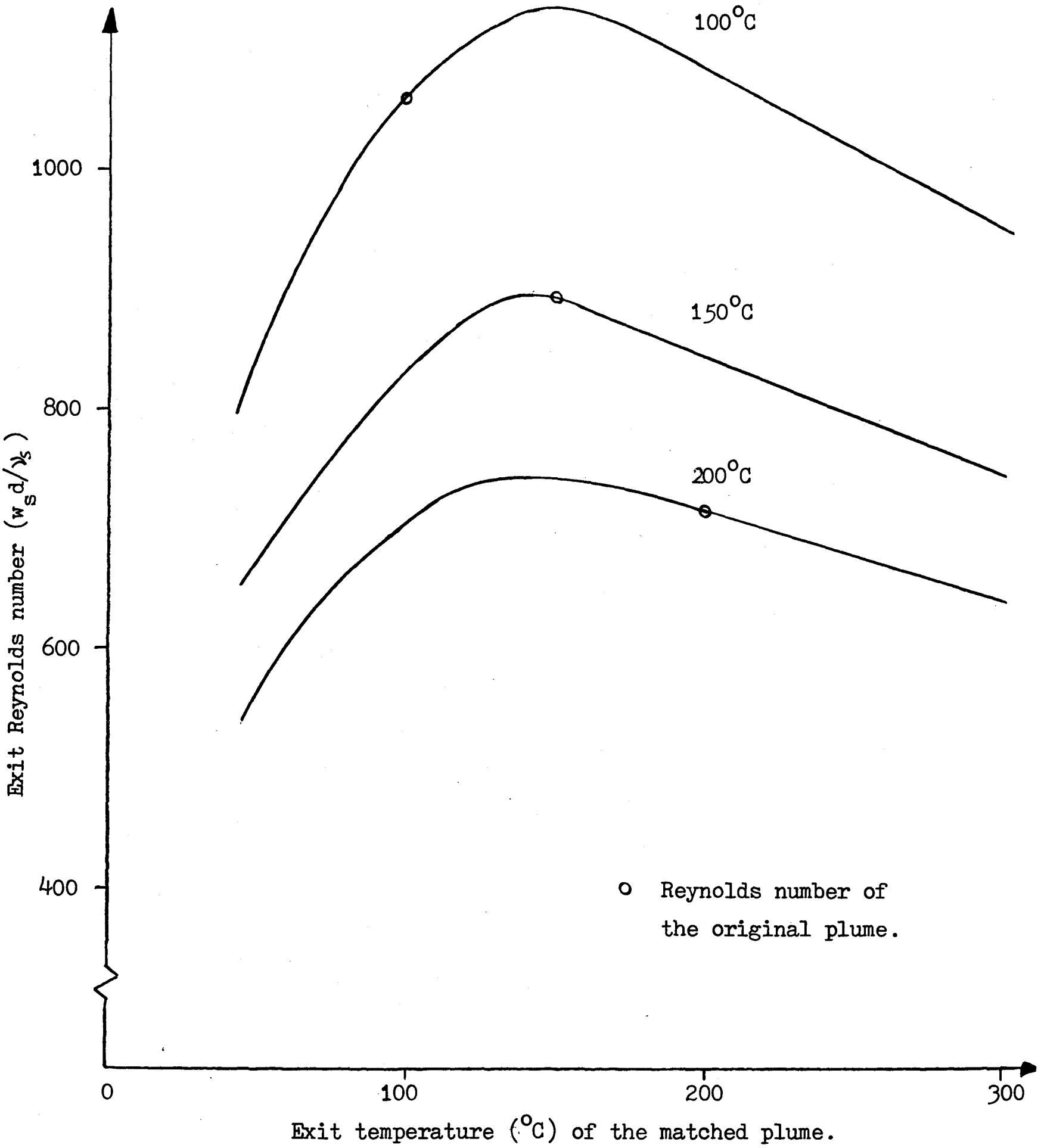

FIG. 6.1 Reynolds Number of Matched Plume Against Exit Temperature

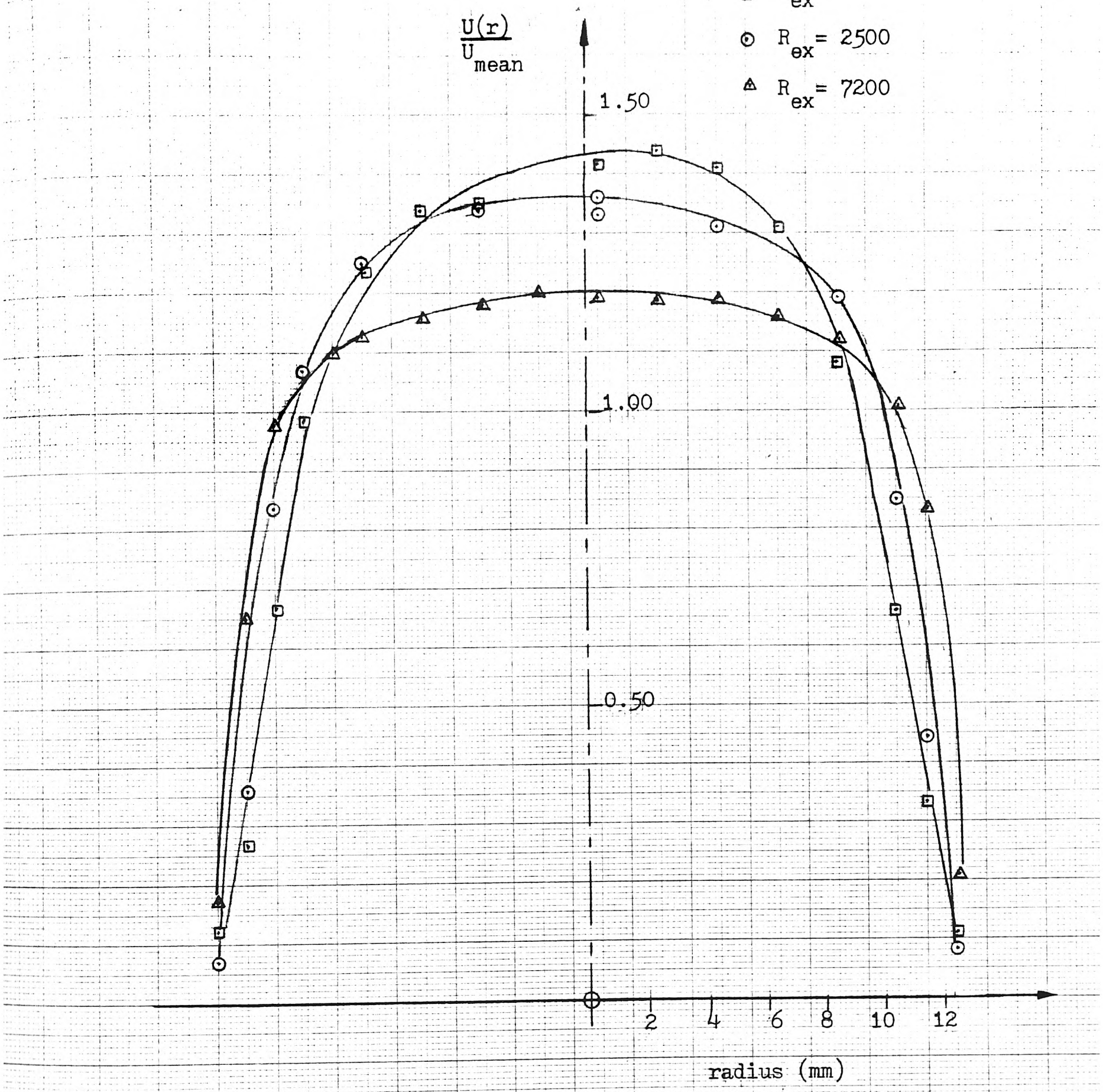

Fig. 6.2 Stack Exit Velocity Profile

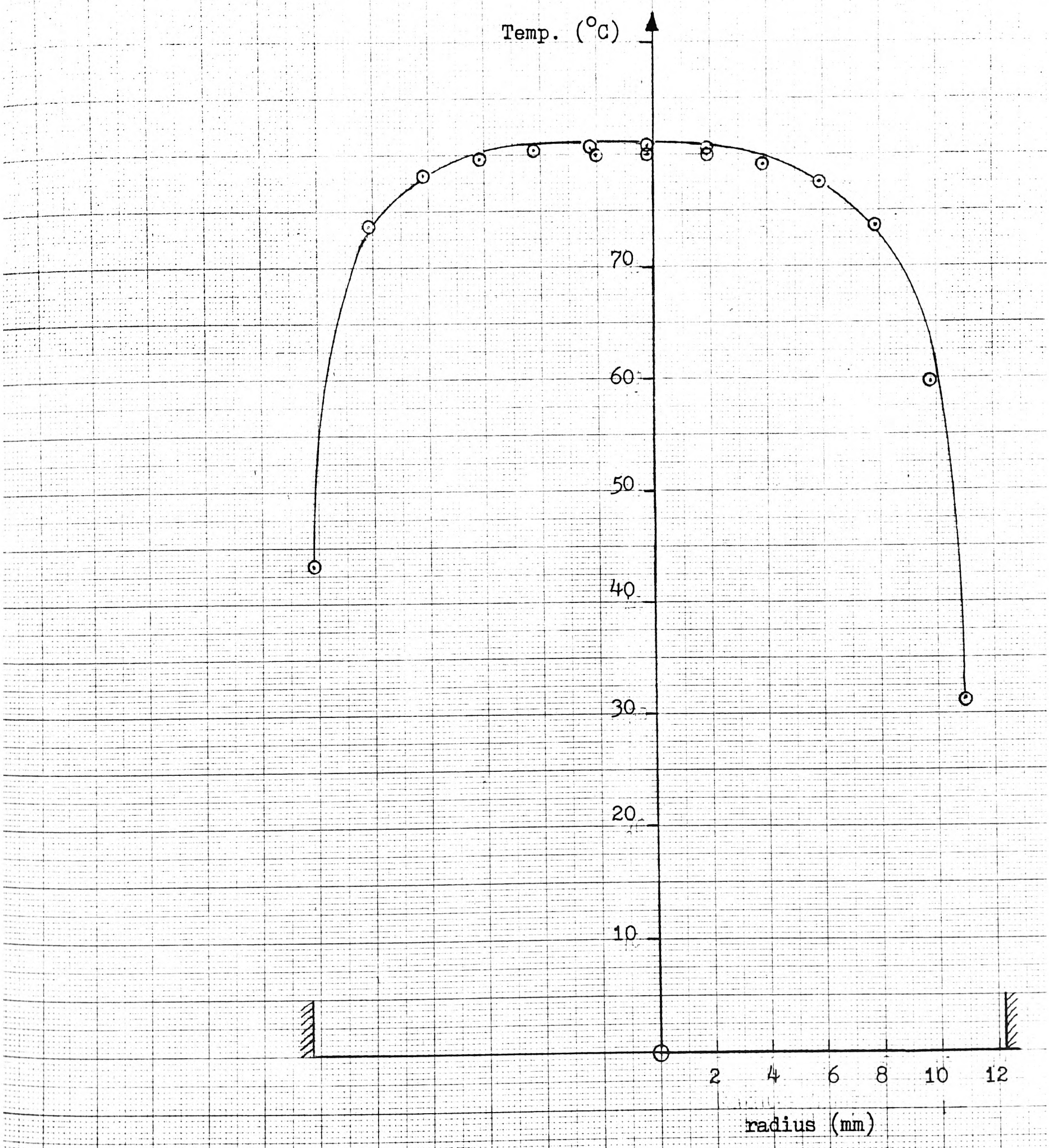

Fig. 6.3 Stack Exit Temperature Profile

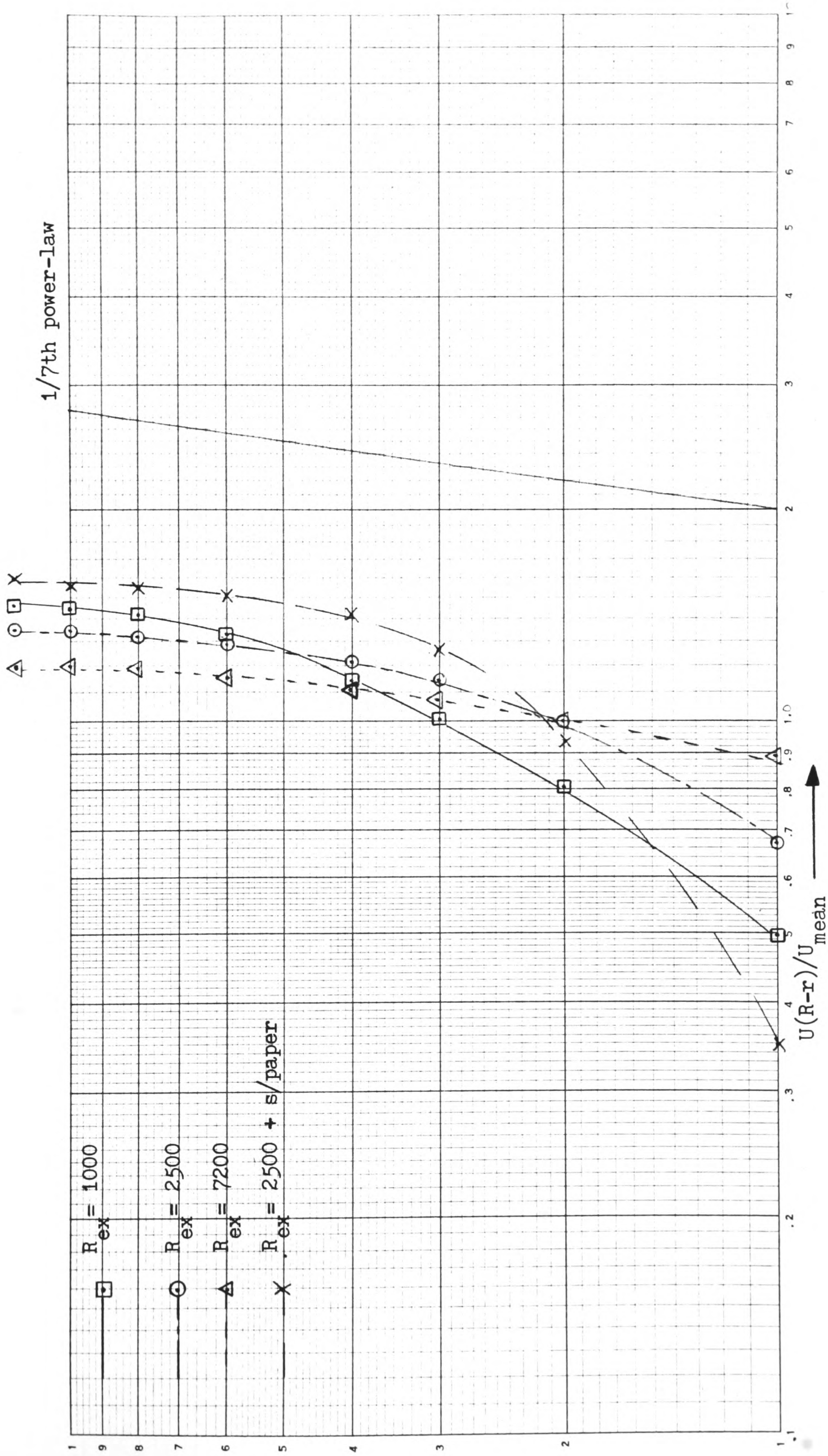

Fig. 6.4 Stack Exit Velocity Profile Plotted in Log-Log Form

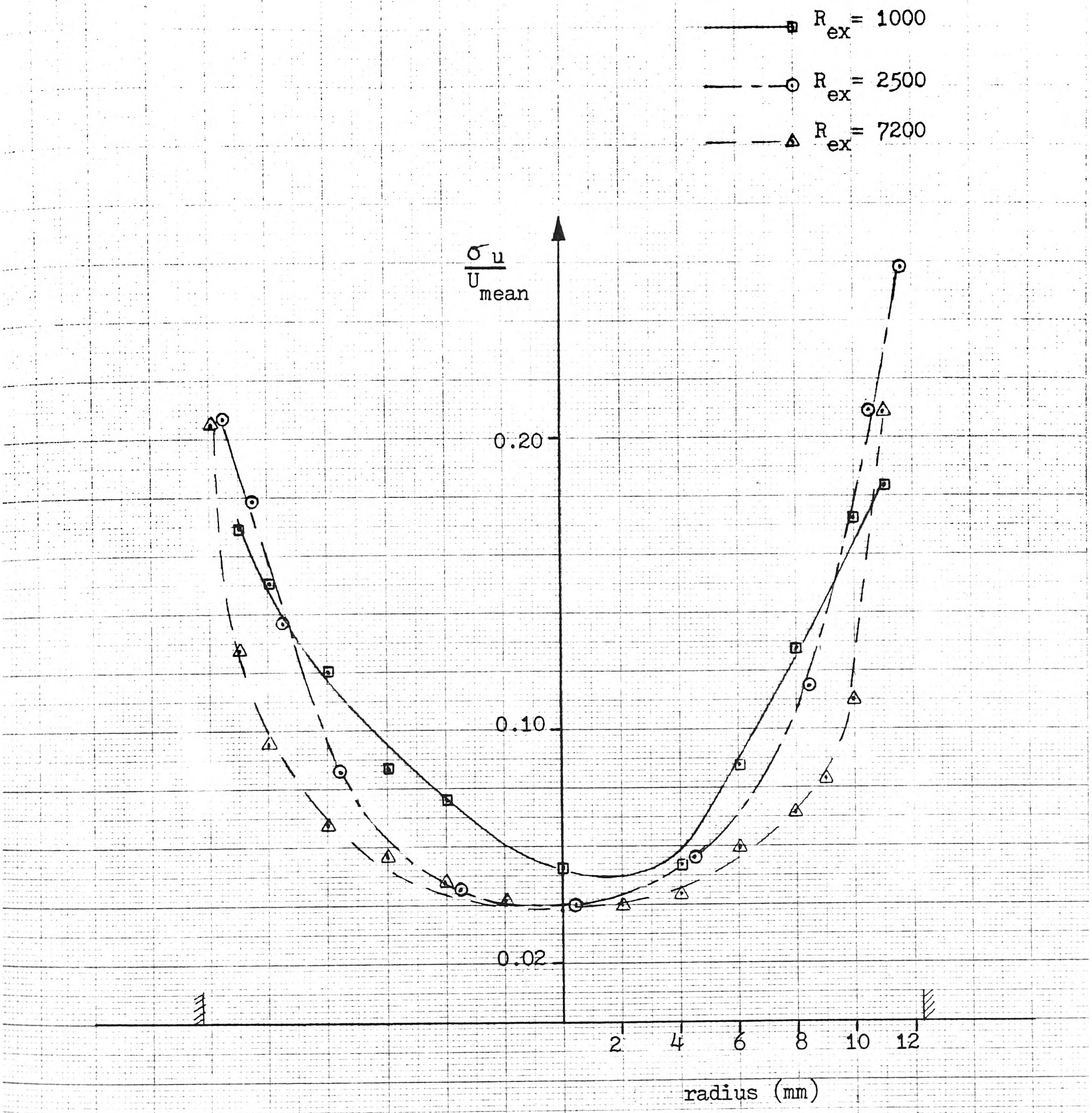

Fig. 6.5 Stack Exit Turbulence Intensity Profile

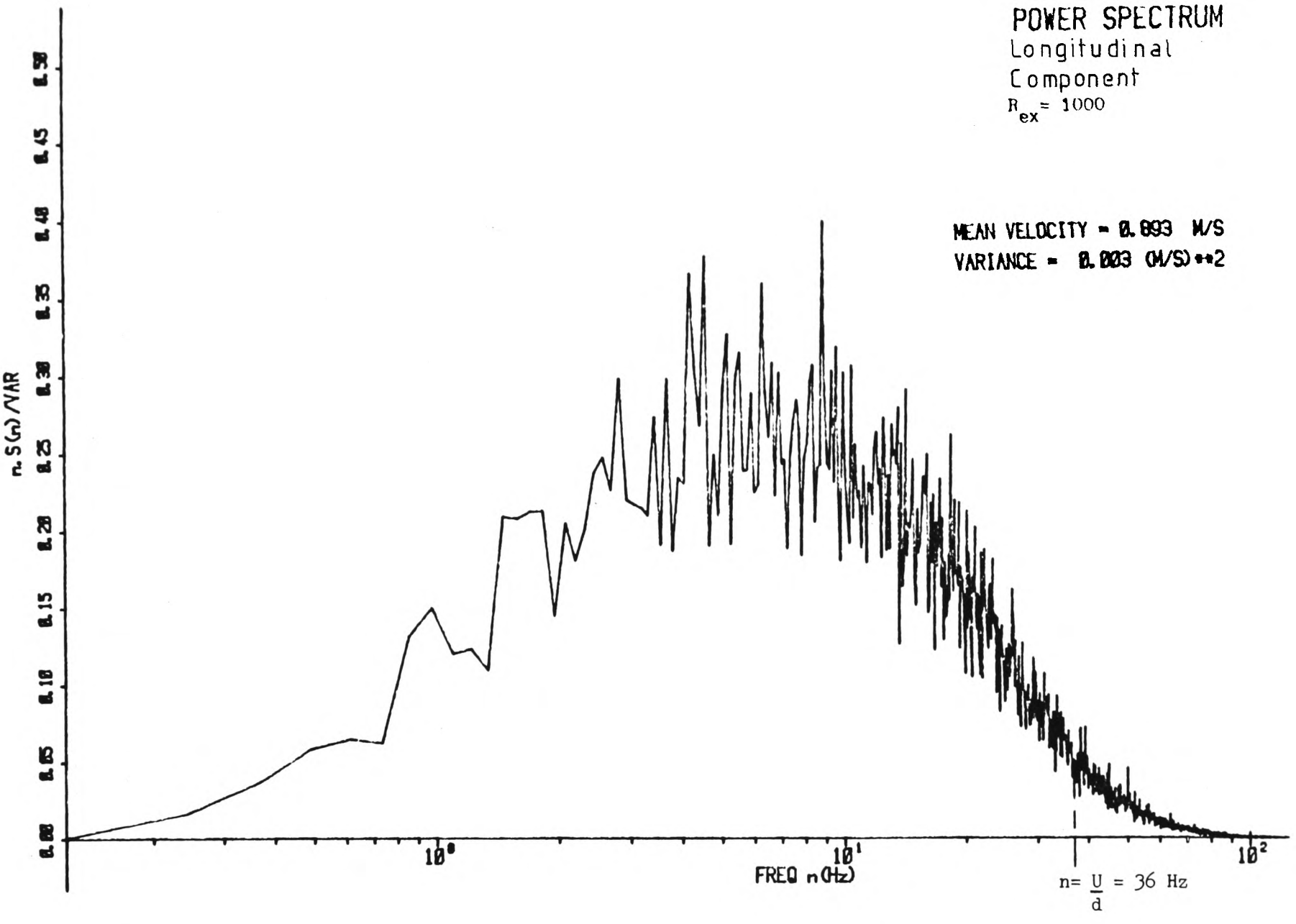

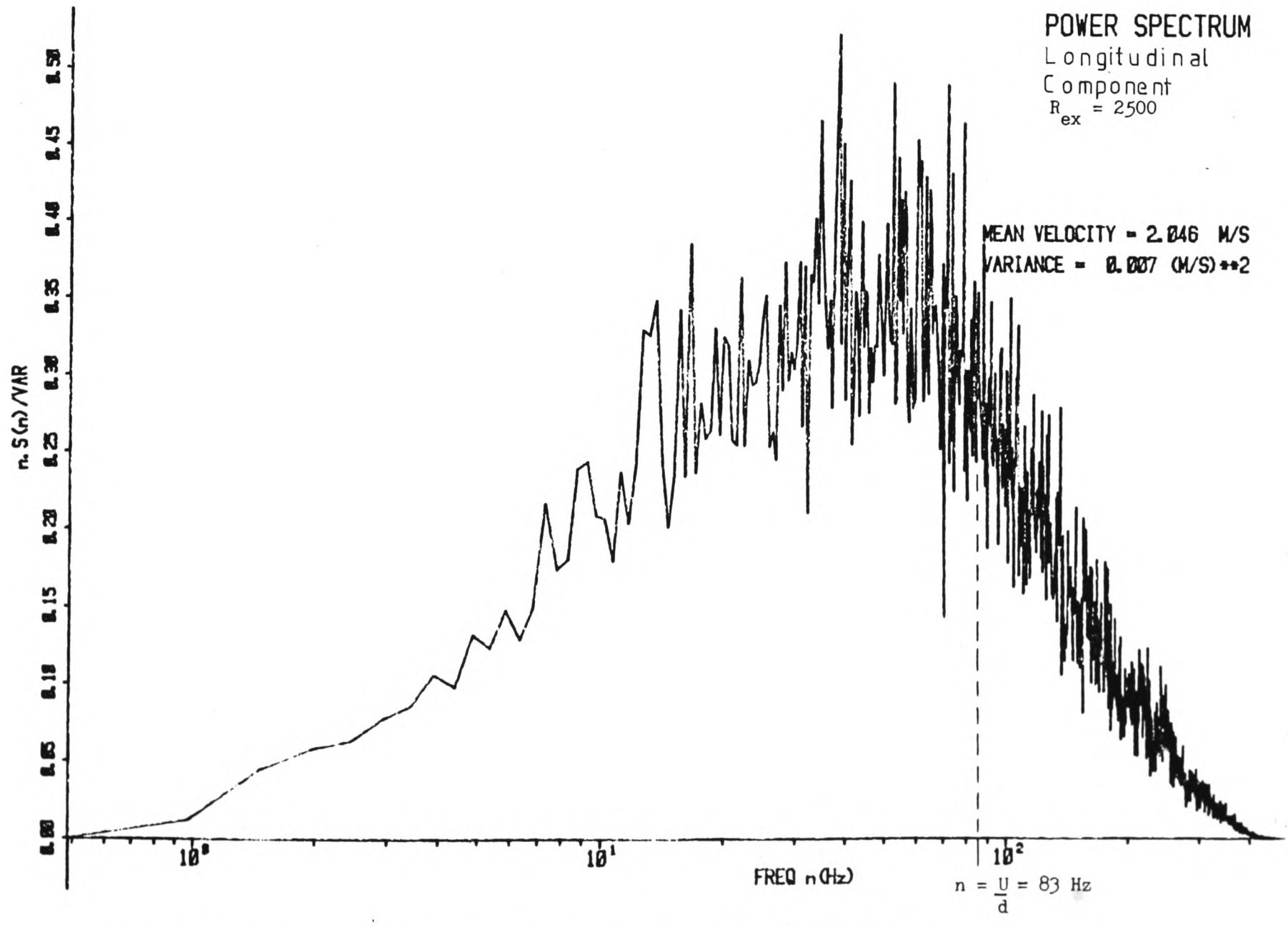

Fig 6.6a Power Spectral Density at Stack Centre

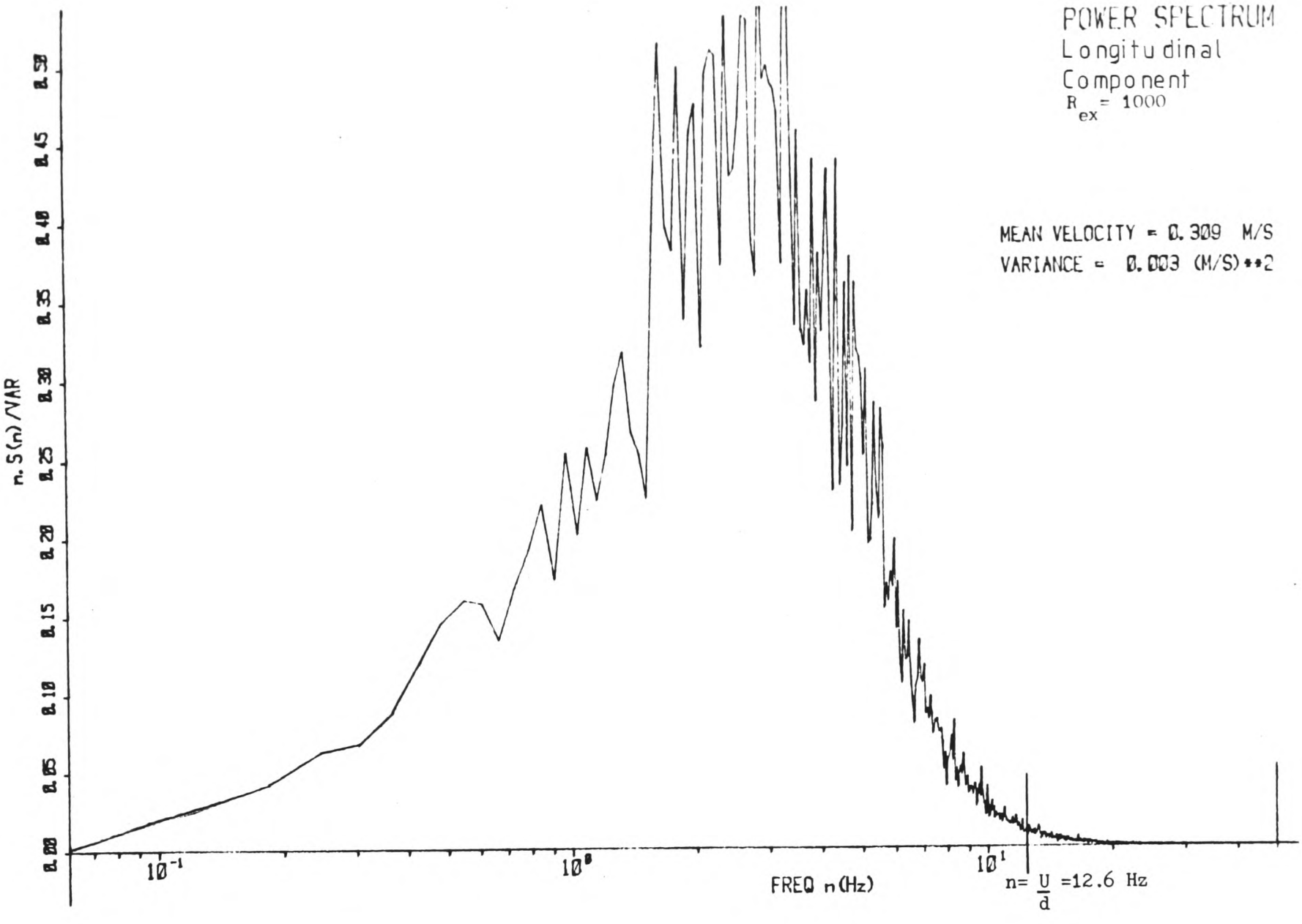

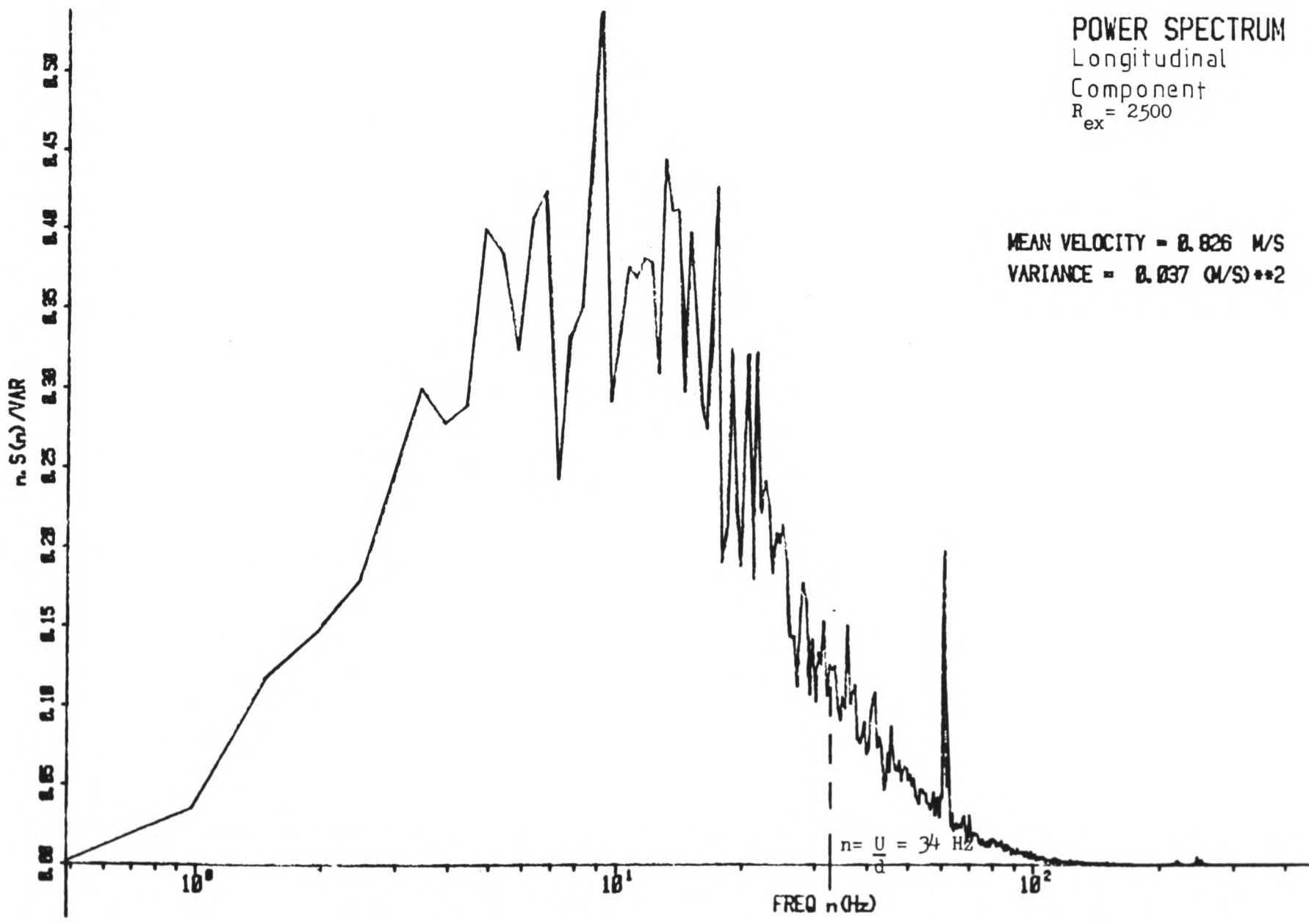

Fig. 6.6b Power Spectral Density at Stack Edge

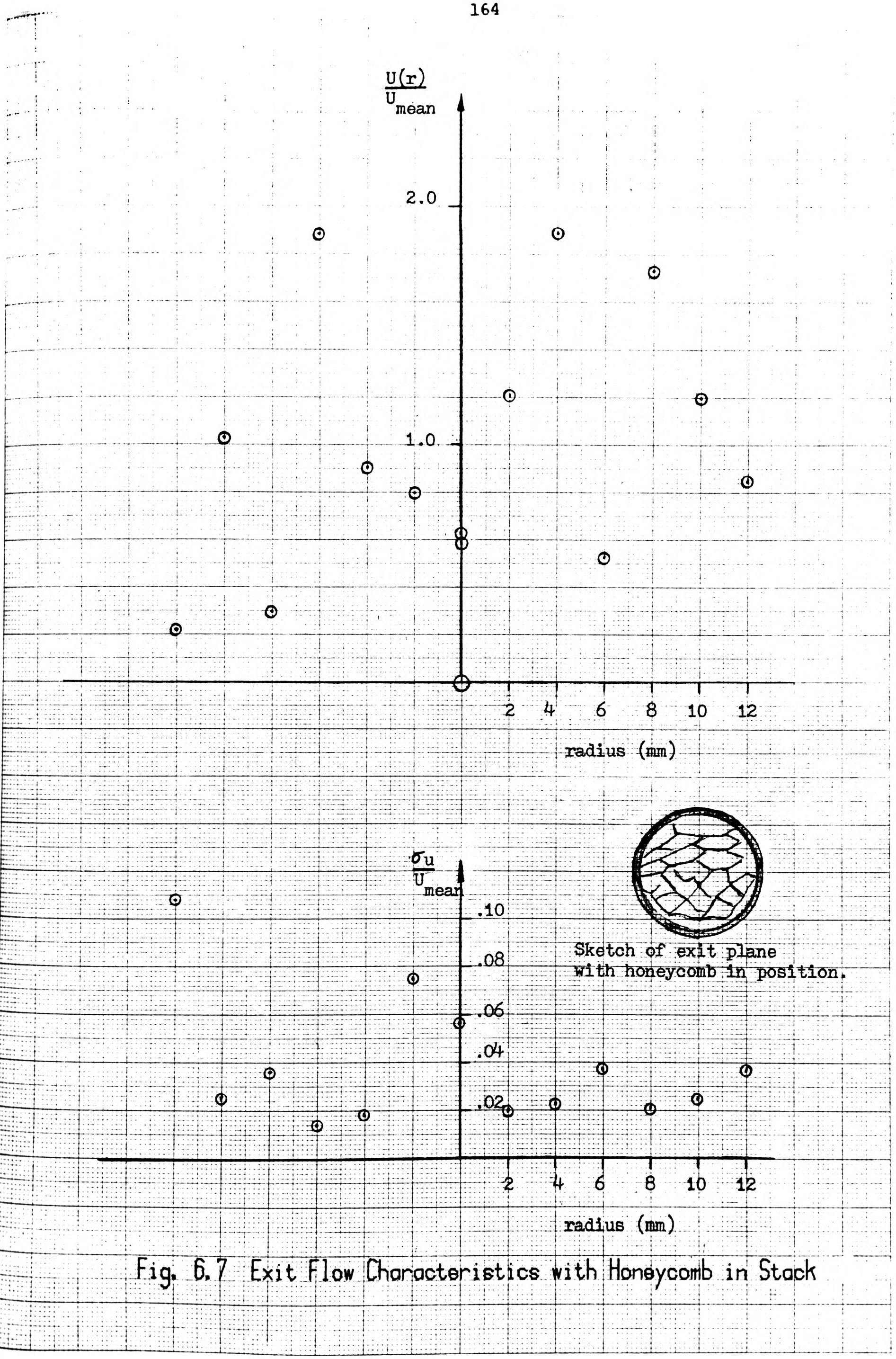

Fig. 6.7 Exit Flow Characteristics with Honeycomb in Stack

Fig. 6.8a Vertical Temperature Profiles for Plume B4b

Simulation B

Plume 4b

T_{amb} = 13.0 °C

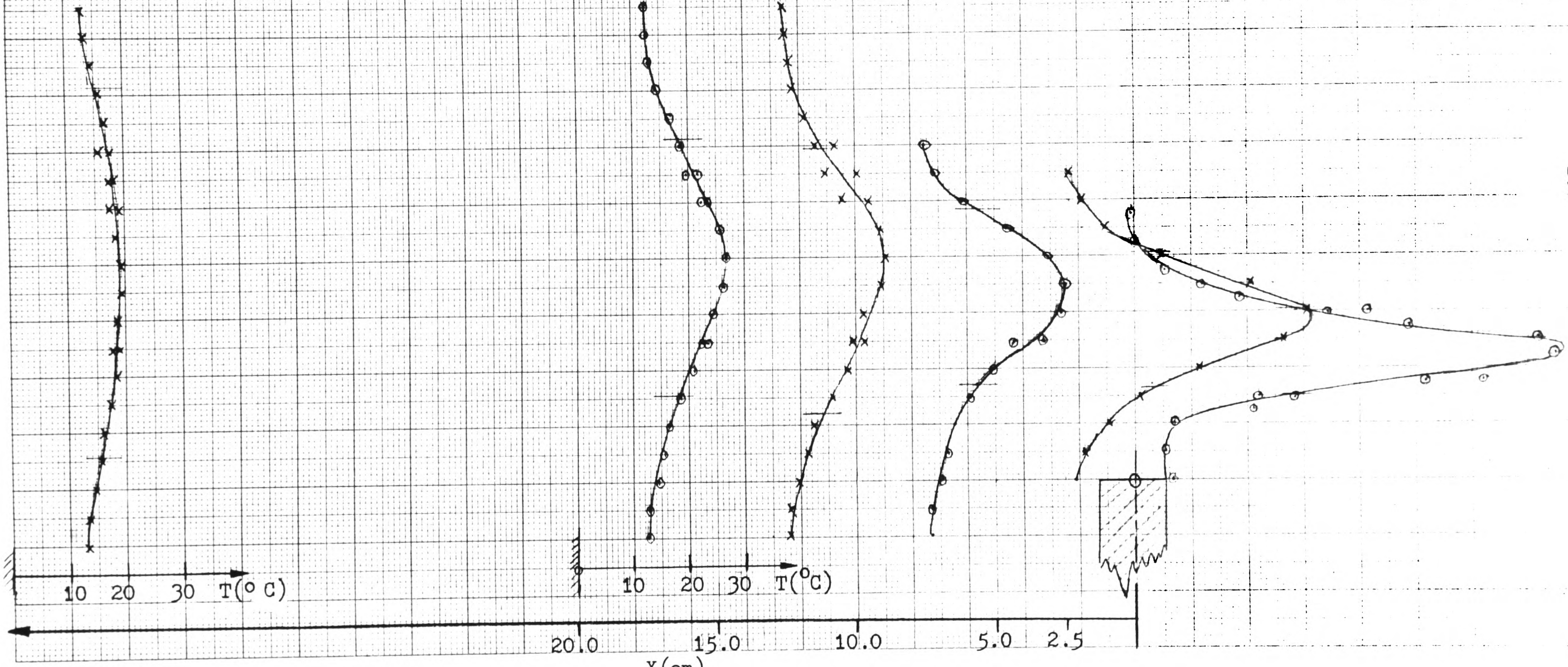

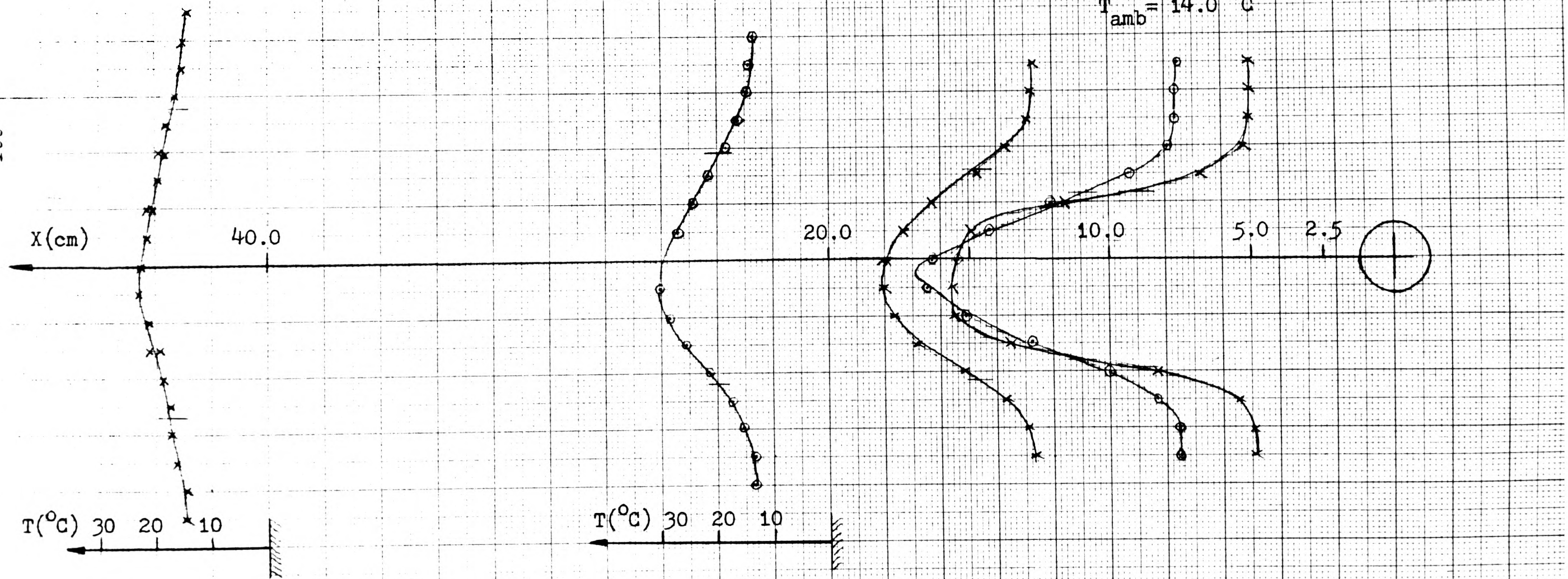

Fig. 6.8b Lateral Temperature Profiles for Plume B4b

Fig. 6.9 Gaussian Curve Fit to Temperature Profiles

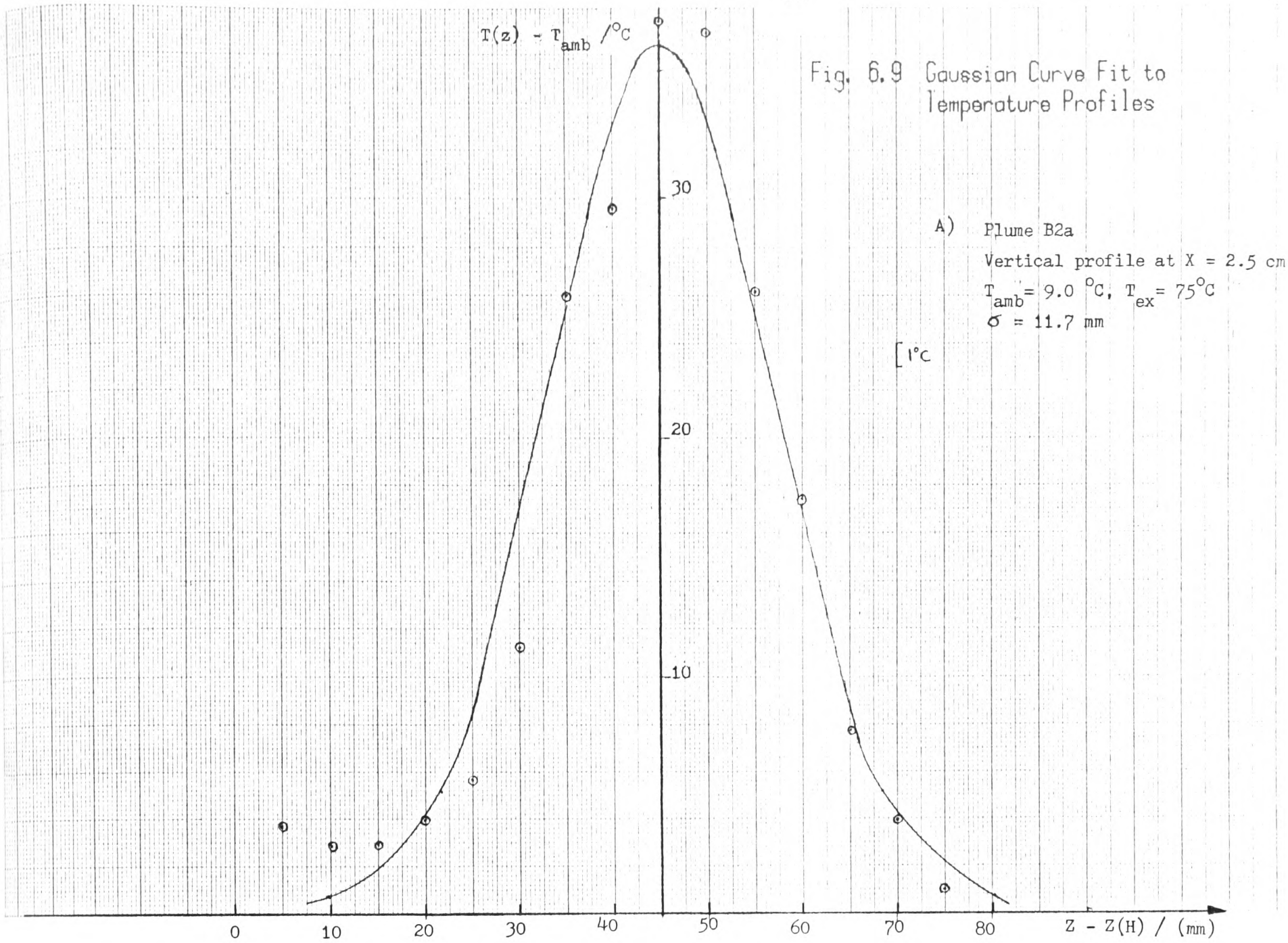

A) Plume B2a
Vertical profile at X = 2.5 cm
T_{amb} = 9.0 °C, T_{ex} = 75°C
σ = 11.7 mm

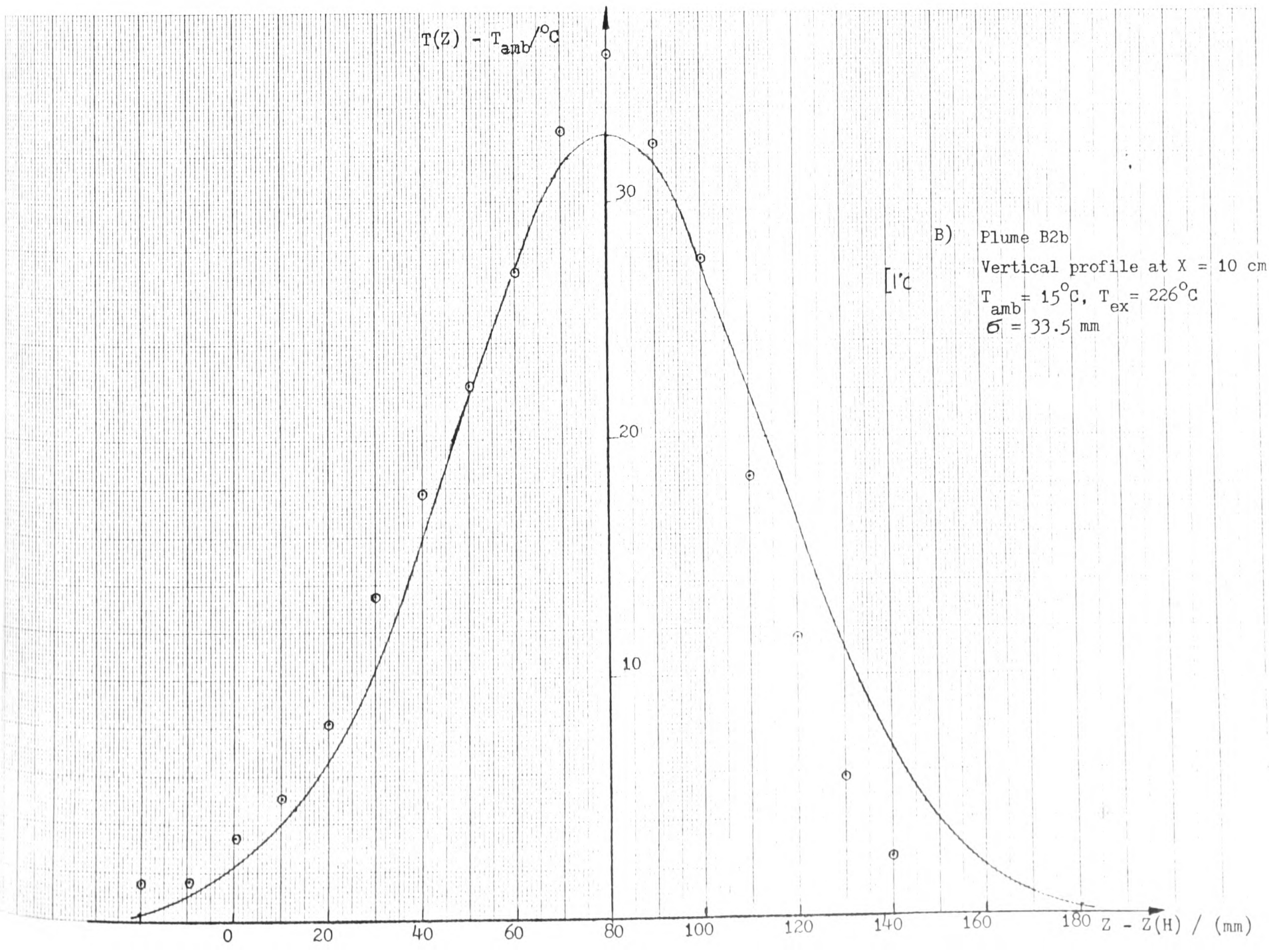

B) Plume B2b
Vertical profile at X = 10 cm
T_{amb} = 15°C, T_{ex} = 226°C
σ = 33.5 mm

Fig. 6.9 Gaussian Curve Fit to Temperature Profiles

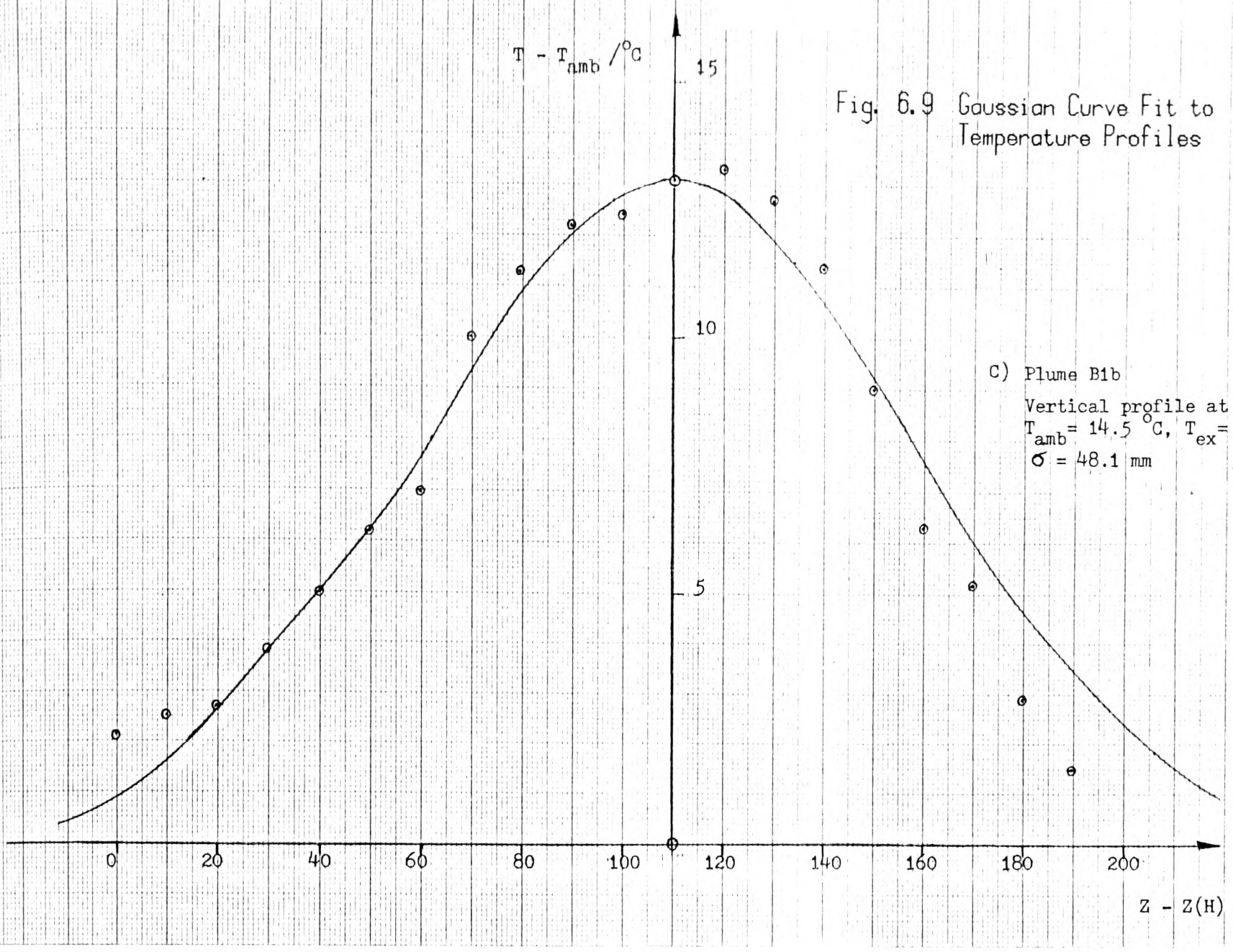

C) Plume B1b
Vertical profile at X = 40 cm
T_{amb} = 14.5 °C, T_{ex} = 265 °C
σ = 48.1 mm

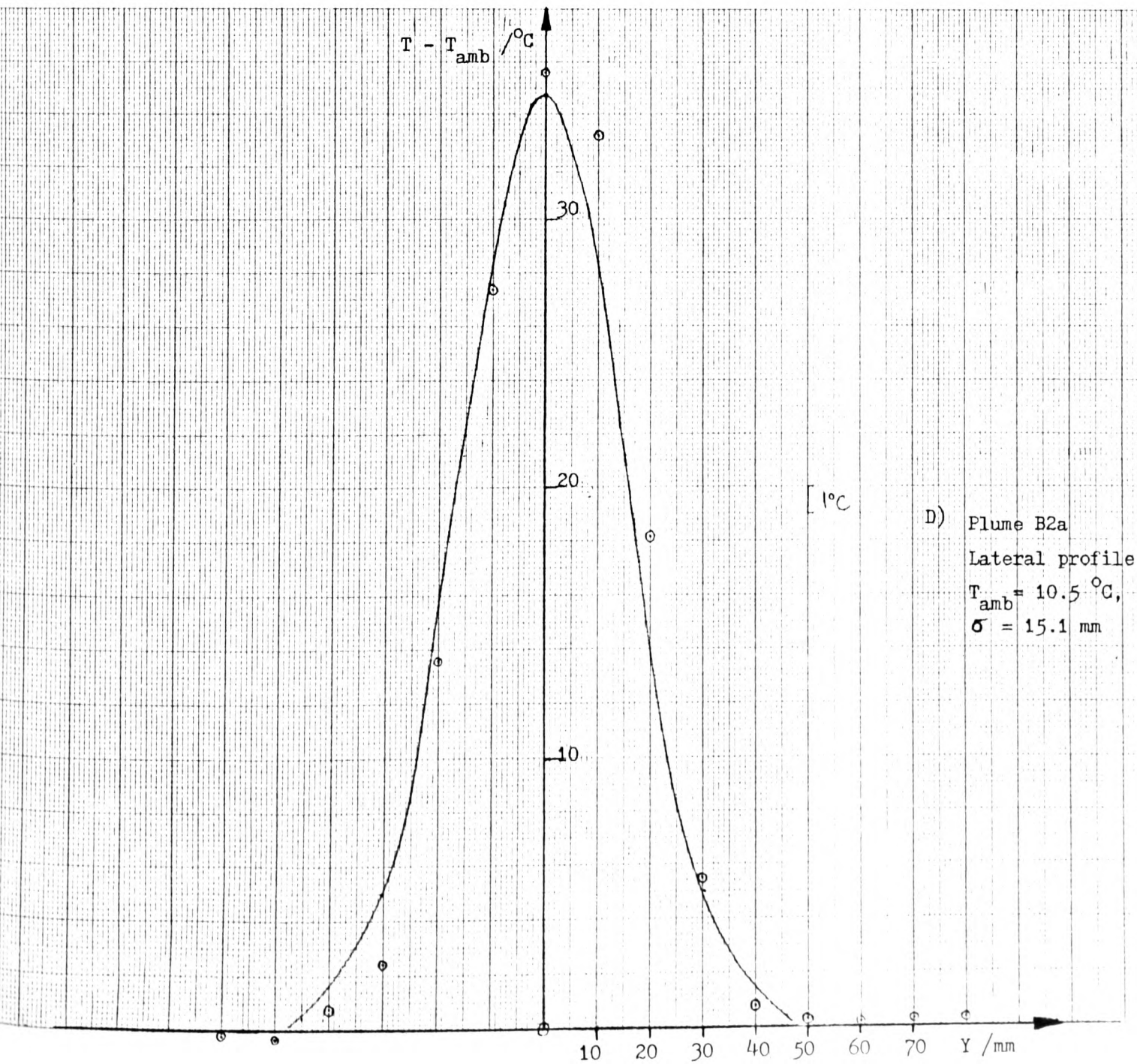

D) Plume B2a
Lateral profile at X = 2.5 cm
T_{amb} = 10.5 °C, T_{ex} = 74.4 °C
σ = 15.1 mm

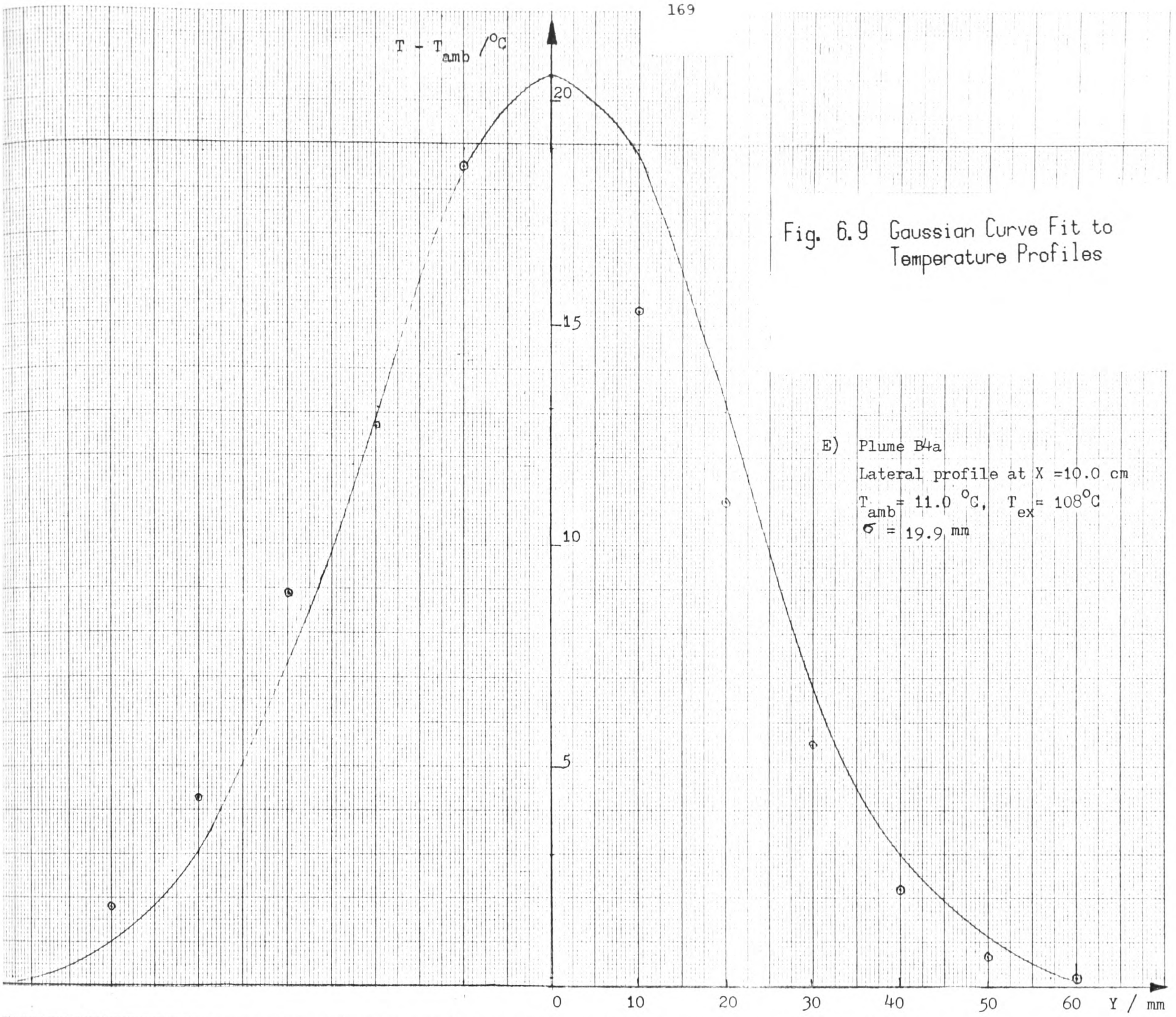

Fig. 6.9 Gaussian Curve Fit to Temperature Profiles

E) Plume B4a
Lateral profile at X =10.0 cm
T_{amb} = 11.0 °C, T_{ex} = 108°C
σ = 19.9 mm

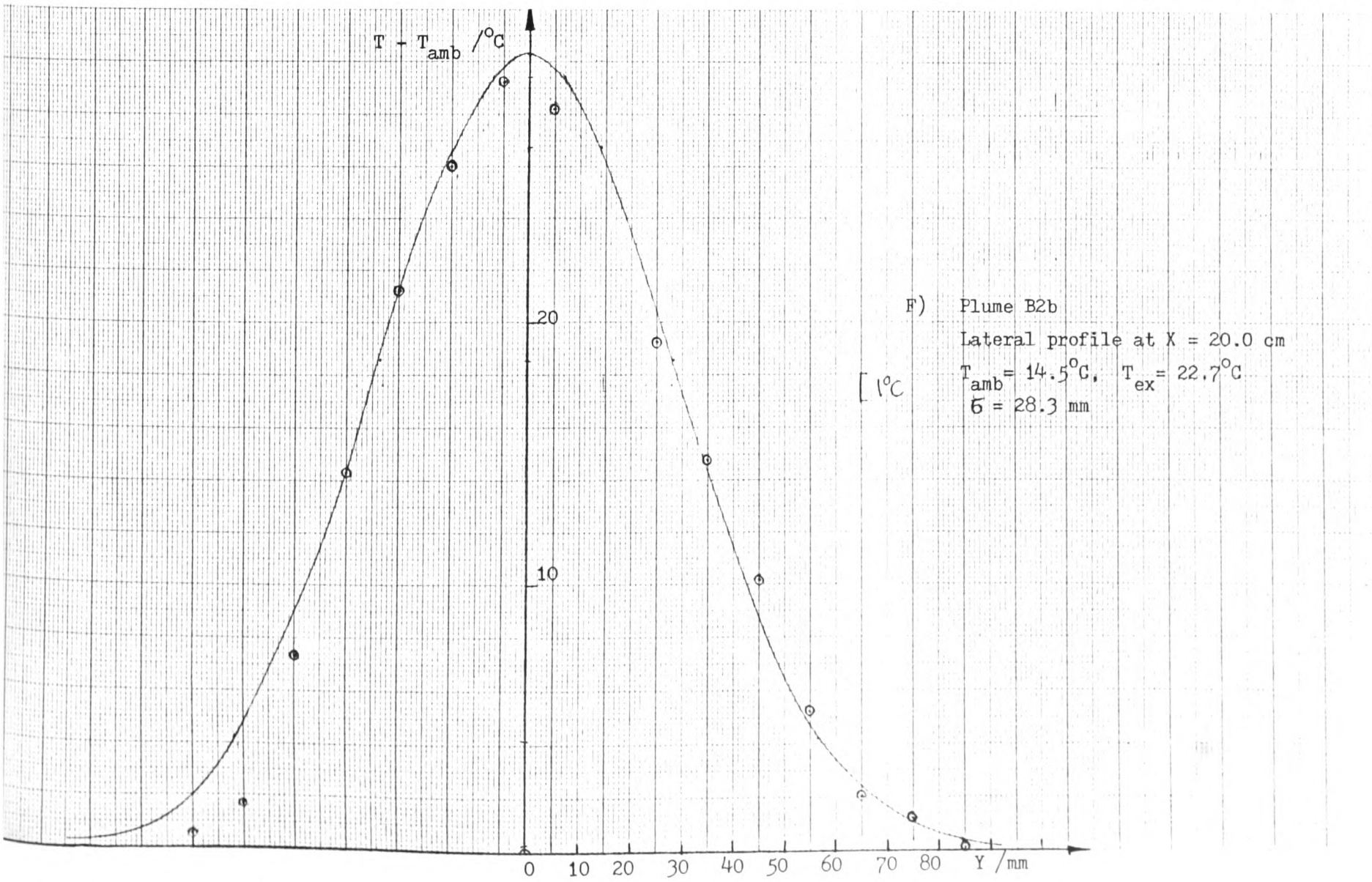

F) Plume B2b
Lateral profile at X = 20.0 cm
T_{amb} = 14.5°C, T_{ex} = 22.7°C
σ = 28.3 mm

[1°C

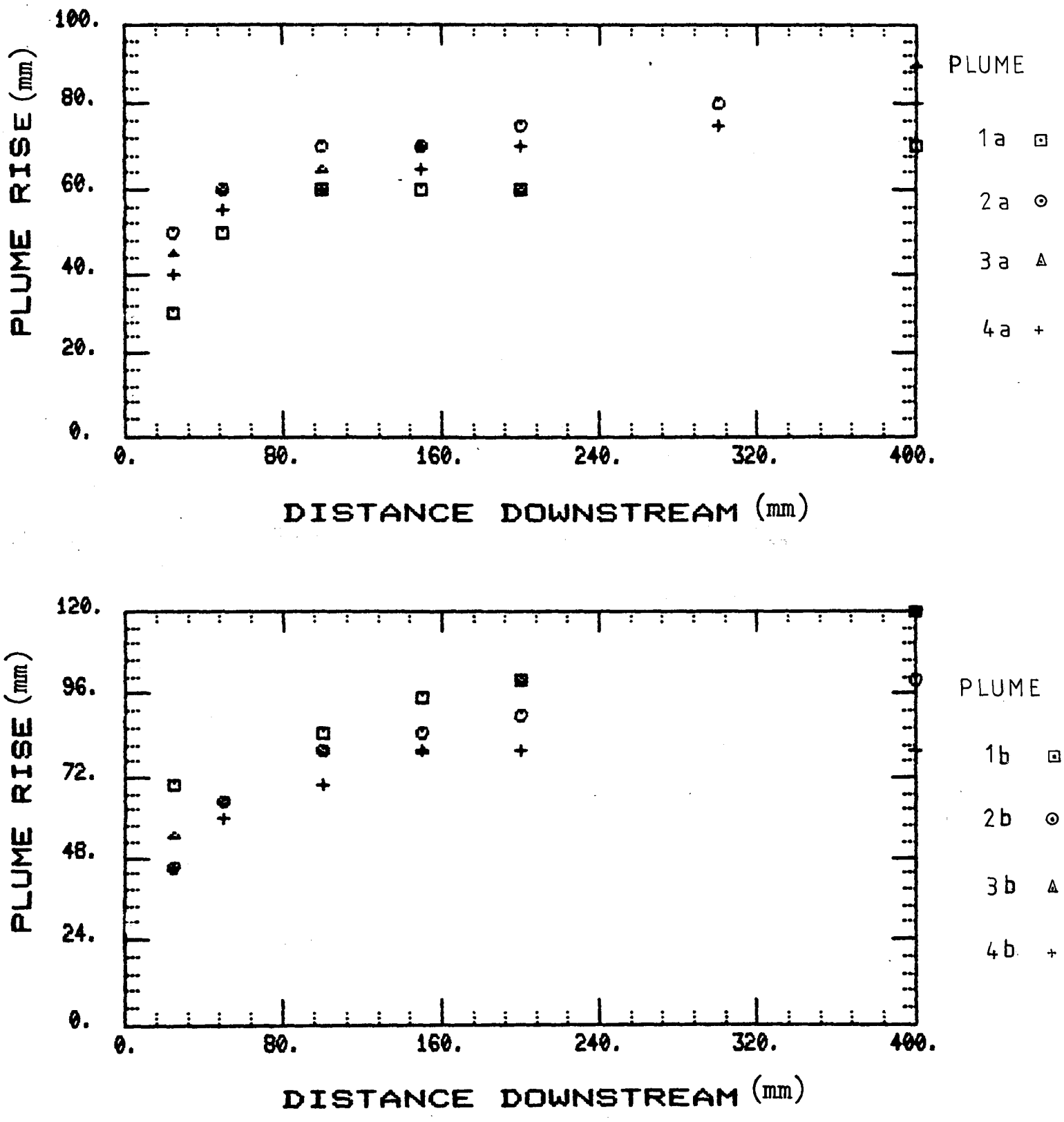

Fig. 6.10 Plume Trajectories in Simulation B
Not Non-dimensionalised

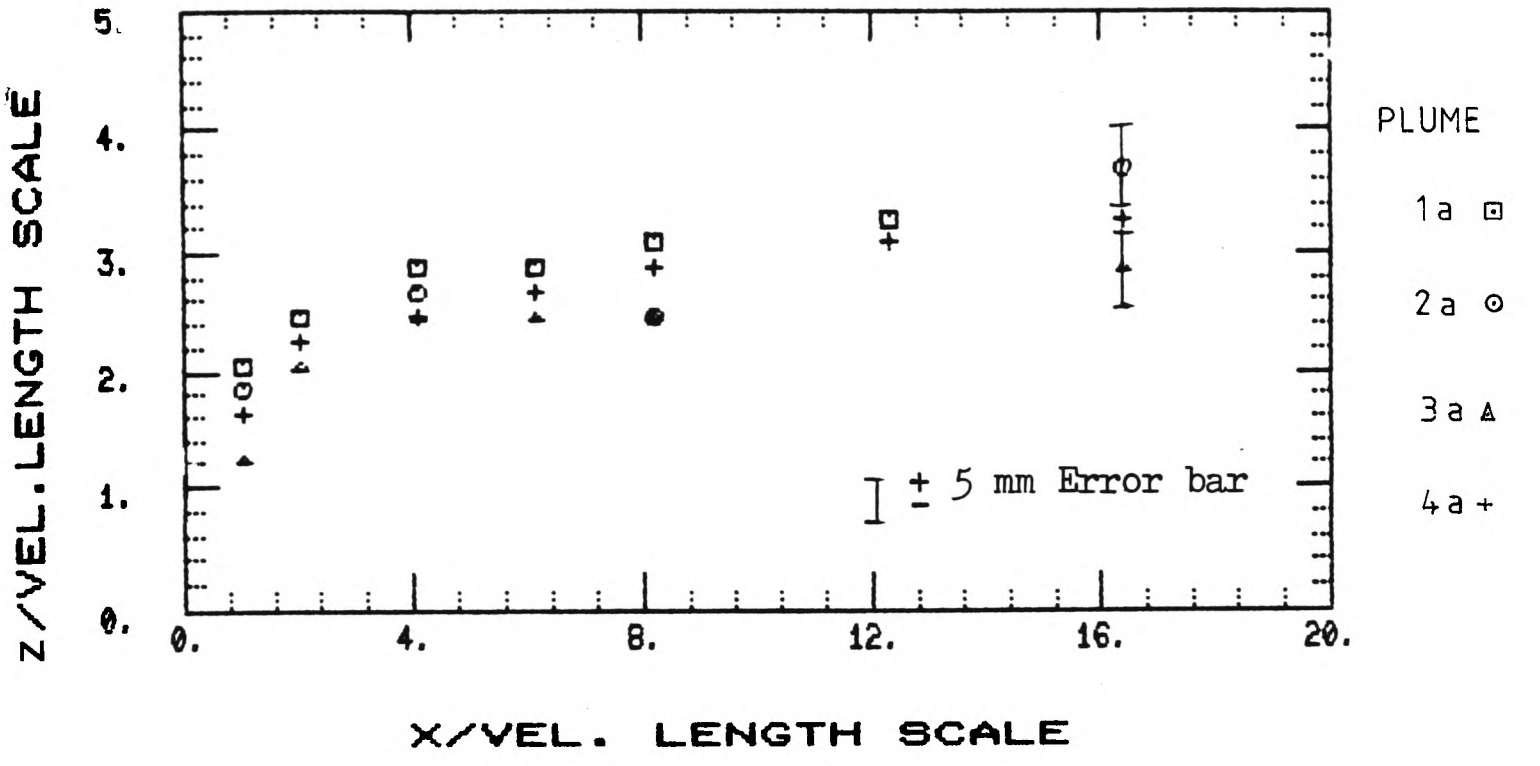

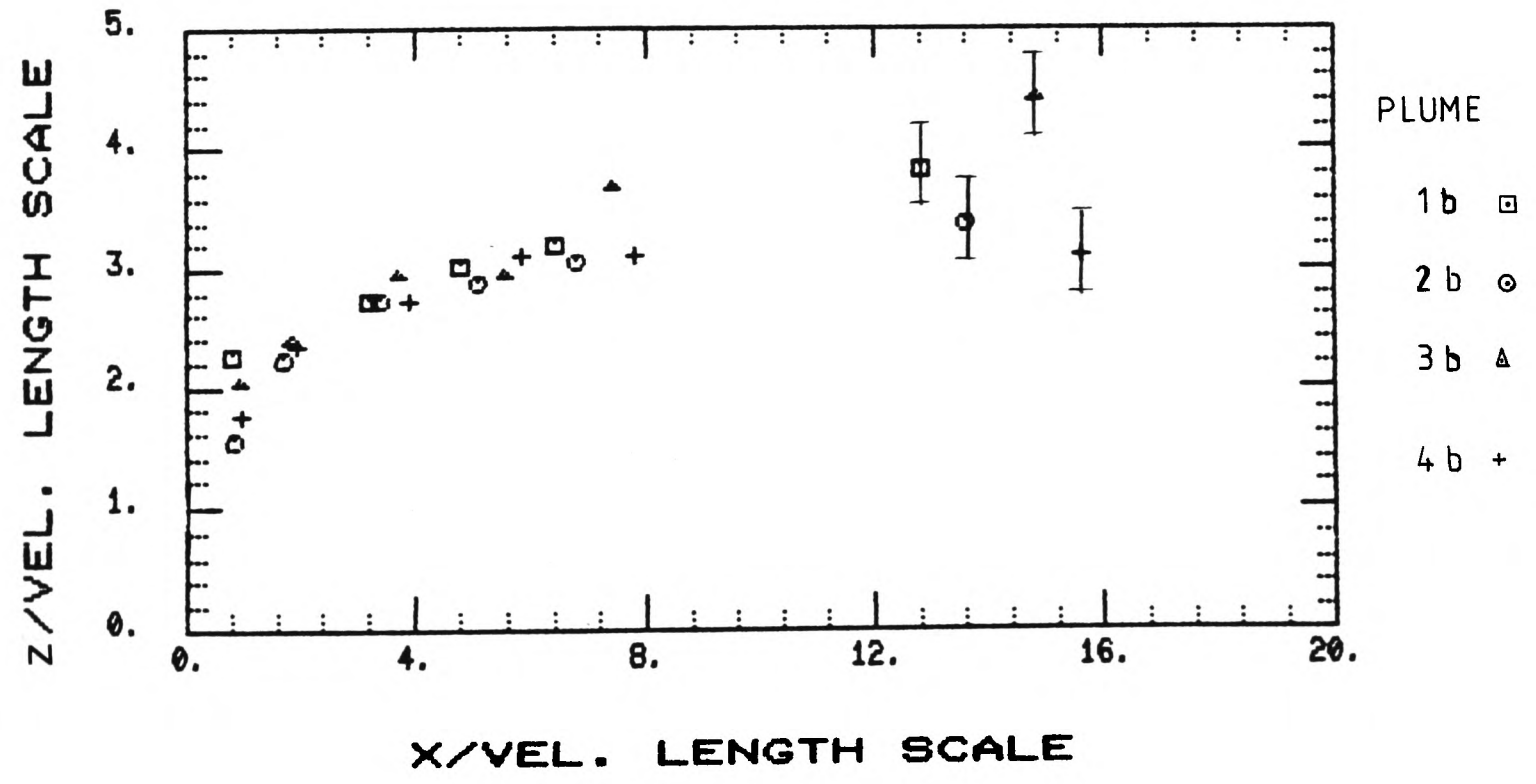

Fig. 6.11 Plume Trajectories in Simulation B
Non-dimensionalised by Velocity Length-scale

Table 6.1a Plume Conditions to Study the Effect of Density Ratio.

No.	T_{ex} (°C)	$\Delta\rho/\rho_a$	U (m/s) (z = 30 cm)	W_s (m/s)	R_{ex}	R_{mom}	F_{rd}
1a	75	.158	.90	2.00	2450	4.2	.047
1b	270	.499	1.51	4.27	2455	4.3	.048
2a	84	.179	.90	2.00	2330	4.1	.053
2b	230	.419	1.36	3.65	2350	4.2	.054
3a	100	.214	.90	2.00	2130	3.9	.063
3b	191	.371	1.18	2.90	2130	3.8	.064
4a	118	.251	.90	2.00	1960	3.7	.075
4b	157	.321	1.01	2.34	1940	3.6	.075

Table 6.1b Plume Conditions to Study the Effect of Reynolds Number.

No.	T_{ex} (°C)	$\Delta\rho/\rho_a$	U (m/s) (z = 30 cm)	W_s (m/s)	R_{ex}	R_{mom}	F_{rd}
5	200	.380	.54	1.50	1075	4.8	.31
6	200	"	.72	2.00	1430	4.8	.18
7	200	"	1.08	3.00	2150	4.8	.08
8	200	"	1.44	4.00	2870	4.8	.04

Stack Centre	R_{ex} = 1000	R_{ex} = 2500	R_{ex} = 2500 + s/paper	R_{ex} =7200
Modal Frequency, $\hat{n}$	7.4	54	75	163
Spectral Width, dn	80	400	440	900
dn/ $\hat{n}$	10.8	7.4	5.9	4.7
Stack Edge				
Modal Frequency, $\hat{n}$	2.7	10.0	11.2	47
Spectral Width, dn	20	100	120	600
dn/ $\hat{n}$	7.4	10.0	10.7	12.8

Table 6.2 Analysis of power spectral densities at various Reynolds numbers.

Plume	B2a	B2b	B1b	B4a	B2a	B2b
σ_{prof}	9.6	30.8	46.0	20.9	15.6	29.4
$\sigma_{b.f.}$	11.7	33.5	48.1	19.9	15.1	28.3
σ_{calc}	11.7	31.0	42.0	20.0	14.5	28.0

Table 6.3 σ values calculated by various methods, in mm.

Plume	B1a	B1b	B2a	B2b	B3a	B3b	B4a	B4b
E_r	.039	.020	.091	.071	.117	.046	.047	.077

Plume	B6	B8	B7	B7b	B6b
E_r	.071	.070	.053	.042	.041

Plume	A3a	A3b	C3a	C3b	D3a	D3b
E_r	.052	.047	.059	.036	.063	.044

Table 6.4 Error Values for Individual Plume Trajectories

length scale / Plume	l_v	l_m	l_b	1
1a,2a,4a	.079	.067	.201	.079
1b,2b,3b 4b.	.083	.081	.154	.101
1a,2a,4a 1b,2b,3b 4b.	.096	.127	>.30	.138
7,8,7b $R_e > 2000$	.084	.084	.208	.084

Table 6.5 Error values for plume trajectories non-dimensionalised by length-scales

Plume	l_v (mm)	l_m (mm)	l_b (mm)
1a	27.2	51.5	.64
1b	34.6	52.7	.83
2a	27.2	50.2	.72
2b	32.9	51.5	.89
3a	27.2	47.8	.86
3b	30.1	46.5	.96
4a	27.2	45.3	1.02
4b	28.4	44.1	1.06
5	34.0	58.8	5.27
6	34.0	58.8	3.06
7	34.0	58.8	1.36
8	34.0	58.8	.68

6.5b Values of the length-scales (model scale)

7. RESULTS AND DISCUSSION

7.1 THE EFFECT OF THE DENSITY RATIO ON PLUME RISE AND SPREAD

Pairs of plumes were studied for which all the dimensionless groups except the density ratio were matched. Temperature profiles were measured for the complete set of plumes, 1 to 4, in simulation B, and for plumes 3a & b in all four simulations. The results for the mean plume trajectory and vertical and lateral spread are given below.

The mean plume trajectories for each of the seven pairs of plumes studied are shown in figs. 7.1a to g (p.176), - non-dimensionalised by the velocity length-scale. Visual examination of these trajectories suggests that in all cases, except B3 (see below), the agreement between the two plumes in each pair is good, bearing in mind the experimental uncertainty, and they appear to collapse onto a single curve. (Error bars showing ± 5 mm uncertainty are shown in fig. 7.1a to illustrate the uncertainty in results.) Also, importantly, there is no observable trend for one plume to rise above the other.

The error analysis of the previous chapter was used to determine how well the pairs of plumes collapsed onto a single curve. A single best-fit curve was fitted to each pair and the root-mean-square error, Er, calculated. This error was then compared with the error when a curve was fitted to each plume individually. The results are given in Table 7.1 and we can see that in all cases, except B1 & B3, the error for the pair is no larger than for the individual plumes. This suggests that within experimental scatter the non-dimensional trajectory of the two plumes is the same. The large error for pair B3 where the two plume trajectories are clearly different, see fig. 7.1c, is thought to be due to an error in measuring the trajectory of plume B3a. The large individual error value for plume B3a (Er = .117) has already been noted

and the fact that the trajectory levels-off rapidly suggests that an error was made while measuring the vertical temperature profiles for plume B3a. Consequently, the result for the pair B3 was not considered in reaching our conclusion. The relatively large error for pair B1 (compared with the individual errors) is suprising. Closer examination shows that although the agreement is good near the stack, at the furthest downstream position the hotter plume (1a) is rising slightly above the colder plume. It is not possible to make a conclusion from only two points but it is worth noting that this pair has the largest temperature difference, i.e. 70 - 270°C.

The results for the vertical rate of spread, σz, plotted in log-log form, are shown in figs. 7.2a to g. Error bars, $\pm$10%, are drawn to show the uncertainty in σ values. Firstly, the relatively large experimental scatter in the results should be noted. Clearly the scatter in the results makes it difficult to come to any definite conclusions. Similar problems are evident in other wind tunnel studies and full-scale measurements of dispersion. Only in a few cases could a meaningful best-fit straight line (or lines) be drawn through the data. Therefore, the error analysis was not applied to these results but rather a best-fit line of the form predicted by theoretical methods was drawn for comparison (- the line drawn is $\sigma_z^2 \propto X$, see sect. 7.4, later).

Examining the results in figs. 7.2, we can see that there is reasonable agreement for the spread of the two plumes in each pair. There is no clear trend for one plume to spread differently from the other, and in several cases, e.g. B3, B4, C3, D3, there is good agreement between the plumes. Only in fig. 7.2a, plumes B1a & b, is there a serious discrepancy. The rate of spread of the colder plume (1b) levels-off for $X/l_v > 4$, while the hotter plume (1a) continues to spread; this was the coldest plume studied (70°C) and the levelling-off

is probably due to the lack of sensitivity of the analysis technique for temperatures only a few degrees above ambient. In fig. 7.2e, plumes A3a & b, the scatter in the results is large but there is no trend for one plume to spread differently from the other. Within the experimental uncertainty due to the scatter in the results, the rate of vertical spread seems to be independent of the exit gas density.

Finally, the results for the lateral spread, σ_y, are shown in figs. 7.3 a to f (-only 5 pairs may be compared since no lateral traverses were made for B1 or D3b). The scatter in the σ_y values appears to be less than for σ_z, and they collapse more readily onto a single curve (a best-fit curve of the form $\sigma_y \propto X^{1/3}$ is plotted for comparison later). Only for plumes B4a & b, fig. 7.3c, is the scatter large and there is no clear discrepancy between the spread of the two plumes. Examining the other results, we observe good agreement between the plumes for lateral spread, especially plumes B2, A3, C3 and no obvious signs of one of the plumes spreading differently from the other.

Bearing in mind the experimental scatter, these results confirm the findings of several authors, Hoult and Weil (1972), Wilson (1979), who found that mismatching the exit density ratio had negligible effect on plume behaviour in the near field provided all the other dimensionless groups were matched. A relatively large range of density differences ($\Delta\rho/\rho_a$) was studied, i.e. 0.15 to 0.46, and no marked discrepancies were found. Hoult et al. (1977) warned that the mechanism of entrainment is modified if $\Delta\rho/\rho_a > .4$; in our experiments there were two pairs of plumes which had one plume below and one above that value and no significant differences were observed.

The results of Ricou and Spalding (1961) for jets in a calm atmosphere would suggest a variation in the entrainment rate (dm/dx) of 30% for the above density difference. Our buoyant bent-over plumes

would not appear to exhibit such a variation in the entrainment rate. Bent-over plumes are clearly less sensitive to the density ratio.

Summarizing the above results, within the experimental uncertainty of the experiments, we have found that for temperatures in the range 70°C to 270°C and for the near-field ($X/l_v < 15$):

i) the mean plume trajectory is unaffected by the exit density ratio,

ii) the mean vertical and lateral spread are also unaffected by the exit density ratio,

provided all the other dimensionless groups are matched.

We can conclude that in wind tunnel studies mis-matching the density ratio, in order to achieve higher operating speeds, is a valid technique for the temperature range studied, i.e. up to 270°C. This range includes most industrial sources and since in many cases the exit temperatures are below 150°C, we could double the density difference in the wind tunnel. Greatly exaggerating the temperature difference, above 300°C, should be considered carefully and verified experimentally.

a) Simulation B ⊡ 1a T_{ex}= 75°C ($\Delta\ell/\ell_a$ = .158) } All other
⊙ 1b T_{ex}= 270°C ($\Delta\ell/\ell_a$ = .499) } conditions matched.

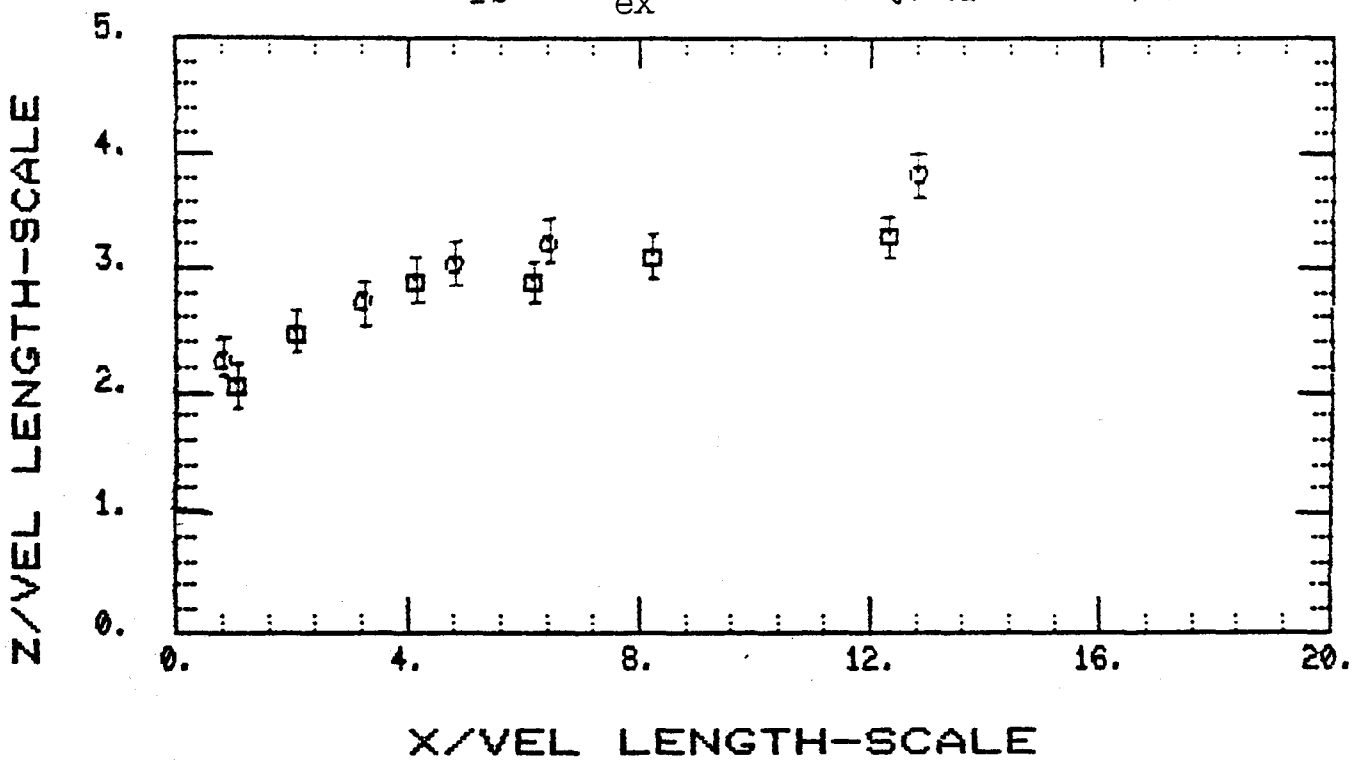

b) Simulation B + 2a T_{ex}= 84°C ($\Delta\ell/\ell_a$ = .179) } All other
× 2b T_{ex}= 230°C ($\Delta\ell/\ell_a$ = .419) } conditions matched.

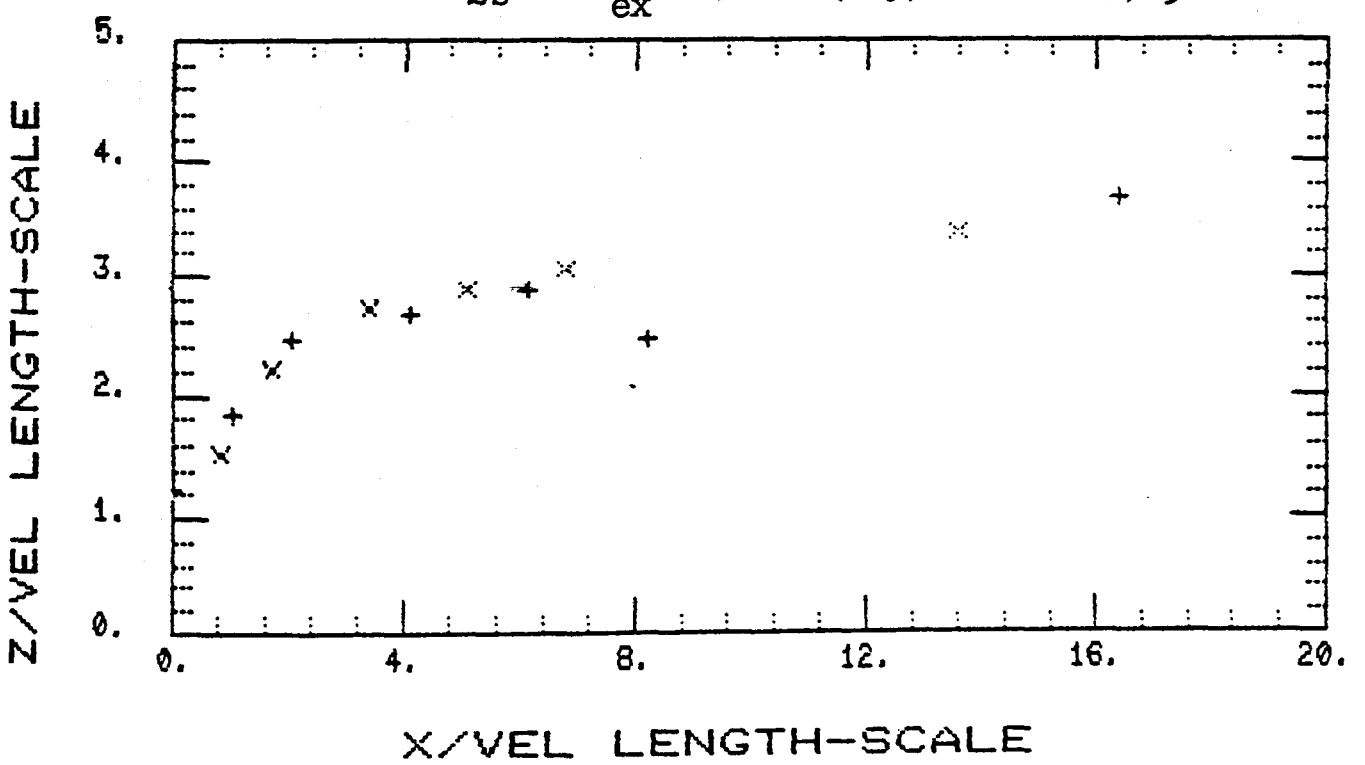

Fig. 7.1a & b Comparison of Pairs of Plumes
with Different Exit Density Ratios

c) Simulation B + 3a T_{ex} = 100°C ($\Delta\ell/\ell_a$ = .214) } All other
× 3b T_{ex} = 191°C ($\Delta\ell/\ell_a$ = .371) } conditions matched.

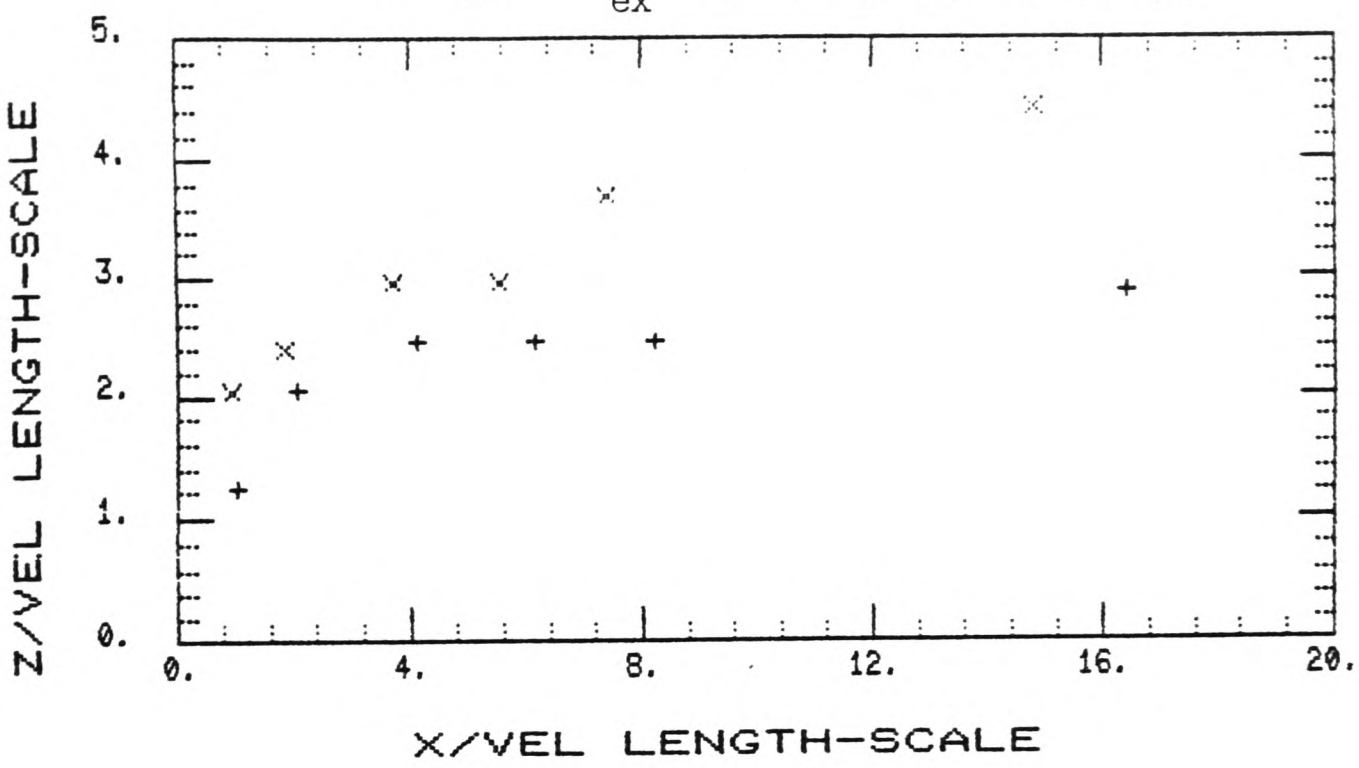

d) Simulation B Y 4a T_{ex} = 118°C ($\Delta\ell/\ell_a$ = .251) } All other
◇ 4b T_{ex} = 157°C ($\Delta\ell/\ell_a$ = .321) } conditions matched.

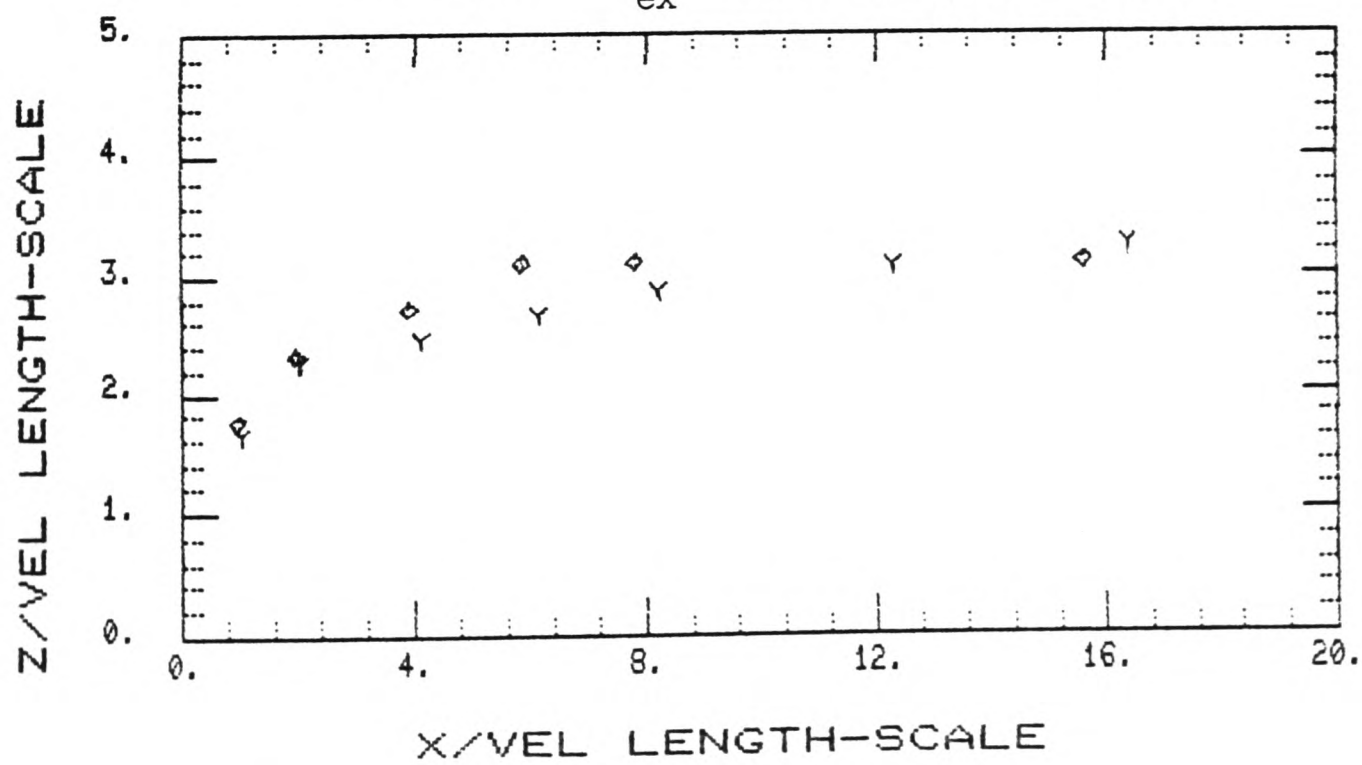

Fig. 7.1c & d Comparison of Pairs of Plumes
with Different Exit Density Ratios

e) Simulation A ⍋ 3a T_{ex} = 100°C ($\Delta\ell/\ell_a$ = .214) } All other
⧖ 3b T_{ex} = 191°C ($\Delta\ell/\ell_a$ = .371) } conditions matched.

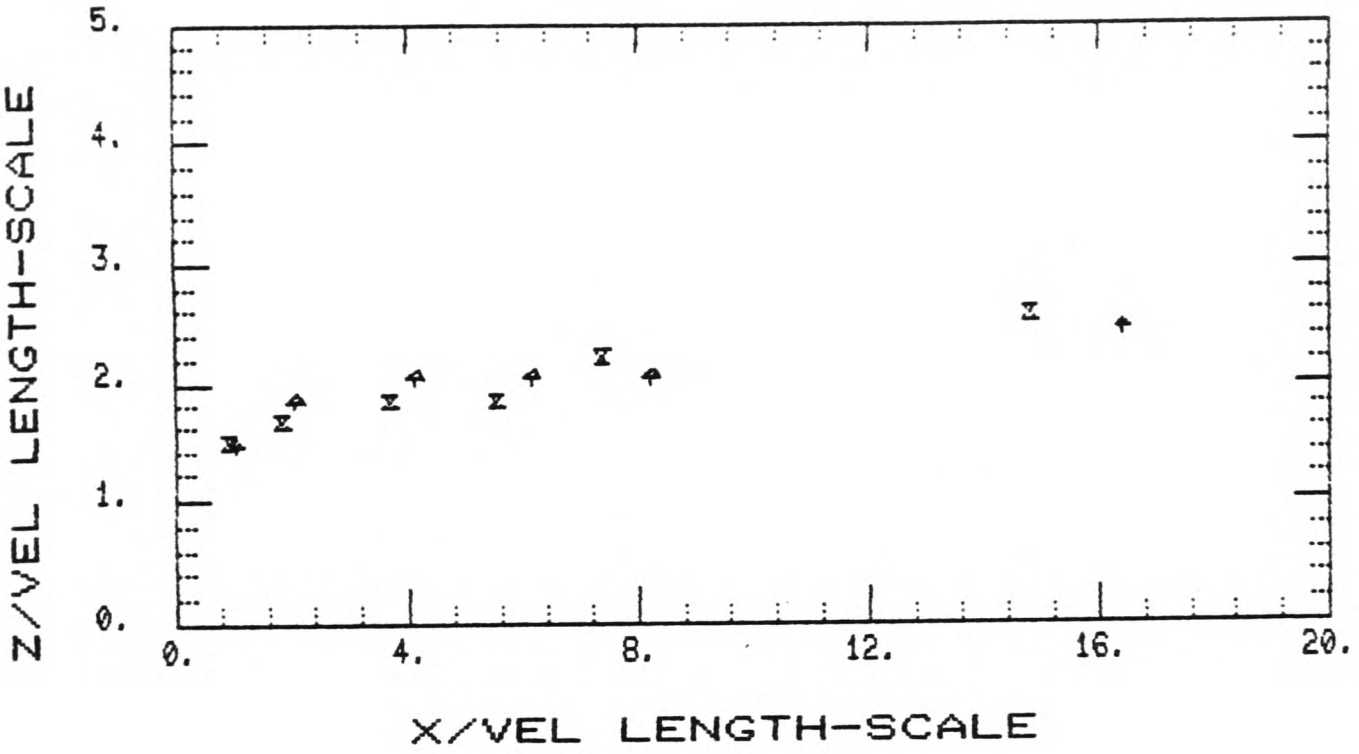

f) Simulation C ⊙ 3a T_{ex}=100°C ($\Delta\ell/\ell_a$ = .214) } All other
△ 3b T_{ex}=191°C ($\Delta\ell/\ell_a$ = .371) } conditions matched.

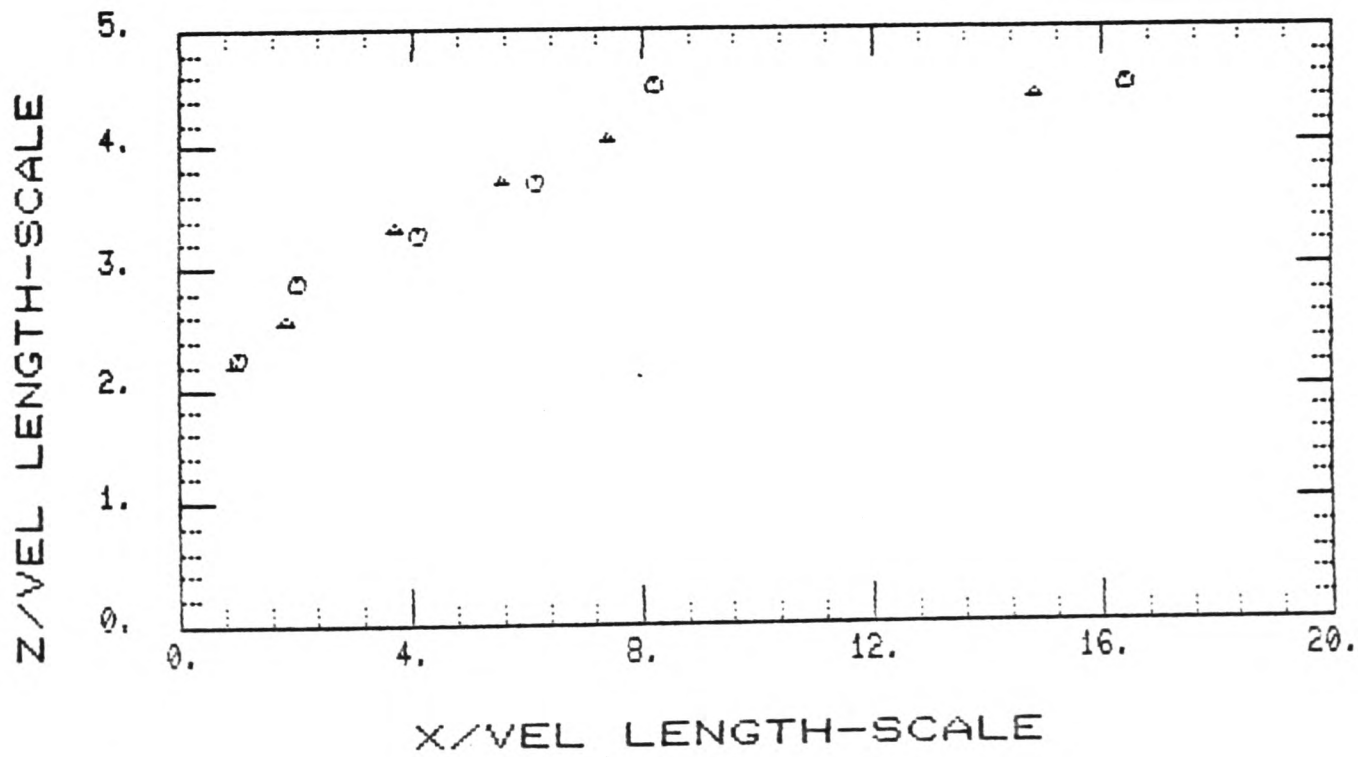

Fig. 7.1e & f Comparison of Pairs of Plumes
with Different Exit Density Ratios

g) Simulation D + 3a T_{ex} = 100°C ($\Delta\ell/\ell_a$ = .214) } All other
× 3b T_{ex} = 191°C ($\Delta\ell/\ell_a$ = .371) } conditions matched.

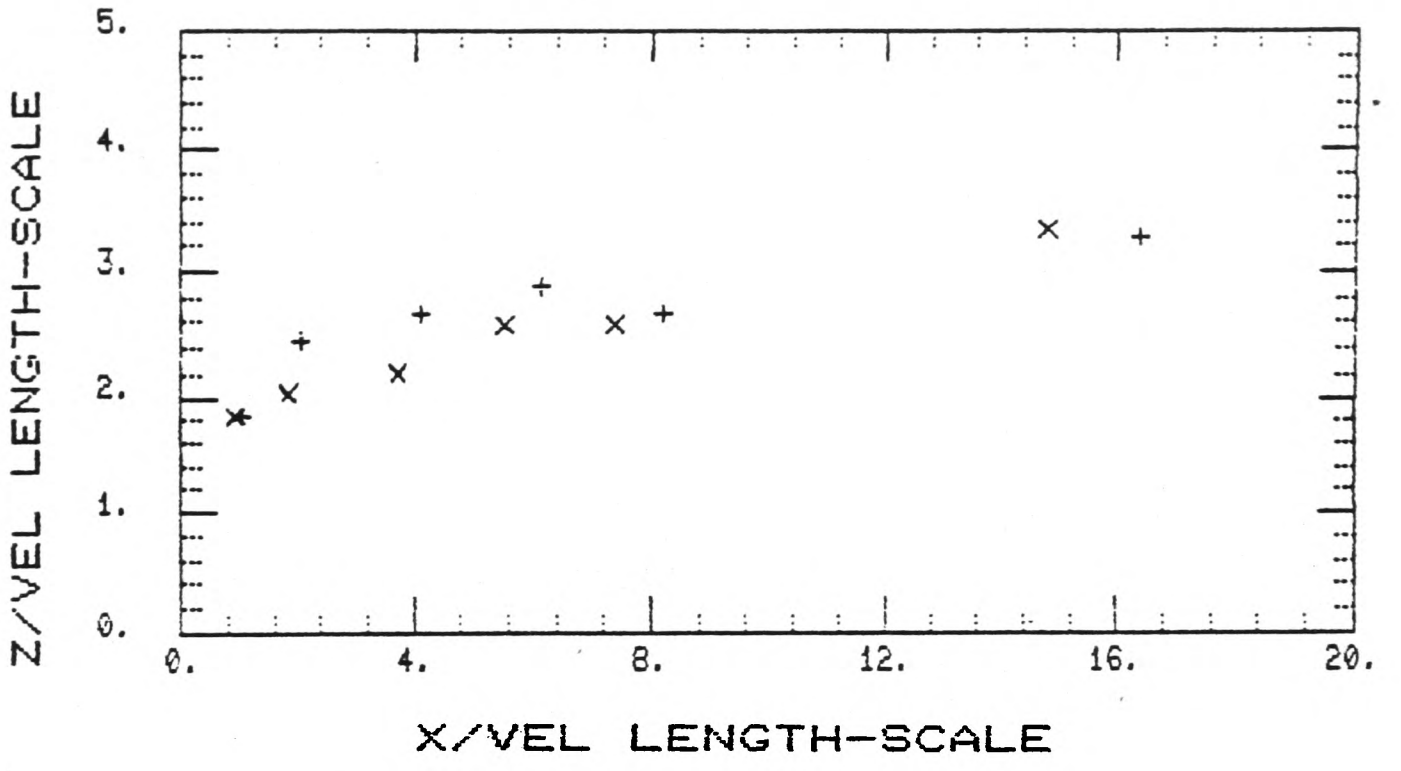

fig. 7.1g Comparison of Pairs of Plumes
with Different Exit Density Ratios

PLUME	a	b	a & b
B1	.039	.020	.063
B2	.091	.070	.087
B3	.117	.046	.188
B4	.047	.077	.078
A3	.052	.047	.051
C3	.059	.036	.049
D3	.063	.044	.064

Table 7.1 R.M.S. Error in Plume Trajectories

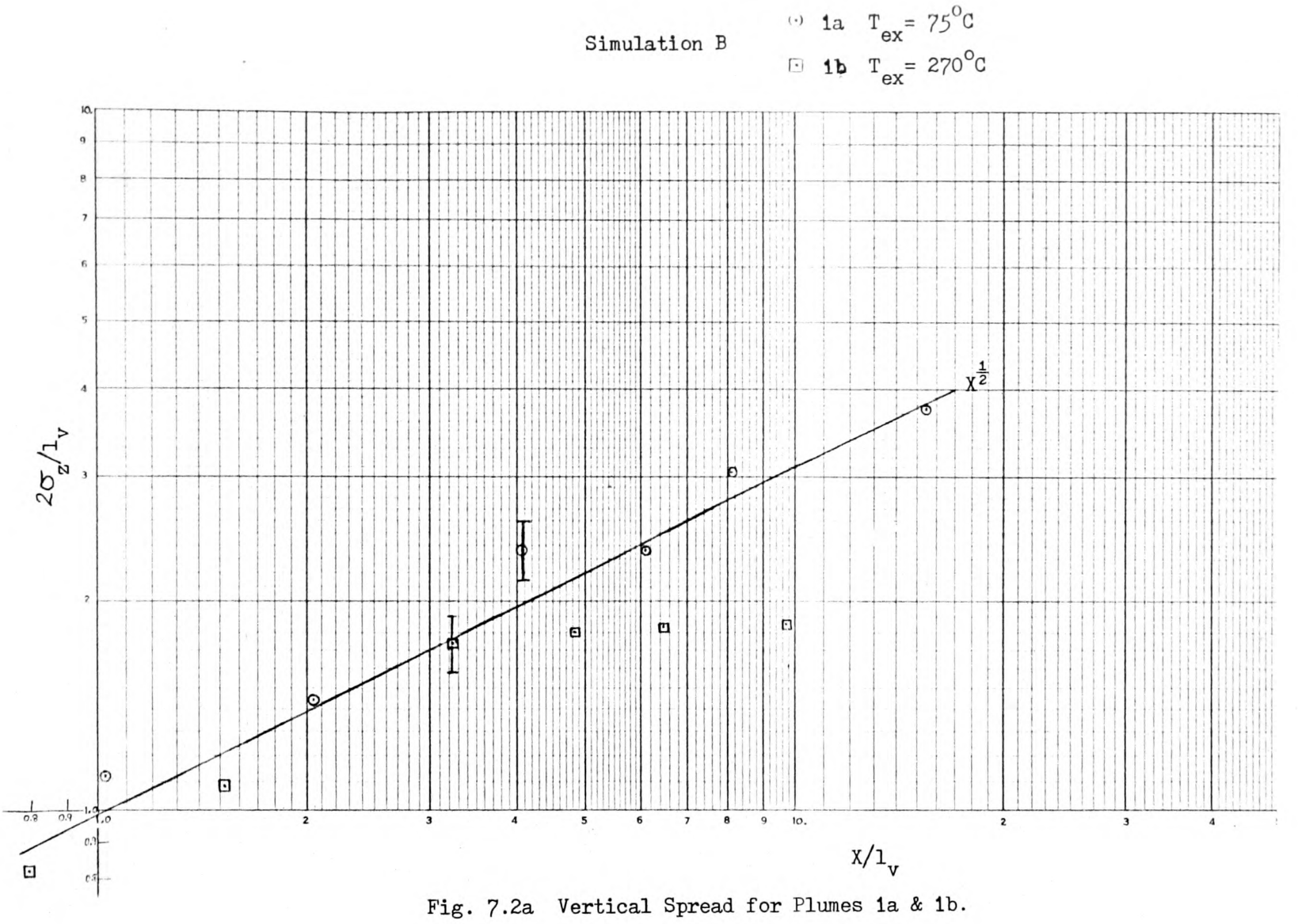

Fig. 7.2a Vertical Spread for Plumes 1a & 1b.

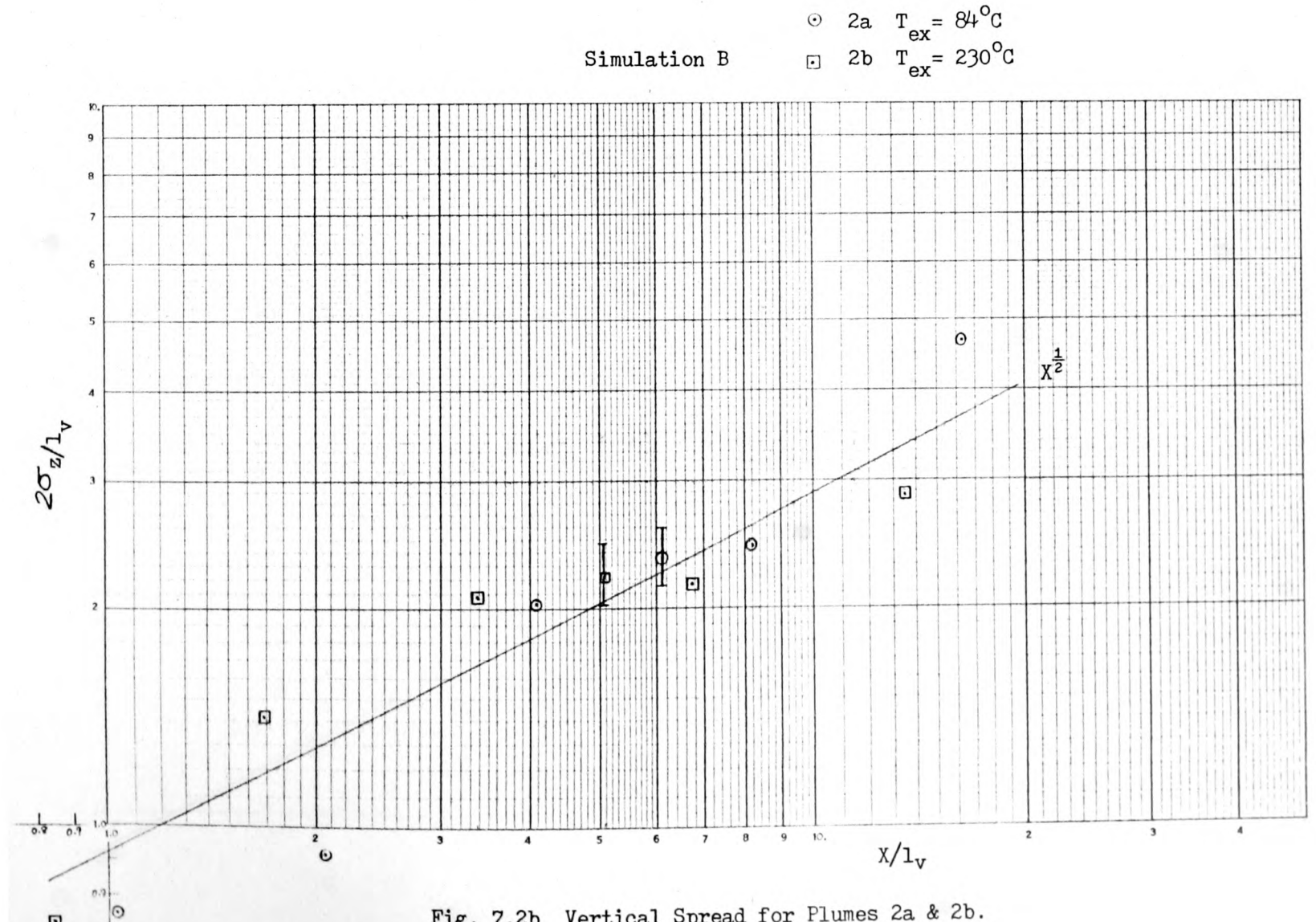

Fig. 7.2b Vertical Spread for Plumes 2a & 2b.

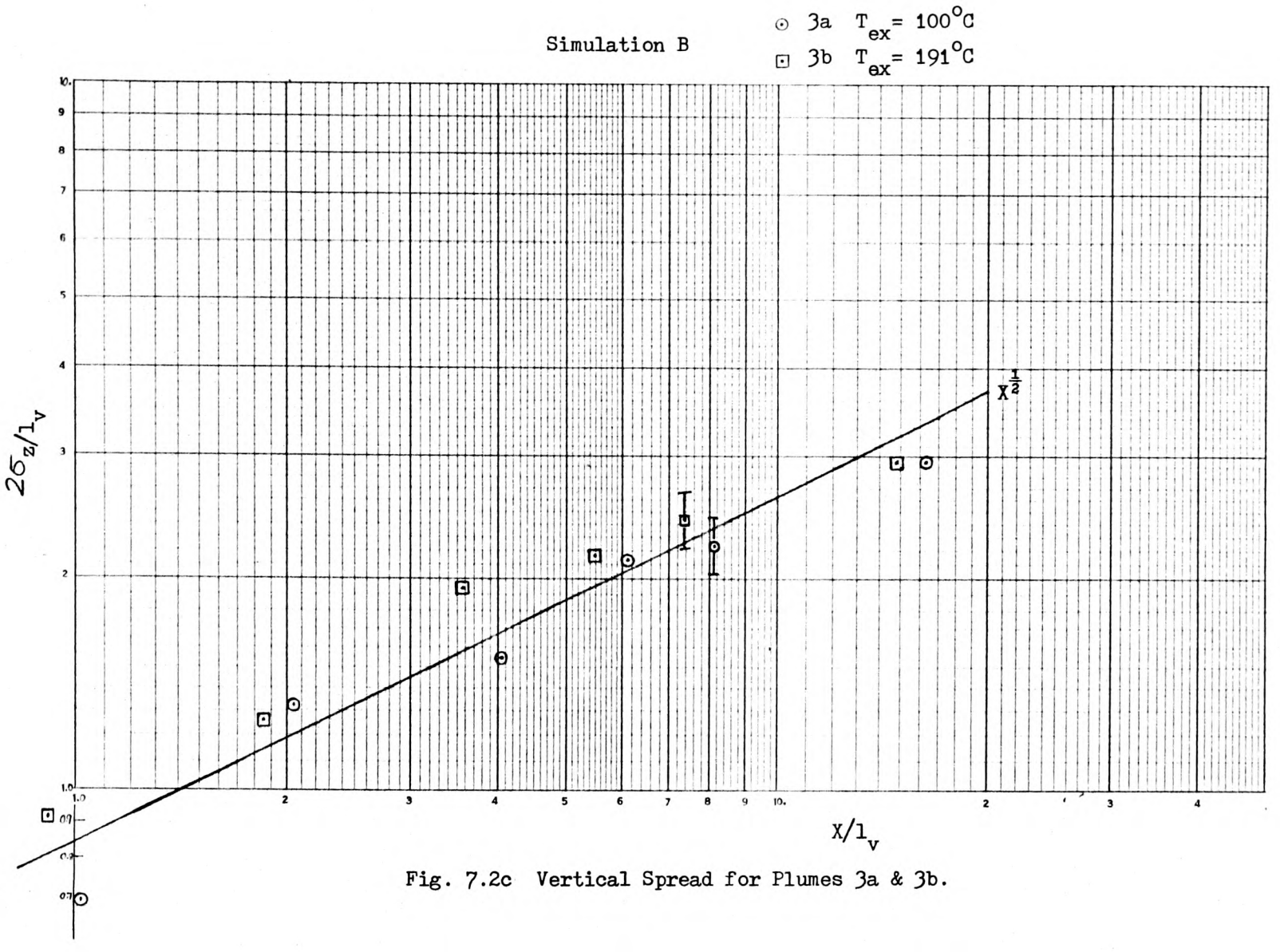

Fig. 7.2c Vertical Spread for Plumes 3a & 3b.

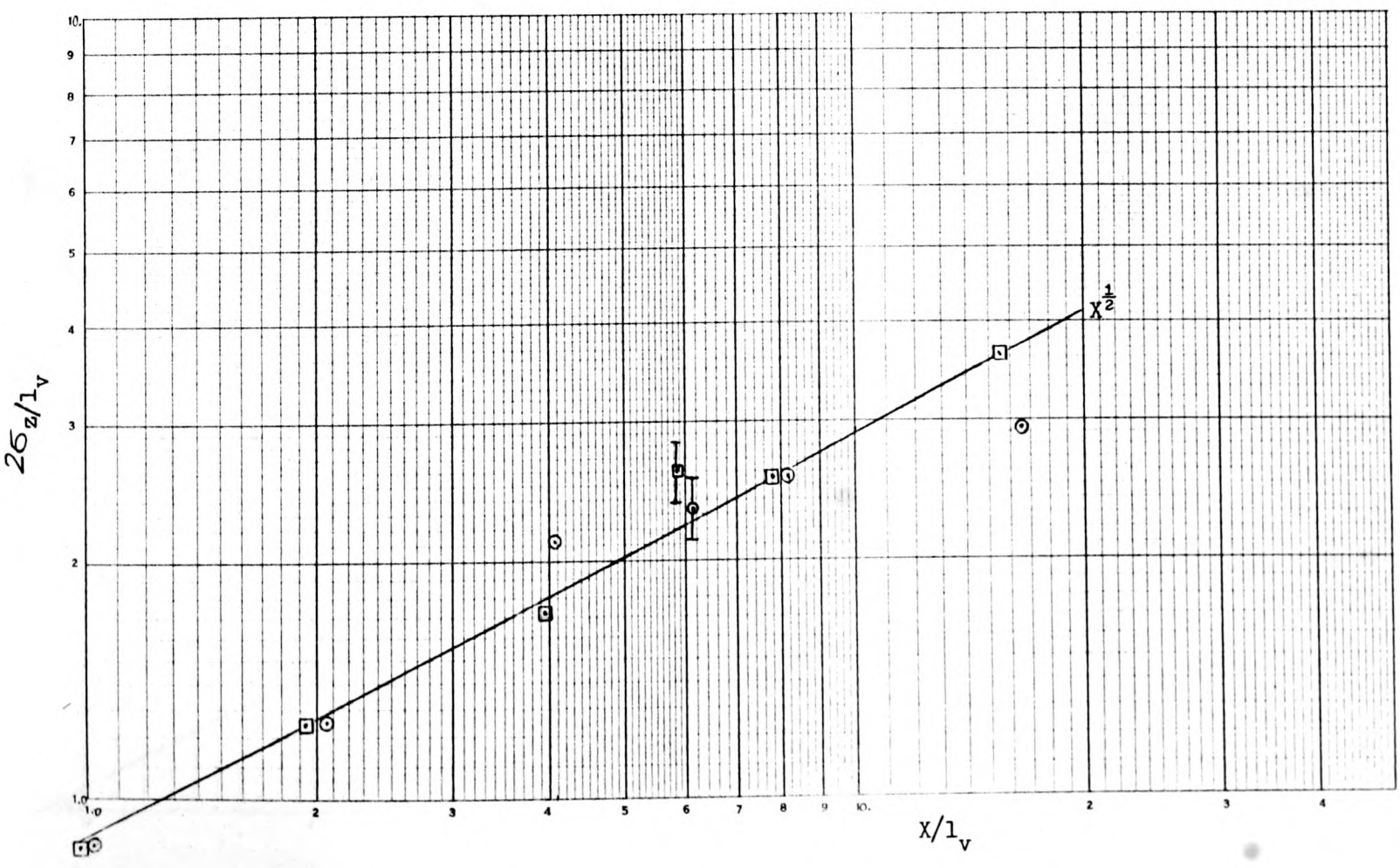

Fig. 7.2d Vertical Spread for Plumes 4a & 4b.

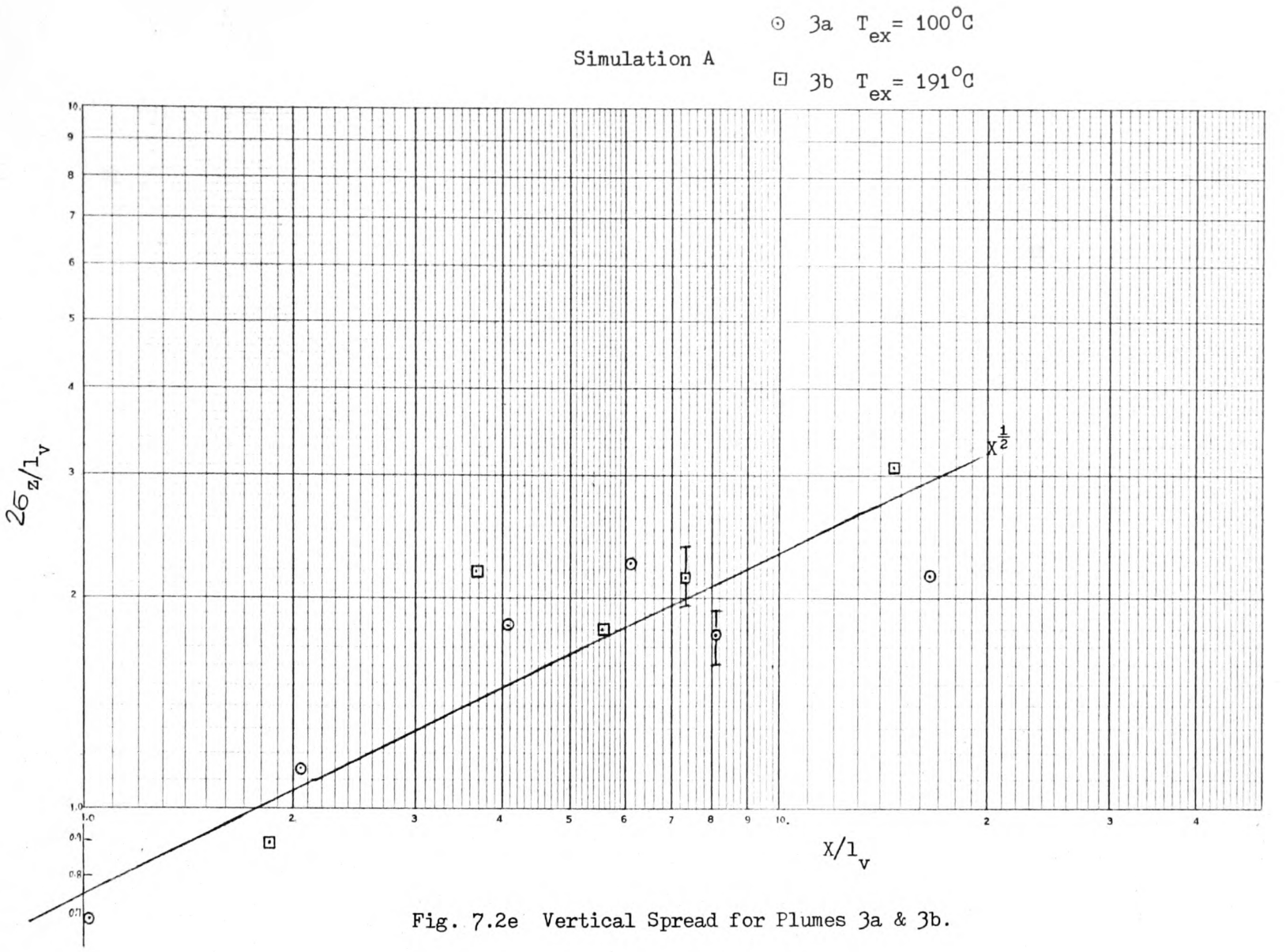

Fig. 7.2e Vertical Spread for Plumes 3a & 3b.

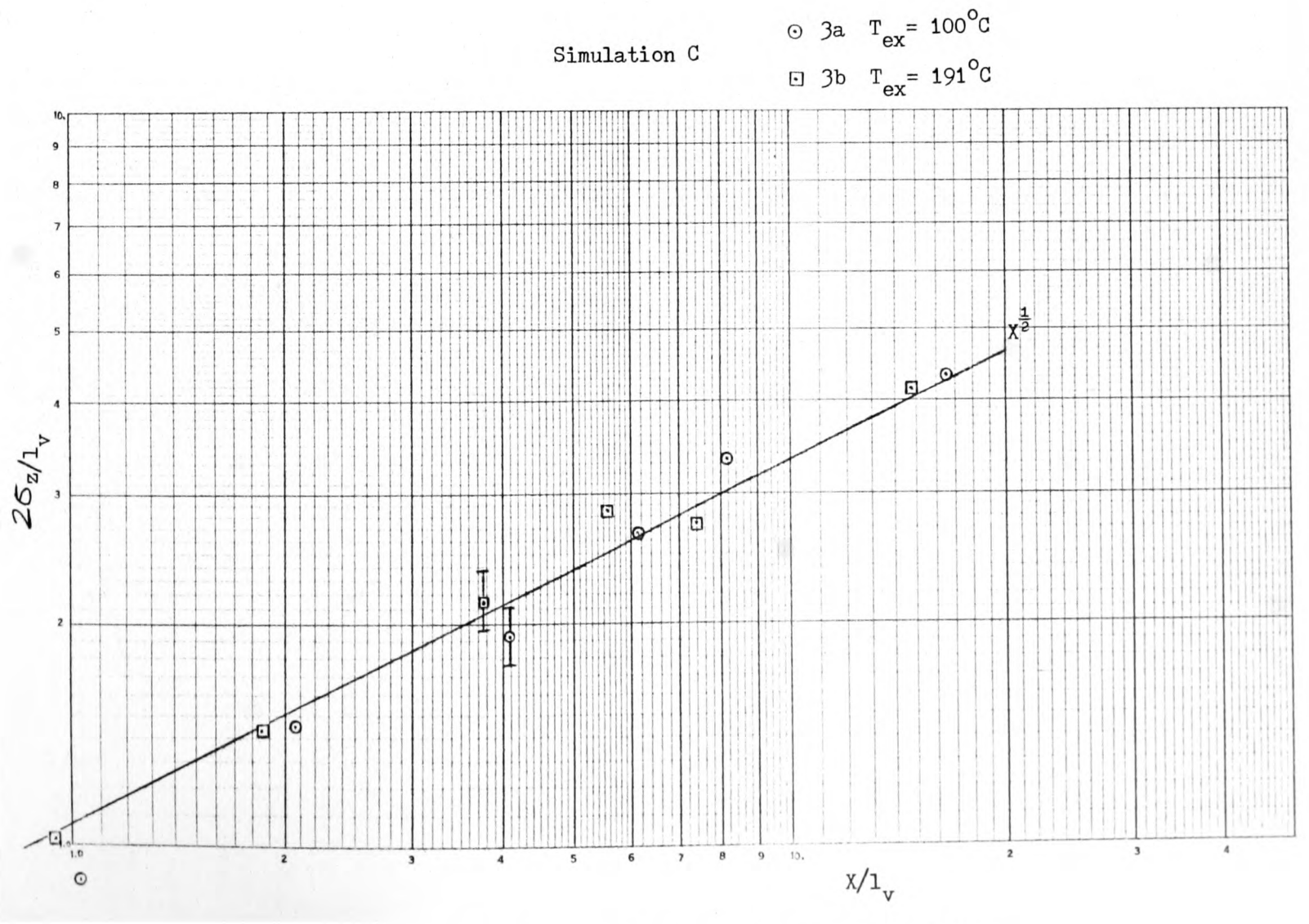

Fig. 7.2f Vertical Spread for Plumes 3a & 3b.

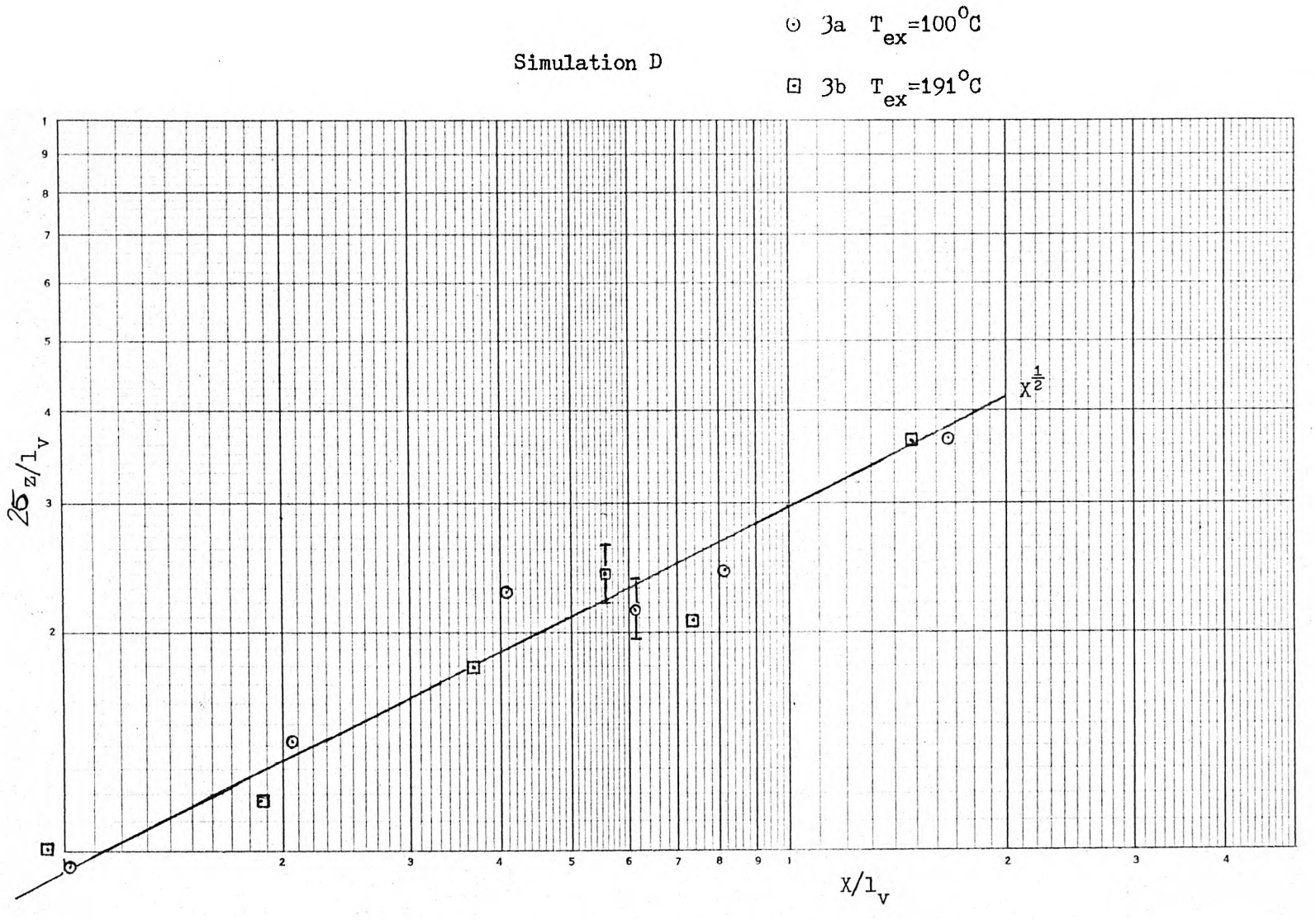

Fig. 7.2g Vertical Spread for Plumes 3a & 3b.

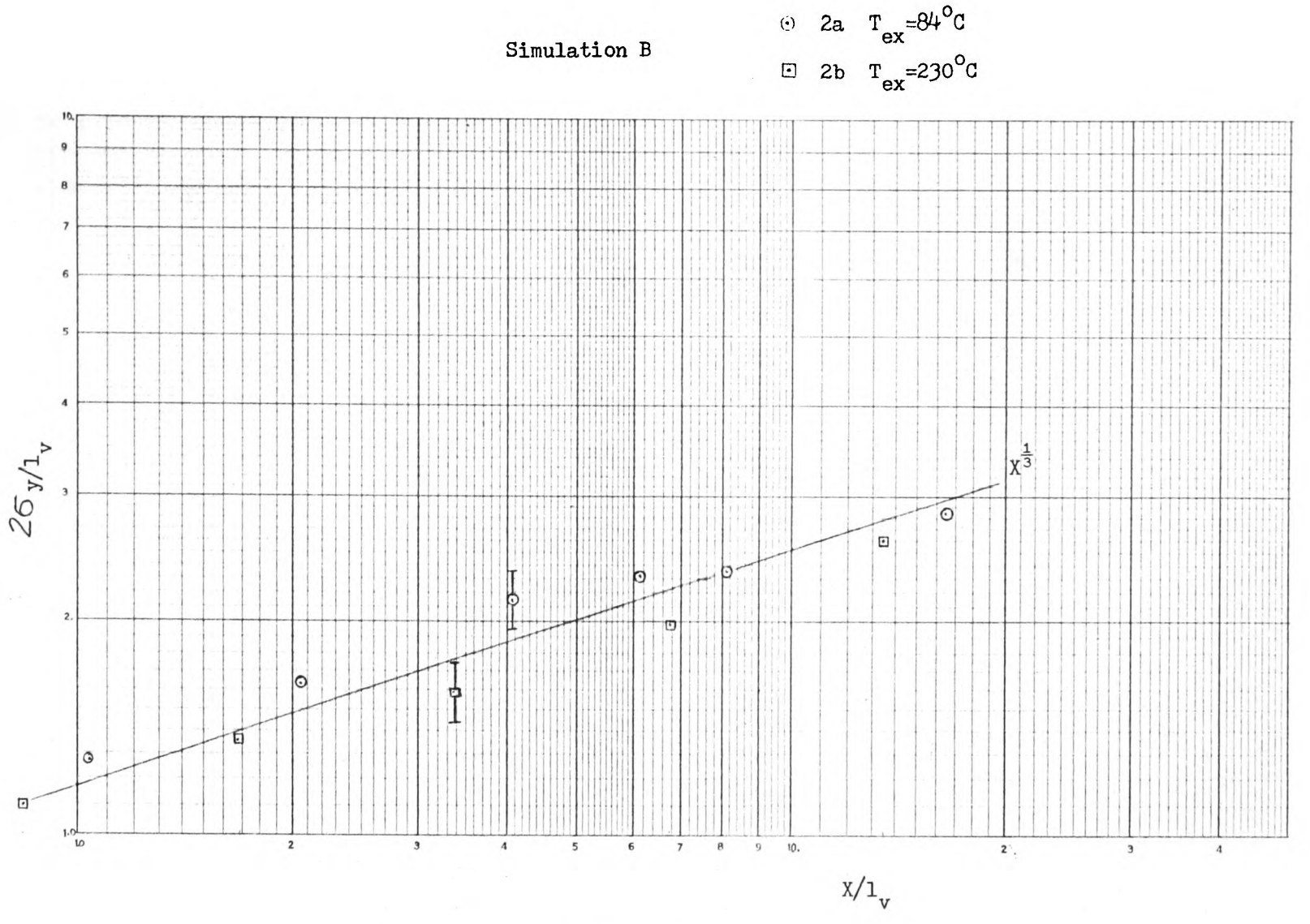

Fig. 7.3a Lateral Spread for Plumes 2a & 2b.

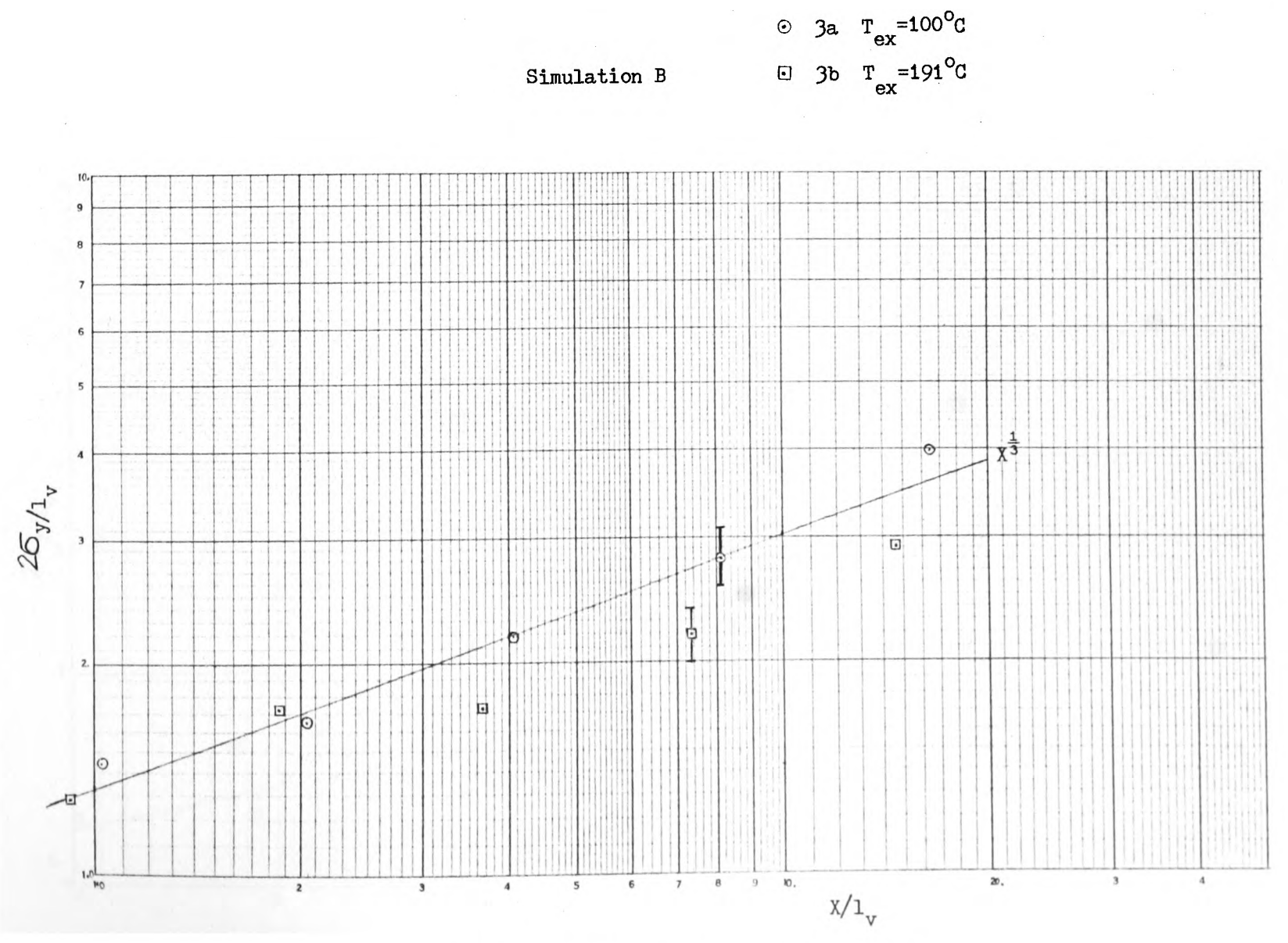

Fig. 7.3b Lateral Spread for Plumes 3a & 3b.

Simulation B

⊙ 4a T_{ex}=118°C

⊡ 4b T_{ex}=157°C

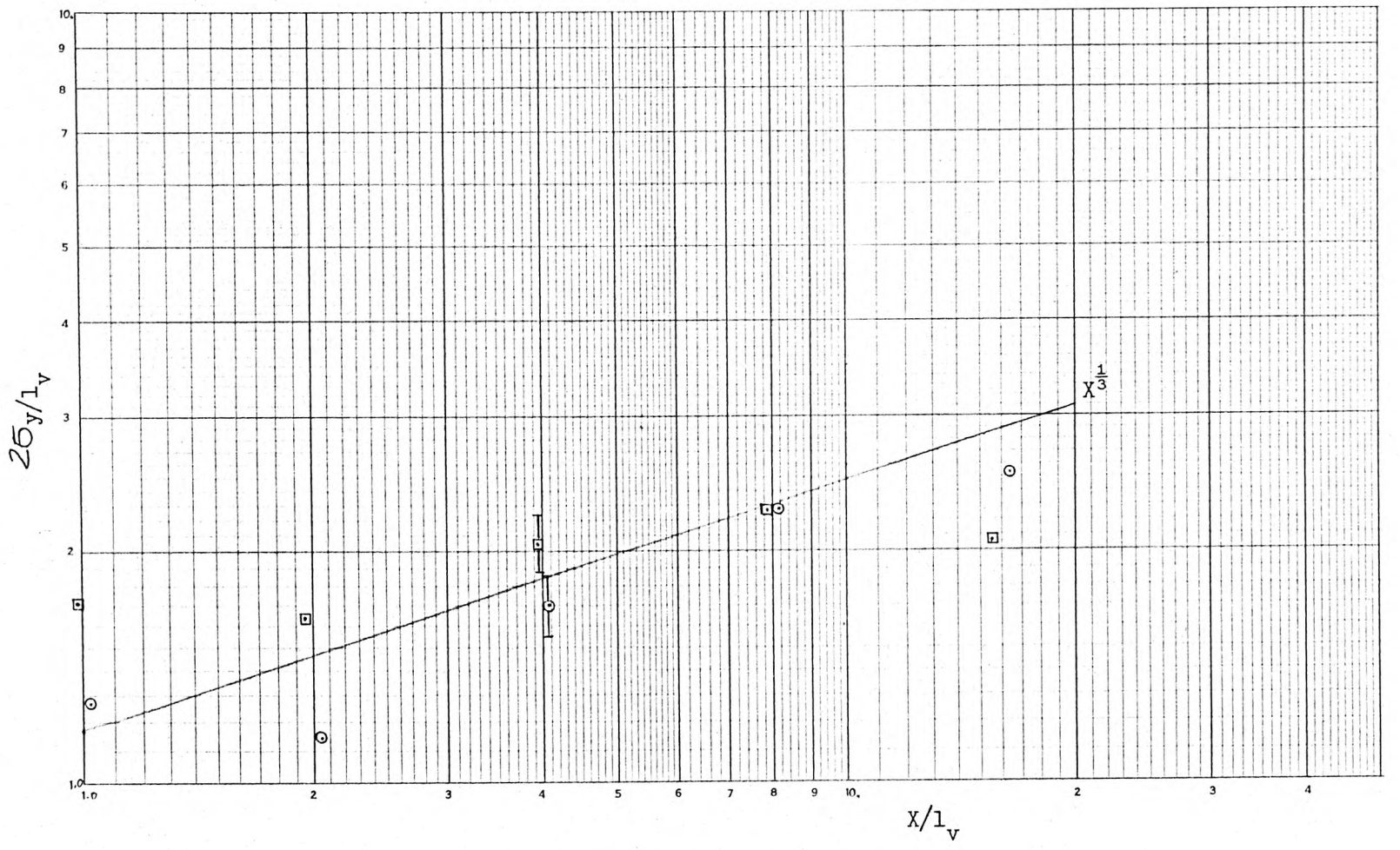

Fig. 7.3c Lateral Spread for Plumes 4a & 4b.

Simulation A

⊙ 3a T_{ex}= 100°C

⊡ 3b T_{ex}= 191°C

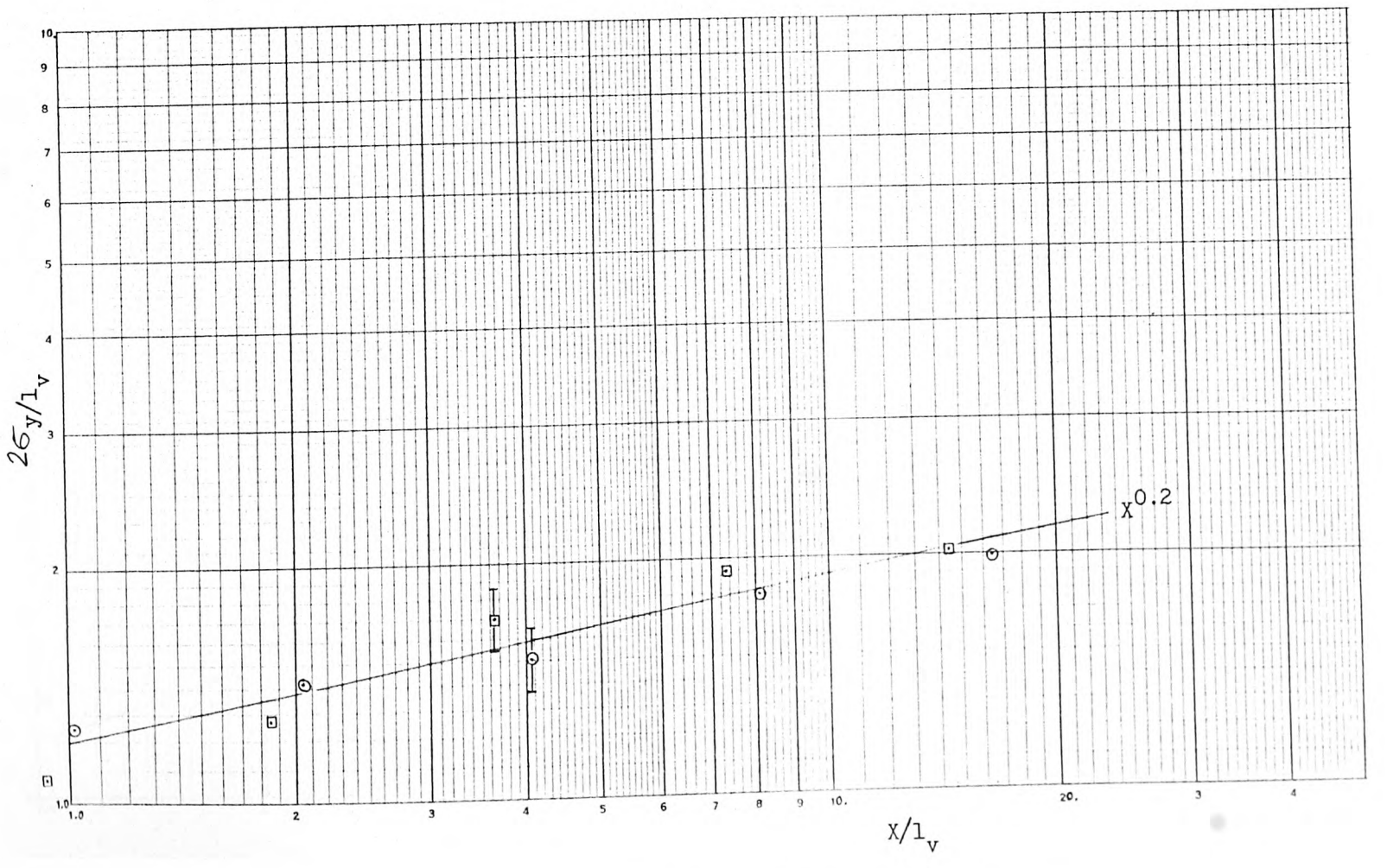

Fig. 7.3d Lateral Spread for Plumes 3a & 3b.

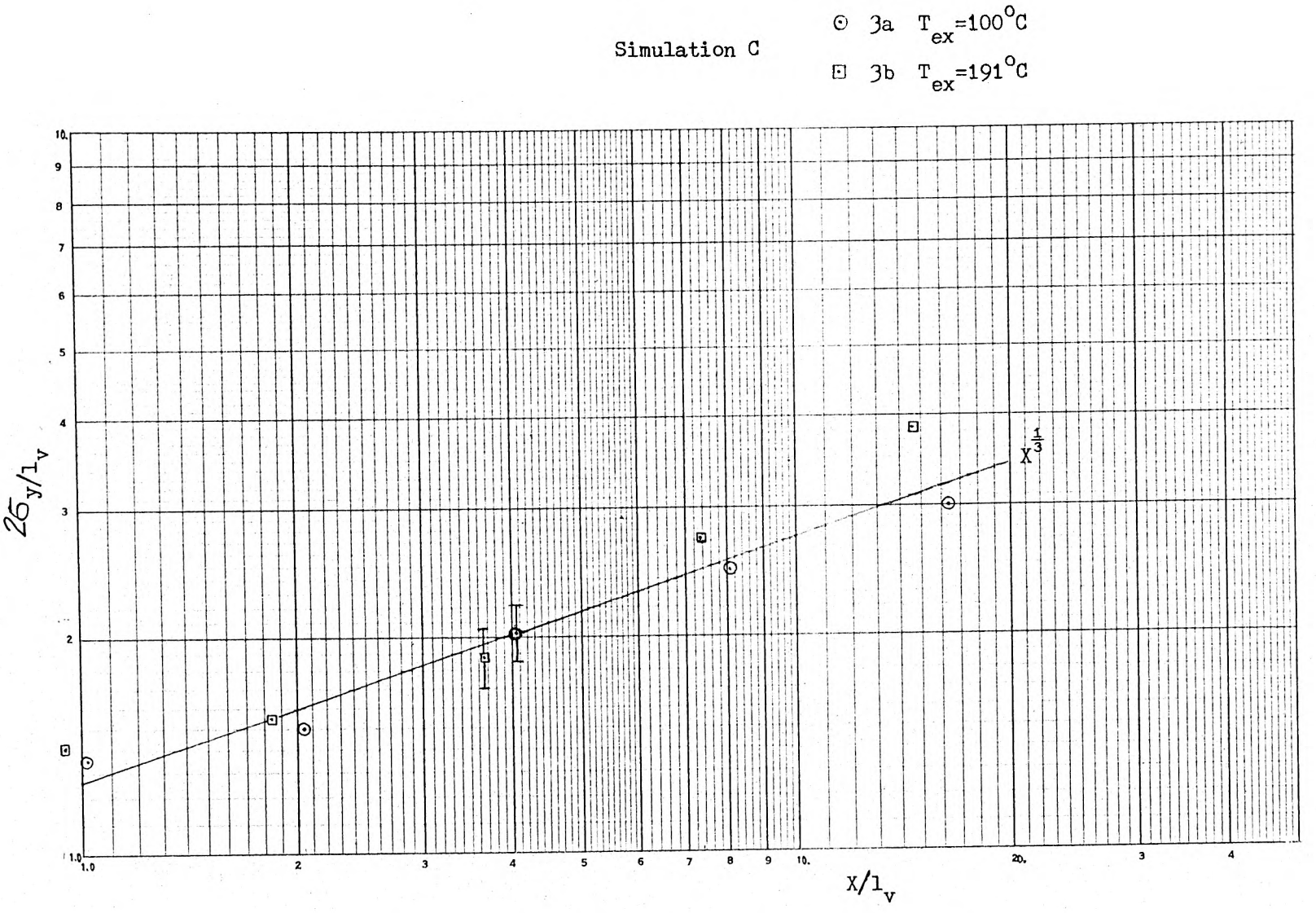

Fig. 7.3e Lateral Spread for Plumes 3a & 3b.

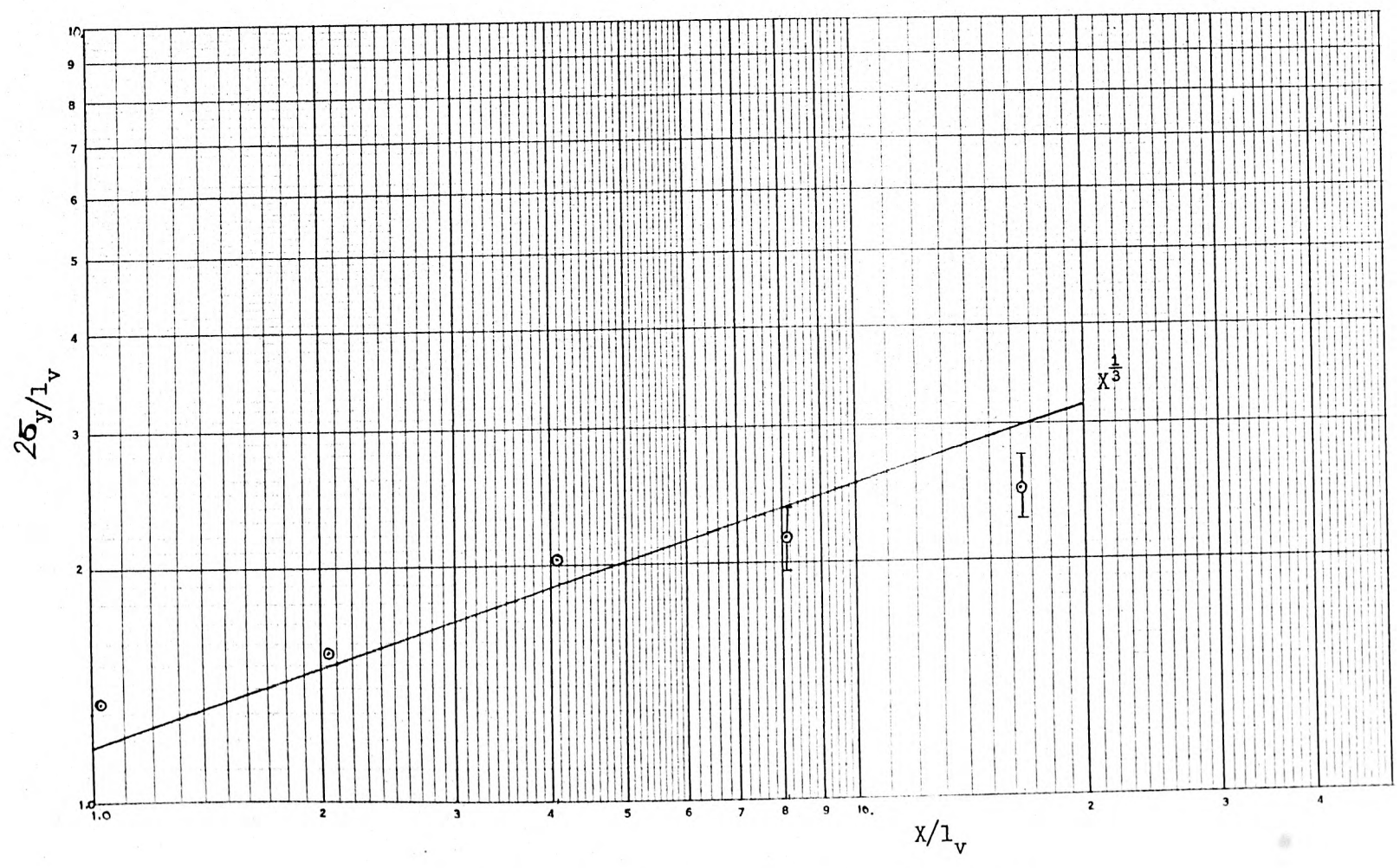

Fig. 7.3f Lateral Spread for Plumes 3a & 3b.

7.2 THE EFFECT OF THE REYNOLDS NUMBER ON PLUME RISE AND SPREAD

Temperature profiles of a set of five plumes with varying exit Reynolds numbers (R_{ex}) and exit flow characteristics were measured in simulation B. Pairs of plumes with different exit Reynolds numbers, i.e. plume 6 (R_{ex} = 1430) and plume 7 (R_{ex} = 2150), were studied in simulations A and C. A set of four plumes with varying exit Reynolds numbers were studied in all four simulations using flow visualisation.

The results for the mean plume trajectories, derived from the temperature profiles, are shown in fig. 7.4. In simulation B (Z_o=.002m -flat farmland), they show clearly that the plume with the lowest Reynolds number is rising significantly above the other plumes. The trajectories of plumes B7 and B8, R_{ex} = 2150 and 2870, are very similar, whereas plume B6, R_{ex} = 1430, rises much higher and by the furthest downstream position has risen almost twice as high as the other plumes.

Further results are shown in fig. 7.4b for plume B6b, R_{ex} = 1450 but with the inside of the stack roughened, and for plume B7b, R_{ex} = 2150 plus the honeycomb gauze inserted in the upper part of the stack. Roughening the inside of the stack is a technique used in many studies to produce a 'turbulent' exit flow. However, in this experiment, roughening the inside of the stack has had no significant effect on the the mean plume trajectory. Only one form of roughness was used and one wonders whether it would have been possible to obtain the same trajectory as the turbulent plumes by only roughening the stack for plume 6. Plume 7b, with the distorted exit velocity profile, rises slightly higher than than plume 7. The difference in trajectory is not as great as we might have expected and this suggests that the exit velocity profile is not the governing factor for plume trajectory.

It should be remembered that for these plumes the densimetric Froude number is also changing. Hence the buoyancy forces acting on each plume will be different. In order to examine whether the difference in buoyancy forces could explain the discrepancy in plume rise, the expected effect of the buoyancy forces on plume rise was considered by using Briggs' (1969) plume rise formula, see eqn. 2.6. Briggs' formula includes the effects of both momentum and buoyancy on the mean plume rise; recalling eqn. 2.6:

$$z = 2.3 \frac{F_m^{1/3} x^{1/3}}{u^{2/3}} \left(1 + \frac{F_b x}{2 F_m u} \right) \qquad (2.6)$$

Then writing eqn. 2.6 in terms of the velocity length-scale yields:

$$\frac{z}{\ell_v} = 2.3 \left(\frac{\ell_s}{\ell_a} \right)^{1/3} \cdot \left(\frac{x}{\ell_v} \right)^{1/3} \left(1 + \frac{F_{rd}}{4} \left(\frac{\ell_a}{\ell_s} \right) \frac{x}{\ell_v} \right)^{1/3} \qquad (2.6b)$$

For plumes 6, 7 and 8 the terms ℓ_s / ℓ_a, R_{mom} and w_s/U are constant (- with values 0.61, 4.8 and 2.78 respectively), while the values of F_{rd} are .18, .08 and .04 respectively. In a later study Briggs (1975) found the value of the constant in the above expression, i.e. 2.3, to vary, see table 2.2. To demonstrate clearly the effect of buoyancy in this study, the actual value, 2.3, was not used. Rather, for each simulation the equation 2.6b was fitted to the downstream region of the measured trajectory of plume 7, R_{ex} = 2,100, and a value for the constant determined. The resulting curves for plume 7 in simulations A,B and C are plotted in figs. 7.4a, c and d. The trajectories for plume 6, R_{ex} = 1400, were then determined from eqn. 2.6b using the value of the densimetric Froude number for plume 6 and the relevant value of the constant for each simulation. The curves predicted by Briggs' formula are shown in figs. 7.4a, c and d as dashed lines. Curves fitted through the experimental data are shown as solid lines.(The predicted curve for plume 8, R_{ex} = 2800, in simulation B will lie approximately 8%

below plume 7 but has not been shown for clarity.)

Firstly, the theoretical curves are not a good fit to the experimental data. We may have expected this since this theoretical plume rise formula is not applicable very close to the stack exit. Briggs' formula assumes a point source and a uniform cross-flow, and it does not implicitly account for the turbulence of the cross-flow. The formula is only being used here to illustrate the potential effect on trajectory due to the mismatch in densimetric Froude number. (Similar results for the effect of the buoyancy mismatch on plume trajectory have been obtained using a computer program based on the work of Petersen and Cermak (1979). The results are shown in fig. 7.15 and discussed in 7.4)

The actual difference measured experimentally between plume 6 (R_{ex}= 1450) and plume 7 (R_{ex} = 2100) is marked on the figures as the difference between the solid lines. The expected difference between the plumes due to the buoyancy mismatch is shown as the difference between the dashed lines, see figure 7.4a, p. 195. We can see that the difference due to the buoyancy mismatch is smaller than the experimentally measured discrepancy in trajectories. Plume 6 will rise higher than plume 7 due to the difference in buoyancy forces but the actual experimentally measured discrepancy in the trajectories is significantly larger. Having accounted for the mismatch in the densimetric Froude number, the only remaining difference between the plumes is the value of the Reynolds number. Therefore, although a fraction of the difference in trajectories may be attributed to the mismatch in the densimetric Froude number, there is still a large discrepancy in trajectories which can only be attributed to the difference in the plume Reynolds numbers.

The results obtained in simulations A and C are shown in fig. 7.4c and d. The difference in plume trajectories is not as marked as in

simulation B. In fact, in simulation A (which is the empty tunnel flow) there is no difference in trajectory until the furthest downstream position. In simulation C (which is quite similar to B) there is no difference in trajectory close to the stack ($X/l_v < 4$) but further downstream the lower Reynolds number plume starts to rise higher than the other plume.

Further evidence is provided by a flow visualisation study which was carried out before the above quantitative studies. The four plumes, 5,6,7,8, were studied in each simulation and the mean trajectory was determined from time-exposure photographs (30 s) as the point mid-way between the visible edges of the plume. (Note: in these earlier experiments the conditions were not exactly the same as later and the exit flow structure would have been different since the wire gauze had not yet been inserted in the base of the stack. Therefore, no comparisons should be made between the two sets of results - temperature measurements and flow visualisation - however, the results do illustrate the main features of plume behaviour.) The results for simulations A, C and D are shown in fig. 7.5. In all cases, they show the lower Reynolds number plumes, i.e. 5 and 6, rising above the other plumes, 7 and 8. The trajectories of the plumes, 7 and 8, are very similar which suggests that they are independent of Reynolds number. Plume 5, R_{ex} = 1075, rises much higher than the other plumes, even plume 6, and it would appear that the discrepancy in trajectory is becoming more marked as the Reynolds number decreases. Thus all the above results suggest that the exit Reynolds number is having an effect on plume trajectory. In view of this result, we might expect an effect on the rate of plume spread.

The results for the vertical spread in simulations A, B and C are shown in fig. 7.6. Firstly, it is interesting to note that the scatter

in the results is relatively small, compared to the previous results. In all three simulations, the agreement in rate of spread for plumes with varying Reynolds numbers is good. It appears that the vertical rate of spread is independent of Reynolds number. It was noted that plume 7 appeared to be spreading slightly more than plume 6 in simulations A and C. However, since this trend was not found in simulation B, and bearing in mind the $\pm$10% uncertainty in σ values, this was not considered to be a significant or definite trend. For clarity, the results for plumes 6b and 7b are not shown in fig. 7.6. The spread of those plumes was very similar to plumes 6, 7, 8 and showed no distinct trends.

Lateral spread measurements were only made in simulation B and C, and the results are shown in fig. 7.7. As for the vertical spread, the agreement between plumes with different Reynolds numbers is good and there are no trends. Thus the rates of spread, vertical and lateral, in the near field ($X/l_j \lesssim 15$) appear to be independent of the Reynolds number.

Relating the above results to those previously reviewed in section 3.6, we find that they are in agreement with Wilson's (1979b) results. Wilson found that a plume with a laminar exit flow rose higher than a turbulent plume. Our results contradict Melbourne's (1968) suggestion that the low Reynolds number has negligible effect in the near field, they also disagree with Hoult and Weil's (1972) result that plume behaviour was independent of Reynolds number above $R_{ex} = 300$. (Note: Hoult and Weil's experiments were carried out in a uniform laminar cross-flow not an a.b.l. simulation. Our results in simulation A do not show the Reynolds number having a great effect and maybe the interaction in laminar and turbulent cross-flows is different.)

The results do show that in the initial phase the rate of spread is independent of the Reynolds number and controlled by self-generated

turbulence. For the range of conditions studied, the resulting self-generated turbulence seems to be independent of the initial exit conditions. Remember the exit conditions of the plumes were different, especially plume 7b with the honeycomb gauze, see section 6.1.3. However, whether this result could be extended to a much wider range of conditions, and to a truly laminar plume, would have to be investigated. The importance of this self-generated turbulence for entrainment of the ambient air into the plume and thus the rate of spread has been mentioned by several authors, Melbourne (1968) and Wilson (1979b). Nevertheless, this does not mean that the initial plume behaviour is independent of the exit conditions. While the rate of spread is unaffected by the initial conditions, the trajectory (or bending) of the plume is affected.

The above seems to suggest that the mean forces acting on the plume are changing as the exit conditions change. To investigate this further, we should return to the Navier-Stokes equations. The important term is $C_D \rho_s W_s^2 / \rho_a U^2$, which determines the bending of the plume. Wilson (1979b) attempted to explain the difference in trajectories by the use of a momentum correction factor (β) for the exit flow. As reported earlier, Wilson was unable to account for the difference by the use of β and in our experiments where the difference in β values was relatively small (<10%) it is unlikely that it would explain the large differences in trajectory. For example, consider the effect of β on Briggs' (1969) expression for plume rise in the near field, $Z' = c l_m^{2/3} X'^{1/3}$. Differentiating to obtain the fractional error, we obtain:

$$\frac{dz}{z} = \frac{2}{3} . \frac{dl_m}{l_m} \qquad (7.1)$$

Allowing for β, the momentum length-scale should be written as $\sqrt{\beta}\, l_m$ and clearly the variation in our values of β is not large enough to explain the differences in trajectory of greater than 25%.

Also, it should be noted that plume 7b, with the distorted exit velocity profile, showed no significant difference in trajectory from plumes 7 and 8. This suggests that the exit velocity profile is not a dominant parameter and that very soon after leaving the stack plume 7b appears like plume 7, with an undistorted velocity profile. All this seems to suggest that there is a bulk interaction between the two flows which is controlling the trajectory.

Returning to the Navier-Stokes equations, we have said little about the drag coefficient C_D. It is frequently mentioned in the literature that in the initial region the jet appears like a solid cylinder to the cross-flow, e.g. Moussa et al. (1976), Crabb et al. (1981). While there have been many studies of the resulting flow field, there have been very few attempts to determine a value for C_D. One such study was carried out by Fan (1967), who fitted his experimental results to a plume rise theory which incorporated a drag term, C_D ; by varying the value of C_D to obtain the best fit to the data he found values for C_D His results are significant in that he found values of C_D varying from 0.1 to 1.7 and they appeared to be a function of F_{rd} and R_{vel} . Clearly, if C_D is varying significantly between laminar and turbulent plumes this may explain the difference in plume trajectory (n.b. in our experiments F_{rd} was varying while R_{vel} was constant).

Considering the physical nature of the interaction further, the velocity profile at the edge of the jet may be significant. At the edge of the turbulent jet the velocity is changing much more rapidly than for a laminar jet. Therefore, the turbulent jet presents a more clearly defined and 'rigid' boundary to the cross-flow which may effect the resulting interaction and forces on the jet. Further, we could consider the edge of the jet to be defined by the point where the velocity falls to a certain fraction of the mean velocity. The resulting effective

diameter of the jet would be smaller for a laminar jet. This may mean that the resulting force on a laminar jet is smaller since it has a reduced effective frontal area.

The implication of the above results for wind tunnel modelling of buoyant plumes is that the Reynolds number <u>will</u> have an effect on plume trajectory. The critical Reynolds number above which the plume's trajectory is unaffected should be determined for each experiment. The exit flow characteristics will vary between experiments and the critical Reynolds number will occur at different values. In many wind tunnel studies where the stack exit diameters are small, i.e. <10 mm, the Reynolds numbers are much smaller than in this study and it would be necessary to run a series of tests at much higher velocities to determine the critical Reynolds number. It may in fact be possible to achieve Reynolds number independence well below R_{ex} = 2000, as the results of Hoult and Weil (1972) would seem to suggest.

The experimental evidence suggests that no general rule may be applied and that each experiment should be examined individually. Certainly, the critical Reynolds number from one experiment will not necessarily apply to another experiment.

In summary, we have found that in the near-field (X/l_v < 15) plumes with low exit Reynolds numbers (R_{ex} < 2000) rise higher than plumes with exit Reynolds numbers above the critical Reynolds number for pipe flow. The difference in plume trajectories could not be accounted for by the difference in the densimetric Froude numbers of the plumes, and would appear to be only dependent on the exit Reynolds number. From limited evidence it would appear that the trajectories of plumes with exit Reynolds numbers greater than 2,000 were very similar. This suggests that above the critical Reynolds number the plume trajectory is

independent of the Reynolds number. Roughening the inside of the stack had no significant effect on the trajectory of a low Reynolds number plume (R_{ex} = 1400). Also, distorting the exit velocity profile had little effect on plume trajectory; this suggests that the exit velocity profile is not of primary importance in determining the plume trajectory.

The lateral and vertical spread of the plumes showed no obvious variation with Reynolds number and within the experimental scatter of the results appeared to be independent of the Reynolds number.

Since the plume trajectory is affected by the exit Reynolds number but the rate of spread is not, this suggests that the bending forces acting on the plume are dependent on the exit Reynolds number of the plume.

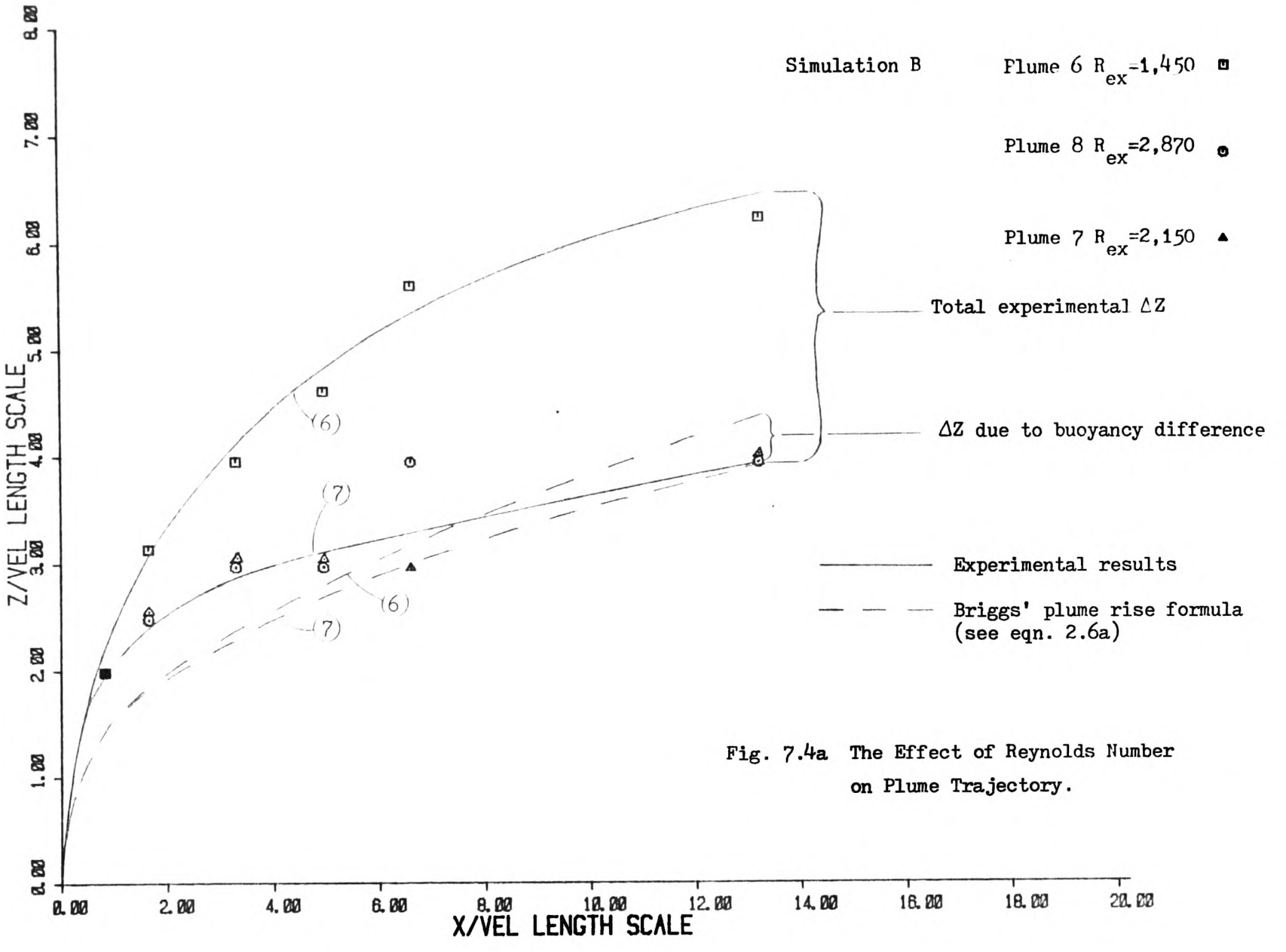

Fig. 7.4a The Effect of Reynolds Number on Plume Trajectory.

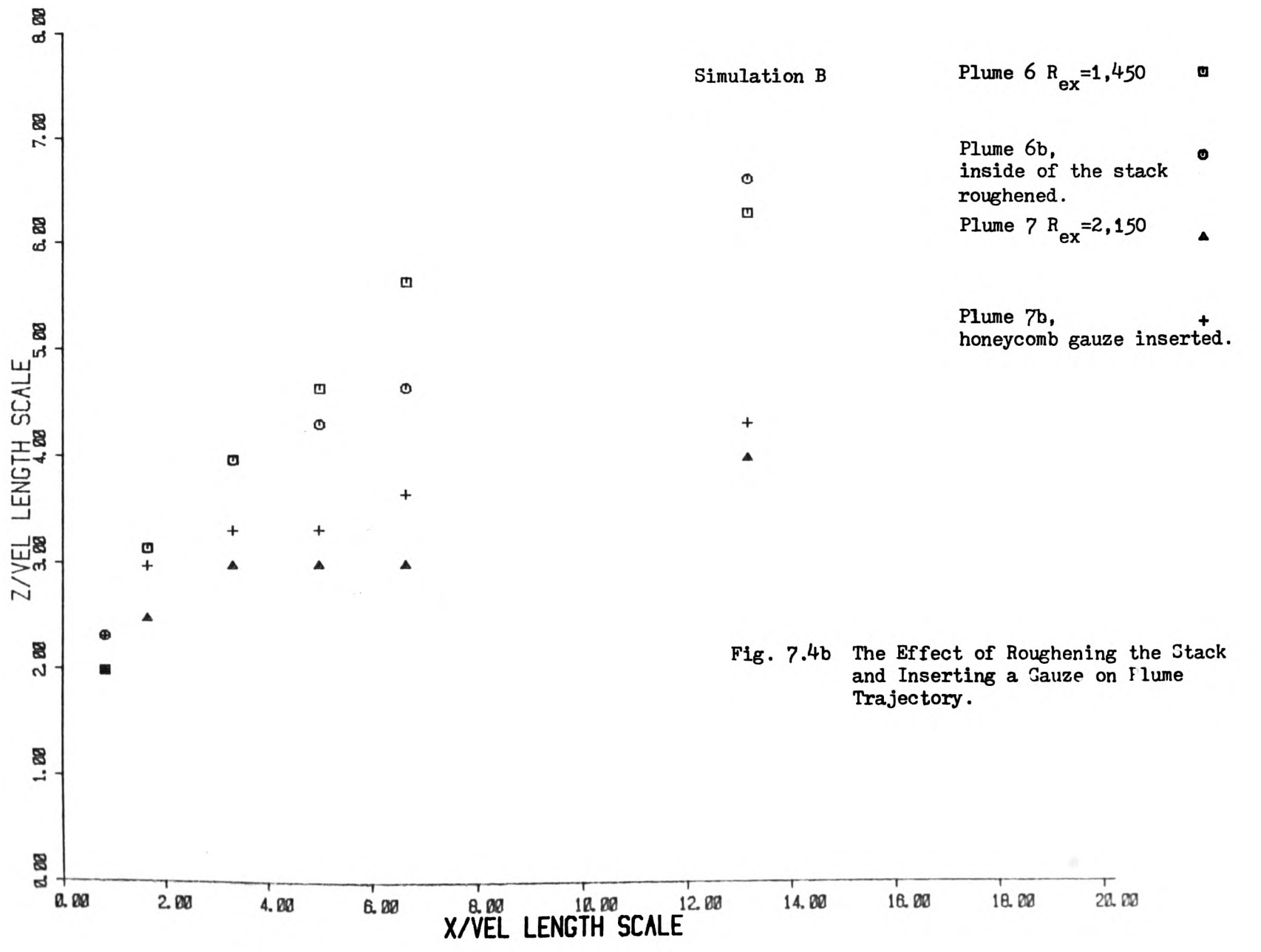

Fig. 7.4b The Effect of Roughening the Stack and Inserting a Gauze on Plume Trajectory.

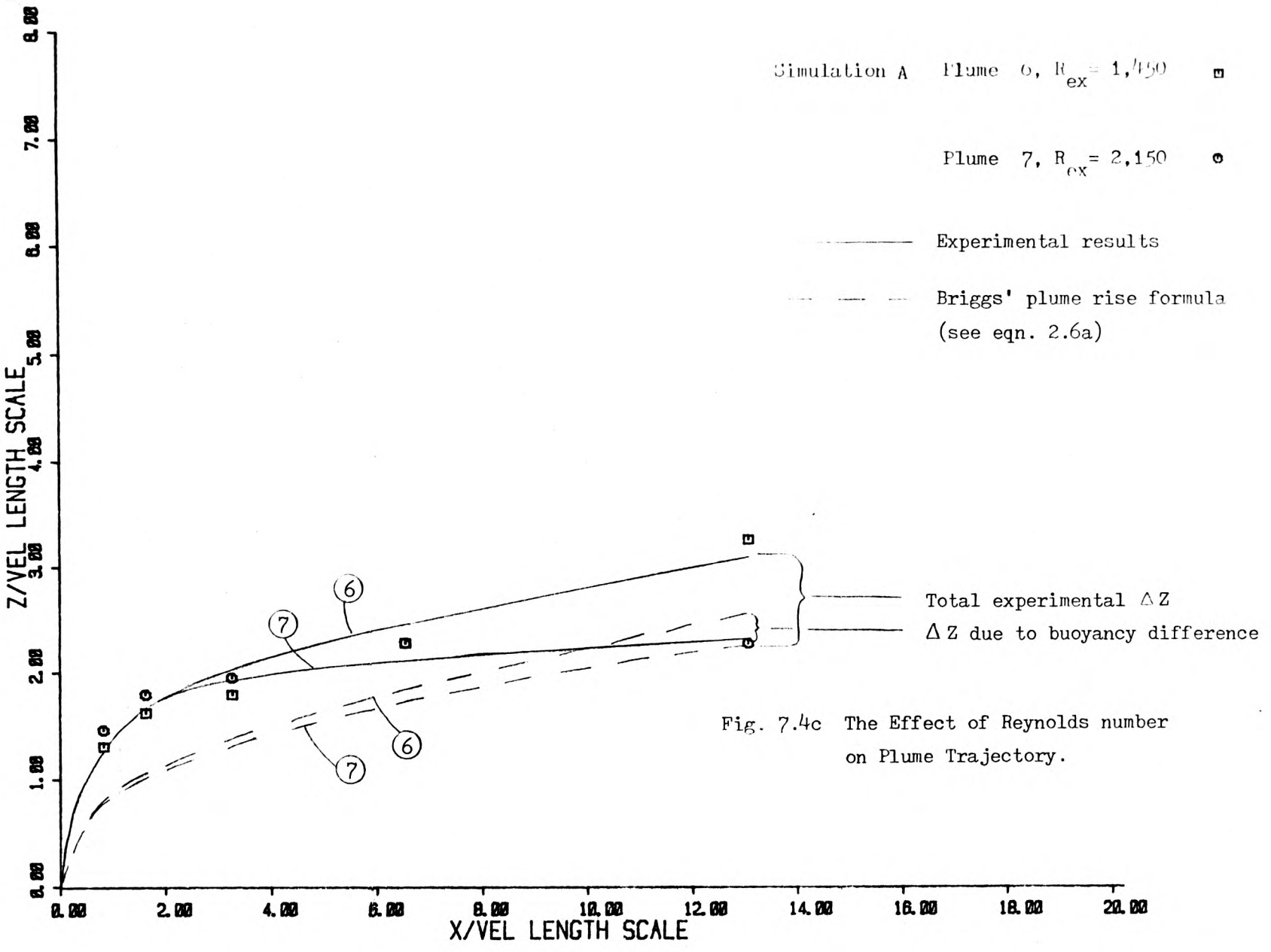

Fig. 7.4c The Effect of Reynolds number on Plume Trajectory.

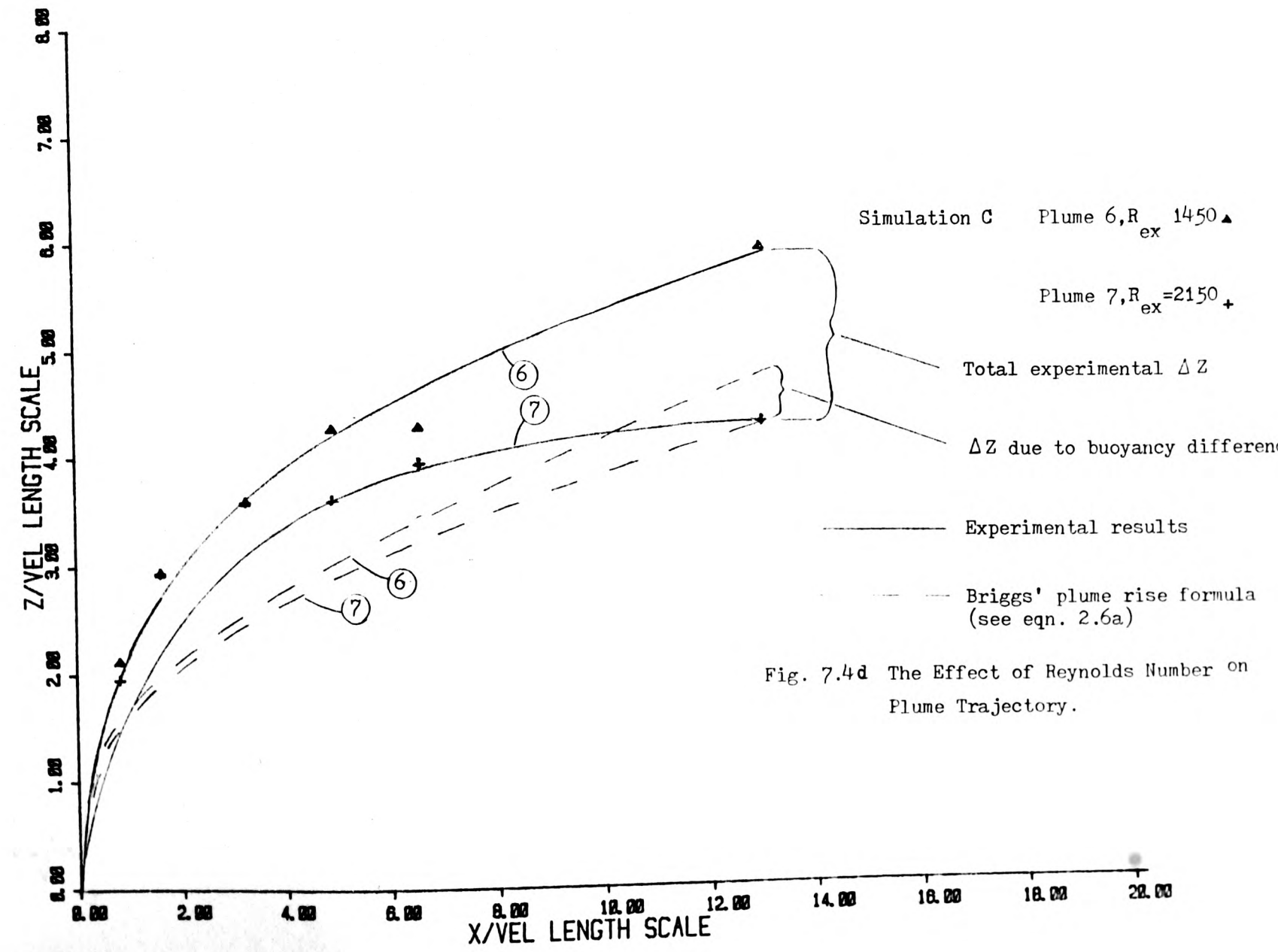

Fig. 7.4d The Effect of Reynolds Number on Plume Trajectory.

Simulation A

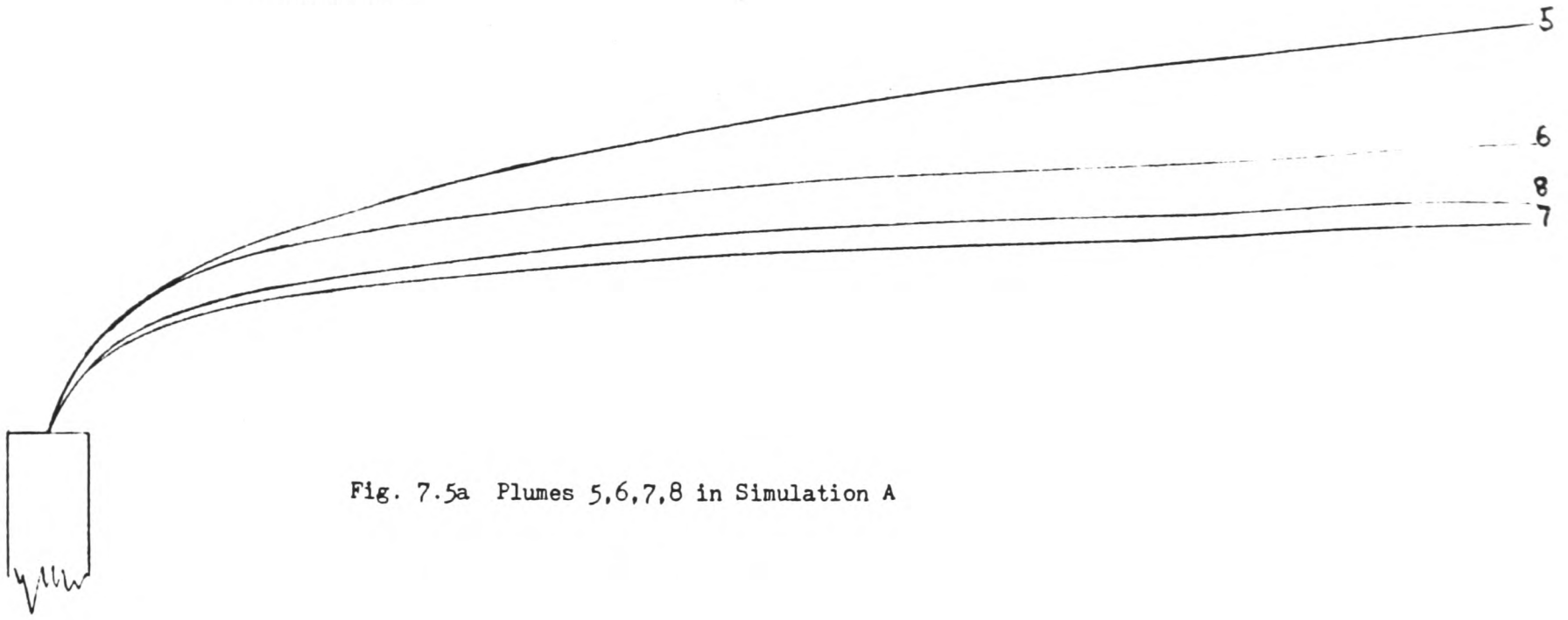

Fig. 7.5a Plumes 5,6,7,8 in Simulation A

Simulation C

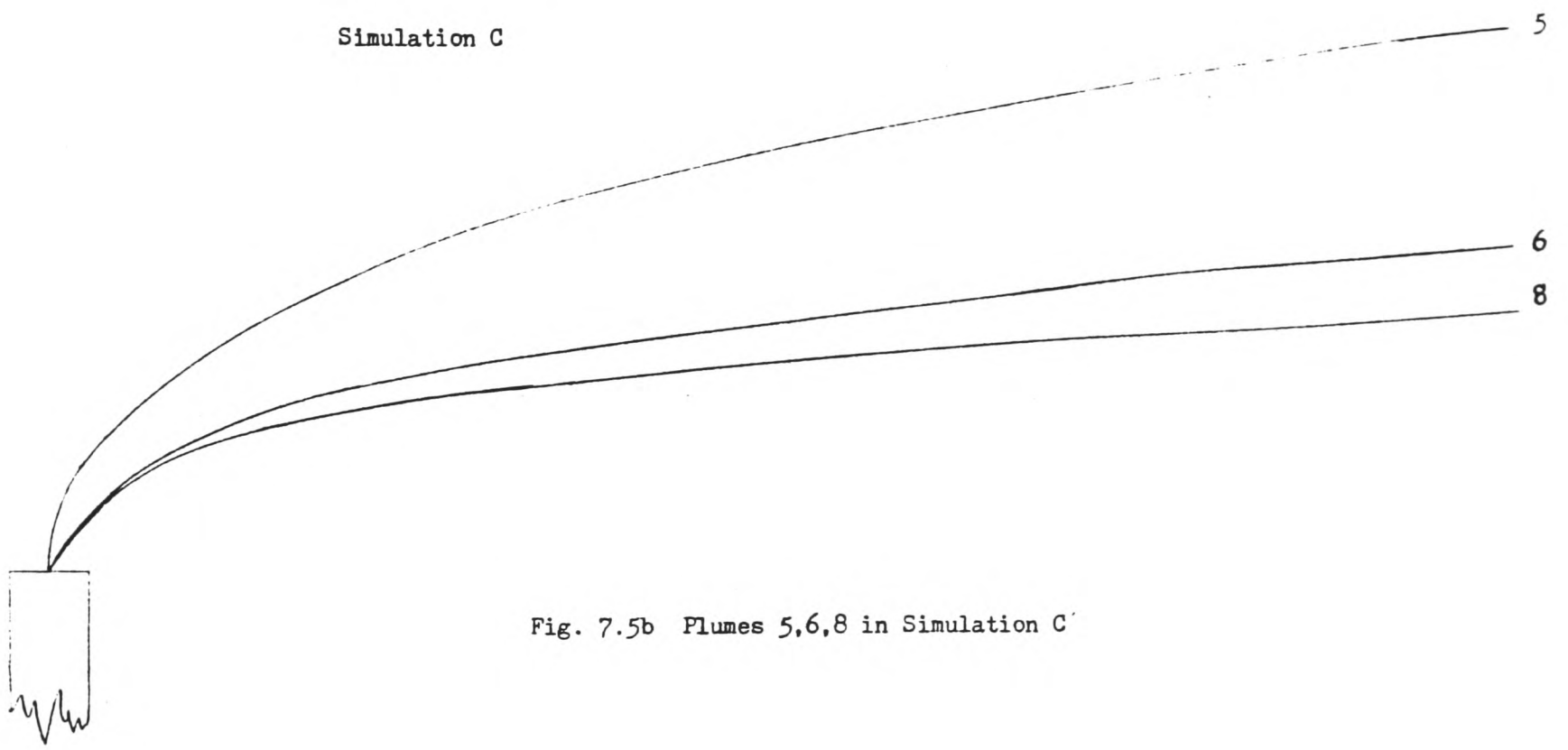

Fig. 7.5b Plumes 5,6,8 in Simulation C

Simulation D

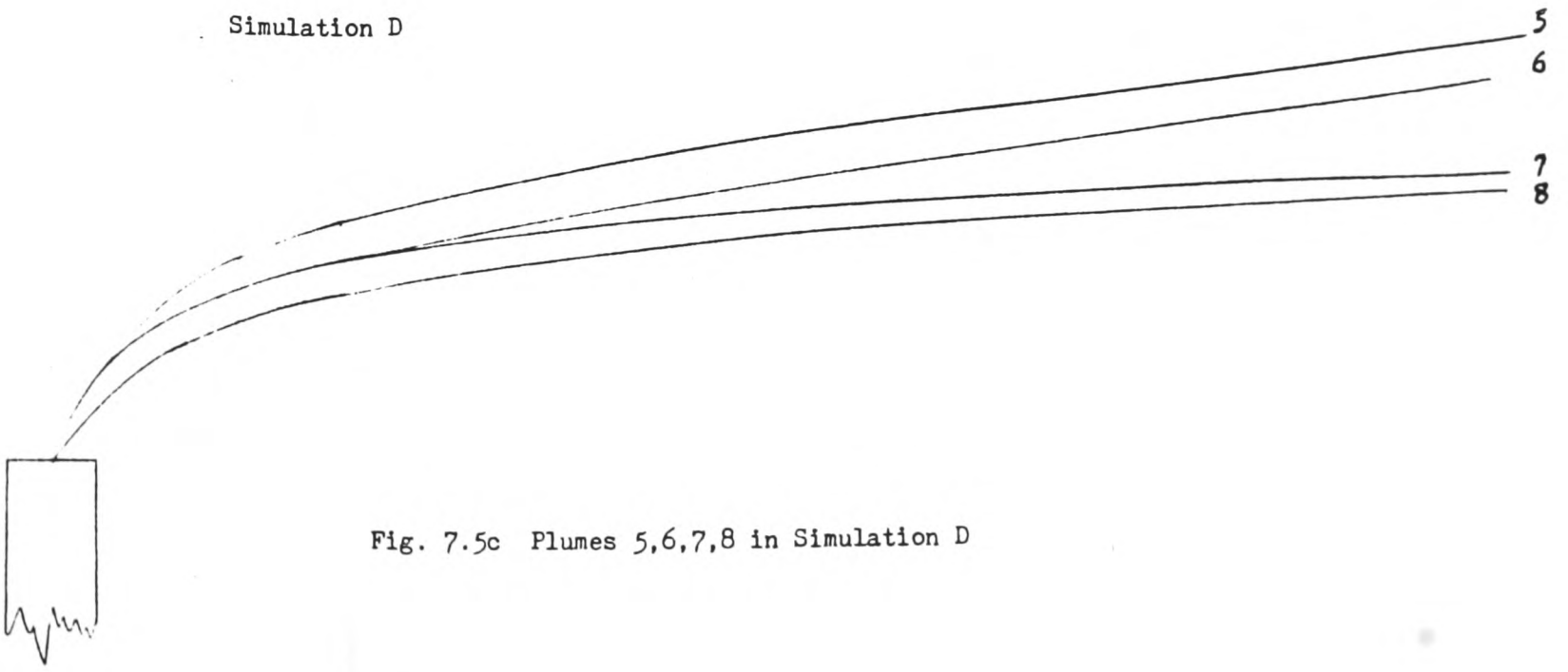

Fig. 7.5c Plumes 5,6,7,8 in Simulation D

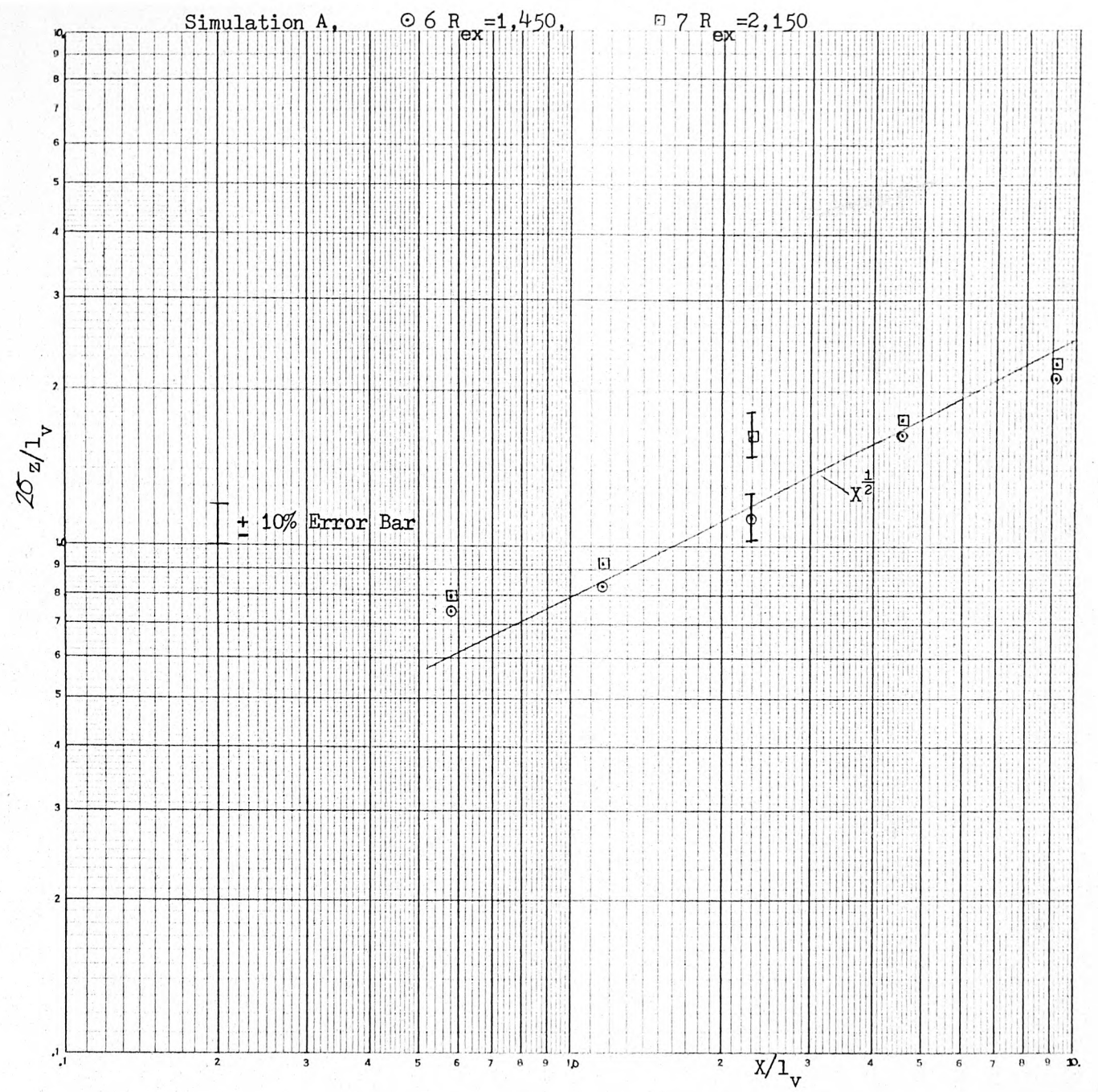

Fig. 7.6a Vertical Spread for Plumes 6 & 7.

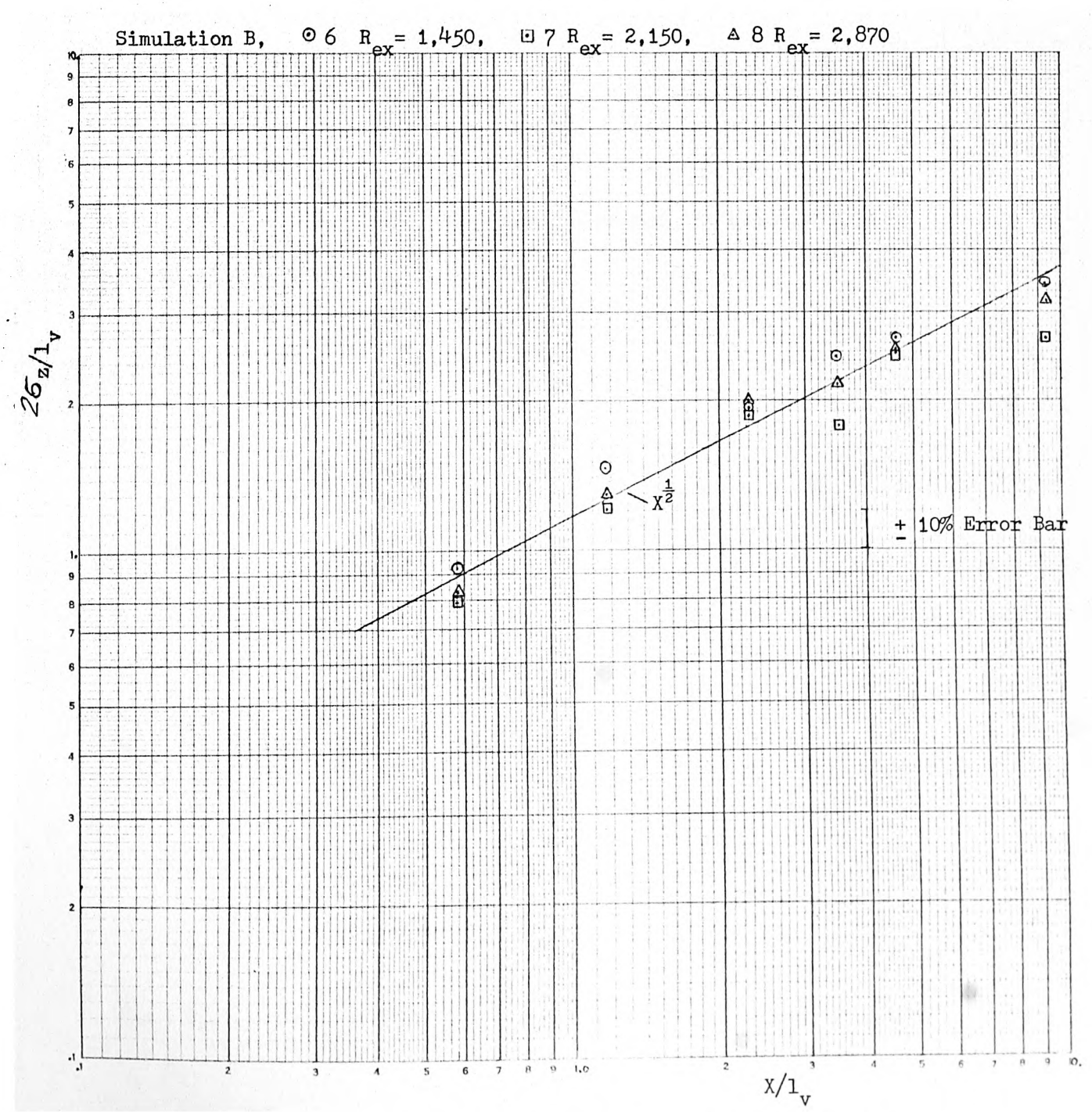

Fig. 7.6b Vertical Spread for Plumes 6,7,8.

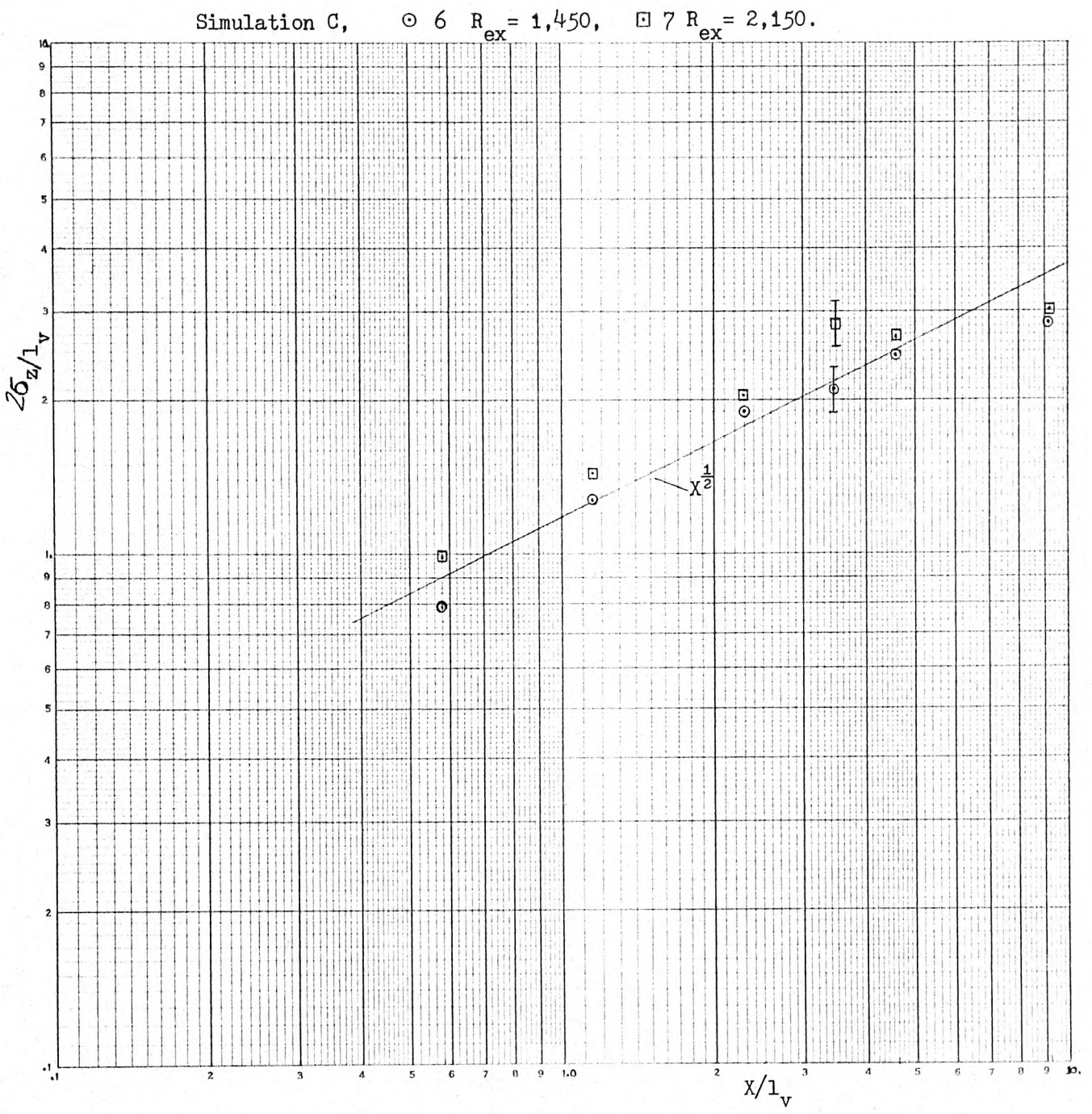

Fig. 7.6c Vertical Spread for Plumes 6 & 7.

Simulation C

⊙ 6 R_{ex} = 1,450

⊡ 7 R_{ex} = 2,150

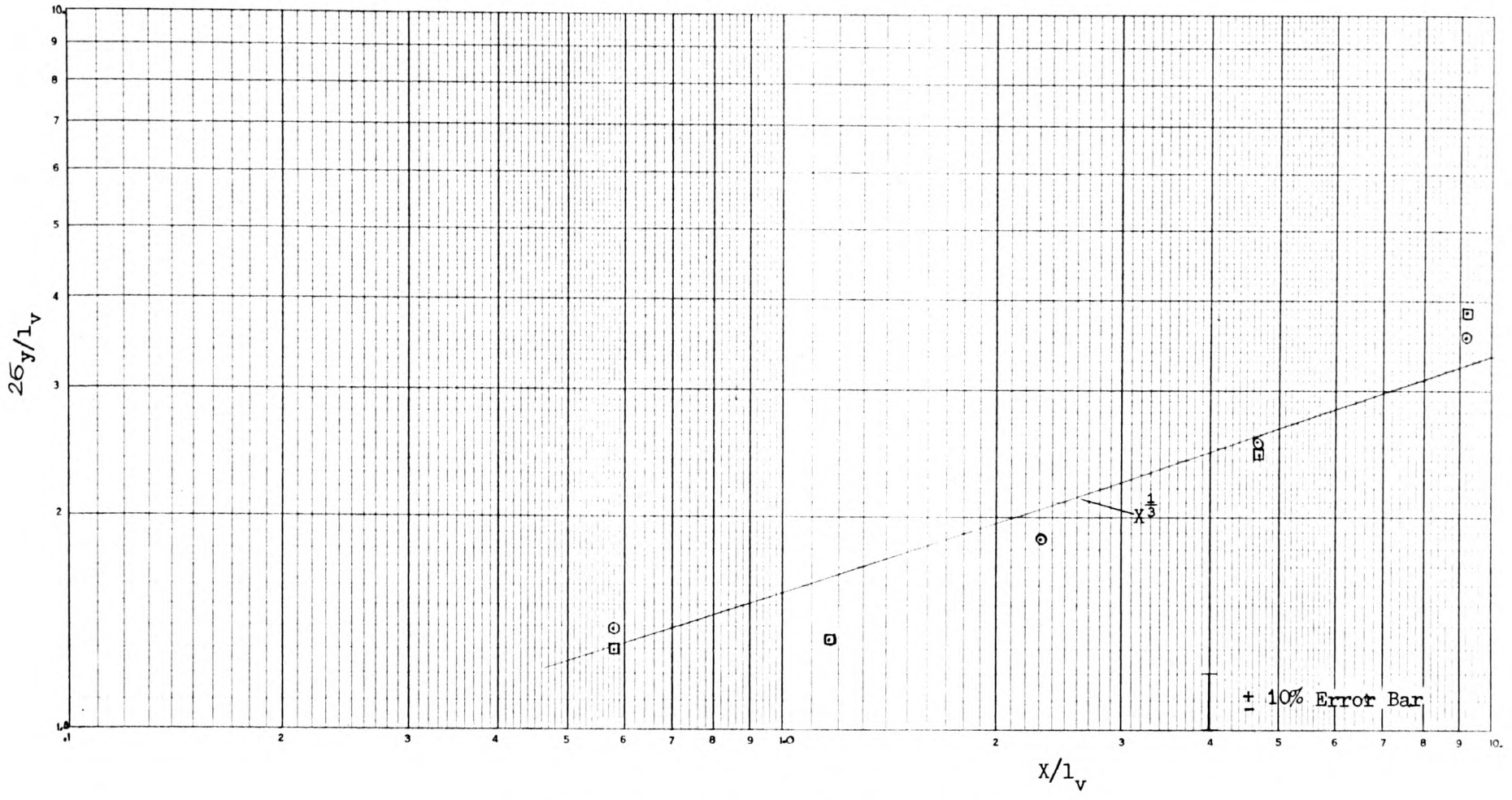

Fig. 7.7b Lateral Spread for Plumes 6 & 7.

Simulation B

⊙ 6 R_{ex} = 1,450

⊡ 7 R_{ex} = 2,150

△ 8 R_{ex} = 2,870

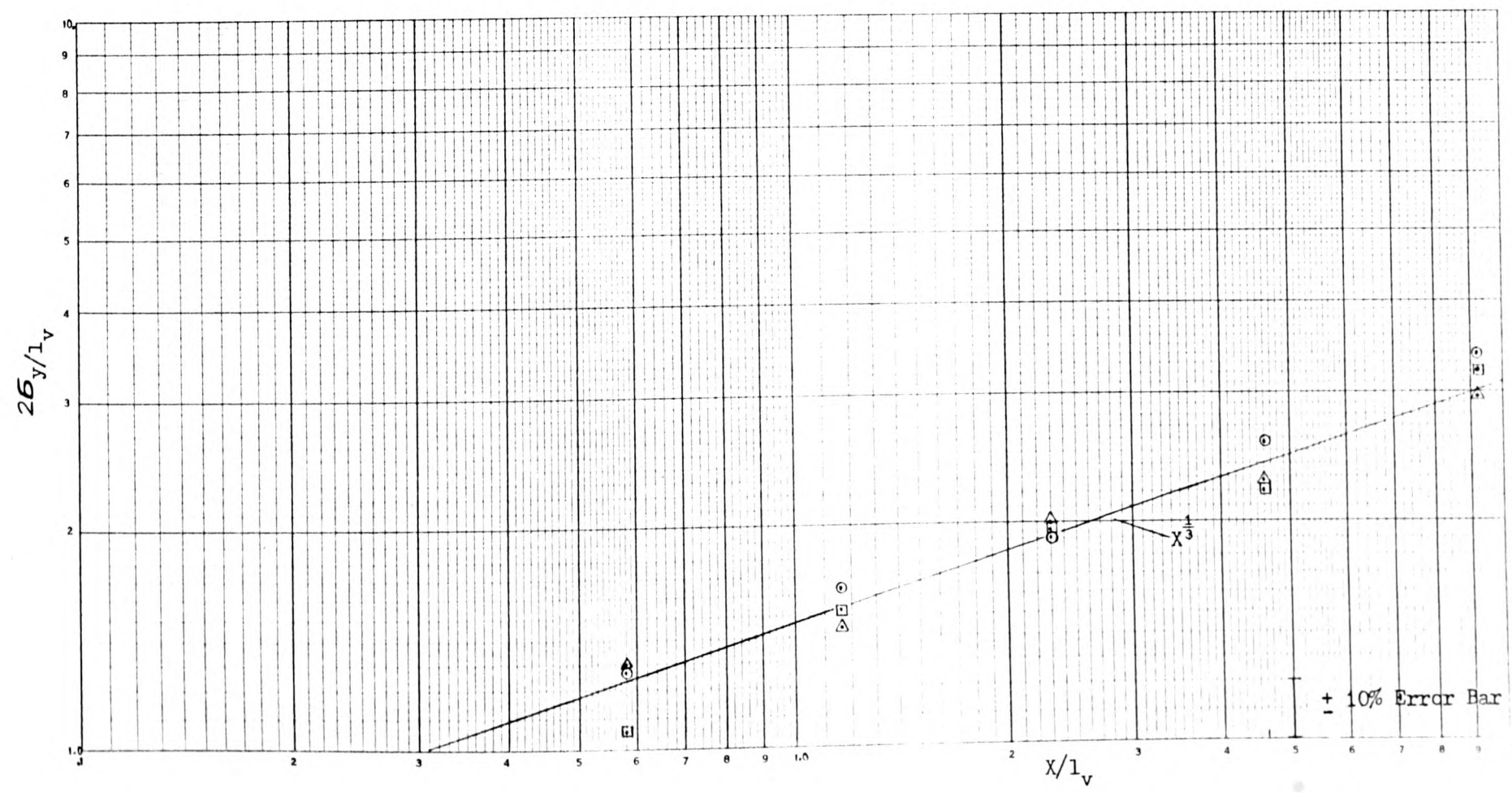

Fig. 7.7a Lateral Spread for Plumes 6,7,8.

7.3 THE EFFECT OF THE ATMOSPHERIC BOUNDARY-LAYER SIMULATION ON PLUME RISE AND SPREAD

From our results it was possible to compare plumes 3a and b in all four simulations, and plumes 6 (R_{ex} = 1430) and 7 (R_{ex} = 2150) in simulations A, B and C. Firstly, it is worth recalling the four simulations: A) low turbulence intensity ($\sim$1%), uniform velocity. All the other simulations represent atmospheric boundary-layer flows, and will be referred to as the a.b.l. simulations, they are:

B) Z_o = 0.002 m, 'natural snow surface (farmland)',

C) Z_o = 0.01 m, ' level grass plains, few trees, winter'

D) Z_o = 1.0 m, 'centre of large towns, (forests)'.

Fig. 5.1a illustrates the main characteristics of the simulations,- the mean velocity profiles are non-dimensionalised by the velocity at the stack height. For the atmospheric boundary-layer simulations, B, C and D, the main differences in the simulations can be summarised as follows. The mean velocity profiles for B and C are essentially identical, while the profile for simulation D shows greater shear, the velocity at 100m is about 5% greater in D than in B and C. Of all the characteristics measured the longitudinal component of turbulence intensity shows the greatest difference between the simulations. At 60m the values of $\sigma u/U$ for simulations B, C and D are .10, .13 and .20 respectively. We would hope that the lateral and vertical components of turbulence intensity would be related by similar ratios, since in the a.b.l. $\sigma v/\sigma u$ =.75, $\sigma w/\sigma u$ = .50; this was not found for our simulations. The values for the lateral and vertical components were very similar in simulations B, C and D, i.e. at 60m $\sigma v/U$ is .080, .085 and .080 in B,C and D; and the $\sigma w/U$ values were .065, .050 and .060 respectively. In summary, the most significant difference between the a.b.l. simulations is in the values of the longitudinal turbulence intensity component, additionally, the

mean velocity profile exhibits greater shear in simulation D than in B and C.

Simulation A has a velocity profile which is constant with height and low values for all three components of turbulence intensity. Thus simulation A has very different characteristics from the a.b.l. simulations, B, C and D.

The mean trajectories for plumes 3a, 3b, 6 and 7 in the different simulations are plotted in figs. 7.8a to d. The first point to note is that for all four plumes studied, the trajectory in simulation A is much lower than in any of the other simulations. Simulation A is a low turbulence intensity, uniform flow, whereas all the other simulations have much higher turbulence intensities (>10%) and a mean velocity which increases with height. The plumes in simulations B and C (-which have very similar characteristics except simulation C has a higher longitudinal turbulence intensity) rise highest. While plumes in simulation D, which has high turbulence intensity and greater shear in the mean velocity profile, do not rise as high as in B and C, they do rise higher than plumes in simulation A.

Before discussing the above results, let us consider the rates of spread in the various wind simulations, starting with the vertical spread σz. Referring to the previous two sections, we found that σz was proportional to $X^{1/2}$ in all four simulations. The magnitude of σz can be inferred graphically from the figures; see figs. 7.2c,e,f & g for plumes 3a & b, see figs. 7.6a,b & c for plumes 6 and 7. We find that the actual standard deviation of the vertical temperature profile, σz, is very similar in the three simulations of the atmospheric boundary-layer but slightly smaller in simulation A, the uniform flow.

For the lateral spread of the plume (σy), we have found σy is proportional to $X^{1/3}$, except in simulation A where $\sigma y \propto X^{0.2}$. Considering

the a.b.l. simulations, i.e. B,C & D, we find that for plumes 3a & b,(see figs. 7.3b, e and f), the magnitude and downstream variation of σ_y is the same for all the simulations. The same result is found for plumes 6 & 7, (see figs. 7.7a and b). The magnitude of σ_y and the variation with downstream distance for plumes 3a & b are found to be significantly smaller in simulation A.

Thus in the near-field, the standard deviations of the temperature profiles, vertical and lateral, for plumes in the a.b.l. simulations were very similar. We may have expected this result since in this region self-generated turbulence dominates the mixing. However, it should be remembered that the lateral and vertical turbulence intensities of the a.b.l. simulations were all very similar. And so the cross-flow conditons should not influence the spreading process differently in the three simulations B,C & D. Therefore, for the a.b.l. simulations, we would expect the rates of spread to be similar even if the cross-flow was affecting the dispersion of the plumes.

In simulation A, which has very low turbulence intensities, the vertical rate of spread, σ_z, was slightly smaller than in the a.b.l. simulations, and the lateral rate of spread was significantly smaller. This suggests that the cross-flow turbulence intensities are having some effect on the initial spreading of the plume.

Returning to the mean plume trajectories, it is clear that the nature of the cross-flow is having a significant effect on plume trajectory. Let us first consider the a.b.l. simulations, B, C and D. Since the rates of spread are very similar this implies that the actual forces acting on the plumes are different in each simulation. We would expect the variation in velocity with height of the cross-flow to be a governing parameter. We would expect plumes in simulation D not to rise as high as those in simulations B and C because the cross-flow velocity

is greater above the stack exit in simulation D than in B and C. By the same argument, we would expect the trajectories of plumes in simulations B and C to be very similar since their mean velocity profiles are almost identical, see fig. 5.1a. These main features are confirmed by the experimental results, figs. 7.8a to d. However, the trajectories in simulation B and C show greater variability than we might have expected. This suggests that the increasing velocity with height of the a.b.l. simulations does not explain the difference in plume trajectories completely. Recalling the characteristics of simulations B, C and D, we noted earlier that the main difference between the simulations was in the longitudinal turbulence intensity component,($\sigma u/U$ at 60m being .10, .13 and .20 respectively). The difference in the longitudinal turbulence intensity components are relatively larger than the difference in the mean velocity profiles and it would appear that the trajectories are sensitive to the $\sigma u/U$ values, although there is no obvious trend.

We may have expected plumes in simulation A to rise higher than those in the a.b.l. simulations, since the cross-wind velocity does not increase with height in simulation A. However, we have found plumes in simulation A to have the lowest trajectories of all. The discussion of the role of the longitudinal turbulence intensity is again relevant, since $\sigma u/U$ in simulation A is much smaller than in B, C and D. The analogy betwen the initial region of the plume and the flow around a cylinder has already been suggested. The drag coefficient for a cylinder in a cross-flow is sensitive to turbulence of the cross-flow. It is well known that a turbulent cross-flow causes the flow around a cylinder to become supercritical at a lower Reynolds number than it would in a less turbulent flow. This will result in a lower C_D value in the more turbulent flow for the same value of the Reynolds number. Our

results for the plumes in simulation A, the low turbulence intensity flow, suggest that a similar effect is happening for plumes in a cross-flow, i.e. in simulation A they have a larger effective C_D than the plumes in the more turbulent a.b.l. simulations.

It has been suggested earlier, Djurfors and Netterville (1978), that the exponent in a power law representation of the trajectory would vary with the exponent in the velocity profile, see eqn. 2.11. To examine this, the trajectories were plotted in log-log form and are presented in figs. 7.9a to d. Although, there is some scatter, it was found that for $X/l_v > 2$ a reasonable straight line could be fitted to each plume. Also, more importantly, the gradient of this line was approximately the same in all simulations for all plumes with $R_{ex} > 2000$, including simulation A which has a zero velocity gradient. A line of the form $Z' \propto X'^{0.2}$ has been drawn for all the plumes. This result is very significant since it provides experimental evidence that the exponent in the expression,

$$Z/l_v = C(X/l_v)^n \qquad (7.2)$$

does not vary with the exponent in the wind velocity profile,

$$U(Z)/U(H) = (Z/H)^{\gamma} \qquad (7.3)$$

for simulations B, C and D, γ is .125,.150 and .320 respectively and for simulation A γ is, of course, 0.0. While the experimental results are for the near-field and Djurfors and Netterville were considering the plume further downstream, the principle of their argument is the same. In fact, we would expect any effect to be more marked in the near-field since the plume's height is changing more rapidly then. It would appear that it is the constant C which is a function of the cross-wind characteristics (-velocity profile and turbulence intensity). If this result could be extended to any value of n, it would explain the wide range of values of C (and hence the entrainment constant α_1) reported in the literature, see Table 2.2, p.44a.

The above results all relate to mean plume behaviour, we would expect the time-dependent plume behaviour to be influenced significantly by the cross-flow simulation. We were able to study the instantaneous plume behaviour by flow visualisation and we will discuss the results below.

The difference in plume behaviour in simulations A and D was very evident when performing the experiments. Plumes in simulation A, (uniform velocity and low turbulence intensity), were relatively narrow and rose smoothly, whereas plumes in simulation D,(high turbulence intensity and increasing velocity with height), were broader and meandered considerably and sometimes broke down into discrete puffs. Plumes in simulations B and C were more like those in simulation D rather than A, though they did not meander as vigorously. Typical plume behaviour is shown in figs. 7.10 and 7.11. In fig. 7.10, the side view of the same plume, 1a (T_s = 75°C, R_{ex} = 2450), is shown in simulations A and D respectively. The plan views of plume 3a (T_s = 100°C, R_{ex} = 2130) in simulations A and D are shown in fig. 7.11; the differences in plume behaviour are evident.

It should be remembered that these photographs only represent the plume at an one instant and the plume may be moving around or 'flapping' considerably. This flapping effect is illustrated in fig. 7.12 where the same plume as in the lower photograph of fig. 7.10 (D1a) is shown at another two instants in time, the change in plume behaviour is considerable. One would expect this fluctuating plume behaviour to be very important if we are interested in instantaneous temperatures and this visual evidence seems to support that hypothesis.

An interesting point arising from the above photographs, is that we might have expected the mean rates of spread to be different in each simulation because of the meandering of the plume. While there is a

difference between the rate of spread in simulation A and the other simulations, there is no difference for the a.b.l. simulations themselves. Thus although the meandering appears to be significant it does not, in fact, transfer significant amounts of enthalpy away from the mean position. This is because visually the smoke exaggerates the spreading of the plume, i.e. the smoke shows up clearly even when the plume temperature is only a few degrees above ambient. This effect should be remembered when using flow visualisation to study dispersion and in most cases a quantitative technique should also be used.

Another interesting feature of plume behaviour is shown in fig. 7.11b, the plan view of plume 3a in simulation D. The plume can be seen to bifurcate into two distinct flows as soon as it leaves the stack. This flow pattern is caused by a pair of counter-rotating vortices which split the plume in half and then travel downstream with the flow. Their motion could be observed clearly by looking upstream from behind the stack. Further examples of this double vortex behaviour are illustrated in fig. 7.13, where plumes 5 (R_{ex} = 1075) and 7 (R_{ex}= 2150) are shown in simulation C. This bifurcating of the plume is frequently observed in full-scale plumes. The double vortices are caused by the flow around the initial jet-like region of the plumes. The flow is like the flow around a cylinder and will be similar to the flow around the stack, with which it must interact and be continuous. These vortices entrain fluid on the downstream side of the plume and are strong enough to separate the plume eventually.

From the wind tunnel modellers point of view, there are several points to note. Firstly, there were no signs of bifurcation for plumes in simulation A, the low turbulence intensity, uniform cross-flow. Bifurcation was observed for plumes in the a.b.l. simulations, though not necessarily in all cases. The effect of bifurcation was not evident

in the lateral mean temperature profiles, where we may have expected a double peak. The magnitude and rate of lateral spread does not appear to be greatly enhanced by bifurcation, though this conclusion is based on the limited evidence that all plumes are spreading similarly in simulations B, C and D.

In conclusion, we have found that in the near-field the mean plume trajectory is influenced by both the mean velocity profile and the longitudinal turbulence intensity. The difference in plume trajectory between plumes in a turbulent a.b.l. simulation and those in a low turbulence intensity uniform cross-flow were marked. For typical a.b.l. simulations the longitudinal turbulence intensity exhibits a greater relative change for different terrain types (i.e. Z_o 's) than the velocity profile. Therefore, in developing an a.b.l. simulation for dispersion studies, it is important to model the longitudinal turbulence intensity as accurately as possible.

The rate of spread of the plumes (σy and σz) was very similar in the three a.b.l. simulations but smaller in the low turbulence intensity simulation A. It should be noted that in the a.b.l. simulations the lateral and vertical components of turbulence intensity (σv & σw) were very similar, therefore if σv and σw were having an effect on plume spread this would not have been evident from the experiments in the a.b.l. simulations. However the difference in the rate of spread between plumes in the a.b.l. simulations and simulation A suggested that a large difference in the turbulence intensities was affecting plume spread. Hence, for plume dispersion studies, the lateral and vertical components of turbulence intensity should be modelled as accurately as possible.

Fig. 7.8a The Effect of Simulation on Plume 3a.

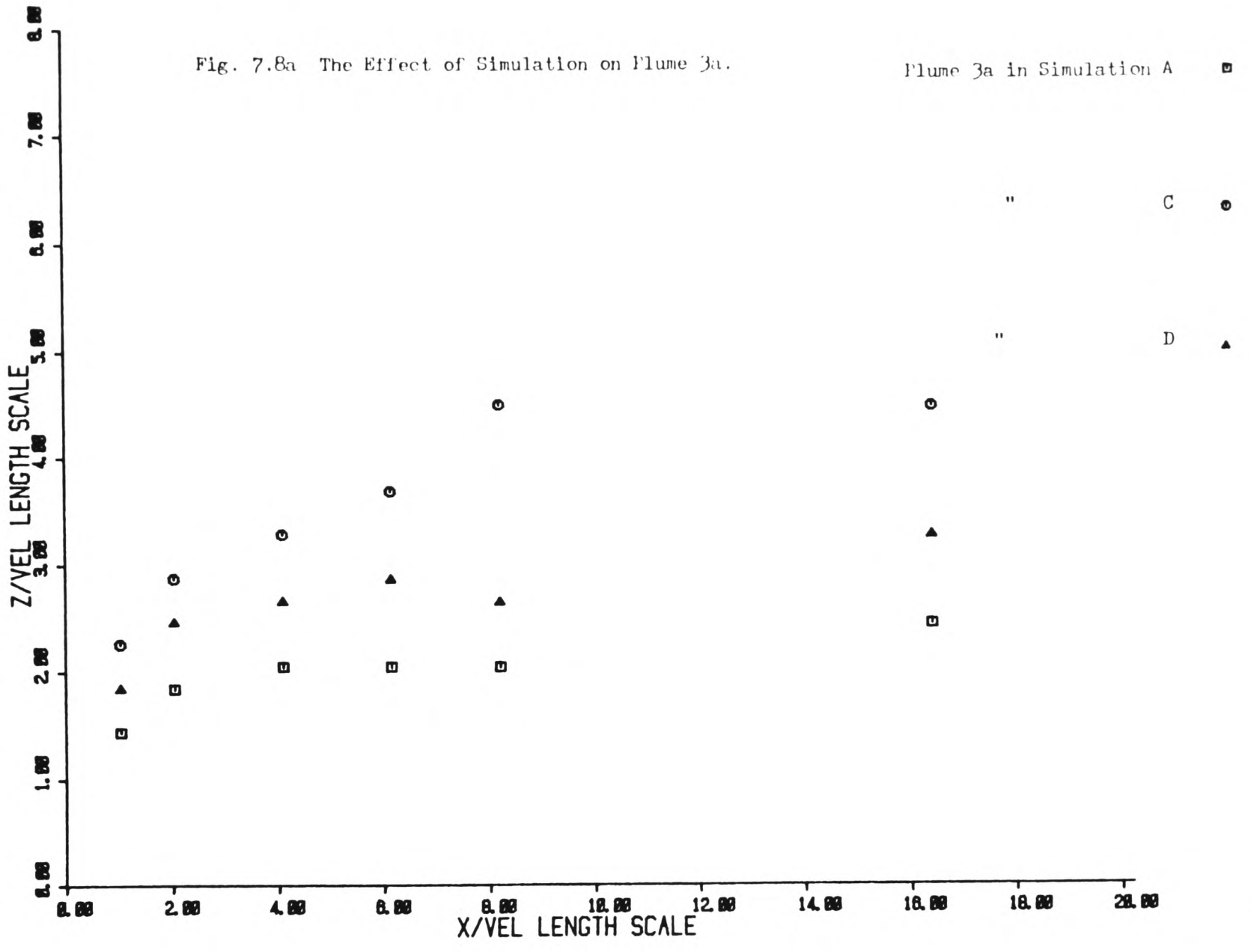

Fig. 7.8b The Effect of Simulation on Plume 3b.

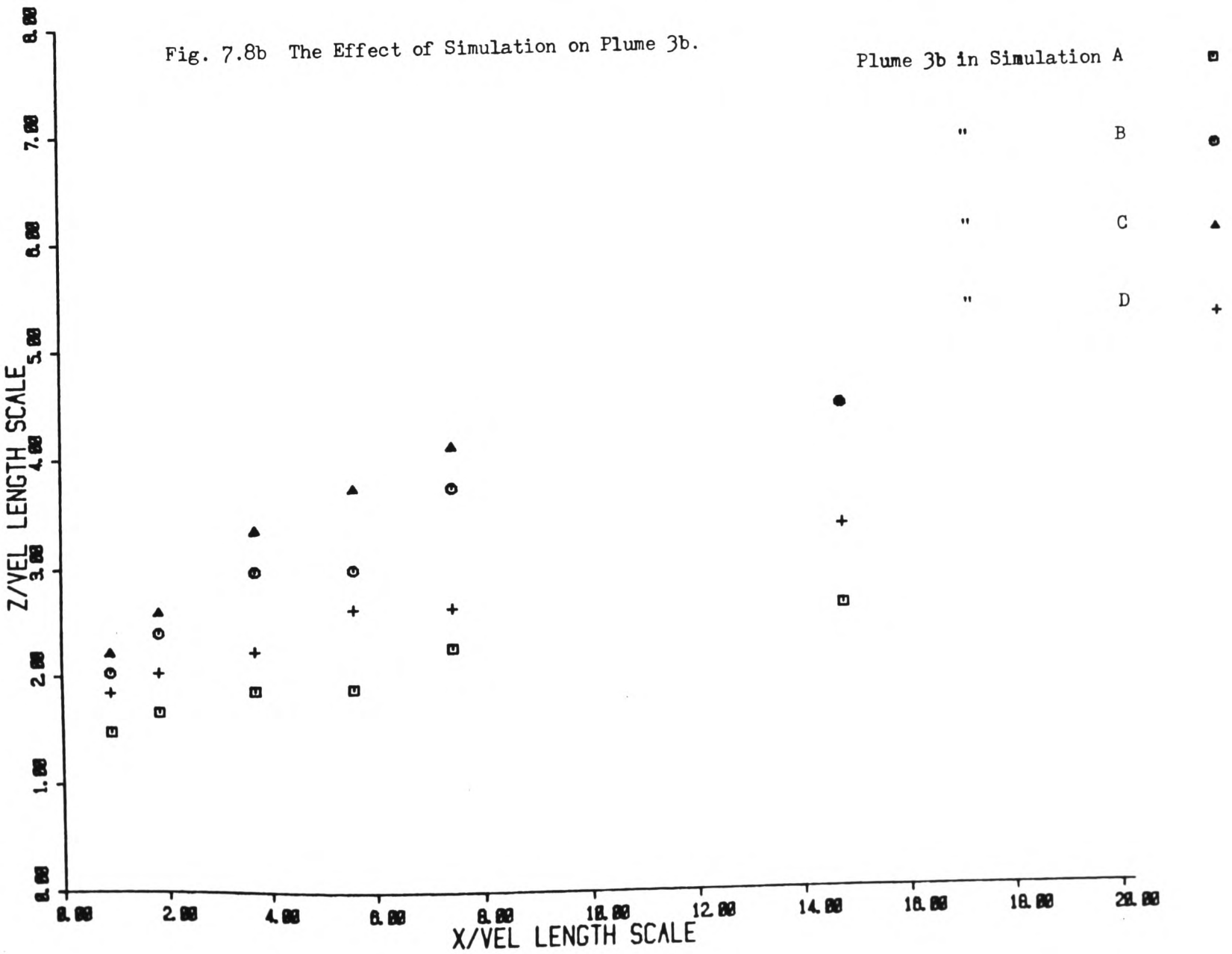

Fig. 7.8c The Effect of Simulation on Plume 6, R_{ex} = 1,450. Plume 6 in Simulation A

" B

" C

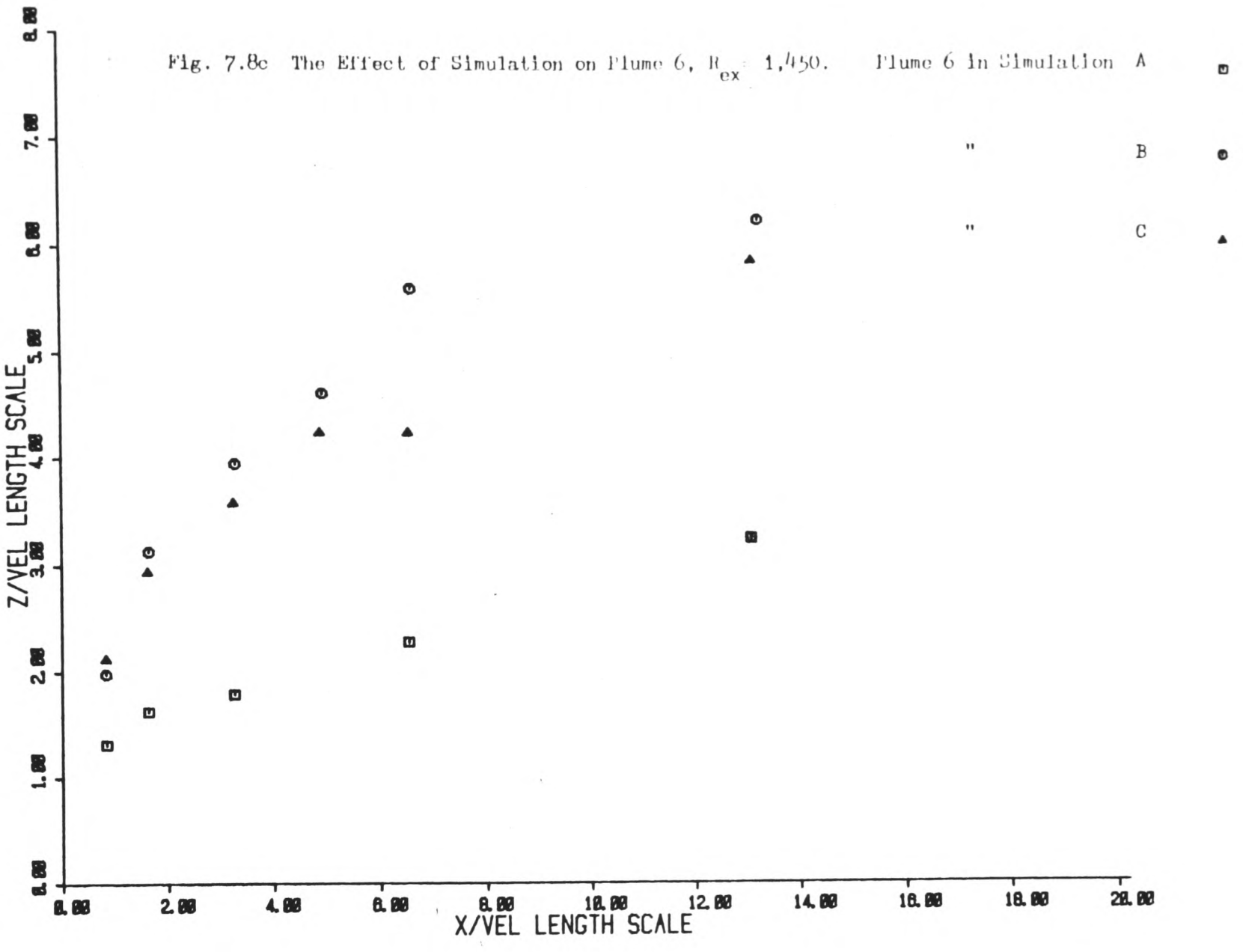

Fig. 7.8d The Effect of Simulation on Plume 7, R_{ex} = 2,150. Plume 7 in Simulation A

" B

" C

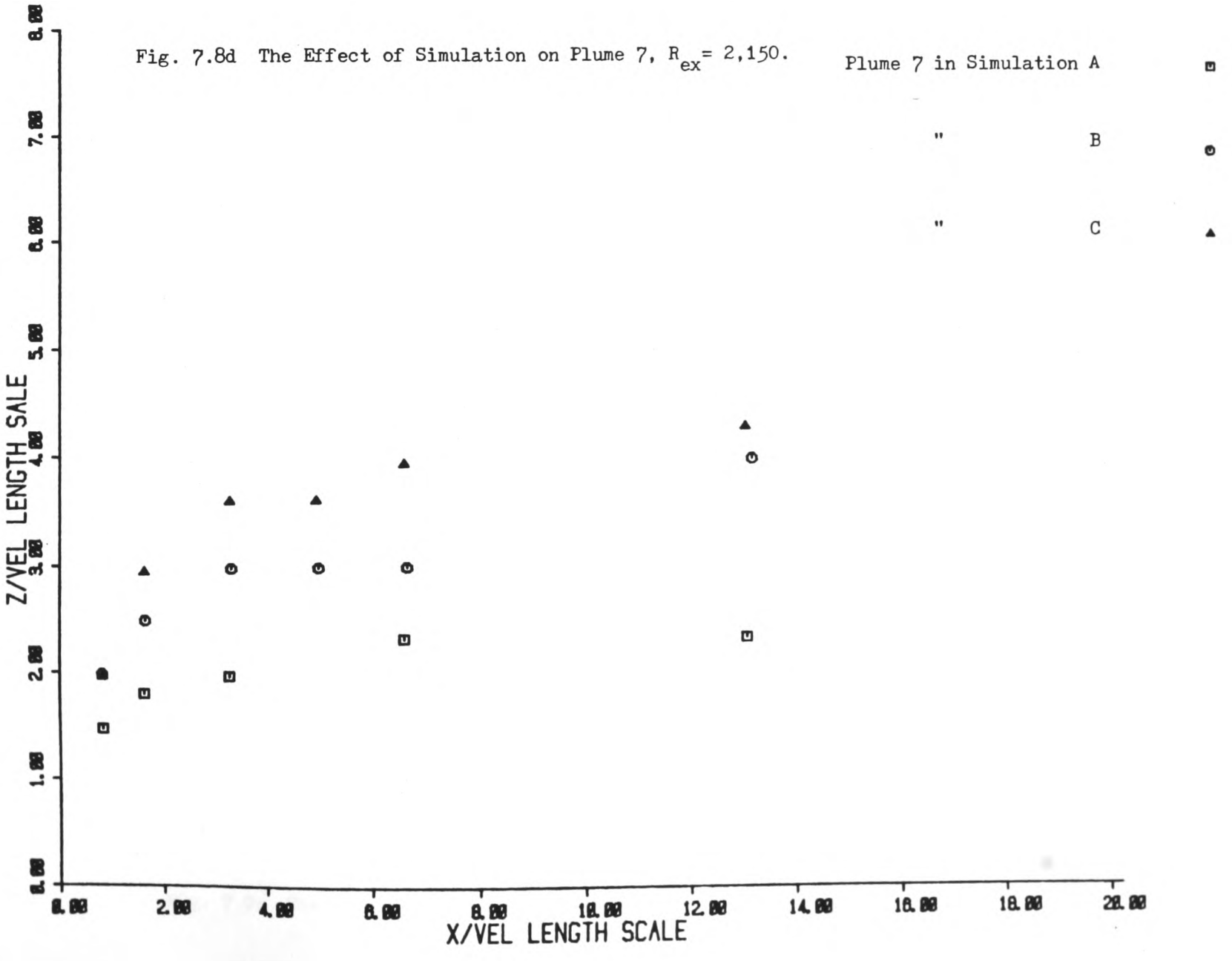

Plume 3a in Simulation A ⊙
" C ⊡
" D △

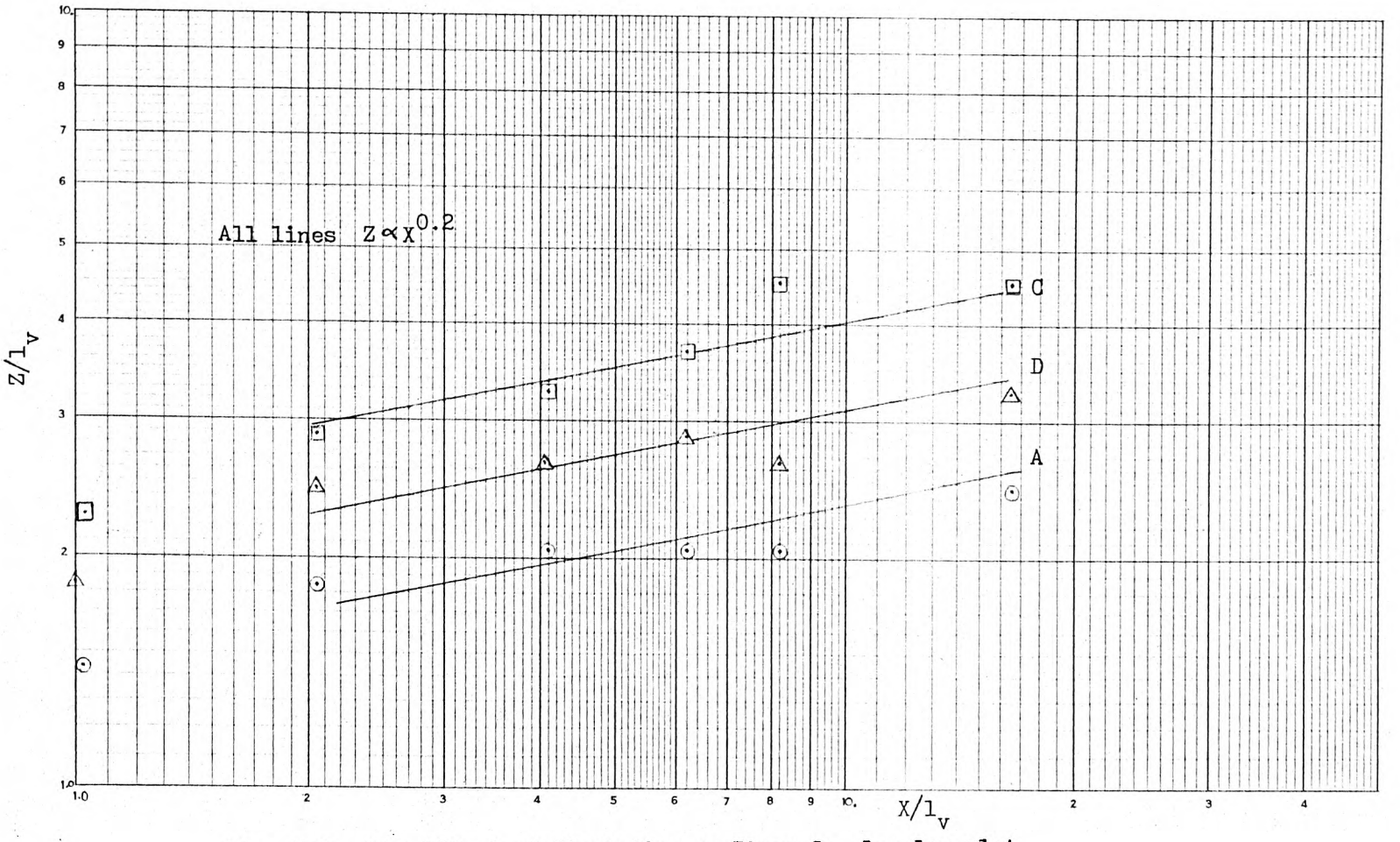

Fig. 7.9a The Effect of Simulation on Plume 3a, log-log plot.

Plume 3b in Simulation A ⊙
" B +
" C ⊡
" D △

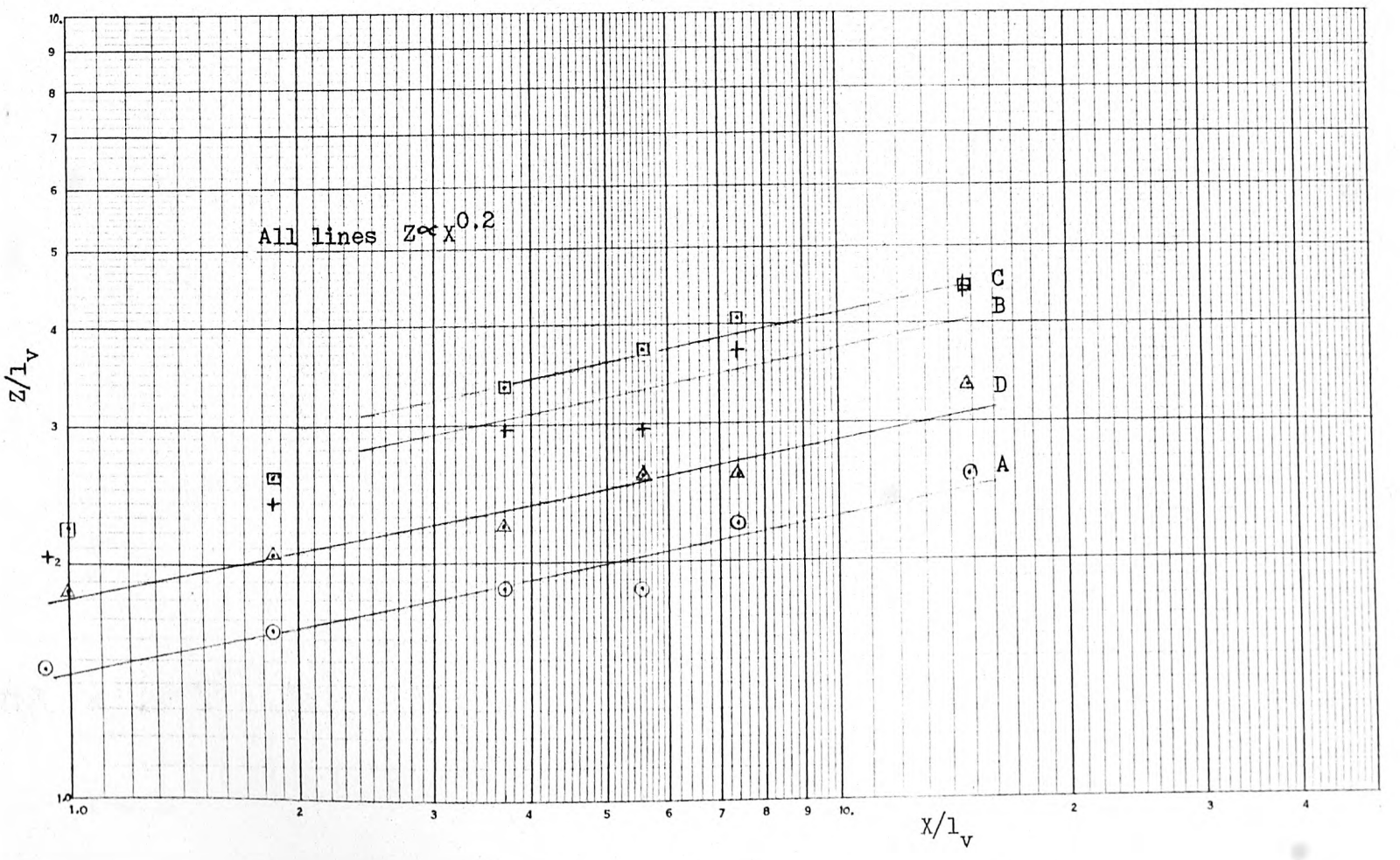

Fig. 7.9b The Effect of Simulation on Plume 3b, log-log plot.

Plume 7 , R_{ex} = 2,150, in Simulation A ⊙
" B ⊡
" C △

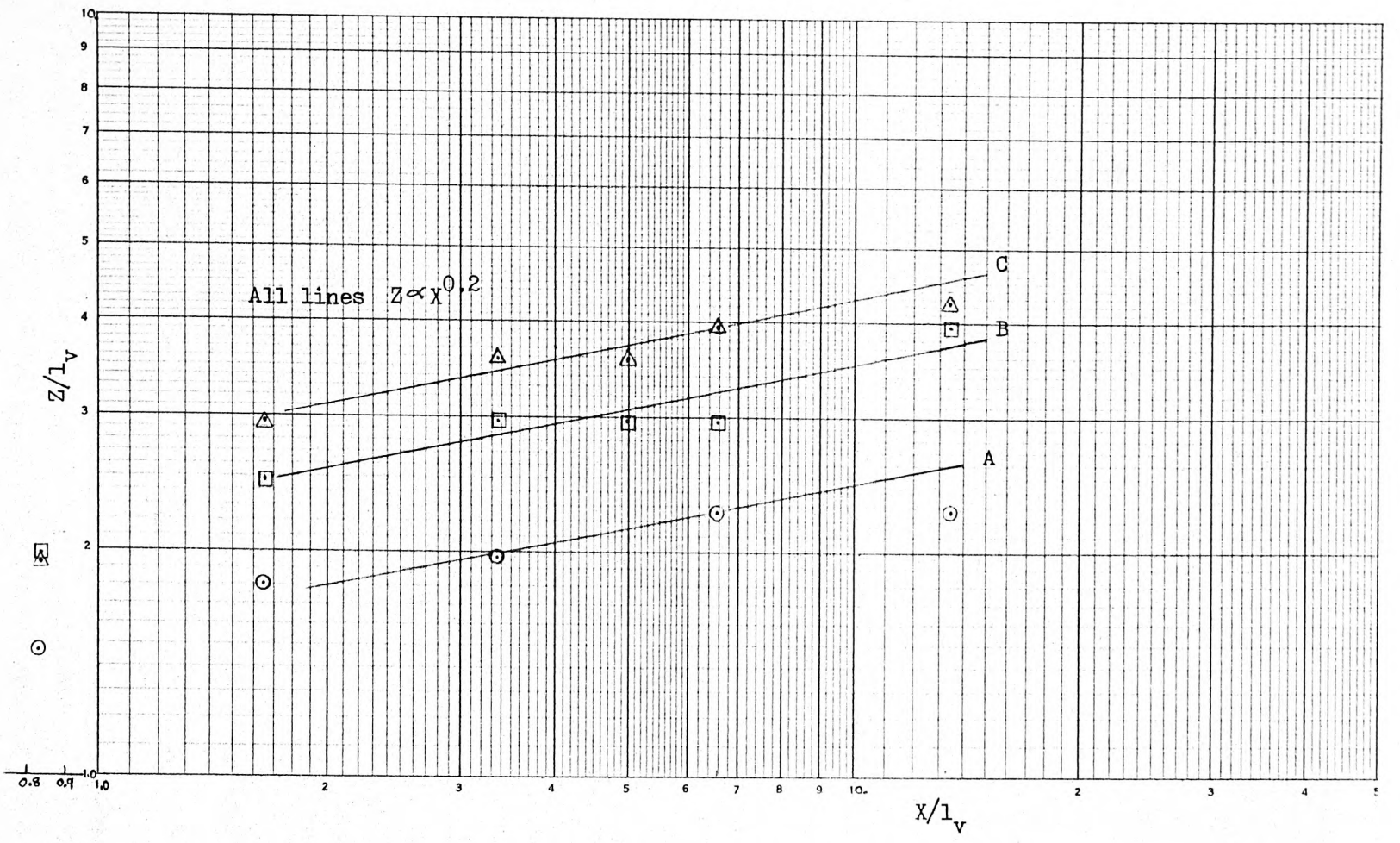

Fig. 7.9c The Effect of Simulation on Plume 7, log-log plot.

Plume 6, R_{ex} = 1,450, in Simulation A ⊙
" B ⊡
" C △

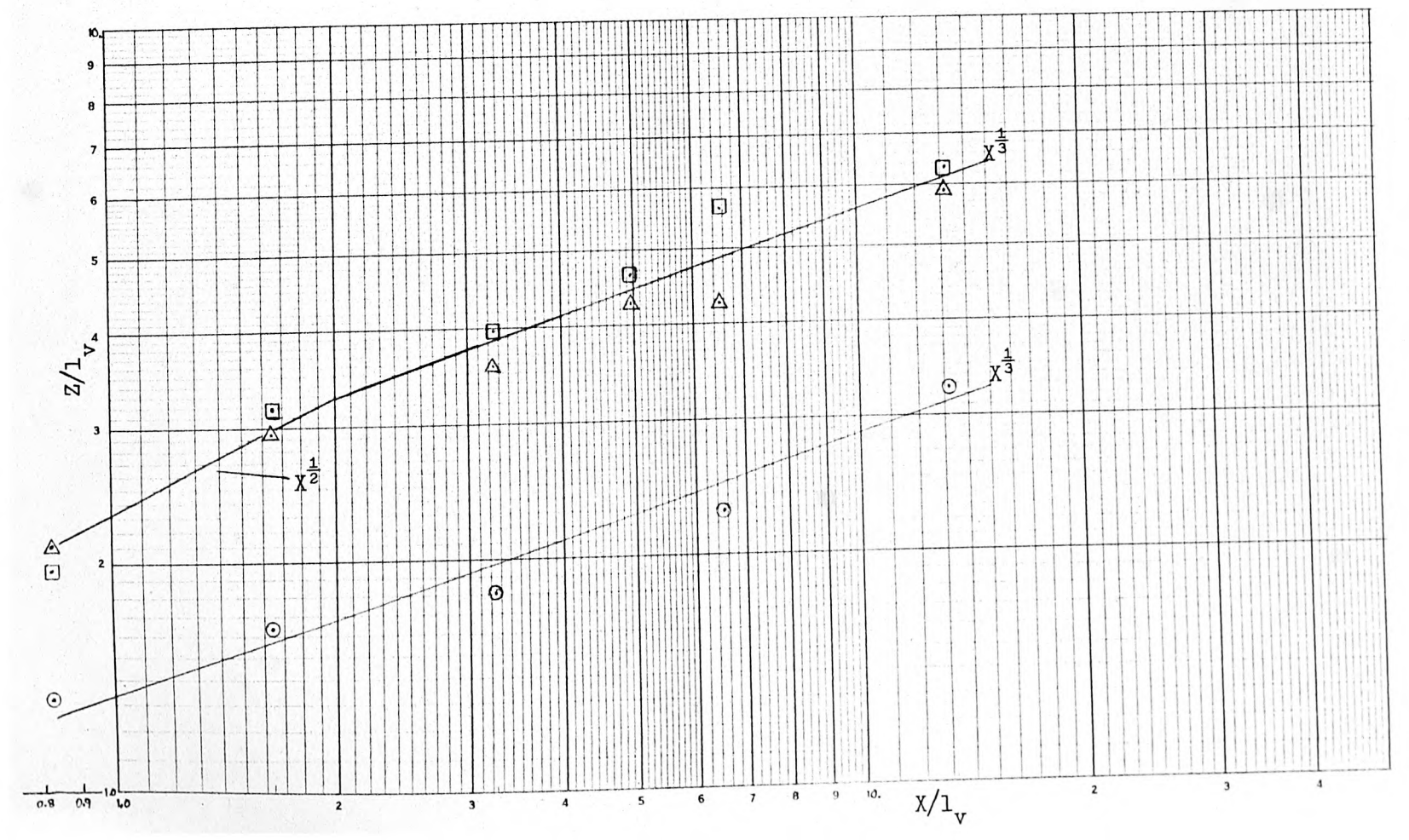

Fig. 7.9d The Effect of Simulation on Plume 6, log-log plot.

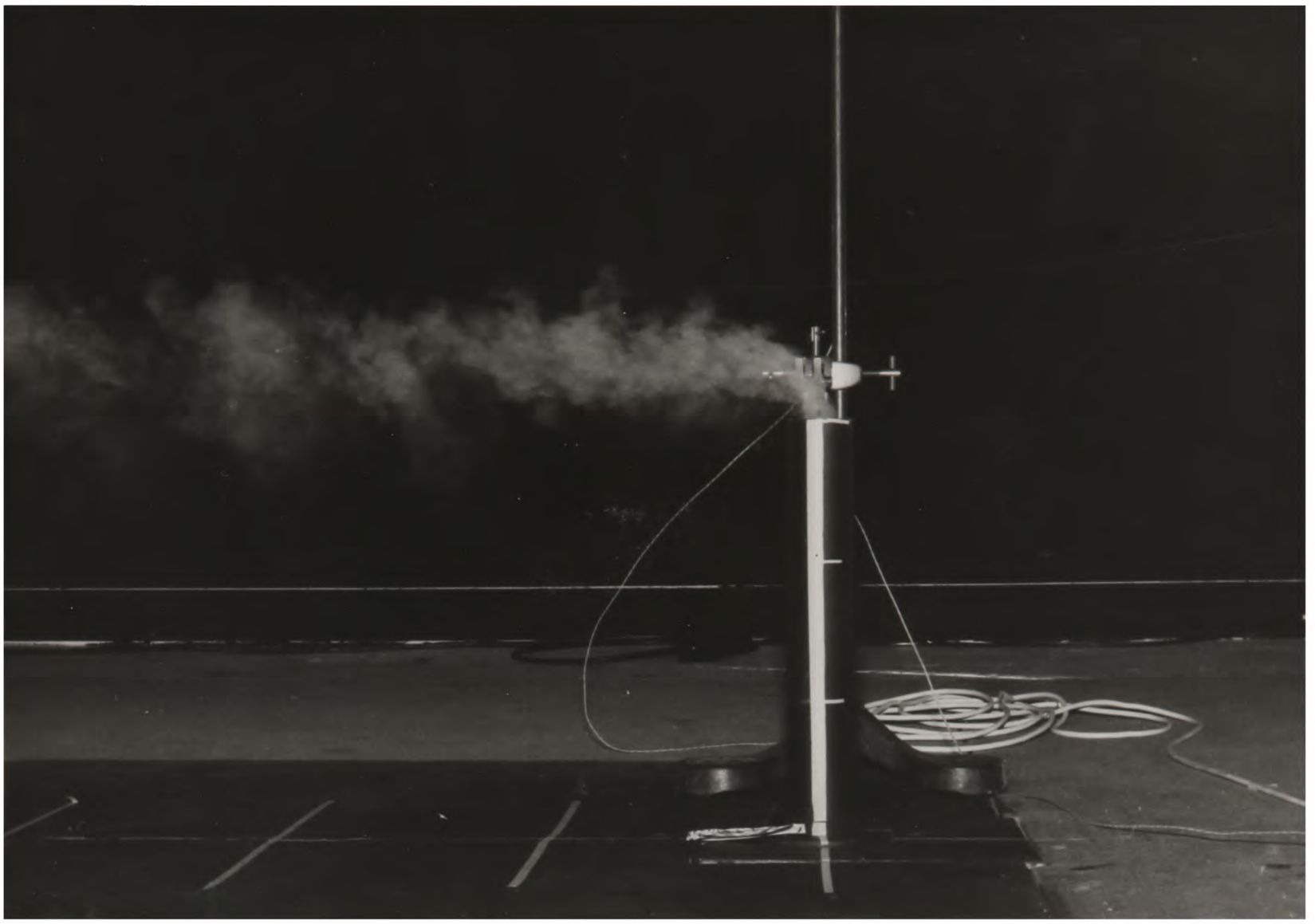

FIG. 7.10 Side View of Plume 1a in Simulations A and D

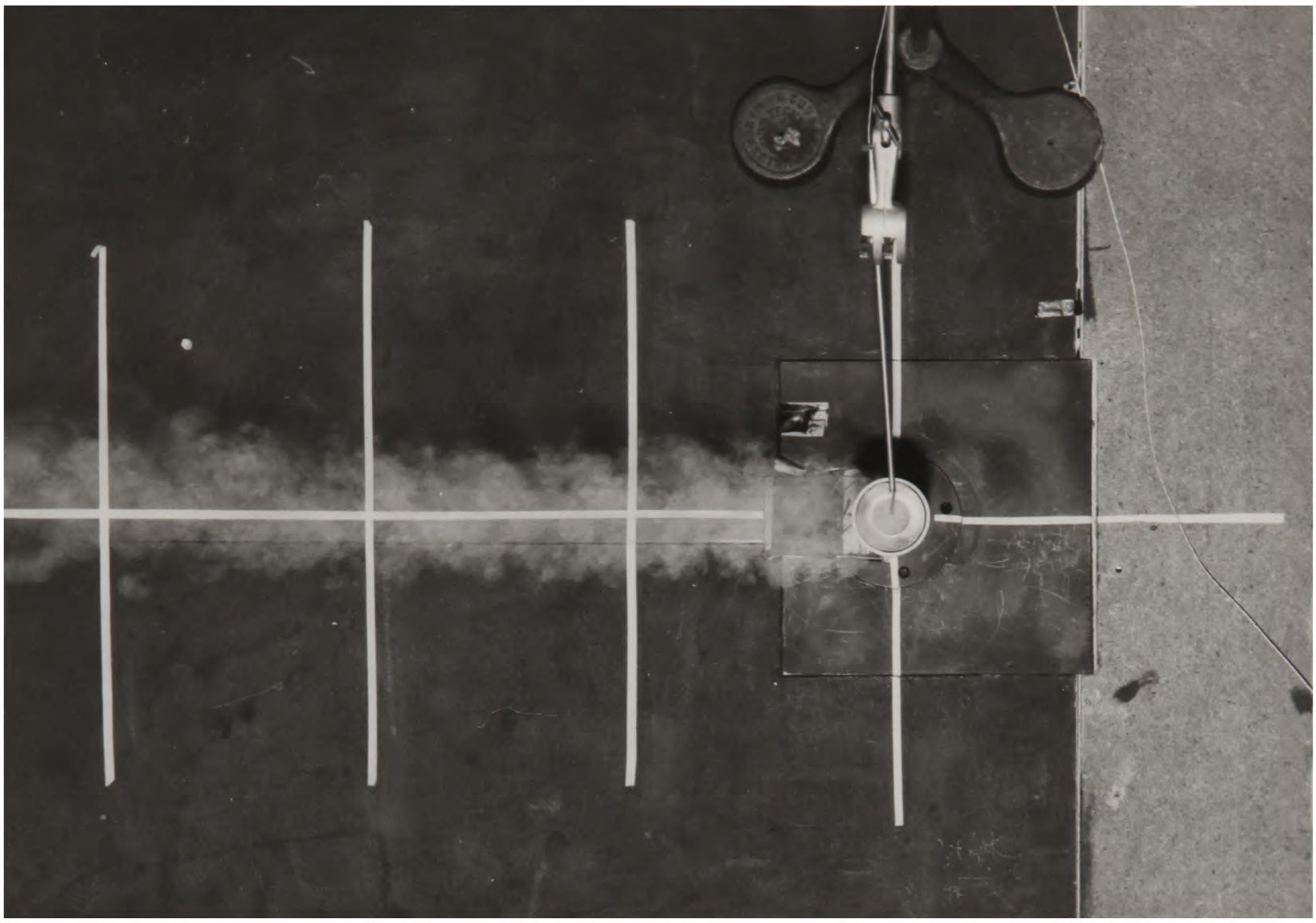

Fig. 7.11 Plan View of Plume 3a in Simulations A and D

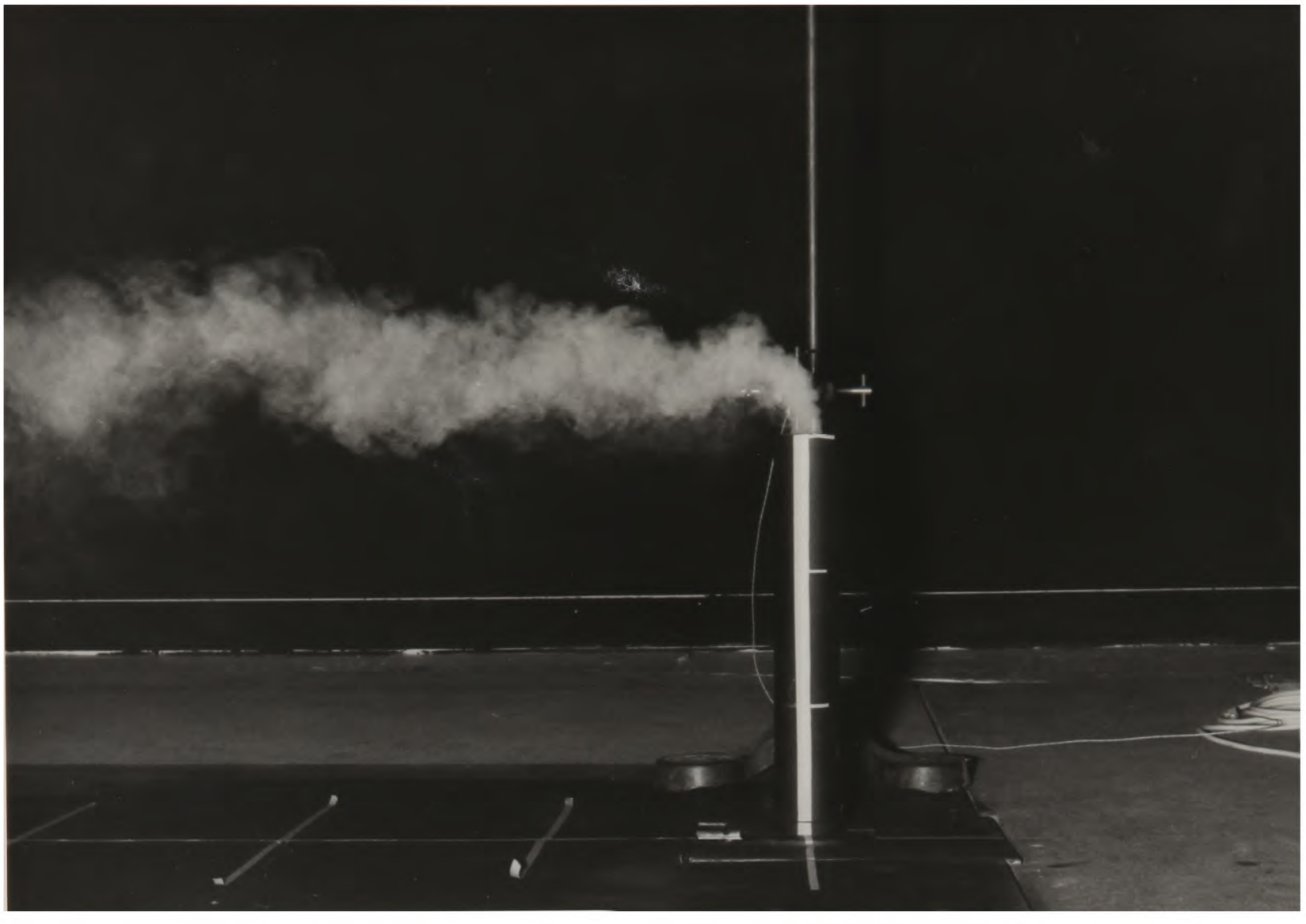

Fig. 7.12 The 'Flapping' Behaviour of Plume 1a in Simulation D

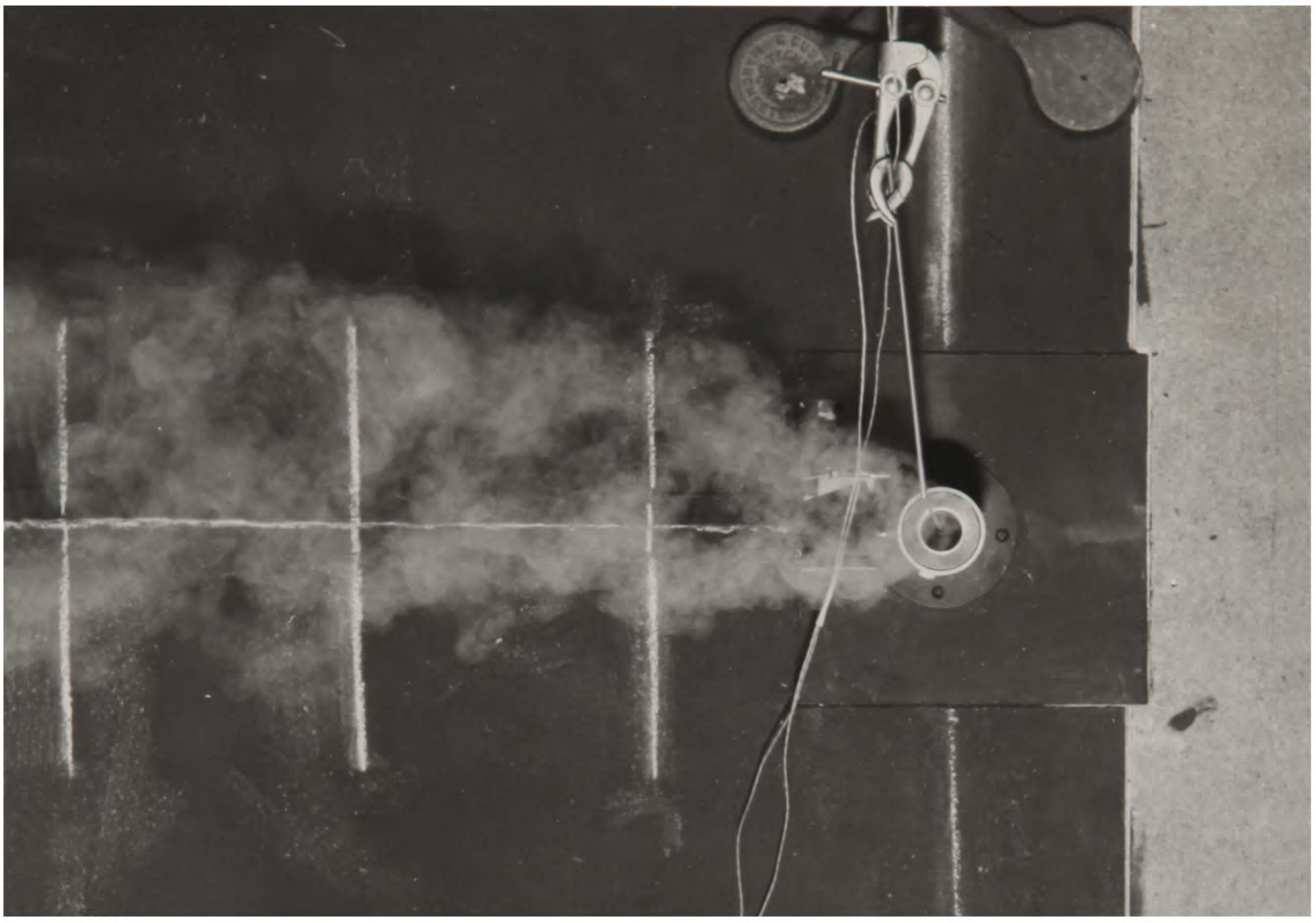

Fig. 7.13 Bifurcation of Plumes 5 and 7 in Simulation C

7.4 COMPARISON OF RESULTS WITH THEORETICAL PREDICTIONS AND PREVIOUS RESULTS

In this section we will compare the results for mean plume trajectory and rate of spread with theoretical methods and the results of previous studies. The aim of this section is to examine how well our results agree with the work of others, rather than suggesting new empirical expressions.

First, let us consider the mean plume trajectory. In sect. 7.2 the predictions of Briggs' plume rise formula were compared with the experimental results, the curves are shown in fig. 7.4 (p. 195) as the dashed lines. Clearly, there is poor agreement between the theoretical plume rise formula and the experimental results. The lack of agreement near the stack should be expected since Briggs' formula is for a bent-over plume (i.e. almost horizontal) from a point source. Briggs' formula does not apply to the bending region of the plume.

Most analytical theoretical methods assume the plume to be either vertical or bent-over, the bending region of the plumes trajectory can be accounted for by computer methods. It was possible to use a commercially available version of Petersen and Cermak's (1979) program to compare the trajectories predicted by the program with some of the experimental results. The computer program was used to predict the trajectories of the following plumes in simulation B, plumes 6, 7, 2a and 2b. The results are shown in figs. 7.15a, b & c. Firstly, considering the results for plumes 6 and 7, fig. 7.15a, the predicted trajectory for plume 7 (R_{ex} = 2100) agrees quite well with the experimental results but for plume 6 (R_{ex} = 1450) the experimentally measured trajectory rises much higher than the predicted trajectory. The relative difference between the trajectories of plumes 6 and 7 predicted by the computer program is very similar to that predicted by

Briggs' formula, see fig. 7.4a. This confirms the expected effect of the buoyancy mismatch between plumes 6 and 7 discussed in sect. 7.2. In figs. 7.15b & c, the results for plumes B2a and B2b are presented. The agreement between the computer program results and the experimental results is good, considering the experimental uncertainty. However, the actual temperatures predicted by the computer program were not in good agreement with the experimental results, the measured temperatures were higher than those predicted by the program.

To compare the experimental results with the various power-laws for plume rise discussed in sect. 2.2.1,the results were plotted in log-log form, see figs. 7.9 and 7.14. For plumes with $R_{ex} > 2000$ and for $X/l_v > 2$, the trajectories fit a curve of the form:

$$Z/l_v = C(X/l_v)^{0.2} \qquad (7.4)$$

Although the exponent may be slightly different for each plume, the general agreement with 0.2 is good. For plumes with low exit Reynolds numbers i.e. plume 6, $R_{ex} = 1450$, and for $X/l_v > 2$ the plume trajectories fitted:

$$Z/l_v = C'(X/l_v)^{1/3} \qquad (7.5)$$

Most theoretical methods predict that for our plumes, $(\text{i.e. } l_v > l_b)$ the plumes will initially rise as $X^{1/2}$ and then as $X^{1/3}$, see tables 2.1 & 2.2; our plumes are not buoyant enough to expect a rise of the form $Z \propto X^{2/3}$. Clearly, although the plumes with $R_{ex} > 2000$ appear to rise initially as $X^{1/2}$ in the first phase, they do not then rise as $X^{1/3}$ in the second phase. However, experimental support for $Z \propto X^{0.2}$ comes from the work of Kamotani and Greber (1972), who fitted curves of the above form to the temperature centreline trajectories for plumes with a wide range of momentum ratios. They found that the exponent varied with momentum ratio and for a momentum ratio of 3.5 (typical of our plumes) they found the exponent to be 0.2. For the exponent to be 1/3 would require a higher

momentum ratio, approximately 10.

Interestingly, the low Reynolds number plumes do appear to rise as $X^{1/3}$ (see fig. 7.9c) this suggests that the interaction between the cross-flow and the plume is basically different for plumes with Reynolds numbers below and above 2,000.

The results for the vertical rate of spread have been presented previously in figs. 7.2 and 7.6, where it was shown that they fitted $\sigma z \propto X^{1/2}$ quite well. This result is in agreement with that of Isyumov and Tanaka (1979) for a plume from an isolated stack. And also agrees with Taylor's Theory of Diffusion for time of travel much greater than the Lagrangian time-scale of the turbulence diffusing the gas. It should be remembered that in the initial phase the spreading is dominated by self-generated turbulence and this result should not be compared with some of the diffusion theories discussed earlier which demand that atmospheric turbulence dominates the mixing. (Though of course, the result does agree with $\sigma^2 z = 2kX$, which is frequently used in the Gaussian plume model.)

The lateral rate of spread was found to follow $\sigma y \propto X^{1/3}$, except in simulation A where $\sigma y \propto X^{0.2}$. Thus the rate of spread is not the same in the vertical and lateral directions. This lateral rate of spread is much smaller than predicted by most theoretical methods and the value frequently used in the Gaussian plume model, i.e. $\sigma y \propto X$. However, there is agreement with the results of Pratte and Baines (1967) who found that for unheated jets, the lateral rate of spread tended towards $X^{1/3}$.

The above results show reasonable agreement with previous experimental results but do not always agree with theoretical predictions. Simple analytical methods do not predict accurately the plume trajectories close to the stack, where the curvature of the plume is greatest, but computer methods show better agreement. Close to the

stack, atmospheric turbulence does not dominate the mixing process and the theoretical methods discussed in sect. 2.2 are not applicable. Hence, the theoretical methods do not predict the temperatures (or concentrations) correctly in the near-field. Of course, the fact that theoretical methods are not applicable in the near-field is one of the justifications for using wind tunnel methods.

Simulation B Plume 1a ⊙
Plume 2a ⊡
Plume 4a △

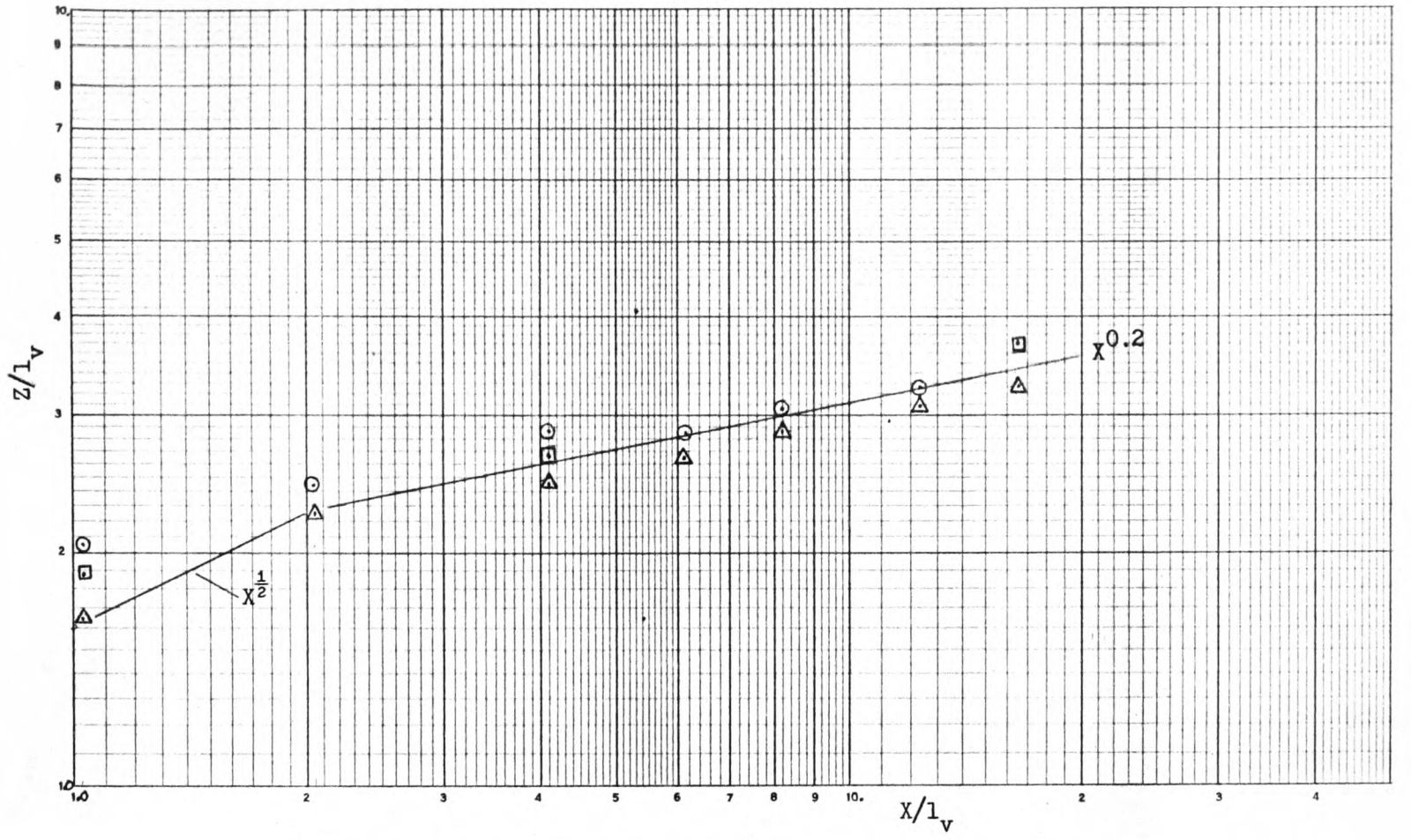

Fig. 7.14a Log-log Plots of Mean Trajectory for Plumes 1a, 2a, 4a.

Simulation B Plume 1b ⊙
Plume 2b ⊡
Plume 4b △

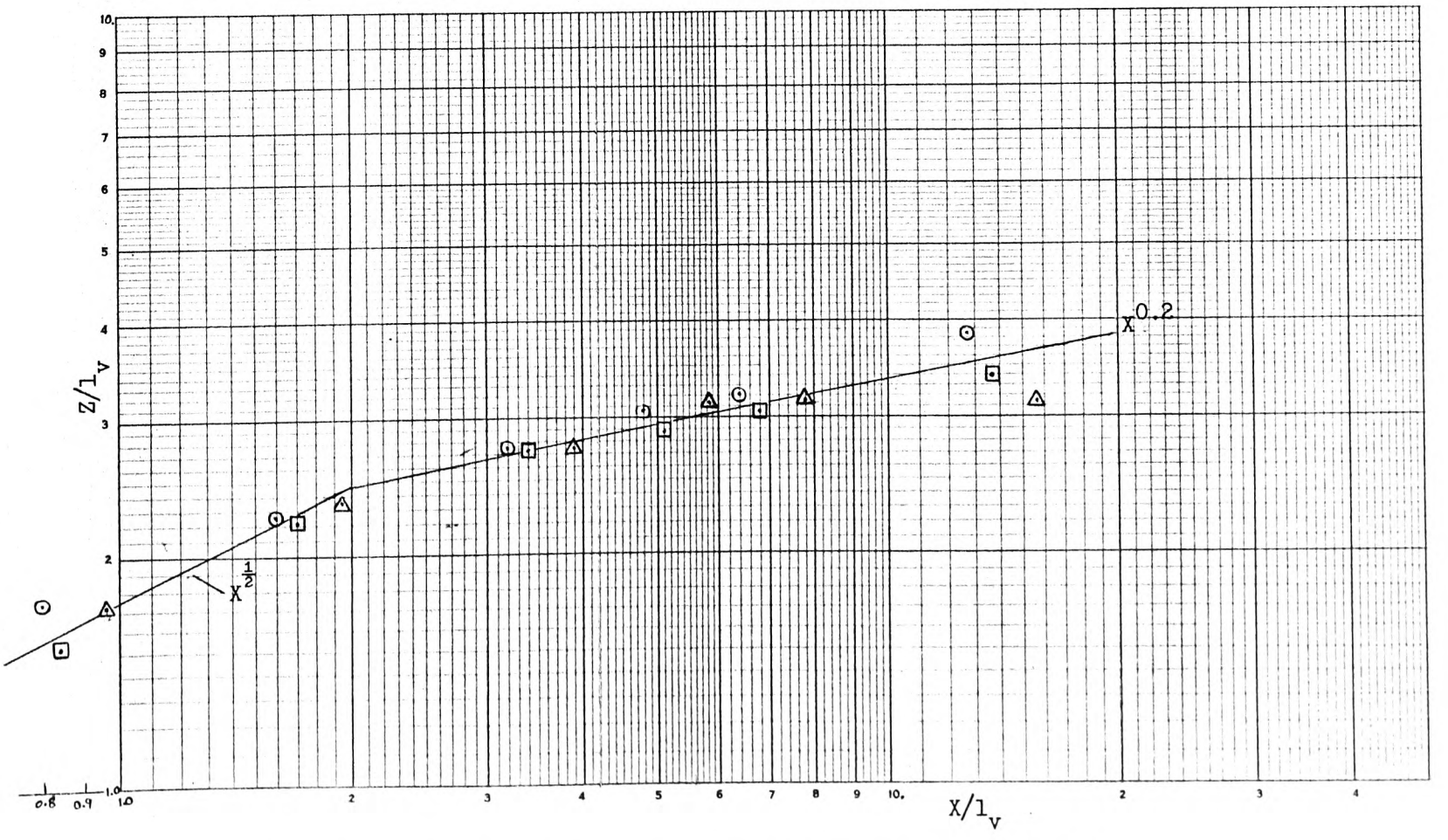

Fig. 7.14b Log-log Plots of Mean Trajectory for Plumes 1b, 2b, 4b.

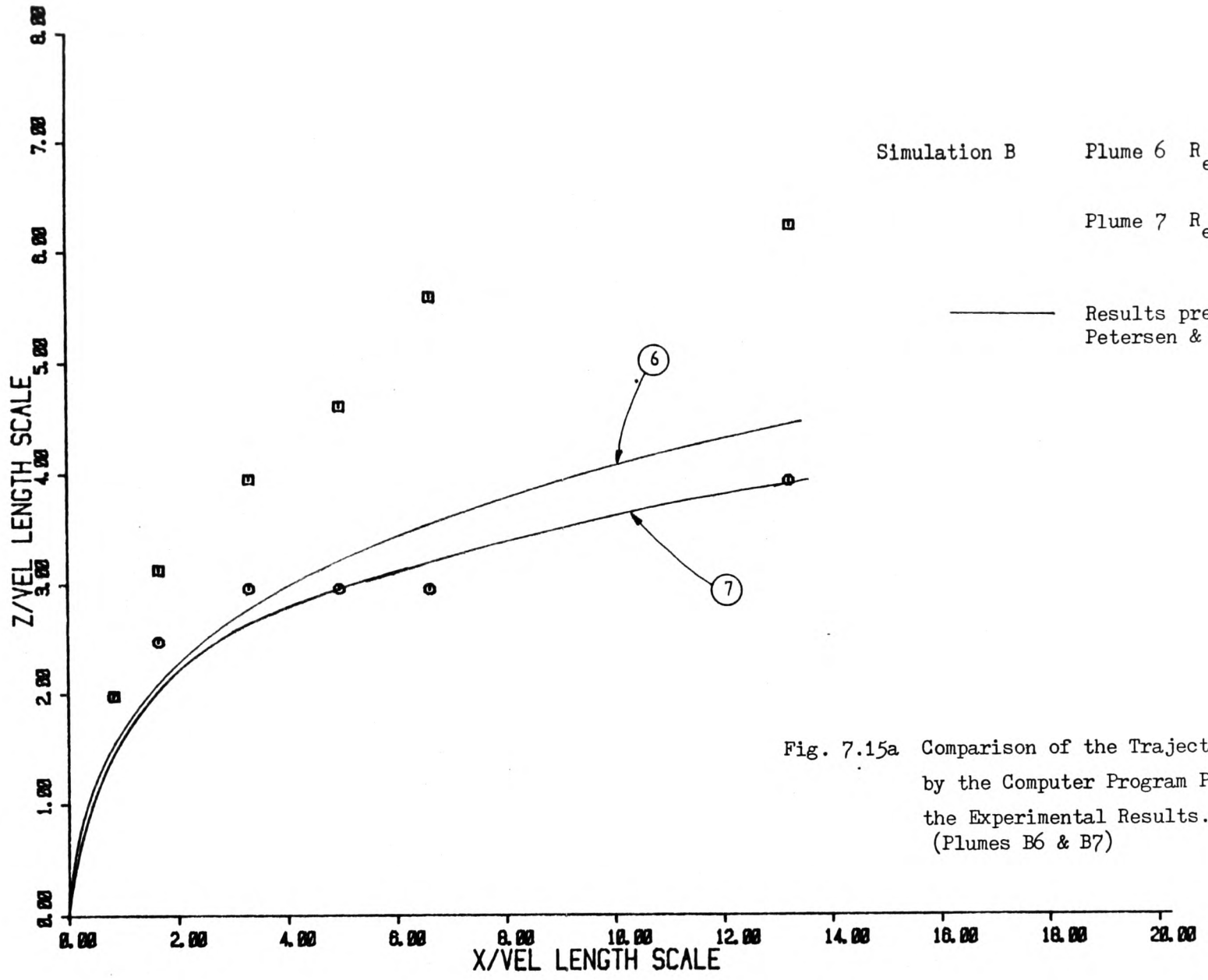

Fig. 7.15a Comparison of the Trajectory Predicted by the Computer Program PLUME with the Experimental Results. (Plumes B6 & B7)

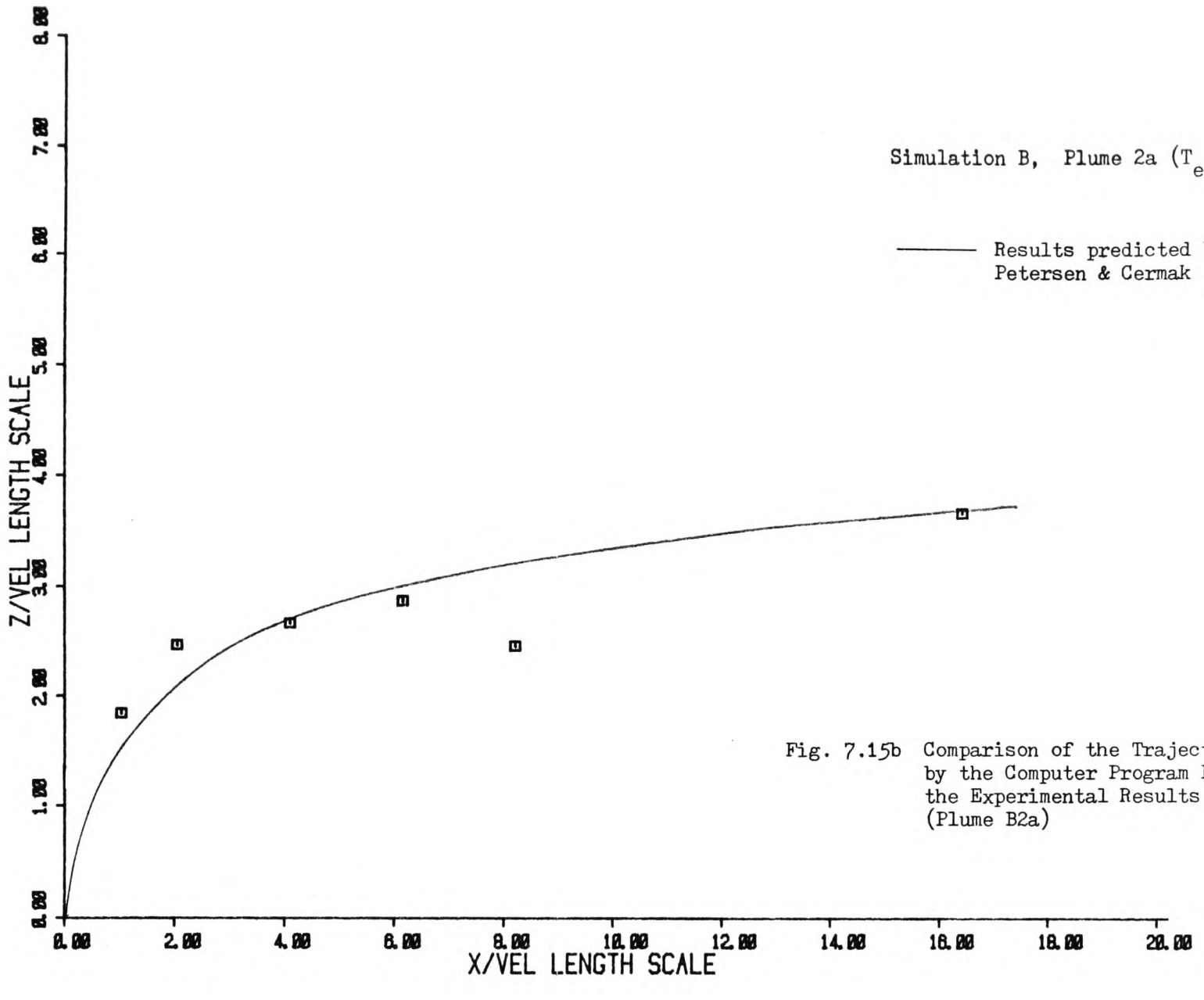

Fig. 7.15b Comparison of the Trajectory Predicted by the Computer Program PLUME with the Experimental Results. (Plume B2a)

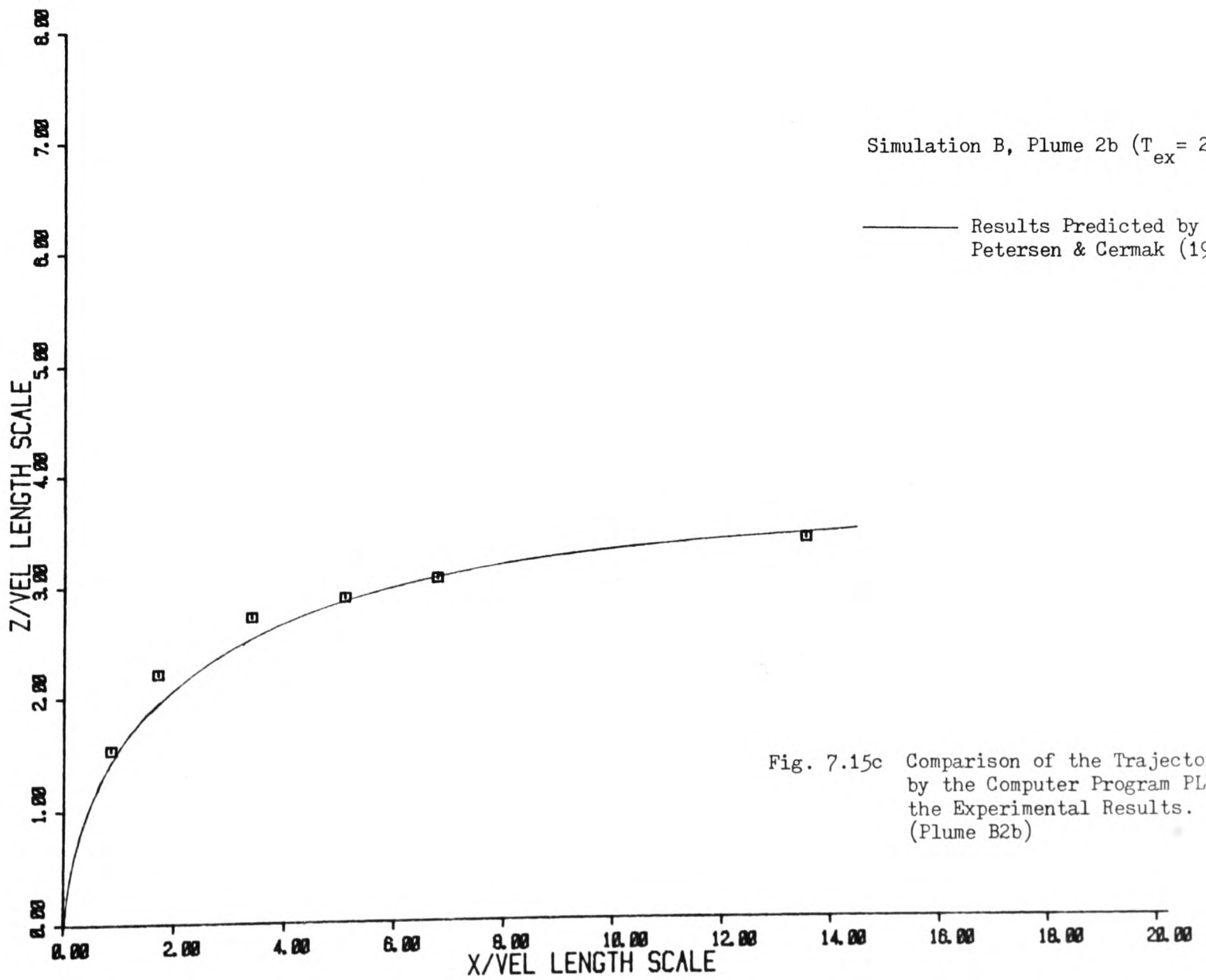

Fig. 7.15c Comparison of the Trajectory Predicted by the Computer Program PLUME with the Experimental Results. (Plume B2b)

8. CONCLUSION

8.1 INTRODUCTION

The aim of this study was to determine how we may examine the near-field behaviour of buoyant gases released into the atmosphere. There are several examples of the release of buoyant gases into the atmosphere being hazardous or dangerous. Hot gases from gas turbine exhausts, either land-based or offshore, can cause thermal pollution problems for man or machinery. For example, on offshore platforms the hot gases from the gas turbines may intefere with helicopters landing on the platform, or create a hostile environment for the personnel. Flammable gases released from pipelines or storage containers are clearly a source of danger. More recently, the accidental release of hot, radioactive gases from nuclear power stations has become a cause for concern.

There are three possible methods of studying the problem:

i) full-scale studies,

ii) theoretical methods,

iii) wind tunnel studies.

Each method has certain advantages and disadvantages.

Full-scale studies are difficult to carry-out and very time-consuming since long averaging times are required and we have no control over the meteorological conditions. As a result, full-scale studies are expensive to perform and few studies have been carried out. Nevertheless, within the experimental accuracy, these experiments do give correct results and do not require any assumptions or scaling relaxations.

Theoretical methods offer a quick and convenient means of examining the problem. The parameters may easily be varied and

hypothetical situations may be studied. However, theoretical methods require certain assumptions to be made and, normally, require some form of empirical input. For these reasons, theoretical methods are limited in their applicability. In complex environments for example, a chemical plant or an offshore platform, theoretical methods cannot be used. The equations of motion for the flow around obstacles cannot be solved and so the dispersion of gases cannot be studied accurately. Thus in many real situations, theoretical methods cannot be used to solve the problem accurately. Therefore, we conclude that an alternative technique is required.

Wind tunnel studies are used as an analogue of the full-scale situation. By constructing a suitable model, dispersion around buildings or obstacles may be studied at reduced-scale in the wind tunnel. The parameters may be easily controlled. Also, shorter averaging times than full-scale are used since the processes occur quicker in the model than at full-scale. The experiments may thus be carried relatively quickly. Wind tunnel methods offer an attractive alternative to full-scale studies and theoretical methods.

In wind tunnel studies we must scale all the governing parameters from the full-scale to model-scale. The necessary similarity requirements may be determined from either dimensional analysis or the governing equations (see Chapter 3). These similarity requirements provide a set of dimensionless groups which should be matched in the model and full-scale for exact similarity. However, we have found that it is not possible to match simultaneously all the groups. If we are going to relax the scaling of a certain group, we must be certain that the group is not having a significant effect on the subsequent dispersion.

The scaling of two groups, the exit density ratio and the exit

Reynolds number, is often relaxed. There is no widely accepted modelling requirement for these groups and there is little experimental evidence to guide us. Additionally, the role of the cross-flow simulation and how accurately we should model the natural wind have not been clearly defined in the past. In an attempt to validate wind tunnel methods, it was decided to study experimentally the following three influences on plume behaviour:

1) the effect of the exit density ratio,

2) the effect of the exit Reynolds number,

3) the effect of the atmospheric boundary-layer simulation.

The study was confined to the dispersion of a buoyant plume from an isolated chimney stack. Buildings or obstacles were not included since they would have created additional effects which would have confused the issue and prevented us from reaching any definite conclusions. In our experiments, the characteristic we were studying was varied while the other dimensionless groups were held constant. The principal findings are now presented.

8.2 THE EFFECT OF THE DENSITY RATIO

Exact scaling of the density ratio is often relaxed since it allows us to exaggerate the density difference in the densimetric Froude number. This in turn allows us to use higher speeds in the wind tunnel and overcome the problems of operating the wind tunnel at low speeds. The experimental evidence for the influence of the density ratio is confusing. Hoult and Weil (1972) and Wilson (1979) studied plumes with different density ratios and found no significant effect on plume trajectory. While, Isyumov and Tanaka (1979) found that plumes with exaggerated density differences rose higher than correctly matched plumes. To examine the effect of the density ratio, we studied pairs of

plumes in which all the dimensionless groups except the density ratio were matched.

We found that mis-matching the density ratio had no significant effect on the plume trajectory or rate of spread(- provided the results were non-dimensionalised by the velocity length-scale and the plume spread was expressed as the standard deviation of the temperature profiles). A wide range of exit temperature differences was used, i.e. 70°C to 270°C. The results provide experimental evidence that the density ratio is not of primary importance for the near-field behaviour of buoyant plumes.

It would appear that we are justified in neglecting to match the density ratio when modelling the near-field behaviour of buoyant plumes, provided all the other dimensionless groups are matched. This makes it much easier to fulfil the other similarity requirements for wind tunnel modelling of buoyant plumes.

8.3 THE EFFECT OF THE EXIT REYNOLDS NUMBER

The Reynolds number of the exit flow is a dimensionless group which cannot be matched since we are using reduced velocity and length scales in the wind tunnel. We are trying to model a full-scale flow which is turbulent and most authors argue that the model exit flow should have the same characteristics as a turbulent pipe flow. The critical Reynolds number for pipe flow is about 2000 and if we can exceed this value, we may argue that the flow characteristics are independent of the Reynolds number. Unfortunately, in wind tunnel studies the exit Reynolds number is normally well below the critical value. Previous studies have tried to overcome this problem by tripping the flow, roughening the inside of the stack to produce turbulence or by using a contraction at the exit to produce a flat-topped velocity

profile. The aim of such devices is rarely explained, other than in the rather vague terms of 'producing a turbulent exit flow' or 'turbulent exit velocity profile'. No reason is given for such properties as the velocity profile being important. The experimental evidence is limited, Isyumov and Tanaka (1979) found that 'improving' the exit flow had little effect on plume dispersion, while Hoult and Weil (1972) found the plume trajectory to be independent of the Reynolds number above a value of 300 (-Hoult and Weil's experiments were carried out in a laminar cross-flow and, in the light of our results, their conclusion should not be extended to a turbulent cross-flow).

We examined several plumes with different Reynolds numbers and exit flow characteristics, and came to some definite conclusions. The Reynolds number had an effect on plume trajectory. We found that the low Reynolds number plumes rose higher than the plumes with $R_{ex} > 2{,}000$. However, above a Reynolds number of 2000, the plume trajectory appeared to be independent of the Reynolds number. The difference in trajectory could not be attributed to the difference in exit velocity profile since, firstly, the exit velocity profiles at different Reynolds number were not very different and, secondly, a plume with a very badly distorted velocity profile rose similarly to an ordinary plume at the same Reynolds number.

The rate of spread was not affected by the Reynolds number, suggesting that the initial entrainment was controlled by self-generated turbulence which was independent of the exit conditions. Thus, the difference in plume behaviour could not be obviously attributed to the exit flow characteristics. The actual Reynolds number itself (based on diameter) appears to be the governing parameter.

Thus, we arrive at the conclusion that producing a turbulent flow by roughening the inside of the stack or producing a turbulent exit

velocity profile would have no effect and there was no justification for such methods. Instead, we must ensure that the critical Reynolds number is exceeded. The critical Reynolds number for each study must be found experimentally, and the Reynolds number independence verified, if we are to be confident of the validity of any such study. Critical Reynolds numbers from one study should not be applied to another study indiscriminately, for example, Hoult and Weil's (1972) value of 300 should not be used for turbulent cross-flows.

8.4 THE EFFECT OF THE ATMOSPHERIC BOUNDARY-LAYER SIMULATION

The final modelling criterion we examined was the atmospheric boundary-layer simulation The characteristics of the a.b.l are reasonably well known and techniques for modelling the a.b.l. in the wind tunnel have been developed. However, there are no guidelines as to which of the many characteristics need to be modelled and how well they need to be modelled to influence the plume's behaviour correctly in the near-field. (At this point, it should be recalled that we only examined the plumes in the near-field and our results cannot be extended to the far-field where atmospheric turbulence dominates the dispersion.)

To investigate the effect of the atmospheric boundary-layer simulation we studied the behaviour of several plumes in four simulations. Three simulations of the a.b.l. were developed and the fourth simulation was a uniform, low turbulence intensity cross-flow. The four simulations had different characteristics. By examining the mean trajectory and rate of spread of the plumes in each simulation, we reached the following conclusions.

The mean plume trajectories were found to be influenced by the cross-flow simulation. The results could not be explained completely by reference to the velocity profiles of the simulations. Plumes in the uniform cross-flow, simulation A, did not rise as high as those in the

a.b.l. simulations where the velocity increased with height. The turbulence intensity of the cross-flow would appear to be an important factor since the turbulence intensity in simulation A was much smaller than in the a.b.l. simulations.

In the a.b.l. simulations the velocity profile did have an effect since plumes in simulation D, which exhibits the greatest increase in velocity with height, do not rise as high as those in the other a.b.l. simulations. However, plume trajectories in simulations B and C, which have almost identical velocity profiles, are not as similar as expected. The main difference between simulations B and C is in the value of the longitudinal turbulence intensity and this again suggests that the turbulence intensity is also influencing the plume trajectory.

The rates of spread of the plumes, lateral and vertical , were very similar in the a.b.l. simulations but slightly smaller in simulation A. The lateral and vertical components of turbulence intensity (σv and σw) were much smaller in simulation A than in the a.b.l. simulations, whereas in the a.b.l. simulations the values of σv and σw were very similar. Therefore, even if the lateral and vertical components of turbulence intensity were affecting the rates of spread, plumes in the a.b.l. simulations would be expected to spread similarly. The fact that plumes in simulation A spread less suggests that the lateral and vertical components are having some effect on plume spread even in the near-field.

These experiments have shown that to model plume dispersion in the near-field, the velocity profile and the three components of turbulence intensity should represent the full-scale conditions as accurately as possible. Since the turbulence intensities show relatively larger changes between different terrain types it is more important to model the turbulence intensities accurately than the velocity profile.

8.5 GENERAL COMMENTS ON THE PLUME AND CROSS-FLOW INTERACTION

We found that plumes in the low turbulence intensity, uniform cross-flow did not rise as high as those in the a.b.l. simulations. We would have expected the opposite effect based the argument presented above. This fact plus the difference in trajectory of the turbulent and laminar plumes led us to the conclusion that the interaction between the plume and the cross-flow is changing. Firstly, considering the exit flow, the interaction between the cross-flow and laminar and turbulent plumes would appear to be fundamentally different. Not only do the laminar plumes' mean trajectories rise higher but they follow a different power-law form, (1/3 as opposed to 0.2 for the turbulent plumes, see fig. 7.9). Considering the cross-flow, the plume trajectories in the uniform cross-flow appear to be different from those in the turbulent simulations. The analogy between the flow around the initial jet-like region and the flow around a cylinder has been suggested. It is well known that the turbulence intensity of the cross-flow around a cylinder may have a marked effect on the values of the drag coefficient (E.S.D.U. 1980) The turbulence intensity of the a.b.l. simulations may be having a similar effect on the drag forces exerted on the plume.

Although there is a wealth of literature on jets in a cross-flow, most of it relates to turbulent jets in a uniform , smooth cross-flow. To understand the interaction more fully would require a series of tests in which jets at various Reynolds numbers were studied in a single cross-flow, and then a series of tests with uniform cross-flows of different turbulence intensities, and then cross-flows with widely differing velocity profiles. Such a study would be of fundamental interest, and has been suggested as a consequence of our attempt to model buoyant plumes accurately.

8.6 POSSIBLE EXTENSIONS OF THE PRESENT STUDY

The present study has examined how we may accurately model in the wind tunnel the near-field behaviour of a buoyant plume from an isolated stack. We have determined which dimensionless groups must be matched and which may be relaxed. We have also examined the modelling requirements for the cross-flow.

However, there are two important aspects of near-field dispersion which we have not examined. They are:

i) the time-dependent behaviour,

and ii) dispersion in the vicinity of buildings.

The time dependent behaviour is of special interest when we are considering the dispersion of flammable gases. We would want to know tha probability of a flammable mixture occurring at possible sources of ignition. This would require the probability density function for concentrations at each point of interest to be determined.

The methods used in this study could be employed to determine the effect of the various parameters on the time-dependent behaviour. Obviously, an instrument with a good frequency response would be required and this may mean that we would have to use hydro-carbon tracer techniques. Also, there are many time-dependent characteristics which we could determine, and we would have to decide which ones were important for our study. Also, the source of gas is unlikely to be a chimney stack and alternative geometries would have to be considered, e.g. pipelines, storage tanks.

Dispersion in the vicinity of buildings is a situation of great practical importance and therefore one of great interest. This kind of problem would require an accurate simulation of the flow around buildings and this is an area of wind engineering which has been the subject of many studies. If we then considered the release of a

pollutant into the flow, we could use the methods of this study to obtain the similarity requirements for the dispersion process. Unfortunately, the possible geometries of source and buildings are numerous and the tendency in the past has been to study only specific cases. Undoubtedly the main problem would be determining the effect of the various Reynolds numbers involved, e.g. for the cross-flow, building and plume. As in this study, the sensitivity of the results to the Reynolds numbers could be determined with a view to providing guidelines for wind tunnel modelling.

REFERENCES

American Meteorological Society,(1978), Position paper on diffusion models, Bull. Amer. Met. Soc., 59, 1025 - 1026.

Barad,M.L.,(1959), Analysis of diffusion studies at O'Neill, in Atmospheric Diffusion and Air Pollution, Ed. Frenkiel,F.N. and Sheppard,P.A., Advances in Geophysics, 6, 389, Academic Press.

Barrett,R.V.,(1973), Use of the wind tunnel to investigate the influence of topographical features on pollution from a tall stack, Chimney Design Symposium., Univ of Edinburgh, April 1973.

Batchelor,G.K.,(1950), The application of the similarity theory of turbulence to atmospheric diffusion, Quart. J. Met. Soc., 76, 133-146.

Batchelor,G.K.,(1952), Diffusion in a field of homogeneous turbulence, Proc. Camb. Phil. Soc., 48, 345-362.

Bayley,F.J., Owen,J.M., Turner,A.B., (1972), "Heat Transfer", Thomas Nelson and Sons Ltd., London.

Bouchardy,A.,(1980), A prediction model for atmospheric pollution caused by a pollutant source, Rech. Aerosp. - No. 1980-3.

Briggs,G.A.,(1965), A plume rise model compared with observations, J. Air Poll. Contr. Assoc., 15, 433-438.

Briggs,G.A.,(1969), Plume Rise, A.E.C. Critical Review Series, TID 25075, 1969, Springfield, Va.

Bringfelt,B.,(1969), A study of buoyant chimney plumes in neutral and stable atmospheres, Atmos. Envir.,3,609-623.

Brotz,W., Schonbucher,A. and Scheller,V.,(1982), Dispersion of plumes from industrial stacks, German Chem. Eng. 5, 240-255.

Builtjes,P.J.H.,(1980), Dispersion around buildings, Atmospheric Pollution 1980, Proc. 14th Int. Coll., Paris, May 1980.

Bultynck,H.,(1972),Evaluation of atmospheric dilution factors for effluents diffused from an elevated continuous point source, Tellus, Vol. 24, No. 5, 455-472.

Carpenter,S.B. et al.,(1971), Principal plume dispersion models T.V.A. power plants, J. Air Poll. Contr. Assoc., 21, 491-495.

Cermak,J.E.,(1971), Laboratory simulation of the atmospheric boundary layer, Trans. A.S.M.E., A.I.A.A. Journal, Vol. 9, No. 9, 1746 - 1754.

Cermak,J.E.,(1975), Applications of fluid mechanics to wind engineering, Freeman Scholar Lecture, J. Fluids Eng. A.S.M.E., 97, 9 - 38.

Cermak,J.E.,(1979), Applications of wind tunnels to investigations of wind engineering problems, A.I.A.A. Jnl., Vol. 17, No. 7.

Cermak,J.E., Peteraka,J.A., Ayad,S.S., and Poreh,M.,(1981), Passive and hybrid cooling developments: Natural ventilation - A wind tunnel study, FMWEP report, Colorado State Univ., Fort Collins, Co., CER81 - 82JEC24, Oct 1981.

Chu,V.H., and Goldberg,M.B.,(1974), Buoyant forced-plumes in cross flow, Proc. A.S.C.E., J Hyd. Div. 100 (HY9), 1203-14.

Cramer,H.E., Record,F.A. and Vaughan,H.C.,(1958), The study of the diffusion of gases in the lower atmosphere, M.I.T. Dept. of Meteorology, Final Report under contract No. AF 19(604)-1058.

Cook,N.J.,(1973), On simulating the lower third of the urban adiabatic boundary-layer in a wind tunnel, Atmos. Envir., 7, 691-705.

Counihan,J.,(1969), An improved method of simulating an atmospheric boundary-layer in a wind tunnel, Atmos. Envir., 3, 197-214.

Davies,M.G., Cole,L.R., and O'Neill,P.G.G.,(1979), Wind tunnel investigation of the temperature field due to the hot exhaust of power generation plants on offshore platforms, N.M.I. Report R54, National Maritime Institute, Feltham, Middx.

Department of Scientific and Industrial Research,(1945), Atmospheric Pollution in Leicester, a scientific survey, H.M.S.O..

Djurfors,S. and Netterville,D.,(1978), Buoyant plume rise in non-uniform winds, J Air Pollut. Control Assoc., vol. 28, no. 8, 780-784.

E.S.D.U. Data Itam No. 72026,(1972), Characteristics of wind speed in the lower layers of the atmosphere near the ground: strong winds, (neutral atmosphere), Engineering Science Data Unit, London.

E.S.D.U. Data Item No. 74031,(1974), Characteristics of atmospheric turbulence near the ground, Part II: single point data for strong winds, (neutral atmosphere), Engineering Science Data Unit, London.

E.S.D.U. Data Item No. 80025/81017,(1980/1), Mean forces, pressures and flow field velocities for circular cylindrical structures: single cylinder with 2D flow / finite length cylinder in uniform and shear flow, Engineering Science Data Unit, London.

Fan,L.N.,(1967), Turbulent buoyant jets into stratified or flowing ambient fluids, California Institute of Technology, Rept. KH-R-15.

Fackrell,J.E.,(1980), A flame ionisation detector for measuring fluctuating concentrations, J. Phys. E : Sci. Instruments, 13, 888 - 893.

Fackrell,J.E. and Robins,A.G.,(1980), Concentration fields associated with emissions from point sources in turbulent boundary layers, Part III, Concentration fluctuations and fluxes, C.E.G.B. Memorandum MM/MECH/TF260, Marchwood Engineering Laboratories, Southampton.

Gifford,F.A.,(1968), An outline of theories of diffusion in the lower layers of the atmosphere, in "Meteorology and Atomic Energy", D.Slade Ed., 66-116.

Goddard,A.J.H., Ghobadian,A. and Gosman,A.D.,(1980), A computer program for the numerical solution of problems in atmospheric dispersion, Atmospheric Pollution 1980, Proc. 14th Int. Coll., Paris, May 1980.

Goldstein,S.,(1938), "Modern Developments in Fluid Dynamics", Clarendon Press, Oxford.

Greenway,M.E. & Wood,C.J.,(1979), The Oxford University 4m x 2m industrial aerodynamics wind tunnel, J.W.E.I.A., 4, 43-70.

Halitsky,J.,(1969), Validation of scaling procedures for wind tunnel modelling of diffusion near buildings, Geophysical Sci. Lab. Report No. TR-69-8, New York University.

Hamilton,P.M.,(1967), Plume height measurements at the Northfleet and Tilbury power stations, Atmos. Envir.,2, 575-98.

Hanna,S.R.,(1982), Turbulent diffusion: chimneys and cooling towers, in "Engineering Meteorology", E.J.Plate Ed., Elsevier 1982.

Hinze,J.O.,(1975), "Turbulence - An Introduction to its Mechanism and Theory (2nd ed.)", McGraw Hill, New York.

Hogstrom,U.,(1964), An experimental study of atmospheric diffusion, Tellus, 16(2), 205-251.

Hoult,D.P., Fay,J.A. and Forney,L.S.,(1969), A theory of plume rise compared with field observations, J. Air Pollut. Control Assoc., 19, 585-590.

Hoult,D.P., O'Dea,S.R., Touchton,G.L. and Ketterer,R.J.,(1977), Turbulent plume in a turbulent cross flow: Comparison of wind tunnel tests with field observations, J. Air Pollut. Control Assoc., Vol. 27, 56-60.

Hoult,D.P. and Weil,J.C.,(1972), Turbulent plumes in a laminar cross-flow, Atmos. Envir., 6, 513-531.

Hunt,J.C.R., and Fernholz,H.,(1975), Wind tunnel simulation of the atmospheric boundary layer: A report on Euromech 50, J.F.M. Vol. 70, part 3, 543-559.

Isyumov,N., Janadali,T., and Davenport,A.G.,(1976), Model Studies and the prediction of full-scale levels of stack gas concentration, J. Air Polut. Control Assoc., Vol. 26, 956 - 964.

Isyumov,N. and Tanaka,H.,(1979), Wind tunnel modelling of stack gas dispersion - Difficulties and approximations, Proc. 5th Int. Conf on Wind Engineering, Colorado State Univ., Colorado, U.S.A., July 1979.

Koga,D.J. and Way,I.L.,(1979), Effects of height and position on pollutant dispersion in building wakes, Proc. 5th Int. Conf. on Wind Engineering, Colorado, U.S.A., July 1979.

Kuhlman,J.M. and Cheng-Chu,L.I.,(1981), Reynolds number and ambient turbulence effects on the near field mean characteristics of a laboratory model thermal plume, Joint A.S.M.E./A.S.C.E. Bioengineering, Fluid and Applied Mechanics Conf., June 22-24, 1981, Boulder Colorado, 81-FE-7.

Lawson,T.V.,(1982), The use of roughness to produce high Reynolds number flows around circular cylinders at lower Reynolds numbers, J.W.E.I.A., 10, 381 - 387.

Li,W.-W. and Meroney,R.N.,(1983), Gas dispersion near a cubical model building. Part I - Mean concentration measurements. Part II - Concentration fluctuation measurements, J.W.E.I.A., Vol. 12, No. 1, 15-48.

List,E.J.,(1982), Turbulent jets and plumes, Ann. Rev. of Fluid Mech. 1982, 14, 189-212.

Lucas,D.H., James,K.W. and Davies,I.,(1967), The measurement of plume rise and dispersion at Tilbury power station, Atmos. Envir.,1,353-66.

Marsh,K.J. and Withers,V.R.,(1969), An experimental study of the dispersion of the emmisions from chimneys in Reading-III, The investigation of dispersion calculations, Atmos. Envir.,3,281-302

Massey,B.S.,(1975), "Mechanics of Fluids (3rd ed.)", Van Nostrand Reinhold, London.

Melbourne,W.H.,(1968), Wind tunnel modelling of buoyant chimney plumes, 3rd Australasian Conference on Hydraulics and Fluid Mechanics,Paper No. 2631, 25th Nov. 1968.

Meroney,R.N.,(1982), Turbulent diffusion near buildings, in "Engineering Meteorology", E.J. Plate Ed., Elsevier, 1982.

Mickelsen,W.R.,(1960), Measurements of the effect of molecular diffusivity in turbulent diffusion, J.F.M., 1960, No. 7, 397 - 400.

Monin,A.S.,(1959), Smoke propagation in the lower layers of the atmosphere, in "Advances in Geophysics; 6, Atmosheric diffusion and air pollution", Frenkiel,F.N. and Sheppard,P.A., editors, Academic Press, London.

Moore,D.J.,(1966), Physical aspects of plume models, Air and Water Pollut. Jnl., 10, 411-417.

Moore,D.J.,(1975), A simple boundary-layer model for predicting time mean ground-level concentrations of material emitted from tall chimneys, Proc. Instn. Mech. Engrs. Vol. 189(4), 33-43.

Morton,B.R., Taylor,G.J. and Turner,J.S.,(1956), Turbulent gravitational convection from maintained and isolated sources, Proc. Roy. Soc. of London, 234A,1-23.

Moussa,Z.M., Trischka,J.W. and Eskinazi,S.,(1977), The near field in the mixing of a round jet with a cross-stream, J.F.M., Vol. 80, 49-80.

Munn,R.E. and Cole,A.F.W.,(1967), Turbulence and diffusion in the wake of a building, Atmos. Envir.,1,33-43.

Murthy,C.R.,(1970), On the mean path of a buoyant chimney plume in a non-uniform wind, J. Appl. Met., 9, 603.

Netterville,D.D.J.,(1979), Concentration fluctuations in plumes, Syncrude Enviromental Research Monograph, 1979-4, Syncrude Canada.

Pasquill,F.,(1969), The influence of the turning of wind with height on crosswind diffusion, Phil. Trans. Roy. Soc. London A, 265, 173.

Pasquill,F.,(1974), "Atmospheric Diffusion (2nd Ed.)", Ellis Horwood, Chichester.

Petersen,R.L. and Cermak,J.E.,(1979), Plume rise for varying ambient turbulence, thermal stratification and stack exit conditions - A numerical and laboratory evaluation, Proc. 5th Int. Conf. on Wind Engineering, Colorado State Univ., Colorado, U.S.A., July 1979.

Poreh,M. and Kacherginsky,A.,(1981), Simulation of plume rise using small wind tunnel models, J.W.E.I.A., Vol. 7, No. 1, 1-14.

Pratte,B.D., and Baines,W.D.,(1967), Profiles of the round turbulent jet in a cross flow, J. Hyd. Div., Proc. A.S.C.E., HY6, Nov. 1967, 53-63.

Priestley,C.H.B. and Ball,F.K.,(1955), Continuous convection from an isolated source of heat, Quart. J. Roy. Met. Soc., 81, 144-157.

Ricou,F.P. and Spalding,D.B.,(1961), Measurements of entrainment by axisymmetrical turbulent jets, J.F.M., 11, 21 - 32.

Rikhter,L.A., Gavrilov,E.I. & Prokhorov,V.B.,(1980), Causes and conditions of the occurrence of downwash of chimney plumes, Thermal Engineering, Vol. 27(11), 610-612.

Robins,A.G.,(1975), Experimental model techniques for the investigation of the dispersion of chimney plumes, Proc. Instn. Mech. Engrs. Vol. 189(4), 44-54.

Robins,A.G.,(1980), Wind tunnel modelling of buoyant emissions, Atmospheric Pollution 1980, Proceedings of the 14th International Colloquium, Paris, May 1980.

Robins,A.G. and Fackrell,J.E.,(1979), Continuous plumes - Their structure and prediction, C.E.G.B. Memorandum MM/MECH/TF148, Marchwood Engineering Laboratories, Southampton.

Robins,A.G. and Fackrell,J.E.,(1980), Laboratory studies of the dispersion near buildings, C.E.G.B. Memorandum MM/MECH/TF 235, Marchwood Engineering Laboratories, Southampton.

Rutledge,K.W. and Thornton,G.K.,(1982), The aspirating gas concentration probe - A review of its use and accuracy in wind tunnel modelling of gas dispersion, O.U.E.L. Report 1391/82, Oxford.

Schlichting,H.,(1979), "Boundary Layer Theory (7th ed.)", McGraw Hill, New York.

Scorer,R.S.,(1958), "Natural Aerodynamics", Pergammon Press, Oxford.

Scriven,R.A.,(1966), On the breakdown of chimney plumes into discrete puffs, Air and Water Pollut. Int. J., 10, 419-25.

Sheppard,C.E. and Warshawsky,I.,(1952), Electrical techniques for compensation of thermal time lag of thermocouples and resistance thermometer elements, N.A.C.A. Tech Note 2703, May 1952.

Skinner,G.T. and Ludwig,G.R.,(1978), Physical modelling of buoyant chimney plumes, Calspan Advanced Technology Centre, Rept. No. 201.

Slawson,P.R. and Csanady,G.T.,(1967), On the mean path of buoyant bent-over chimney plumes, J. Fluid. Mech. Vol. 28, 311-22.

Slawson,P.R., Davidson,G.A., McCormick,W. and Raithby,G.,(1978), A study of the dispersion characteristics of the G.C.O.S. plume, Syncrude Canada Ltd. Report.

Slawson,P.R., Davidson,G.A. and Maddukuri,C.S.,(1980), Dispersion modelling of a plume in the Tar Sands area, Syncrude Enviromental Research Report 1980-1, Syncrude Canada Ltd.

Smith,F.B. and Jeffrey,G.H.,(1971), The prediction of high concentrations of sulphur dioxide in London and Manchester air, Meteorolgical Office, Met. O. 14, Turbulence and Diffusion Note 19.

Smith,M.E., and Singer,I.A.,(1966), An improved method of estimating concentrations and related phenomena from a point source emission, J. Appl. Met., 5, 631-639.

Snyder,W.H.,(1981), Guideline for fluid modelling of atmospheric diffusion, Fluid Modelling Rept No. 10, EPA-600/8-81-009, Sci. Res. Lab., Research Triangle Park, NC, U.S.A., April 1981.

Standen,N.M.,(1972), A spire array for generating thick turbulent shear layers for natural wind simulation in wind tunnels, Tech. Rept. No. LTR-LA-94, National Aeronautical Est., Ottawa.

Taylor,G.I.,(1921), Diffusion by continuous movements, Proc. London Math. Soc., Ser. 2, 20,196.

Thornton,G.K. and Rutledge,K.W.,(1981), A wind tunnel study of buoyant plumes - Comparison of hot air and helium-air plumes, O.U.E.L. Report No. 1345/81, Oxford.

Townsend,A.A.,(1976), "The Structure of Turbulent Shear Flows (2nd ed.)" Cambridge University Press.

Wilson,D.J.,(1979a), Wind tunnel plume modelling, Unpublished report, Dept. Mech. Eng., Univ. of Alberta, 1979.

Wilson,D.J.,(1979b), Wind tunnel simulation of plume dispersion at Syncrude Mildred Lake site, Syncrude Enviromental Research Monograph 1979-1, Syncrude Canada Ltd.

Wood,C.J. and Halstead,A.G.,(1982), The calibration of an aspirating gas concentration probe for thermal experiments, J.W.E.I.A., 9(1982), 237 - 249.

Wright,S.J.,(1977), Mean behaviour of buoyant jets in a cross flow, Proc. A.S.C.E., J. Hyd. Div. 103 (HY5), 499-513.

Yih,C.S.,(1981), Similarity solutions for turbulent jets and plumes, J. Engineering Mechanics Division, A.S.C.E., Vol. 107, No.EM3, 455-478.

ADDENDA

Chatwin,P.C.,(1968), The dispersion of a puff of passive contaminant in the constant stress region, Quart J. Roy. Met. Soc., 94, 350-360.

McCormick,R.A.,(1971), Air pollution in the locality of buildings, Phil. Trans. Roy. Soc. London A, 269, 515-526.

Moore,D.J.,(1974), A comparison of the trajectories of rising buoyant plumes with theoretical/empirical models, Atmos. Env., 8, 441-457.

Sommers,H. et al.,(1980), Flue gas dispersion in the vicinity of buildings: Wind tunnel simulation and comparison with field measurements, Int. Conf. on Air Pollution, Paris, May 1980.

Start,G.E. et al.,(1977), Rancho Seco building wake effects on atmospheric diffusion, NOAA Tech. Memo ERL, ARL-69.